Volume 67A
Number 6
Nov.-Dec. 1963

Physics and Chemistry

6

U.S. DEPARTMENT OF COMMERCE

SECTION A

JOURNAL OF RESEARCH

NATIONAL BUREAU OF STANDARDS

Journal of Research

of the

National Bureau of Standards

A. Physics and Chemistry

NOV.–DEC. • 1963

VOLUME • 67A

NUMBER • 6

Editor: C. W. Beckett

Associate Editors: D. D. Wagman
J. M. Richardson

Publication dates:
Feb. 1, Apr. 1, June 1, Aug. 1, Oct. 1, Dec. 1, 1963

JOURNAL OF RESEARCH

The National Bureau of Standards Journal of Research reports research and development in the fields of activity shown at right. Also included from time to time are survey articles on topics closely related to the Bureau's scientific and technical program.

The Journal is published in four separate sections as follows:

A. Physics and Chemistry

Contains papers of interest primarily to scientists working in these fields. Issued six times a year. Annual subscription: domestic, $4.00; foreign, $4.75.

B. Mathematics and Mathematical Physics

Presents studies and compilations designed mainly for the mathematician and the theoretical physicist. Issued quarterly. Annual subscription: domestic, $2.25; foreign, $2.75.

C. Engineering and Instrumentation

Reports research and development results of interest chiefly to the engineer and the applied scientist. Issued quarterly. Annual subscription: domestic, $2.25; foreign, $2.75.

D. Radio Propagation

Reports work in radio propagation, upper atmospheric physics, and communications. Issued six times a year. Annual subscription: domestic, $4.00; foreign, $4.75.

U.S. DEPARTMENT OF COMMERCE
Luther H. Hodges, Secretary
NATIONAL BUREAU OF STANDARDS
A. V. Astin, Director

Functions and Activities

The functions of the National Bureau of Standards are set forth in the Act of Congress, March 3, 1901, as amended. These include the development and maintenance of the national standards of measurement and the provision of means and methods for making measurements consistent with these standards; the determination of physical constants and properties of materials; the development of methods and instruments for testing materials, devices, and structures; advisory services to government agencies on scientific and technical problems; invention and development of devices to serve special needs of the Government; and the development of standard practices, codes, and specifications. The work includes basic and applied research, development, engineering instrumentation, testing, evaluation, calibration services, and various consultation and information services. The Bureau also serves as the Federal technical research center in a number of specialized fields. The scope of activities of the National Bureau of Standards is suggested in the following listing of the divisions and sections engaged in technical work.

Washington, D.C.

Electricity. Resistance and Reactance. Electrochemistry. Electrical Instruments. Magnetic Measurements. Dielectrics. High Voltage. Absolute Electrical Measurements.

Metrology. Photometry and Colorimetry. Refractometry. Photographic Research. Length. Engineering Metrology. Mass and Volume.

Heat. Temperature Physics. Heat Measurements. Cryogenic Physics. Equation of State. Statistical Physics.

Radiation Physics. X-ray. Radioactivity. Radiation Theory. High Energy Radiation. Radiological Equipment. Nucleonic Instrumentation. Neutron Physics.

Analytical and Inorganic Chemistry. Pure Substances. Spectrochemistry. Solution Chemistry. Standard Reference Materials. Applied Analytical Research. Crystal Chemistry.

Mechanics. Sound. Pressure and Vacuum. Fluid Mechanics. Engineering Mechanics. Rheology. Combustion Controls.

Polymers. Macromolecules: Synthesis and Structure. Polymer Chemistry. Polymer Physics. Polymer Characterization. Polymer Evaluation and Testing. Applied Polymer Standards and Research. Dental Research.

Metallurgy. Engineering Metallurgy. Metal Reactions. Metal Physics. Electrolysis and Metal Deposition.

Inorganic Solids. Engineering Ceramics. Glass. Solid State Chemistry. Crystal Growth. Physical Properties. Crystallography.

Building Research. Structural Engineering. Fire Research. Mechanical Systems. Organic Building Materials. Codes and Safety Standards. Heat Transfer. Inorganic Building Materials. Metallic Building Materials.

Applied Mathematics. Numerical Analysis. Computation. Statistical Engineering. Mathematical Physics. Operations Research.

Data Processing Systems. Components and Techniques. Computer Technology. Measurements Automation. Engineering Applications. Systems Analysis.

Atomic Physics. Spectroscopy. Infrared Spectroscopy. Far Ultraviolet Physics. Solid State Physics. Electron Physics. Atomic Physics. Plasma Spectroscopy.

Instrumentation. Engineering Electronics. Electron Devices. Electronic Instrumentation. Mechanical Instruments. Basic Instrumentation.

Physical Chemistry. Thermochemistry. Surface Chemistry. Organic Chemistry. Molecular Spectroscopy. Elementary Processes. Mass Spectrometry. Photochemistry and Radiation Chemistry.

Office of Weights and Measures.

Boulder, Colo.

Cryogenic Engineering Laboratory. Cryogenic Processes. Cryogenic Properties of Solids. Cryogenic Technical Services. Properties of Cryogenic Fluids.

Central Radio Propagation Laboratory

Ionosphere Research and Propagation. Low Frequency and Very Low Frequency Research. Ionosphere Research. Prediction Services. Sun-Earth Relationships. Field Engineering. Radio Warning Services. Vertical Soundings Research.

Troposphere and Space Telecommunications. Data Reduction Instrumentation. Radio Noise. Tropospheric Measurements. Tropospheric Analysis. Spectrum Utilization Research. Radio-Meteorology. Lower Atmosphere Physics.

Radio Systems. Applied Electromagnetic Theory. High Frequency and Very High Frequency Research. Frequency Utilization. Modulation Research. Antenna Research. Radiodetermination.

Upper Atmosphere and Space Physics. Upper Atmosphere and Plasma Physics. High Latitude Ionosphere Physics. Ionosphere and Exosphere Scatter. Airglow and Aurora. Ionospheric Radio Astronomy.

Radio Standards Laboratory

Radio Standards Physics. Frequency and Time Disseminations. Radio and Microwave Materials. Atomic Frequency and Time-Interval Standards. Radio Plasma. Microwave Physics.

Radio Standards Engineering. High Frequency Electrical Standards. High Frequency Calibration Services. High Frequency Impedance Standards. Microwave Calibration Services. Microwave Circuit Standards. Low Frequency Calibration Services.

Joint Institute for Laboratory Astrophysics-NBS Group (Univ. of Colo.).

Order all publications from the Superintendent of Documents
U.S. Government Printing Office, Washington, D.C. 20402

Use of funds for printing this publication approved by the Director of the Bureau of the Budget (June 19, 1961).

JOURNAL OF RESEARCH of the National Bureau of Standards—A. Physics and Chemistry
Vol. 67A, No. 6, November–December 1963

Analysis of the Spectrum of Neutral Atomic Bromine (Br I)

Jack L. Tech

(August 7, 1963)

The spectrum of the neutral bromine atom, Br I, has been newly investigated by using electrodeless discharge tubes as light sources. The observations have led to a list of wavelengths and estimated intensities for 1253 spectral lines in the range 1067 to 24100 Å. The number of known energy levels has been increased to 123 even and 128 odd levels, as compared with the 27 even and 33 odd levels previously known. All predicted energy levels of the $4s^2\,4p^4\,ns$, np, nd, nf electron configurations from 0 to ~93250 K have been discovered. The observations in the vacuum ultraviolet establish that the positions of all the levels lying above those of the ground configuration as given in the compilation *Atomic Energy Levels*, Vol. II (1952) should be increased by 6.7 K. All but 26 faint lines of Br I have been classified. A total of 67 levels has been ascribed to the $4s^2\,4p^4\,nf$ configurations. It is demonstrated that the nf configurations exhibit almost pure pair coupling. The very regular $(^3P_2)nf[5]^\circ_{11/2}$ series yields for the principal ionization energy of Br I the value 95284.8 K.

1. Introduction

It has been part of the recent program of this laboratory to obtain improved descriptions and analyses of the first and second spectra of the heavier halogens. Work on the Br II and Cl I spectra is currently in progress, and the results for I I and I II have already been published [1, 2].[1] It is the purpose of the present paper to report the results for the first spectrum of bromine, Br I.

Iodine and bromine are very frequently used in electrodeless metal-halide lamps [3] serving as light sources for the study of rare-earth and other metallic spectra. Since the spectrum of both the metal and the halogen will appear when such a lamp is excited, it is essential that the user have available a complete and accurate description of the spectrum of the halogen in order to separate the halogen lines from those of the metal under investigation.

The most thorough study of Br I hitherto available is that contained in the excellent paper on the structure of the arc spectrum of bromine published 30 years ago by C. C. Kiess and T. L. de Bruin [4]. That paper gives, also, a summary of the investigations of Br I carried out prior to 1930. The Br I analysis by Kiess and de Bruin appears with minor revisions in the compilation "Atomic Energy Levels" [5], and when we refer to the analysis given by those authors we shall mean the form as presented in AEL.

The most significant contributions to the study of Br I to appear since 1930 are those by P. Lacroute [6], who studied the Zeeman effect in this spectrum and made some wavelength measurements in the Schumann region; and by Tolansky and Trivedi [7], who made a rather extensive study of hyperfine structure (hfs) in Br I. In the course of the latters' analysis of the structure of 64 lines in the range 4390 to 8700 Å it was found that a number of lines exhibited hfs patterns that could not be satisfactorily explained on the basis of the interpretation of these lines as offered by Kiess and de Bruin. Without going into details, we merely state that all the anomalies encountered by Tolansky and Trivedi have been eliminated by the extended analysis of this spectrum given in the present work.

This considerably improved analysis results largely from the use of more refined apparatus, photographic emulsions, and light sources than were formerly available. The analysis rests chiefly on the 1035 spectral lines that we have recorded for Br I by using electrodeless discharge sources in the photographic air region. In comparison, Kiess and de Bruin's line list contained only 330 lines, which is reduced to 274 when the 56 lines listed by them but not confirmed in our work are rejected.

The analysis of Br I as given in AEL has undergone a number of changes as a result of clues furnished by the greatly augmented line list. These changes can be summarized briefly as follows:

	Number	
	Even	Odd
Original levels	39	39
Rejected	12	6
J or designation changed	7	17
Total real	27	33

[1] Figures in brackets indicate the literature references at the end of this paper.

The new wavelengths have permitted us to find 123 even and 128 odd levels for Br I compared with the 27 even and 33 odd levels listed in AEL.

2. Wavelength Material

(a) Vacuum region: We have observed the bromine spectrum below 2000 Å by use of a vacuum spectrograph having as dispersing element a concave grating of two-meter radius and ruled with 30,000 lines per inch directly on Pyrex. The plate factor at the normal (1920 Å) is 4.26 Å/mm, and the plateholder covers the range 0 to 2570 Å in the first order.

The light source was an end-on glass discharge tube having two side-arms set off by stopcocks and containing reservoirs of bromine and iodine. The discharge tube was affixed to the slit housing of the spectrograph by means of an O-ring seal, so that the slit opened directly to the discharge. The bromine vapor was retarded from entering the main spectrograph chamber by continuous pumping through a trap that entered the discharge tube just before the slit. The bromine vapor pressure in the discharge, excited in the field of 2450 Mc/s radiation from a microwave oscillator, was partly controlled by regulating the temperature at the bromine reservoir. Helium was also admitted into the discharge. The auxiliary iodine reservoir was used to provide standards [1] to supplement the impurity standards of hydrogen, helium, carbon, nitrogen, oxygen, and chlorine [8, 9]. We used EK 103a-O UV and SWR plates and measured the 1000 to 1280 Å region in the second order and the 1000 to 1650 Å region in the first order.

Table A1 in the appendix lists the 124 spectral lines in the vacuum region that we have attributed to Br I. The observed wavelengths in the first column of this table represent the weighted means of only two measurements in the second order for the range 1067 to 1120 Å and of three or more measurements in the first and second orders for the range 1120 to 1633 Å. We have also made use of measurements by W. C. Martin and C. H. Corliss of certain bromine lines that occurred on their iodine spectrograms.

The new wavelengths have made it possible to establish the ground Br I energy separation $4p^5\ ^2P^\circ_{3/2}-{}^2P^\circ_{1/2}$ as 3685.2 K with an estimated error of ± 0.3 K.[2] Since none of the higher Br I energy levels make transitions to the ground term that yield lines in the air region, it is necessary to fix the energies of these higher levels with respect to the ground $^2P^\circ_{3/2}$ level by use of the vacuum observations only. Our new vacuum wavelengths establish the absolute positions of all levels above the ground level to an estimated accuracy of ± 0.3 K and require that the corresponding values for Br I levels in AEL be increased by 6.7 K.

[2] Throughout this paper we use the name kayser, with symbol K, for the unit of wave number cm^{-1}.

Since the relative positions of the higher Br I levels have been accurately fixed by observations in the air region, we can calculate the Br I lines in the vacuum region on an accurate and uniform scale once we have made the energy connection between the ground and excited levels through our measured vacuum wavelengths. These calculated wavelengths are given in column 2 of table A1; they agree to a better extent with the measured wavelengths over the entire range than to the ± 0.01 Å we would have ventured to estimate solely on the basis of examination of the agreement of wavelengths derived from the different exposures, and especially in recognition of the inadequate standards in certain parts of the region.

(b) Air region: A preliminary list of Br I wavelengths in the photographic air region was given earlier by Tech and Corliss [10]. One will find in that paper a thorough description of the experimental procedure and the preparation of the light sources, which we summarize briefly.

Workers have encountered in the past two major difficulties in obtaining a light source suitable for the investigation of the bromine spectrum: (i) bromine is so chemically active a material that it attacks hot internal electrodes; and (ii) water vapor in the bromine causes the appearance of troublesome extraneous bands. Both these difficulties were eliminated in the present work by using electrodeless discharge lamps, excited by a Raytheon Microtherm microwave generator at 2450 Mc/s. For our first series of observations, we used lamps containing $BeBr_2$, but for the more recent series we used lamps containing pure bromine vapor at a pressure of the order of several millimeters of mercury and dried by means of several passes through P_2O_5 as described in [10]. The absence of water vapor in our lamps is attested to by figure (1), displaying the bromine spectrum in the vicinity of Hα (6563 Å). It will be noticed that Hα does not appear at all in the bromine exposure. On the other hand, this figure shows clearly the highly objectionable Br_2 background that occurs on spectrograms of long exposure and that reduces the effective resolving power. Furthermore, the presence of such bands often makes it difficult to decide whether certain faint lines are of atomic or molecular origin.

The spectrograms were made in the first and, wherever possible, second orders with concave gratings having 7,500, 15,000, and 30,000, lines per inch, and mounted in parallel light (Wadsworth mounting), giving first order plate factors of 10, 5, and 2.4 Å/mm respectively. All the spectrograms bore exposures to an electrodeless lamp containing thorium or iron, or to the iron arc, to serve as secondary standards in the determination of the bromine wavelengths. The plates were reduced either by linear interpolation and a correction curve, or by putting the micrometer readings of the lines on punched cards and carrying out the reduction by use of an IBM 704 computer, which adjusted all wavelengths to fit a fourth degree equation determined by least squares.

Table A2 contains the wavelengths, intensities, wave numbers, and classifications of 1035 Br I lines

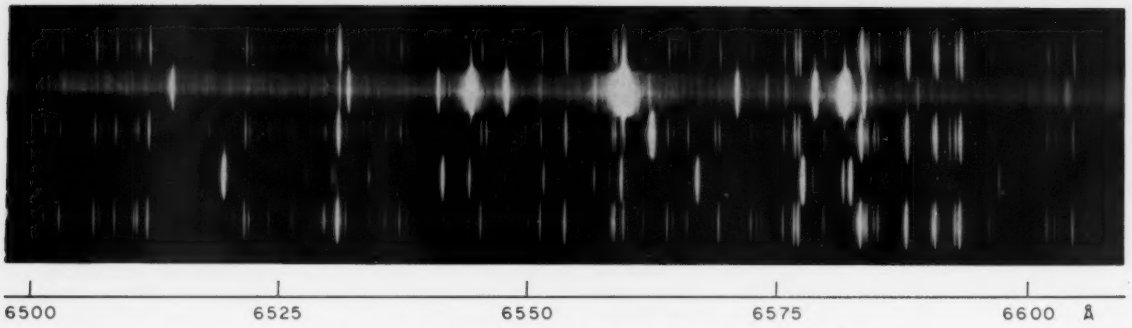

FIGURE 1. *The bromine spectrum in the vicinity of* Hα *(6563 Å).*

Exposure (b) was made with an electrodeless discharge tube containing bromine vapor excited by a microwave diathermy unit. Exposure (d) is of bromine excited by a high voltage ring discharge apparatus that enhanced Br II. The other exposures are of thorium, which served as secondary standards. Hα occurs only in the middle thorium exposure (c).

observed in the range 3325 to 12810 Å. Except for the weaker lines in the region 4264 to 5721 Å, and except for very faint lines over the whole range, the wavelengths in the table represent the weighted means of from two to eight measurements. Because of the inherent broadness of many of the lines, partly as a result of unresolved hyperfine structure, and because the weaker lines were only measured once or twice, the accuracy of the wavelengths is not as great as one would wish. The estimated error of the wavelengths according to spectral region is:

λ	Error
3325–4300 Å	±0.005 Å
4300–7400 Å	±0.02 Å
7400–11000 Å	±0.03 Å
11000–12900 Å	±0.06 Å

Lines in table A2 whose wavelengths are connected by braces are individually measured components of resolved or partially resolved hyperfine structure. Most of the Br I lines exhibiting such wide, resolved hfs patterns result from transitions involving the $4p^4(^1D_2)5s\ ^2D_{5/2},\ ^2D_{3/2}$ levels or the $4p^4(^3P_2)5s\ ^4P_{5/2}$ level, a clue that was very useful in the analysis.

The character of certain lines is indicated by inserting the following symbols after the intensity of the line:

c almost resolved hyperfine structure
d unresolved double line
h hazy, diffuse
H very hazy, very diffuse
s shaded to shorter wavelengths
w wide
W very wide.

The numbers in column 2 of the table are visual estimates of the intensities on an approximately linear scale where the faintest line is assigned an intensity 1. It must be emphasized that these relative intensities are valid only over small wavelength ranges, and no attempt has been made to adjust the values to take into account the varying sensitivity of the photographic emulsions.

Lines of wavelength greater than 11316 Å were measured also on the infrared recordings described in the next section. For comparison, the intensities derived from these recordings are listed in parentheses following the photographic intensities for these lines in table A2. The symbol (*m*) indicates that the line was masked on the recorder charts either by a standard line or by a bromine line of another order.

Table A2 incorporates several improvements over our earlier list of wavelengths. Additional chlorine lines were deleted by consulting the unpublished chlorine line list of Corliss. Chlorine accounted for nearly all the impurity lines found on our spectrograms. Furthermore, several faint lines, measured only once, especially in the region 4725 to 4825 Å have been ascribed to Br_2 and removed from the list. The line at 4358.33 Å has been attributed to Hg and probably originated in the scattered light entering the slit from fluorescent illumination in our source room.

More importantly, additional plates have been measured in parts of the spectrum above 7400 Å. This has not only yielded a number of new lines in this region, but also has allowed us to correct a small systematic error of uncertain origin that was present in some of the earlier measurements in this region. The new wavelengths from 7400 to 9700 Å differ, if at all, by only about +0.01 Å from the earlier values. Above 9700 Å the correction averages somewhat less than +0.04 Å.

Finally, W. F. Meggers and R. Zalubas have generously provided us with some Br I wavelengths that they had measured on their Yb and Th spectrograms, respectively. These measurements have also been averaged into our new mean wavelengths.

(c) Lead sulfide region: The infrared description of Br I was extended to 24100 Å by the use of recording infrared spectrometers. The wavelengths of 94 new lines were measured by the author from radiometric records in the form of recorder charts generously supplied expressly for this investigation by C. J. Humphreys at the Naval Ordnance Laboratory,

TABLE 1. *Wavenumbers and intensities of selected multiplets observed in the radiometric region*

	$4d$ $^4F_{1/2}$ 80587. 61	$^4F_{7/2}$ 81081. 10	$^4F_{5/2}$ 81672. 28	$^4F_{3/2}$ 81842. 02	$^4D_{7/2}$ 79044. 50	$^4D_{5/2}$ 79260. 91	$^4D_{3/2}$ 80630. 67	$^4D_{1/2}$ 80026. 40	$4d$ $^4P_{1/2}$ 81429. 97
$5p$ $^4P^\circ_{5/2}$ 74672. 32		(18) 6408. 78	——	——	(950) 4372. 18	(469) 4588. 59	(138) 4958. 35		
$^4P^\circ_{3/2}$ 75009. 13			(35) 6663. 15	——		(206) 4251. 78	(359) 4621. 54	(138) 5017. 27	(219) 6420. 84
$^4P^\circ_{1/2}$ 75814. 00				(250) 6028. 02				(40) 4212. 40	(330) 5615. 97
$5p$ $^4D^\circ_{7/2}$ 75521. 50	(3450) 5066. 11	(40) 5559. 60	(90) 6150. 78						
$^4D^\circ_{5/2}$ 75697. 05		(500) 5384. 05	(1800) 5975. 23	——					
$^4D^\circ_{3/2}$ 76743. 08			(500) 4929. 20	(263) 5098. 94					

	$4d'$ $^2F_{7/2}$ 83358. 84	$4d'$ $^2F_{5/2}$ 83723. 08
$5p'$ $^2D^\circ_{5/2}$ 78511. 60	(547) 4847. 24	(266 *bl*) 5211. 48
$5p'$ $^2D^\circ_{3/2}$ 78676. 65		(452) 5046. 43

Corona, and by E. D. Tidwell at the Bureau. In both laboratories electrodeless discharge lamps, containing pure bromine and excited by 2450-megacycle microwave diathermy units, served as light source. The records made at Corona were obtained by scanning the spectrum with the high-resolution grating spectrometer designed and built at the National Bureau of Standards. This apparatus has been described by Humphreys and Kostkowski [11]. The bromine wavelengths were measured on these records by linear interpolation between krypton standards that were introduced by reflection from back of the various filters used to sort out the higher order bromine lines. This procedure does not yield the most precise wavelengths, but it was entirely satisfactory for our purposes. For nearly all lines, the departure of the measured wavelengths from those calculated by the combination principle was less than 1 Å. All lines (except 19317 Å and 21093 Å) of intensity 40 and above in the region beyond 19000 Å were also measured on the tracings made by Tidwell, who used the infrared spectrometer at NBS. These wavelengths could be measured with precision by interpolation between the white-light fringes of a Fabry-Perot interferometer that were recorded simultaneously with the bromine spectrum. This technique, as well as the spectrometer apparatus, has been described by Plyler, Blaine, and Tidwell [12].

With the exception of a single chlorine line,[3] every line established from these records can be classified as a transition between Br I levels whose values have been accurately determined from observations in the photographic air region. Precise wavelengths for these lines can therefore be calculated by use of the combination principle. It is these calculated wavelengths that are listed in table A3, which includes four lines above 12000 Å that were also observed photographically.

The relative intensities given in the second column of this table express, in tenths of an inch, the heights of the recorded line profiles above the continuum. One of the tracings furnished by Humphreys was selected to provide the standard scale to which the intensities of lines measured on other tracings would be referred. As the spectrum was being scanned, lines of intensity greater than 85 were attenuated by manual adjustment of a resistance network introduced in the input of the amplifier. The measured heights of these lines were multiplied by the known attenuation factors corresponding to the various resistance box dial settings. Since the amplifier is linear within the limits of loading, and the response of the detector is almost flat within the range covered, the relative intensities are considered to be very reliable over intervals of several hundred angstroms, but not over the entire region covered, inasmuch as no correction was made for the spectral response of the detector or angular distribution of energy from the grating.

In table 1 are displayed the wave numbers and intensities (in parentheses) of certain important multiplets observed in the radiometric region. Observed multiplets that helped to establish the important $(^3P)6s$ ^4P levels are shown in table 2. In both these tables, transitions allowed by the selection rules, but unobserved, are indicated by horizontal bars.

[3] 15730.1 Å. This is the only impurity line found on the tracings; it occurred with intensity 5 on our scale. According to the recent work of Humphreys and Paul [13], it is the second strongest Cl line in the region studied. The strongest Cl line, at 15869.7 Å, was masked by a Br line of another order.

TABLE 2. *Some observed multiplets involving the* 6s $^4P'$ *levels*

	$6s$ $^4P_{5/2}$ 82236. 17	$6s$ $^4P_{3/2}$ 82661. 57	$6s$ $^4P_{1/2}$ 85576. 93
$5p\ ^4P^\circ_{5/2}$ 74672. 32	(1700) 7563. 85	(20) 7989. 25	
$^4P^\circ_{3/2}$ 75009. 13	(750) 7227. 04	(110) 7652. 44	(500d)[a] 10567. 80
$^4P^\circ_{1/2}$ 75814. 00		(338) 6847. 57	——
$5p\ ^4D^\circ_{7/2}$ 75521. 50	(1250) 6714. 67		
$^4D^\circ_{5/2}$ 75697. 05	——	(1800) 6964. 52	
$^4D^\circ_{3/2}$ 76743. 08	——	——	(10w)[a] 8833. 85
$^4D^\circ_{1/2}$ 78865. 72			(55) 6711. 21
$5p\ ^4S^\circ_{3/2}$ 79178. 33			(24) 6398. 60

[a] These two lines were observed photographically.

3. Term Structure of Br I

The unexcited state of the neutral bromine atom is characterized by the electron configuration $4s^2\ 4p^5$, which yields an inverted ^2P term of odd parity. From the vacuum ultraviolet observations discussed above, the position of $4s^24p^5\ ^2P^\circ_{1/2}$ is found to be 3685 K, relative to $^2P^\circ_{3/2}$ taken as zero. The $4s4p^6$ configuration gives one even level, $^2S_{1/2}$, while all other known Br I levels arise from excited configurations of the type $4s^2\ 4p^4\ nl$, where l stands for the letters s, p, d, f indicating the orbital angular momentum quantum number, and n is the principal quantum number. It is convenient to refer to $4s^2\ 4p^4\ nl$ configurations simply as nl configurations. The terms that are expected theoretically for each of these configurations are displayed in table 3, built in the LS scheme. The nl levels are based on, and can be derived from, the parent $^3P_{2,1,0}$ $^1D_2$ and $^1S_0$ terms of the $4p^4$ configuration of the ion, Br^+. The observed distribution of the levels in each of the Br I nl configurations indicates that the coupling energies of the $4p^4$ core dominate the structure of the Br I levels. With just a few exceptions the coordination of Br I levels to specific components of the limiting $4p^4$ terms is unambiguous. When discussing Br I levels in text, this limit is stated explicitly. However, in our tables of observed lines, the levels involved in the classification of the lines are written in an abbreviated notation, which affixes no prime, one prime, and two primes to the symbol for l-value to designate that the level is based on the $^3P_2$, $^3P_1$, and $^3P_0$ parent, respectively. For levels based on $^1D_2$ and $^1S_0$, the parent is stated explicitly.

The positions of the Br II $4p^4$ levels have been accurately determined by Martin and Tech [14], who established the $4p^4\ ^3P_{2,1,0}$ levels from new observations of the vacuum ultraviolet spectrum and the $^1D_2$ and $^1S_0$ levels from observations in the air region of the "forbidden" magnetic dipole transitions, $4p^4\ ^3P_2 - 4p^4\ ^1D_2$ and $4p^4\ ^3P_1 - 4p^4\ ^1S_0$. Since the distribution of these parent levels manifests itself in the structure of all the Br I configurations, the positions of the observed parent levels are repeated here in table 4, together with a slightly different fit to intermediate coupling theory from that given earlier.

The spin-orbit interaction energies in the $4p^4$ configuration may be obtained by reversing the sign of ζ_p in the matrices for p^2 given in *The Theory*

TABLE 4. *Observed and calculated positions for the energy levels of the* $4p^4$ *configuration in* Br II

Energies and coupling parameters are stated in kaysers

Level	Observed position	Obs.-Calc.	Obs.-Calc.
		$F_2 = 1690$ $\zeta_{4p} = 2800$	$F_2 = 1698.1$ $\zeta_{4p} = 2795.0$
$^3P_2$	0.0	0	0
$^3P_1$	3136.4	+6	+13
$^3P_0$	3837.5	−18	−14
$^1D_2$	12089.1	−111	−153
$^1S_0$	27867.1	+112	0

TABLE 3. *Predicted terms of* Br I

Configuration	Predicted terms				
$4s^2\ 4p^5$	$^2P^\circ$				
$4s\ 4p^6$	^2S				
	ns $n \geq 5$	np $n \geq 5$	nd $n \geq 4$	nf $n \geq 4$	ng $n \geq 5$
$4s^2\ 4p^4(^3P)nl$	^4P	$^4(SPD)^\circ$	$^4(PDF)$	$^4(DFG)^\circ$	$^4(FGH)$
	^2P	$^2(SPD)^\circ$	$^2(PDF)$	$^2(DFG)^\circ$	$^2(FGH)$
$4s^2\ 4p^4(^1D)nl$	^2D	$^2(PDF)^\circ$	$^2(SPDFG)$	$^2(PDFGH)^\circ$	$^2(DFGHI)$
$4s^2\ 4p^4(^1S)nl$	^2S	$^2P^\circ$	^2D	$^2F^\circ$	^2G

TABLE 5. *Odd*

Parent	LS Designation	J_cl Designation	E	$\{T$ / n^*	E	$\{T$ / n^*	E	$\{T$ / n^*	E	$\{T$ / n^*	E	$\{T$ / n^*
	$4s^24p^4+$	→	$5p$		$6p$		$7p$		$8p$		$9p$	
$(^3P_2)$	$^4D^\circ_{7/2}$	7/2 [3]°	75521.50	19763.30 2.35638	85762.98	9521.82 3.39481	89636.84	5647.96 4.40788	91538.33	3746.47 5.41208	92620.21	2664.59 6.41742
	$^4D^\circ_{5/2}$	5/2	75697.05	19587.75 2.36692	85820.53	9464.27 3.40512	89669.07	5615.73 4.42051	91557.11	3727.69 5.42570	92626.84	2657.96 6.42542
	$^4P^\circ_{5/2}$	5/2 [2]°	74672.32	20612.48 2.30733	85526.82	9757.98 3.35348	89548.83	5735.97 4.37393	91489.10	3795.70 5.37687	92584.19	2700.61 6.37448
	$^4P^\circ_{3/2}$	3/2	75009.13	20275.67 2.32642	85586.30	9698.50 3.36375	89540.42	5744.38 4.37073	91529.22	3755.58 5.40552	92594.47	2690.33 6.38665
	$^4D^\circ_{3/2}$	3/2 [1]°	76743.08	18541.72 2.43277	85943.86	9340.94 3.42752	89786.18	5498.62 4.46734	91667.59	3617.21 5.50794	92677.31	2607.49 6.48731
	$^4P^\circ_{1/2}$	1/2	75814.00	19470.80 2.37402	85799.19	9485.61 3.40129	89764.81	5519.99 4.45868	91598.86	3685.94 5.45634	92608.84	2675.96 6.40377
$(^3P_1)$	$^2D^\circ_{5/2}$	5/2 [2]°	78511.60	19909.60 2.34771	88848.01	9573.19 3.38569	92755.81	5665.39 4.40110				
	$^2D^\circ_{3/2}$	3/2	78676.65	19744.55 2.35750	88953.76	9467.44 3.40455	92818.85	5602.35 4.42579				
	$^4S^\circ_{3/2}$	3/2 [1]°	79178.33	19242.87 2.38804	89031.84	9389.36 3.41867	92839.36	5581.84 4.43391				
	$^4D^\circ_{1/2}$	1/2	78865.72	19555.48 2.36887	89147.30	9273.90 3.43989	92890.80	5530.40 4.45448				
	$^2S^\circ_{1/2}$	[0]°—1/2	78076.00	20345.20 2.32244	88712.98	9708.22 3.36206	92728.53	5692.67 4.39054				
$(^3P_0)$	$^2P^\circ_{3/2}$	3/2 [1]°	79695.89	19426.41 2.37673	89947.93	9174.37 3.45850	93500.15	5622.15 4.41799				
	$^2P^\circ_{1/2}$	1/2	79868.03	19254.27 2.38733	89905.88	9216.42 3.45060	93491.41	5630.89 4.41456				
$(^1D_2)$	$^2F^\circ_{7/2}$	7/2 [3]°	87225.16	20148.74 2.33374								
	$^2F^\circ_{5/2}$	5/2	87061.23	20312.67 2.32430								
	$^2D^\circ_{5/2}$	5/2 [2]°	88483.42	18890.48 2.41021								
	$^2D^\circ_{3/2}$	3/2	88438.78	18935.12 2.40736								
	$^2P^\circ_{3/2}$	3/2 [1]°	87259.29	20114.61 2.33572								
	$^2P^\circ_{1/2}$	1/2	87499.03	19874.87 2.34976								

Parent	J_cl Designation
$(^3P_2)$	[5]° 11/2, 9/2
	[4]° 9/2, 7/2
	[3]° 7/2, 5/2
	[2]° 5/2, 3/2
	[1]° 3/2, 1/2
$(^3P_1)$	[4]° 9/2, 7/2
	[3]° 7/2, 5/2
	[2]° 5/2, 3/2
$(^3P_0)$	[3]° 7/2, 5/2

E	$\left\{\begin{matrix}T\\n^*\end{matrix}\right.$
10*p* 93291.38	1993.42 7.41953
93339.31	1945.49 7.51037

Ground Configuration of Br I, $4s^24p^5$		E
	$^2P_{3/2}$	0.00
	$^2P_{1/2}$	3685.24

E	$\left\{\begin{matrix}T\\n^*\end{matrix}\right.$	E	$\left\{\begin{matrix}T\\n^*\end{matrix}\right.$	E	$\left\{\begin{matrix}T\\n^*\end{matrix}\right.$	E	$\left\{\begin{matrix}T\\n^*\end{matrix}\right.$	E	$\left\{\begin{matrix}T\\n^*\end{matrix}\right.$	E	$\left\{\begin{matrix}T\\n^*\end{matrix}\right.$
4*f*		5*f*		6*f*		7*f*		8*f*		9*f*	
88392.18	6892.62 3.99010	90873.70	4411.10 4.98772	92222.74	3062.06 5.98644	93036.08	2248.72 6.98567	93563.77	1721.03 7.98512	93925.35	1359.45 8.98450
		90873.78	4411.02 4.98777	92222.80	3062.00 5.98650	93036.13	2248.67 6.98575	93563.82	1720.98 7.98523	93925.36	1359.44 8.98453
88339.16	6945.64 3.97484	90845.55	4439.25 4.97188	92207.32	3077.48 5.97143	93026.10	2258.70 6.97022	93556.94	1727.86 7.96932	93919.84	1364.96 8.96635
88340.71	6944.09 3.97528	90846.78	4438.02 4.97257	92208.27	3076.53 5.97235	93026.67	2258.13 6.97110	93557.34	1727.46 7.97025		
88351.10	6933.70 3.97826	90851.30	4433.50 4.97511	92187.93	3096.87 5.95270	93028.44	2256.36 6.97383	93558.51	1726.29 7.97295		
88350.78	6934.02 3.97817										
88371.32	6913.48 3.98407	90869.64	4415.16 4.98543	92222.01	3062.79 5.98573	93035.35	2249.45 6.98453				
88363.97	6920.83 3.98196	90868.76	4416.04 4.98493	92221.57	3063.23 5.98530	93034.99	2249.81 6.98398	93562.65	1722.15 7.98252		
88425.48	6859.32 3.99977	90891.56	4393.24 4.99785	92233.08	3051.72 5.99658	93042.65	2242.15 6.99590				
88424.88	6859.92 3.99960	90890.88	4393.92 4.99746	92232.69	3052.11 5.99619	93042.39	2242.41 6.99549				
91496.23	6924.97 3.98077	93994.02	4427.18 4.97866								
91497.14	6924.06 3.98103	93994.73	4426.47 4.97905							10*f*	↓
91545.72	6875.48 3.99507	94017.80	4403.40 4.99208					($^3P_2$) 10*f*	[4]$_{3/2}$	94180.82	1103.98 9.97000
91542.44	6878.76 3.99412	94018.21	4402.99 4.99231								
91483.01	6938.19 3.97697	93988.36	4432.84 4.97548								
91482.30	6938.90 3.97677	93987.61	4433.59 4.97506								
92228.30	6894.00 3.98970	94700.23	4422.07 4.98153								
92228.60	6893.70 3.98978	94700.41	4421.89 4.98163								

Parent	*LS* Designation	*Jd* Designation	*E*	$\left\{\begin{matrix}T\\n^*\end{matrix}\right.$	*E*	$\left\{\begin{matrix}T\\n^*\end{matrix}\right.$	*E*	$\left\{\begin{matrix}T\\n^*\end{matrix}\right.$	*E*	$\left\{\begin{matrix}T\\n^*\end{matrix}\right.$	*E*
	$4s^2\,4p^4+$	→	*5s*		*6s*		*7s*		*8s*		*9s*
	$^4P_{5/2}$	5/2	63436.45	31848.35 1.85623	82236.17	13048.63 2.89997	88135.07	7149.73 3.91770	90788.90	4495.90 4.94046	92161.45
($^3P_2$)		[2]									
	$^4P_{3/2}$	3/2	64907.19	30377.61 1.90064	82661.57	12623.23 2.94843	88275.49	7009.31 3.95674	90797.55	4487.25 4.94522	92182.30
	$^2P_{3/2}$	3/2	67183.58	31237.62 1.87429	85435.33	12985.87 2.90697	91284.03	7137.17 3.92114	93906.64	4514.56 4.93024	
($^3P_1$)		[1]									
	$^4P_{1/2}$	1/2	66883.87	31537.33 1.86536	85576.93	12844.27 2.92295	91347.68	7073.52 3.93875	93983.18	4438.02 4.97257	
($^3P_0$)	$^2P_{1/2}$	[0]—1/2	68970.21	30152.09 1.90773	86279.41	12842.89 2.92310	92089.61	7032.69 3.95016			
	$4s^2\,4p^4+$	→	*4d*		*5d*		*6d*		*7d*		*8d*
	$^4F_{9/2}$	9/2	80587.61	14697.19 2.73249	87191.97	8092.83 3.68235	90244.89	5039.91 4.66621	91851.14	3433.66 5.65323	92807.81
		[4]									
	$^4F_{7/2}$	7/2	81081.10	14203.70 2.77955	87440.02	7844.78 3.74012	90267.85	5016.95 4.67688	91880.64	3404.16 5.67768	92843.81
	$^4D_{7/2}$	7/2	79044.50	16240.30 2.59943	86768.28	8516.52 3.58959	89860.70	5424.10 4.49792	91755.54	3529.26 5.57614	92729.66
		[3]									
	$^4D_{5/2}$	5/2	79260.91	16023.89 2.61693	86933.28	8351.52 3.62487	89947.97	5336.83 4.53455	91810.29	3474.51 5.61990	92753.69
($^3P_2$)	$^4F_{5/2}$	5/2	81672.28	13612.52 2.83927	87754.92	7529.88 3.81752	90354.93	4929.87 4.71800	91956.55	3328.25 5.74206	92743.16
		[2]									
	$^4F_{3/2}$	3/2	81842.02	13442.78 2.85714	87769.96	7514.84 3.82134	90416.44	4868.36 4.74771	91926.88	3357.92 5.71664	92853.62
	$^4D_{3/2}$	3/2	79630.67	15654.13 2.64765	87131.65	8153.15 3.66871	89867.69	5417.11 4.50082	91800.15	3484.65 5.61172	92774.91
		[1]									
	$^4D_{1/2}$	1/2	80026.40	15258.40 2.68177	87271.73	8013.07 3.70063	89729.40	5555.40 4.44445	91690.94	3593.86 5.52580	92650.45
	$^4P_{1/2}$	[0]—1/2	81429.97	13854.83 2.81433	87754.17	7530.63 3.81733	90428.50	4856.30 4.75360	91823.95	3460.85 5.63098	92824.33
	$^2F_{7/2}$	7/2	83358.84	15062.36 2.69916	90427.64	7993.56 3.70515	93244.35	5176.85 4.60408			
		[3]									
	$^2F_{5/2}$	5/2	83723.08	14698.12 2.73240	90565.85	7855.35 3.73760	93342.44	5078.76 4.64833			
	$^4P_{5/2}$	5/2	84305.76	14115.44 2.78823	90585.26	7835.94 3.74223	93473.77	4947.43 4.70962			
($^3P_1$)		[2]									
	$^4P_{3/2}$	3/2	84077.52	14343.68 2.76596	90537.52	7883.68 3.73088	93452.77	4968.43 4.69966			
	$^2P_{3/2}$	3/2	83578.50	14842.70 2.71906	90459.75	7961.45 3.71261	93117.18	5304.02 4.54855			
		[1]									
	$^2P_{1/2}$	1/2	83101.09	15320.11 2.67636	90292.34	8128.86 3.67418	92992.67	5428.53 4.49609			
	$^2D_{5/2}$	5/2	84945.16	14177.14 2.78216	91175.18	7947.12 3.71596	94088.98	5033.32 4.66926			
($^3P_0$)		[2]									
	$^2D_{3/2}$	3/2	85191.59	13930.71 2.80666	91001.35	8120.95 3.67597	94082.60	5039.70 4.66631			

$\left\{\begin{matrix}T\\n^*\end{matrix}\right.$	E	$\left\{\begin{matrix}T\\n^*\end{matrix}\right.$	E	$\left\{\begin{matrix}T\\n^*\end{matrix}\right.$	E	$\left\{\begin{matrix}T\\n^*\end{matrix}\right.$		Parent	LS Designation	E	$\left\{\begin{matrix}T\\n^*\end{matrix}\right.$
	10*s*		11*s*				$4s^2\,4p^4+$				
3123. 35 5. 92741	92905. 81	2288. 99 6. 92395	93544. 55	1740. 25 7. 94090			5*s*	($^1D_2$)	$^2D_{5/2}$	75890. 33	31483. 57 1. 86695
3102. 50 5. 94730	93039. 29	2245. 51 6. 99066	93557. 98	1726. 82 7. 97172					$^2D_{3/2}$	75908. 53	31465. 37 1. 86749
							5*s*	($^1S_0$)	$^2S_{1/2}$	91937. 95	31213. 95 1. 87500
	$4s\,4p^5$	$^2S_{1/2}$	84825. 60	----------			6*s*	($^1D_2$)	$^2D_{5/2}$		
				----------					$^2D_{3/2}$	94470. 7	12903. 2 2. 91626
	9*d*		10*d*		11*d*		12*d*		$4s^2\,4p^4+$	4*d*	
2476. 99 6. 65600	93411. 48	1873. 32 7. 65367	93818. 96	1465. 84 8. 65232	94106. 70	1178. 10 9. 65127	94317. 40	967. 40 10. 65056	$^2G_{9/2}$	91921. 86	15452. 04 2. 66491
2440. 99 6. 70491	93431. 26	1853. 54 7. 69440	93859. 09	1425. 71 8. 77324	94126. 43	1158. 37 9. 73312			$^2G_{7/2}$	91998. 55	15375. 35 2. 67155
2555. 14 6. 55342	93403. 86	1880. 94 7. 63815	93798. 76	1486. 04 8. 59331					$^2D_{3/2}$	93088. 62	14285. 28 2. 77160
2531. 11 6. 58446	93405. 91	1878. 89 7. 64231	93815. 57	1469. 23 8. 64233				($^1D_2$)	$^2D_{3/2}$	92516. 91	14856. 99 2. 71775
2541. 64 6. 57081									$^2F_{7/2}$	93682. 82	13691. 08 2. 83111
2431. 18 6. 71842									$^2F_{5/2}$	93671. 92	13701. 98 2. 82998
2509. 89 6. 61223	93335. 31	1949. 49 7. 50266	93821. 47	1463. 33 8. 65973					$^2P_{3/2}$	93609. 89	13764. 01 2. 82360
2634. 35 6. 45415	93282. 58	2002. 22 7. 40320							$^2P_{1/2}$	93650. 35	13723. 55 2. 82776
2460. 47 6. 67831	93451. 49	1833. 31 7. 73673							$^2S_{1/2}$	93701. 48	13672. 42 2. 83304

of Atomic Spectra [15, p. 268]. The diagonal electrostatic energies to be added are[4]

$$\begin{aligned} {}^3P &: 6F_0 - 15F_2 \\ {}^1D &: 6F_0 - 9F_2 \\ {}^1S &: 6F_0 \end{aligned}$$

where $F_0 = F_0(4p, 4p)$ and $F_2 = \frac{1}{25} F^2(4p, 4p)$. The choice of coupling parameters in the previous calculation of the distribution of Br II $4p^4$ levels [14] resulted in the fit shown in the third column of table 4. Since these discrepancies reappear to some extent in the calculation of Br I $4p^5 5s$ levels presented below, it has seemed worthwhile to recalculate the parents in order to demonstrate that, with just a small change in parameters, the calculation of Br II $4p^4\ {}^1S_0$ can be improved without appreciably affecting the fit for the ${}^3P_{2,1,0}$ levels. The new fit, shown in the last column of table 4, is a strict least squares fit to the four levels other than ${}^1D_2$. It predicts the total energy spread of the configuration exactly, and emphasizes that the larger discrepancy for $4p^4\ {}^1D_2$ may actually be due to a perturbation by a higher level, since the discrepancy is in the right direction.

Tables 5 and 6 contain all the energy levels of the neutral bromine atom that we have been able to find by using the new wavelengths. The tables are arranged so as to display clearly the level parentage, configuration, and series. For each level are given the energy (E) relative to $4p^5\ {}^2P^o_{3/2}$ taken as zero, the absolute energy value (T) measured from the principal ionization limit, i.e., from Br II $4p^4\ {}^3P_2$, and the effective quantum number (n^*) calculated according to $n^* = \sqrt{(R/T)}$, where R is the Rydberg constant for bromine, 109736.56 K. The designations of the levels, usually in both the LS scheme and the $J_c l$ scheme, are given just to the left of the first member of each series and hold for all other levels of the series. In all except the nf configurations one might say that the coupling is "midway between" the LS, $J_c j$, and $J_c l$ coupling schemes. The almost pure pair-coupling in the nf configurations permits positive assignment of $J_c l$ symbols to the nf levels. All other levels are consistently referred to in terms of the adopted LS symbols, for reasons of tradition, of the general familiarity of this notation, and of the lack of any really satisfactory solution to the vexing problem of notation for intermediate couplings.

Figure 2 shows the distribution of ns, np, nd, nf levels through $n=9$. The small horizontal bars in each nl column represent the position of one *or more* levels. The scale of the diagram does not allow an individual representation for each level. The vertical lines in each column separate groups of levels having different parents, the lowest group of levels in each column being based on the $({}^3P_2)$ parent. It should be remembered that when a level group appears to be intersected by a vertical line (by virtue

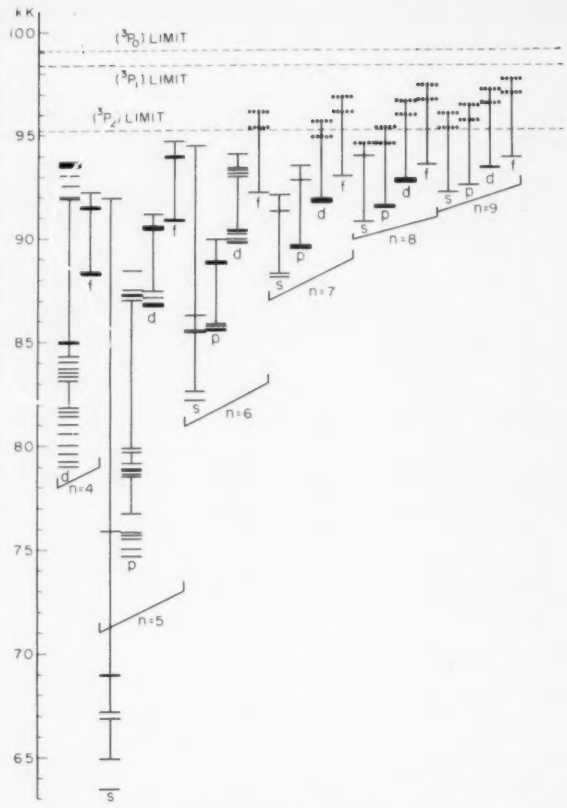

FIGURE 2. *The distribution of* Br I *energy levels for* $n=4$ *to* $n=9$, *as discussed in the text.*

of being met from above and from below by such a line), then there is a change of parent in either going to the next higher or the next lower group. The separation of the level groups for each nl clearly reflects the energy differences of the parent limits shown by the dashed lines in the figure. Thus, except for absolute energy position, the levels of many nl sets have the same appearance in this figure: three groups of levels held apart by the parent differences. This "building-block" character is well observed at $4f$, $5f$, $6p$, and $7s$, for example, and can be expected to hold at all high n. The dotted level positions represent some predicted, but unobserved, levels based on $({}^3P_{1,0})$. It is seen that the only unobserved levels based on parents other than $({}^3P_2)$ and lying below the $({}^3P_2)$ limit are those of $({}^3P_1)\ 8p$, $({}^3P_1)7d$, and $({}^3P_0)8s$. The other dotted positions fall above the $({}^3P_2)$ limit, and the atoms excited to these levels can be expected to autoionize.

It is convenient at this point to discuss the extent to which significance may be attached to the symbols used in this paper to describe the energy levels. The LS symbols are based on an examination of the intensities in the transition arrays, with symbols being assigned in such a way that the

[4] These electrostatic expressions differ by a constant amount from those given on p. 199 in TAS, which are not entirely correct. See footnote on page 102 of reference [22].

intensity relations most nearly conform to the well-known LS rules. The arrays used were those containing levels of low principal quantum number n, the assignments being retained along series without regard to intensities. LS symbols assigned to levels in this way will not necessarily survive if the actual energy matrices in the LS scheme are diagonalized and the eigenvectors found, because when the coupling strongly departs from the LS scheme, the intensities then being governed more by, say, the J_cl rules, the LS symbols to which one is led depend more on J_c and K and will not with assurance correspond to the major LS contribution to the composition of the levels. A preliminary rough diagonalization of the Br I $5p$ energy matrices suggests, for example, that the "percentage-method" would require the $(^3P_2)5p\,^4D^\circ_{5/2}$ and $(^3P_1)5p\,^2D^\circ_{5/2}$ levels to have their designations interchanged, whereas the intensities would not suggest this. In any case, the departure from LS coupling is so great that L and S are not good quantum numbers anyway, making meaningless any involved procedure for naming the levels. In the absence of reliable eigenvectors, the "intensity-method" seems to be the most attractive. The np LS assignments in Br I turn out to correspond exactly to those in F I [16], but are quite different from those adopted for the I I np levels by Kiess and Corliss [1], who assigned LS symbols by forming a one-to-one best correspondence of Landé g-factors to observed g-factors. For small departures from pure LS coupling, all three methods should result in the same designations.

Ideally, one should like to designate observed levels in the notation of the coupling scheme in which the energy matrices are already most diagonal, that is, in which there is the least nondiagonal contribution to the energies (eigenvalues). In this sense, the Br I nf configurations are very nearly pair-coupled, and J_cl symbols should certainly be used for the nf levels. For the sake of consistency, J_cl symbols have also been assigned to the other Br I levels, as alternatives to the LS symbols. This is justifiable on the grounds that for ns the choice of J_cl or J_cj notation is arbitrary owing to the identity of the matrices built in the two schemes, while for np and nd the notation could be equally well J_cl or J_cj since the coupling is intermediate. In these cases only exact calculation would allow us to decide in favor of one or the other scheme, and this would still be difficult for nd because of the sizeable perturbations that afflict the nd configurations. The J_cl designations for the Br I np levels have been chosen on the basis of approximate calculations by using the diagonal J_cl energy expressions. Diagonal expressions are less valid for nd, so that only general considerations of level positions could be invoked in the assignment of J_cl notation, the primary emphasis being placed on the intensities of $(^3P_2)4d$–$(^3P_2)nf$ transitions for the $(^3P_2)4d$ designations and $5p$–$4d$, $5p$–$5d$ transitions for the other nd designations.

The main features of J_cl coupling and the theoretical treatment of electronic configurations exhibiting this type of coupling are discussed at length by Minnhagen [17] in his fine paper on Ar II. The theoretical treatment is based upon the general formulas of Möller [18], who calculated the p^1l matrices of electrostatic energy in the J_cl scheme. The corresponding matrices of spin-orbit interaction have recently been provided by Källén and appear in the appendix of reference [19].

A pair-, or J_cl coupled configuration is characterized by (i) a domination by the core coupling energies, and (ii) an electrostatic interaction of the outer electron with the core that is stronger than the spin coupling of this electron. The second requirement means, in the case of the $4p^4nl$ configurations of Br I, that the contribution of $F^2(4p, nl)$ to the level energies must be greater than that of ζ_{nl} and the $G^k(4p, nl)$. The notation used for a level in a pair-coupled configuration is that suggested by Racah [20], in which the level is designated as $(\ )nl\ [K]_J$, where the parent is placed in the parentheses, and where K, the intermediate quantum number, is the quantized resultant of the coupling of the total angular momentum J_c of the parent ion with the orbital angular momentum of the external electron. The coupling of K with the spin of this electron gives the J-value of the level. Each K-value thus has two J-values associated with it, $J=K\pm\frac{1}{2}$. For Br I, J_c can take the values 2, 2, 1, 0, and 0, corresponding to the five levels of the ground configuration $4p^4$ in the ion. The selection rules governing electric dipole transitions between J_cl coupled levels are

$$\Delta J_c=0;\ \Delta K=0,\pm1;\ \Delta l=\pm1;\ \text{and}\ \Delta J=0,\ \pm1.$$

The last two are, of course, independent of coupling, but the first two are easily violated when departures from pure pair coupling occur, because the energy matrices are not diagonal in J_c or K.

Owing to the departures in Br I from any pure coupling scheme, the single level eigenfunctions of any such scheme are mixed. L, S, J_c, and K are not very good quantum numbers, and the only restrictions on transitions seem to be those on parity and ΔJ.

4. Ionization Limits

A very sharp determination of the principal ionization limit of the neutral bromine atom is possible now that the $(^3P_2)nf[5]^\circ_{11/2}$ series has been observed. This series is found not only empirically to provide the best value for the limit; it is also the series one might expect on theoretical grounds to provide such a best value. The theoretical criterion one should use in the selection of the least perturbed series for the limit determination is that the effect of nondiagonal matrix elements connecting the levels to other levels of common l and J value shall be very small or zero. In general, this criterion restricts consideration to series of levels with high l and J values.

Since no level with $J=11/2$ can occur in the np configurations, there will be no perturbation of the $(^3P_2)nf[5]^\circ_{11/2}$ series by levels of those configurations. Indeed, the only nondiagonal element that makes a connection to this series is the ζ_{4p} element between

$(^3P_2)[5]^\circ_{11/2}$ and $(^1D_2)[5]^\circ_{11/2}$, but the latter nf series is well above the $(^3P_2)$ ionization limit, the lowest member of the series, $(^1D_2)4f[5]^\circ_{11/2}$, being already more than 5000 K above the $(^3P_2)$ limit.

The actual determination of the limit from the $(^3P_2)nf[5]^\circ_{11/2}$ series has been carried out graphically. The effective (principal) quantum number, n^*, of a series member is defined by the relation $T=R/(n^*)^2$, where T is the position of the level measured from the series limit and R is the Rydberg constant, which for bromine equals 109736.56 K. If the series is Ritzian, then $n^*=n-\alpha-\beta T_n$, where n is the running principal quantum number and α and β are constants for a given series. The position of the series limit is taken as that value for which the plot of $(n-n^*)$ versus T_n yields the best straight line. The quantity $(n-n^*)$ defines the quantum defect, $\delta=\alpha+\beta T_n$. In practice it is usually more convenient to plot T_n against $(C-\delta)$, where C is some integer for the series such that $(C-\delta)$ is the part of n^* to the right of the decimal.

Figure 3 shows that a very nearly straight line results if the $4p^4(^3P_2)$ limit is taken to be 95284.80 K above the $4p^5\ ^2P^\circ_{3/2}$ ground level of Br I. The vertical lines through the points represent the deviation of $(1-\delta)$ resulting from a change in the limit of ± 0.10 K. If the adopted series limit is reduced by only one kayser, we obtain the unsatisfactory and unreasonable behavior of this series depicted by the second plot in figure 3.

With the adopted $IP=95284.80$ K, we have made a least squares calculation of the constants α and β by using the first five series members. How well these constants reproduce the series members can be seen from table 7. The position of $(^3P_2)9f[5]^\circ_{11/2}$ would have to be raised by 0.09 K in order to bring its point in figure 3 onto the line. This is certainly within the experimental error, since the level has been established on the basis of two measurements of a wide, hazy line at 7495.46 Å. A change of 0.05 Å in this wavelength would bring the corresponding level into line.

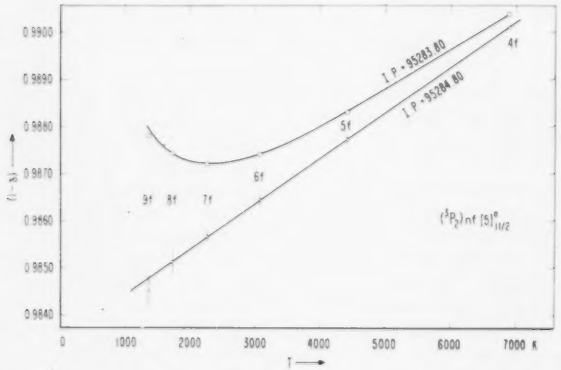

FIGURE 3. *The* $(^3P_2)nf[5]^\circ_{11/2}$ *series plotted for two different values of the limit.*

The upper curve results from changing the value of the Br I ionization potential by only 1.00 K from the value adopted for Br I on the basis of the lower plot. The vertical bars in the lower plot show the effect on $(1-\delta)$ of a change of $\pm$ 0.1 K in the limit.

The value of 95284.80 K for the principal ionization energy is well supported by other series. The $(^3P_2)nf[5]^\circ_{9/2}$ series gives an identical limit, although the point for $9f$ again falls about 0.1 K below the line, and again the spectral line establishing the level is wide and faint (7783.44 Å). With this limit, the plots of the higher members of the $(^3P_2)nd\ ^4F_{9/2}$ and $(^3P_2)np\ ^4D^\circ_{7/2}$ series are also very nearly linear, while the greater deviation from linearity in the first few members of each of these series is a result of the changing coupling conditions along the series.

TABLE 7. *Observed* Br I $(^3P_2)nf[5]^\circ_{11/2}$ *series members compared with positions calculated by use of the Ritz formula*

$\alpha=0.016505$
$\beta=-9.585\times10^{-7}$

Config.	Observed	Calc.	Obs.-calc.
$4f$	88392. 18	88392. 19	−0. 01
$5f$	90873. 70	90873. 70	0. 00
$6f$	92222. 74	92222. 73	+0. 01
$7f$	93036. 08	93036. 07	+0. 01
$8f$	93563. 77	93563. 78	−0. 01
$9f$	93925. 35	93925. 44	−0. 09

It may be pointed out that, although the apparent depression of $(^3P_2)9f[5]^\circ_{11/2}$ and $(^3P_2)9f[5]^\circ_{9/2}$ is within the experimental uncertainty, the depression of these levels might more interestingly be a result of an inter-ionic Stark effect. The conditions at $9f$ are ripe for such an effect, and the character of the observed lines from these levels are certainly suggestive of Stark broadening. Such an interpretation is strengthened by the fact that the lines $(^3P_2)4d\ ^4F_{9/2}$–$(^3P_2)7f[5]^\circ_{11/2}$ and $(^3P_2)4d\ ^4F_{7/2}$–$(^3P_2)7f[5]^\circ_{9/2}$, as well as 9 out of 13 of the observed $(^3P_2)4d$–$(^3P_2)8f$ lines have been recorded as hazy or wide. The regularity of the $(^3P_2)nf[5]^\circ_{11/2}$ series used to determine the ionization limit leaves no doubt, however, that the determination is an excellent one, accurate to probably ± 0.15 K relative to the levels used in the determination, even allowing a small Stark effect on the $n=7$, 8 members. Such an effect would have no more influence than the normal experimental error on the limit determination.

It seems reasonable therefore to adopt 95284.8 ± 0.5 K as the position of Br II $4p^4\ ^3P_2$ above the ground level of Br I. We have included in the stated error the estimated accuracy of the absolute positions of the higher levels. With the conversion factor 12395×10^{-8} ev/K as adopted in AEL, we obtain 11.811 ev for the principal ionization energy of Br I. If we use a more recent value [25] for the conversion factor, 8066.03 ± 0.14 K/ev, we obtain 11.8131 ± 0.0003 ev for this ionization energy.

Although several Br I series having three members and based on the higher $(^3P_{1,0})$ are known, none of them is unperturbed. More accurate values for the positions of the higher limits can be found by com-

bining the above ($^3P_2$) limit with the positions of the Br II $4p^4$ levels as given by Martin and Tech [14]. It is estimated that these Br II levels are accurate to ± 0.5 K. The five limits are then as follows:

($^3P_2$)	95284.8
($^3P_1$)	98421.2
($^3P_0$)	99122.3
($^1D_2$)	107373.9
($^1S_0$)	123151.9

These are the limits that were used in the calculations of n^* for the Br I levels.

The ($^3P_2$) limit found in this investigation is 265 K lower than that given in AEL, Vol. II. It is noteworthy that Catalán and Rico predicted a value of 95300 K for this limit on the basis of their study of the Ga I—Rb I sequence [21].

5. Levels of Even Parity

(a) $4p^4ns$: Except for ($^3P_0$) $8s\ ^2P_{1/2}$, which is calculated to fall around 94650 K, every (^3P)ns level through $11s$ that is predicted to lie below the ($^3P_2$) limit is now known. The (^3P)$5s$ group and the two ($^3P_2$)$7s$ levels were known before. With the exception of ($^3P_2$)$8s\ ^4P_{5/2}$, assigned to the $6d$ configuration in AEL, all other ns levels are new. The (^3P)$7s$ $^2P_{3/2,1/2}$ levels listed in AEL are spurious.

The most important of the new (^3P)ns levels are those belonging to (^3P)$6s$. The strongest lines from these levels fall in the lead-sulfide and vacuum regions, but it has been possible to determine all the levels accurately from weaker lines observed in the photographic air region. Catalán and Rico [21], who made a graphical study of the Ga I—Rb I sequence by means of term values and the constants α and β appearing in the expression defining the quantum defect, predicted the positions of the then unknown ($^3P_2$)$6s\ ^4P_{5/2}$ and ($^3P_1$)$6s\ ^2P_{3/2}$ levels as 82300 K and 85649 K, respectively, which are remarkably close to their observed positions 82236 K and 85435 K. Catalán and Rico also came to the conclusion that ($^3P_2$)$5s\ ^2P_{3/2}$ at 67184 K was considerably perturbed, its "unperturbed" position being 67969 K. However, the results of certain calculations, presented below, do not support such a conclusion. It seems that the differing coupling conditions in the elements of the sequence studied by Catalán and Rico are responsible for the appearance that the 67184 level was perturbed.

In both the $5s$ and $6s$ configurations the ^2D term based on the ($^1D_2$) parent falls below the ($^3P_2$) limit. The term belonging to $5s$ is discussed below. The ($^1D_2$)$6s\ ^2D_{3/2}$ level, 94470.7 K, has been established on the basis of only one line, identified as $4p^5\ ^2P^\circ_{1/2}$—($^1D_2$)$6s\ ^2D_{3/2}$, at 1101.498 Å in the vacuum ultraviolet. This line was long regarded by us as belonging to Br II, but its intensity and the fact that it establishes the ($^1D_2$)$6s\ ^2D_{3/2}$ level within just a few kaysers of its predicted position (table 11), make us believe that our identification is almost certainly correct. One then wonders whether the unclassified line at 5139 Å might not be ($^3P_2$)$5p\ ^4P^\circ_{3/2}$—($^1D_2$)$6s$ $^2D_{5/2}$, placing the latter level at 94460.97 K.

The only ns configuration in which the $^2S_{1/2}$ level based on the ($^1S_0$) parent falls below the ($^3P_2$) parent is $5s$. The results of calculations presented below give ~91940 K for the position of ($^1S_0$)$5s\ ^2S_{1/2}$. There are three eligible levels in this vicinity that have $J=1/2$, at 91691, 91824, and 91938 K. (For intensity reasons and on the basis of calculations, the level at 92090 K has been assigned to ($^3P_0$)$7s\ ^2P_{1/2}$.) Since the 91938 level agrees so well with the predicted position, we have interpreted this level as the ($^1S_0$)$5s\ ^2S_{1/2}$. The other two levels have been assigned to the ($^3P_2$)$7d$ configuration. It is felt that this interpretation of the two lower levels also leads to the most consistent nd series. An observed g-factor for the level at 91938 K will be required in order convince us that this interpretation is correct, however.

The (^3P)$5s$ levels were all known before, but a curious circumstance led Kiess and de Bruin to adopt incorrect ($^1D_2\ ^1S_0$)$5s$ and ($^1D_2\ ^1S_0$)$5p$ levels. This caused some confusion in the preparation of AEL about the correct order of the ($^1D_2$) and ($^1S_0$) limits in Br II. The $5s$ levels in question, adjusted to our energy scale, are:

	This work	Ref. [1]	
($^1D_2$) $^2D_{5/2}$	75890.3	77330.8	$\Delta = 1422.2$ K
	(−18.2)	(+18.2)	
($^1D_2$) $^2D_{3/2}$	75908.5	77312.6	
($^1S_0$) $^2S_{1/2}$	91938.0	75908.6	

It is seen that Kiess and de Bruin's $^2S_{1/2}$ level is real and corresponds to our $^2D_{3/2}$. Although their ^2D term is inverted with respect to ours, it has the *same* separation, 18.2 K. This led to a qualitatively correct interpretation of many lines in Kiess and de Bruin's work, even though most of their ($^1D_2$)$5s$,$5p$ levels are spurious. Both levels of their ($^1S_0$)$5p\ ^2P^\circ$ term are real but are actually based on the ^3P parent. Since Kiess and de Bruin established the ($^1D_2$)$5p$ levels on the basis of strong lines having the 18.2 K separation of their spurious ($^1D_2$)$5s$ levels, all (except $^2P^\circ_{3/2}$) of their ($^1D_2$)$5p$ levels are spurious as well, and are all (except $^2P^\circ_{1/2}$) raised above real levels by an amount corresponding to the difference $\Delta = 1422.2$ K. The reason that this fortuitous system could have appeared so convincing—the transition array is displayed in reference [4]—is that Br I is a prime example of a spectrum in which chance numerical relationships occur among the levels and give support to gross errors in the analysis. It is through such relationships that additional errors can easily

be generated; in this case they also account for some of the incorrect J-values given by Kiess and de Bruin.[5]

The energy levels of the Br I $4p^4 5s$ configuration have been calculated by diagonalizing the second-order energy matrices built in the LS scheme. The matrices of spin-orbit interaction are obtained from those of $p^2 s$ on page 268 of TAS by reversing the sign of the spin-orbit integral associated with the core, ζ_p. The diagonal electrostatic energies to be added to the spin-orbit matrices are as follows:

$$
\begin{aligned}
&^4P : F_0 - 15F_2 - 3G_1 \\
&^2P : F_0 - 15F_2 \\
&^2D : F_0 - 9F_2 - 2G_1 \\
&^2S : F_0 - 2G_1
\end{aligned}
$$

where $F_2 = (1/25)F^2(4p, 4p)$, $G_1 = (1/3)G^1(4p, 5s)$, and $F_0 = 6F_0(4p, 4p) + 4F_0(4p, 5s)$.

In the first diagonalization we adopted the values ζ_{4p} and F_2 found above for the $4p^4$ configuration of parent levels. In order to compensate approximately for the discrepancy in the calculated position of the ($^1D_2$) parent, we have added an electrostatic correction term $C = -150$ K to the diagonal energy expression above for the ^2D term, built on ($^1D_2$). A least squares fit, holding C constant, was then made to the $5s$-levels other than $^2D_{5/2,3/2}$, since this term is known to be perturbed. The calculation yielded $G_1 = 733.8$. The results of the fit are given in table 8 and show that the ^2D levels have apparently been pushed down by about 300 K. It is for this reason that any attempt to determine physically meaningful parameters from the diagonal-sum rule necessarily leads to failure. In fact, this method yields an imaginary value for ζ_{4p} and a negative G_1.

In order to obtain better eigenvectors for a calculation of g-factors, we attempted to improve the parametric representation of the $5s$ levels by making a strict least squares fit to the levels other than $^2D_{5/2,3/2}$ and by allowing all parameters (except C) to vary. The main effect on the parameters was a reduction of the value of ζ_{4p}. The fit is shown in table 8. By means of the eigenfunction expansion coefficients (table 9) obtained in this calculation, the theoretical g-factors can be calculated. These are compared in table 10 with the observed g-factors. The g-factors for these $5s$ levels are derived from measurements of the Zeeman patterns we obtained by exposing to an electrodeless lamp placed in a field of about 37000 oersteds. Since our exposure times were not long for these preliminary exposures, only the stronger Br I lines were recorded. These included most of the lines in the $5s$–$5p$ transition array, however. Also averaged with our own measurements were values generously furnished us by W. F. Meggers, who had measured some Br I Zeeman patterns occurring on his ytterbium spectrograms. The final observed g-factors should be accurate to better than 0.015. The agreement between observed and calculated values is seen to be very good. The observed g-sums also agree well with the theoretical sums. It should be noticed that the LS levels $^2P_{3/2}$ and $^4P_{3/2}$ are thoroughly mixed.

It is gratifying that two effects predictable on the basis of the perturbation of the ($^1D_2$)$5s$ ^2D levels are actually observed. The first concerns the group of moderately strong lines in the region 7975 to 8035 Å. These lines all show resolved hyperfine structure and are ($^1D_2$)$5s$ ^2D–($^3P_2$)$4f$ transitions,

[5] The difficulty rests on the fact that three pairs of real odd levels in Br I have almost the same separation, *equal to the above difference* Δ. They are

($^3P_2$)$7p$ $^4D^0_{3/2}$ 89786.2 − ($^3P_2$)$4f[2]^0_{1/2}$ 88364.0 = 1422.2 K
($^1D_2$)$5p$ $^2D^0_{5/2}$ 88483.4 − ($^1D_2$)$5p$ $^2F^0_{5/2}$ 87061.2 = 1422.2 K
($^3P_0$)$6p$ $^2P^0_{1/2}$ 89065.9 − ($^1D_2$)$5p$ $^2D^0_{5/2}$ 88483.4 = 1422.5 K

Owing to the appearance of the 88483.4 level in two of the pairs, the line at 7950.2 Å falls at a "junction" in Kiess and de Bruin's system, so that it could be, and indeed was, classified twice by them. The entire puzzle is compounded by the fact that the real pairs of levels,

($^3P_0$)$5s$ $^2P_{1/2}$ 68970.2 − ($^3P_1$)$5s$ $^2P_{1/2}$ 67183.6 = 1786.6 K
($^3P_1$)$6p$ $^2D^0_{3/2}$ 88848.0 − ($^1D_2$)$5p$ $^2F^0_{7/2}$ 87061.2 = 1786.8 K,

have separations almost equal to Δ = 1422.2 added to the separation

($^3P_1$)$6p$ $^2D^0_{3/2}$ 88848.0 − ($^1D_2$)$5p$ $^2D^0_{5/2}$ 88483.4 = 364.6.

TABLE 8. *Observed and calculated* Br I $4p^4 5s$ *energy levels*

All energies and parameters are stated in kaysers.

Level desig.	Observed position	$F_2(4p,4p) = 1698.1$, $G_1(4p,5s) = 733.8$, $\zeta_{4p} = 2795.0$		$F_2(4p,4p) = 1698.0$, $G_1(4p,5s) = 748.5$, $\zeta_{4p} = 2712.0$	
		Calc.	Obs-Calc.	Calc.	Obs-Calc.
($^3P_2$)$5s$ $^4P_{5/2}$	63436	63389	+47	63439	−3
($^3P_2$)$5s$ $^4P_{3/2}$	64907	64848	+59	64905	+2
($^3P_1$)$5s$ $^4P_{1/2}$	66884	66938	−54	66888	−4
($^3P_1$)$5s$ $^2P_{3/2}$	67184	67185	−1	67173	+11
($^3P_0$)$5s$ $^2P_{1/2}$	68970	68984	−14	68977	−7
($^1D_2$)$5s$ $^2D_{5/2}$	75890	76185	−295	76172	−282
($^1D_2$)$5s$ $^2D_{3/2}$	75909	76239	−330	76225	−316
($^1S_0$)$5s$ $^2S_{1/2}$	91938	91975	−37	91938	0

TABLE 9. *Eigenvectors of the* Br I $4p^4 5s$ *levels, calculated with* $F_2(4p, 4p) = 1698.0$, $G_1(4p, 5s) = 748.5$, $\zeta_{4p} = 2712$

	$(^1D_2)\ ^2D_{5/2}$	$(^3P_2)\ ^4P_{5/2}$
$(^1D_2)\ ^2D_{5/2}$	0. 9883	0. 1524
$(^3P_2)\ ^4P_{5/2}$	−0. 1524	0. 9883

	$(^1D_2)\ ^2D_{3/2}$	$(^3P_2)\ ^4P_{3/2}$	$(^3P_1)\ ^2P_{3/2}$
$(^1D_2)\ ^2D_{3/2}$	0. 9837	0. 1581	−0. 0851
$(^3P_2)\ ^4P_{3/2}$	−0. 0585	0. 7302	0. 6807
$(^3P_1)\ ^2P_{3/2}$	0. 1698	−0. 6646	0. 7276

	$(^3P_2)\ ^4P_{1/2}$	$(^3P_0)\ ^2P_{1/2}$	$(^1S_0)\ ^2S_{1/2}$
$(^3P_1)\ ^4P_{1/2}$	0. 9794	0. 1561	0. 1283
$(^3P_0)\ ^2P_{1/2}$	−0. 1693	0. 9805	0. 0994
$(^1S_0)\ ^2S_{1/2}$	−0. 1102	−0. 1191	0. 9867

The eigenvector of each level is given in the column under the adopted designation of the level. The designations on the extreme left refer to pure LS states. The elements of the eigenvectors are the expansion coefficients that occur in the corresponding eigenfunction. For example, the eigenfunction of the level called $^2D_{5/2}$ is a linear combination of those for $^2D_{5/2}$ and $^4P_{5/2}$ and is given by

$$\psi(\text{“}^2D_{5/2}\text{”}) = 0.9883\psi(^2D_{5/2}) - 0.1524\psi(^4P_{5/2}).$$

The $^2D_{5/2}$ level thus has a purity of 97.7 percent in this approximation.

which point to apparent violations of the selection rule on the orbital angular momentum of the external electron, $\Delta l = \pm 1$. A reasonable interpretation of these lines is that $(^1D_2)5s\ ^2D$ contains an admixture of $(^3P_2)4d$ eigenfunctions. Probably each of the $(^1D_2)5s\ ^2D$ levels is mixed with both of the two possible $(^3P_2)4d$ levels of the same J-value, but the $5s\ ^2D_{5/2} \times 4d\ ^4D_{5/2}$ and $5s\ ^2D_{3/2} \times 4d\ ^4D_{3/2}$ interactions are perhaps the stronger because of the proximity of the levels. This would explain both the $\Delta l = 3$ transitions and the fact that the $(^1D_2)5s\ ^2D$ levels have apparently been pushed downward. The situation is actually more complicated than this, because the strong $(^1D_2)5s\ ^2D - (^3P_2)4f[2]^\circ$ combinations are caused partly by the additional $(^1D_2)5p\ ^2D^\circ \times (^3P_2)4f[2]^\circ$ interaction.

The $(^3P)5s$ levels also combine weakly with $(^3P)nf$ levels, partly because of small $5s \times 4d$ interactions and also through the $(^1D_2)5s\ ^2D$ levels.

The other effect of the $(^1D_2)5s \times (^3P_2)4d$ interaction is a reciprocal one to the above and concerns the unexpected intensity of the $(^3P_2)4d - (^1D_2)5p$ transitions, particularly the line at 10840 Å, resulting from the transition $(^3P_2)4d\ ^4D_{5/2} - (^1D_2)5p\ ^2D^\circ_{5/2}$.

Already at $5s$ the separation of the level groups according to parentage is obvious. For $n \geqq 6$ the dominance of ζ_{4p} should permit the calculation and identification of the ns levels by use of simplified matrices for $J_c j$ or J_d coupling. Since these are identical in the two schemes for $l = 0$, the coupling might be called $J_c s$ coupling. The complete $J_c s$ matrices for $p^4 s$ have been given by Minnhagen [19].[6]

[6] Two typographical errors appear in those matrices: In the $J = 3/2$ matrix the off-diagonal $(-f_p/\sqrt{2})$ element should connect the levels based on the $(^3P_2) - (^1D_2)$ parents rather than $(^3P_1) - (^1D_2)$, which should be zero. Further, the coefficient of G^1 in the diagonal element for the $J = 1/2$ level based on $(^3P_1)$ should be 2/3 rather than 1/3.

TABLE 10. *Observed and calculated* g*-factors for the* Br I $4p^4 5s$ *levels*

Level design.	Energy	g		
		Obs.	Calc.	Landé
	K			
$(^3P_1)\ ^4P_{1/2}$	66884	2. 608	2. 601	2. 667
$(^3P_0)\ ^2P_{1/2}$	68970	0. 734	0. 734	0. 667
$(^1S_0)\ ^2S_{1/2}$	91938	----------	(1. 998)	(2. 000)
	g-sum=	3. 342	3. 335	3. 333
$(^3P_2)\ ^4P_{3/2}$	64907	1. 532	1. 533	1. 733
$(^3P_1)\ ^2P_{3/2}$	67184	1. 522	1. 515	1. 333
$(^1D_2)\ ^2D_{3/2}$	75909	0. 826	0. 819	0. 800
	g-sum=	3. 880	3. 867	3. 867
$(^3P_2)\ ^4P_{5/2}$	63436	1. 595	1. 591	1. 600
$(^1D_2)\ ^2D_{5/2}$	75890	1. 210	1. 209	1. 200
	g-sum=	2. 805	2. 800	2. 800

As was the case in I I, the relative magnitudes of the $J_c s$ matrix elements permit a simplification such that the p^4s levels in Br I may be calculated by use of the following approximate expressions:

$$(^3P_2)\ {}^4P_{5/2} = B + (^3P_2)$$

	$(^3P_2)\ {}^4P_{3/2}$	$(^3P_1)\ {}^2P_{3/2}$
$(^3P_2)\ {}^4P_{3/2}$	$B + (^3P_2) + \frac{5}{6} G^1$	$\frac{\sqrt{5}}{6} G^1$
$(^3P_1)\ {}^2P_{3/2}$	$\frac{\sqrt{5}}{6} G^1$	$B + (^3P_1) + \frac{1}{6} G^1$

	$(^3P_1)\ {}^4P_{1/2}$	$(^3P_0)\ {}^2P_{1/2}$
$(^3P_1)\ {}^4P_{1/2}$	$B + (^3P_1) + \frac{2}{3} G^1$	$\frac{\sqrt{2}}{3} G^1$
$(^3P_0)\ {}^2P_{1/2}$	$\frac{\sqrt{2}}{3} G^1$	$B + (^3P_0) + \frac{1}{3} G^1$

$$(^1D_2)\ {}^2D_{5/2,3/2} = B + (^1D_2) + \frac{1}{3} G^1$$

$$(^1S_0)\ {}^2S_{1/2} \quad = B + (^1S_0) + \frac{1}{3} G^1,$$

where the parent symbols stand for the observed values: $(^3P_2)=0$, $(^3P_1)=3136$, $(^3P_0)=3838$, $(^1D_2)=12089$, and $(^1S_0)=27867$ K. *LS* symbols are given the Br I p^4s levels in the company of $J_c s$ energy expressions, but the $J_c l$ correspondence can be found in table 6.

The *LS* eigenvectors for $(^3P)5s$ show that the $J=1/2$ levels are relatively pure in the *LS* scheme while the $J=3/2$ are thoroughly mixed. As might be expected, the calculation of $(^3P)5s$ from the above $J_c s$ expressions gives just the opposite results, i.e., the $J=1/2$ levels are thoroughly mixed in the $J_c s$ scheme while the $J=3/2$ levels are pure. This same behavior was found by Minnhagen in I I. The large electrostatic interaction of the $J=1/2$ levels is also present for $n \geq 6$ and reveals itself through a larger nondiagonal contribution to the energy than for the (^3P) $J=3/2$ levels. The comparison of observed $6s$ and $7s$ levels with those calculated from the $J_c s$ expressions is given in table 11. Since the agreement is excellent for a rather large range of G^1, and since small perturbations are present at both $6s$ and $7s$, it makes little sense to debate the exact value of G^1 in this approximation. A strict least squares fit gives $G_1 = \frac{1}{3} G^1$ as 172 K and 62 K for $6s$ and $7s$, respectively. In the preparation of table 11, however, we have assumed that G_1 varies approximately as $(n^*)^{-3}$ in accordance with theory and have taken $G_1(4p, 6s) = 190$ K and $G_1(4p, 7s) = 78$ K, both based on the value of $G_1(4p, 5s)$ found above. The nondiagonal contributions in kaysers to the $(^3P)6s$, $7s$ energies for ^4P, ^2P are as follows:

	$6s$	$7s$
$J=1/2$	± 115	± 19
$J=3/2$	± 16	± 3

where the upper sign is always taken with the higher level of a given J. It is seen that even at $7s$ a positive confirmation of the level assignments can be effected by use of diagonal expressions only.

Coupling diagrams of the type found in TAS, chapter 11, cannot be constructed for a p^4s configuration because the number of parameters necessary to determine the level intervals is greater than two. However, since the splitting of Br II (^3P) is small compared to the distance from (^3P) to $(^1D_2)$ or $(^1S_0)$, the Br I $(^3P)ns$ levels can be described to a satisfactory approximation as a function of the ratio $G_1(4p,ns)/\zeta_p$. This is accomplished by omitting in the energy matrices the elements associated with $(^1D_2)$ and $(^1S_0)$. A coupling diagram showing the structure of $p^4(^3P)ns$ in the transition from *LS* to $J_c j$- or $J_c l$-coupling has been constructed by Edlén [22, p. 132]. An equivalent diagram for the observed Br I levels is presented in figure 4 and strikingly agrees with the theoretical behavior of these levels.

TABLE 11. *Observed* Br I $4p^4 6s$, $7s$ *energy levels compared with calculations using the simplified* $J_c s$ *matrices*

All energies and parameters are stated in kaysers.

Level design.	Observed position	Calc.	Obs.-Calc.	Parameters
$(^3P_2)6s\ {}^4P_{5/2}$	82236	82199	+37	
$(^3P_2)6s\ {}^4P_{3/2}$	82662	82658	+4	
$(^3P_1)6s\ {}^4P_{1/2}$	85577	85601	−24	B = 82199
$(^3P_1)6s\ {}^2P_{3/2}$	85435	85447	−12	$G_1 = 190$
$(^3P_0)6s\ {}^2P_{1/2}$	86279	86342	−63	
$(^1D_2)6s\ {}^2D_{3/2}$	94471	94478	−7	
$(^3P_2)7s\ {}^4P_{5/2}$	88135	88100	+35	
$(^3P_2)7s\ {}^4P_{3/2}$	88275	88292	−17	B = 88100
$(^3P_1)7s\ {}^4P_{1/2}$	91348	91373	−25	$G_1 = 78$
$(^3P_1)7s\ {}^2P_{3/2}$	91284	91278	+6	
$(^3P_0)7s\ {}^2P_{1/2}$	92090	92035	+55	

Since G_1 varies approximately as $(n^*)^{-3}$ and ζ_p remains essentially constant along the series, we have plotted in figure 4 the *ns* levels, referred to the center of gravity of each group, against $(n^*)^{-3}$. The mean values $\frac{1}{2}(^4P_{1/2}+{}^2P_{1/2})$ and $\frac{1}{2}(^4P_{3/2}+{}^2P_{3/2})$ are also plotted and found to give two approximately straight parallel lines, as expected. The slight irregularities are caused partly by small perturbations of the levels. The observed crossover of the $^4P_{1/2}$ and $^2P_{3/2}$ levels is in accordance with theory. It should be noticed that the plot yields an unambiguous coordination of the levels to specific levels of the (^{3}P) limit.

From a comparative study of the plots in figures 4 and 5 one can obtain a qualitative picture of the perturbations present in the (^{3}P)*ns* series, mostly caused by $ns \times nd$ interactions. The displacements of the perturbed levels are all small, being of the order of 20 to 50 K.

The ($^3P_0$) $6s\ ^2P_{1/2}$ level seems to be about 75 K too low, but the cause is not clear, unless this displacement results from the influence of the $J=\frac{1}{2}$ levels in the ($^3P_2$)5*d* configuration that lie 1000 to 1500 K higher. The ($^1D_2$)$4d\ ^2P_{1/2}$, $^2S_{1/2}$ levels are probably responsible for the perturbation of ($^3P_1$)$8s\ ^4P_{1/2}$, which is about 50 K too high. The higher ($^3P_2$) *ns* series members all suffer slight perturbations owing to $ns \times nd$ interactions. While the plots in figure 5 seem to be highly irregular at the end corresponding to high *n*, it should be remembered that *T* is there relatively small, and n^* is therefore quite sensitive to changes in *T*, as is evident from the expression

$$\Delta n^* \sim -\frac{R^{1/2}}{2T^{3/2}}\Delta T.$$

(b) $4p^4nd$: Sorting out and interpreting the Br I *nd* energy levels is perhaps the most intricate problem in the analysis of this spectrum. Abundant perturbations and an intermediate type of coupling severely complicate the analysis. We have in the analysis attempted to make the best possible use of the observations. The interpretation of the Br I *nd* levels as presented in table 6 seems to be the most reasonable derivable from general arguments, observed line intensities, application of the Ritz formula, approximate calculations, and the like. A more detailed study of the *nd* configurations based on accurate calculations including interconfigurational interaction might well necessitate the revision of some of the assignments, particularly of those levels having low *J*-values. Reconsideration of the *nd* $J=\frac{1}{2}$ levels might even bring the interpretation of ($^1S_0$) $5s\ ^2S_{1/2}$ into question, as pointed out above.

The separation of the *nd* levels of each configuration into groups according to the parent limits is quite apparent. The ($^3P_{1,0}$)4*d*, 5*d*, 6*d* levels all lie below the ($^3P_2$) limit and have been found. The ($^3P_1$)7*d* levels are predicted to fall below the ($^3P_2$) limit but are so close (~94900 K) to this limit that they have not been discovered. All ($^3P_2$)*nd* series are complete through 8*d*; each series thus contains five members. The ($^3P_2$)$nd\ ^4F_{9/2}$ series is known through 12*d*. Of the *nd* levels based on the high ($^1D_2$) and ($^1S_0$) parents, only the ($^1D_2$)4*d* group falls below the ($^3P_2$) limit. All levels in this group have been identified at least tentatively.

The grouping of the *nd* levels according to parent suggests that the coupling of these configurations is intermediate between the J_cl and J_cj schemes. The diagonal energy expressions for p^4d in these two schemes have been calculated by Möller and Källén, respectively, and can be found in the paper by Minnhagen [19]. A comparison of the J_cl expressions with the observed levels reveals that even the observed ordering of *K*-pairs with respect to energy is not reproduced by the diagonal J_cl expressions on the assumption that the dominant contribution to the energy is due to $F^2(4p, nd)$.

It is felt that the reason for this lies, at least in the case of 4*d*, in the magnitude of the G^1 integral, whose effect on the energies is probably greater than that of F^2, implying a large departure from J_cl coupling, which requires a small G^k contribution. The large G^1 contribution probably accounts in part for the high position of the ($^3P_2$)$4d[2]_{5/2,3/2}$ levels. It may be that the levels ($^3P_2$)$4d[3]_{5/2}$ and $[2]_{5/2}$ should have their designations interchanged. The interaction of the 4*d* levels having $J=5/2$, 3/2 with the ($^1D_2$)$5s\ ^2D_{5/2,3/2}$ levels contributes to the high position of the 4*d* pair just mentioned, but this effect is probably less significant than the size of the G^1 integral.

The large departures from any pure coupling scheme in the *nd* configurations, as well as sizeable perturbations, render the assignment of designations to the levels a rather difficult problem. Both the *LS* and J_cl symbols assigned these levels in table 6 are based on the intensities of the $4d-nf$, $5p-4d$, and $5p-5d$ combinations. There still remain several inconsistencies; in particular the combining properties of some levels vary irregularly along a series. Only a very detailed consideration of perturbations, together with accurate calculations, can aid in the solution of this problem. Even a cursory examination of the effective quantum numbers of the *nd* levels reveals marked irregularities along series. Apart from small interaction with some *ns* levels, the perturbations are primarily a result of the overlapping or proximity of groups of levels with different *n* and based on different parents. The most striking case of this is the ($^3P_1$)$5d\times$($^3P_2$)6*d* interaction, which causes the ($^3P_1$)5*d* group of levels to be slightly higher than expected. It is very possible that the ($^3P_2$)$6d\ ^4F_{7/2}$ and ($^3P_1$)$5d\ ^2F_{7/2}$ levels should have their designations interchanged. A ($^3P_1$)$6d\times$($^3P_2$)9*d* interaction has apparently pushed the ($^3P_1$)6*d* group down. The separation of these latter groups is difficult, however, and the assignments should be regarded as tentative. Their further interaction with the slightly higher ($^1D_2$)4*d* levels is also probable.

The ($^1D_2$)$4d\ ^2G_{9/2,7/2}$ levels have been established with certainty (see table 6). The other seven levels of the ($^1D_2$)4*d* group have received their designations primarily on the basis of their position being such that they do not fit well into any (^{3}P) groups.

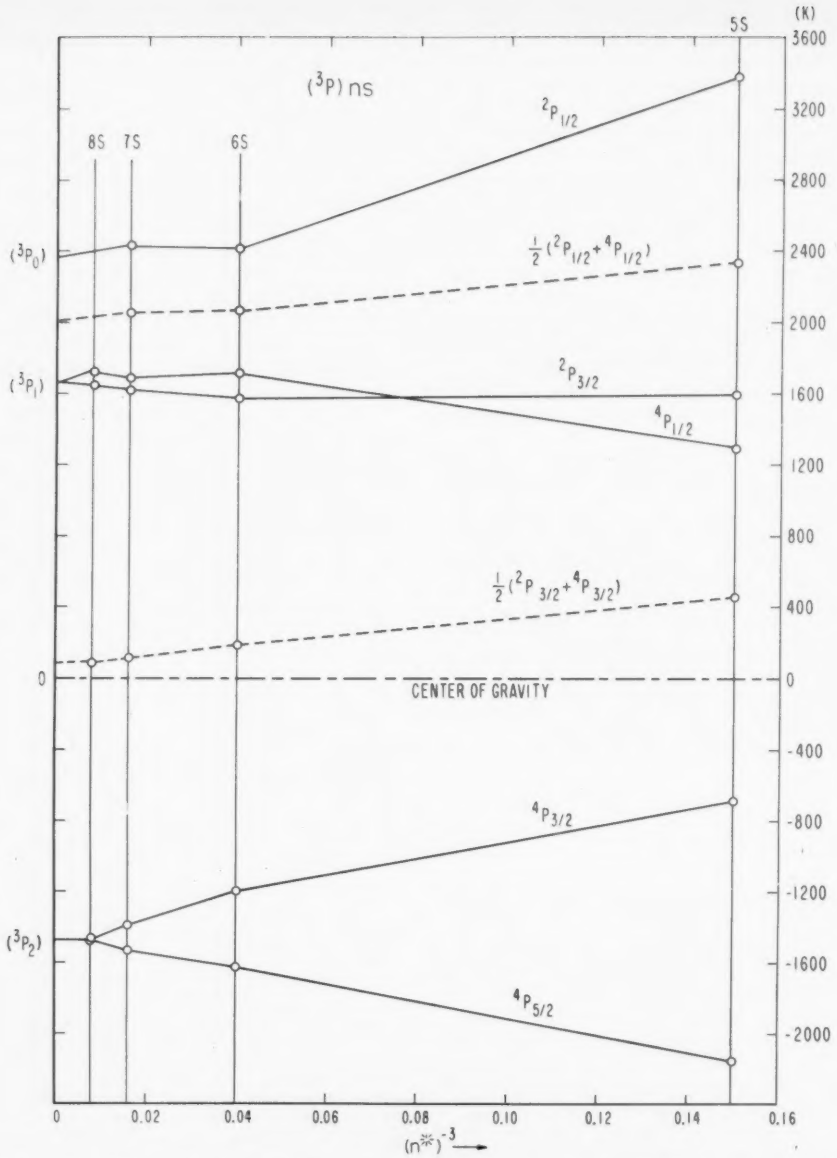

FIGURE 4. *Observed levels of* $4p^4(^3P)ns$, *referred to center of gravity, and plotted against* $(n^*)^{-2}$ *to show the convergence toward the* Br II $4p^4\ ^3P_{2,1,0}$ *limits.*

(Furthermore, we had just seven levels left over after unraveling the $(^3P)nd$ levels.) The order of the $(^1D_2)4d$ levels bears a striking resemblance to the corresponding group in Kr II, but is in sharp disagreement with the Jd diagonal expressions (assuming dominant F^2), which predict the $J=½$ levels to be the lowest.

The most important nd series showing any degree of regularity is the $(^3P_2)nd\ ^4F_{9/2}$ series, for which $(2-\delta)$ is plotted against T in figure 6. The nonlinearity of this plot is interpreted not as a failure to have the correct ionization potential, but as the effect of a gradual change in coupling along the series. The members from $9d$ through $12d$ are almost exactly linear. A change in the assumed ionization potential would cause the line connecting these levels to curve up or down. A least squares calculation of the Ritz constants α and β from these levels gives $\alpha=1.35276$, $\beta=-3.442\times10^{-6}$, from which the entire series has been calculated. The results, given in table 12, reveal not only by how much the early series members lie too high because of the different coupling conditions, but also by how

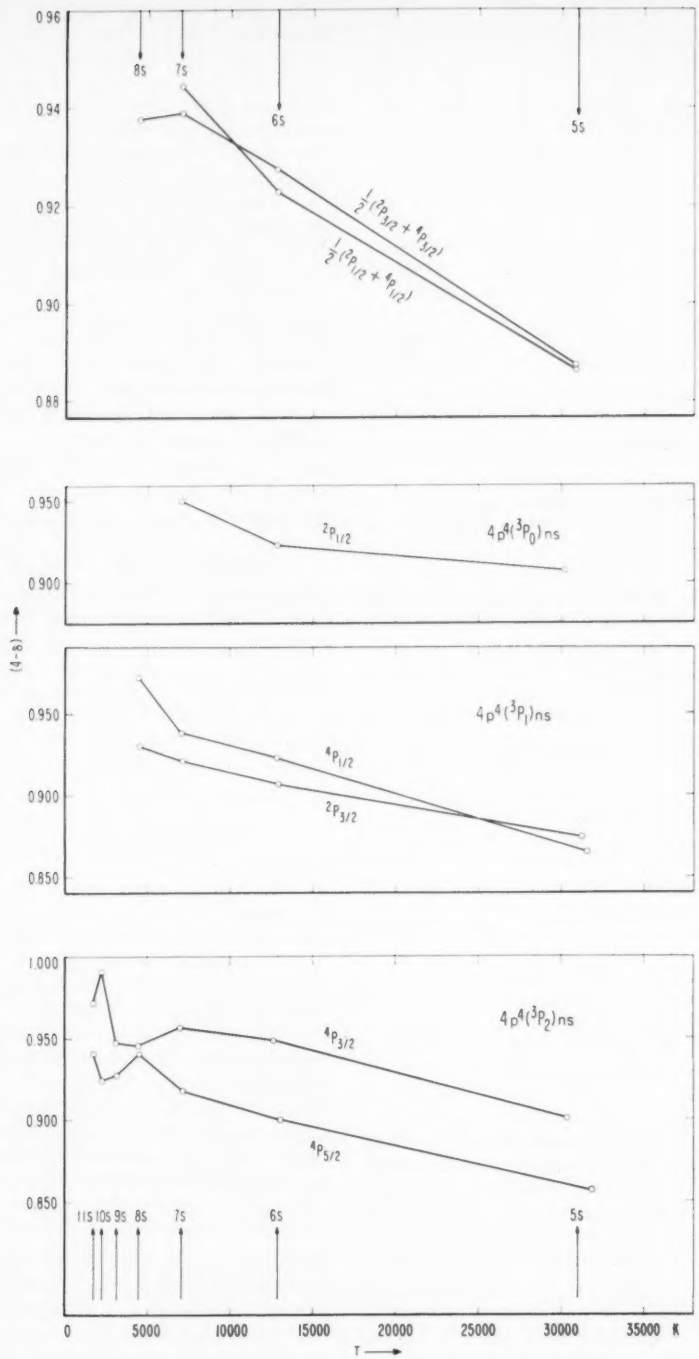

FIGURE 5. *Diagram showing the observed* Br I ns *series.*

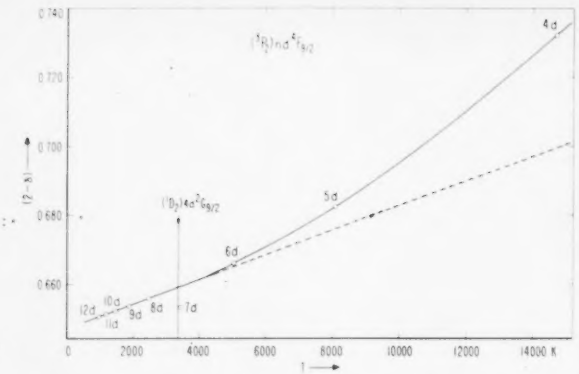

FIGURE 6. *Diagram showing the very regular* $(^3P_2)$nd $^4F_{9/2}$ *series.*

The $(^1D_2)4d\ ^2G_{9/2}$ level was found from its influence on the 7*d* member of this series.

much the 7*d* and 8*d* levels have been pushed down and up, respectively, by the $(^1D_2)4d\ ^2G_{9/2}$ level between them.

TABLE 12. *Observed energy levels of the* $4s^4(^3P_2)$nd $^4F_{9/2}$ *series compared with calculations using the Ritz formula, as described in the text.*

All energies are stated in kaysers.

$\alpha = 1.35276$

$\beta = -3.442 \times 10^{-6}$

Config.	Observed	Calculated	Obs.-calc.
4*d*	80587. 61	80221. 57	+366. 04
5*d*	87191. 97	87160. 44	+31. 53
6*d*	90244. 89	90241. 40	+3. 49
7*d*	91851. 14	91858. 17	−7. 03
$4p^4(^1D_2)4d\ ^2G_{9/2} = 91921.86$			
8*d*	92807. 81	92807. 63	+0. 18
9*d*	93411. 48	93411. 49	−0. 01
10*d*	93818. 96	93818. 95	+0. 01
11*d*	94106. 70	94106. 70	0. 00
12*d*	94317. 40	94317. 40	0. 00

These slight deviations of the points representing $(^3P_2)7d$, 8*d* $^4F_{9/2}$ indicate with certainty the presence of the nearby perturbing level, which can be only $(^1D_2)4d\ ^2G_{9/2}$. Until this perturbation was recognized, the only strong Br I lines still remaining unclassified were those at 6096 and 6133 A. That the line at 6096 Å results from the transition $(^3P_2)5p\ ^4D^o_{7/2} - (^1D_2)4d\ ^2G_{9/2}$ is unquestionably correct, because (i) it fortunately happens to be one of the two unclassified lines whose hfs were reported by Tolansky and Trivedi [7], its observed structure fitting fairly well the splitting of $(^3P_2)5p\ ^4D^o_{7/2}$ derived from other lines, and (ii) it yields a value 91922 K for $(^1D_2)4d\ ^2G_{9/2}$, which is the proper position to account for the perturbation of the *nd* $^4F_{9/2}$ series.

The other line, at 6133 A, is interpreted as the transition $(^3P_2)5p\ ^4D^o_{5/2} - (^1D_2)4d\ ^2G_{7/2}$. One additional line has been observed in the radiometric region for each of the ^2G levels. These are combinations with $(^1D_2)5p\ ^2F^o_{7/2,5/2}$ and serve as further evidence for the reality of the ^2G levels.

(c) $4s4p^6$: The $4s4p^6$ configuration yields only one level, $^2S_{1/2}$. Bromine is the only halogen for which this level has been found with certainty. A calculation based upon the irregular-doublet law predicts the $^2S_{1/2}$ term to lie near 87000 K. Of the nine even levels with $J = 1/2$ that were found in the range 80000 −90000 K, only eight can arise from configurations other than $4s4p^5$. These can all be unambiguously identified on the basis of position and intensity considerations. The remaining level, at 84825.60 K, must be $4s4p^6\ ^2S_{1/2}$. This identification explains the high intensity of the ultraviolet lines at 1232 Å, resulting from the transition $4s^24p^5\ ^2P^o_{1/2}$—84825, and at 1179 Å, $4s^24p^5\ ^2P^o_{3/2}$—84825: the ground $^2P^o$ term is the only known term to which the $4s4p^6\ ^2S_{1/2}$ can make transitions in a one-electron jump.

In addition to the ultraviolet lines and a faint, wide line at 12369 A, the only other lines from $^2S_{1/2}$ that have been observed are two moderately strong doublets at 10184 Å and 11094 Å. The doublet character of each of these lines is assumed to result from the wide hfs splitting of $^2S_{1/2}$, which is expected, since the unpaired 4*s* electron in the $4s4p^6$ configuration should couple strongly with the nucleus. The classifications of these lines are as follows:

10184 Å	$5p\ ^4P^o_{3/2} - sp^6\ ^2S_{1/2}$
11094 Å	$5p\ ^4P^o_{1/2} - sp^6\ ^2S_{1/2}$

The components of 11094 Å appear single with our resolution but there is slight shading in the two components of 10184 Å. This results from the hfs splitting of $5p\ ^4P^o_{3/2}$, which according to Tolansky and Trivedi has a structure (0.127, 0.086, 0.043) in K. To get an estimate of the splitting of the $^2S_{1/2}$ level, we note that the separations of the components of 10184 Å and 11094 Å are 0.45 and 0.59 K, respectively. The large difference between these two values might at first seem disturbing. But a simple sketch of the appropriate transitions, taking into account the known hyperfine structure of $^4P^o_{3/2}$ (four *F*-levels) and adopting any reasonable value for the unknown structure of $^4P^o_{1/2}$ (two *F*-levels), reveals that one would expect the components of 10184 Å to be about 0.1 K closer together than the components of 11094 A. Furthermore, it is apparent from such a sketch that the measured separation of the centers of gravity of the 11094 Å components very nearly represents the true hfs splitting of the $^2S_{1/2}$. We therefore adopt 0.59 K as the splitting of the $^2S_{1/2}$ level.

A calculation of the theoretical structure of this level is revealing. Following Slater [23], we can

write the expectation value of the nuclear interaction contribution to the total Hamiltonian as

$$\langle H' \rangle = \frac{\alpha^2}{3} g_N R^2(0) K \qquad \text{rydbergs.}$$

(This formula holds only for configurations containing a single unpaired s-electron.)[7] Here α is the fine structure constant (1/137), g_N is the weighted average bromine nuclear g-factor ($=7.93\times10^{-4}$), $R(0)$ is the value of the normalized s-eigenfunction at the origin, and

$$K = F(F+1) - I(I+1) - J(J+1).$$

Since $J=1/2$ and the nuclear spin $I=3/2$, the energy separation of the two F-levels will be

$$\Delta E = \frac{4\alpha^2}{3} g_N R^2(0) \qquad \text{rydbergs.}$$

We have calculated $R(0)$ from recently published [24] Hartree-Fock radial wave functions for the bromine $4s^24p^5$ configuration. The 4s-orbital of this configuration will not be very different from that of the $4s4p^6$ configuration. We find $R(0)=15.6$. Inserting numerical values in the above equation, we finally obtain

$$E = 1.37\times10^{-3} \qquad \text{rydbergs}$$

$$= 1.50 \qquad \text{kaysers.}$$

(A relativity correction would increase this value by about 14%.) The above result is to be compared with the observed value 0.59 K. Some of the discrepancy between these values must arise from configuration interaction. Such an interaction is undoubtedly present, because the two lines under discussion are examples of so-called two-electron jumps. The occurrence of these lines at all indicates that the sp^6 configuration is mixed with a configuration that would make the transition in a one-electron jump. The interaction involved here is probably with one of the $J=1/2$ levels of the 4d configuration, possibly $4d\ ^4P_{1/2}$. One would expect the level with which the $sp^6\ ^2S_{1/2}$ is mixed to share some of the latter's hyperfine structure. Each of the 4d levels with $J=1/2$ was checked for hfs, but none could definitely be established from our observations.

6. Levels of Odd Parity

(a) $4p^4np$: The analysis of the system of odd levels of Br I was enormously simplified by the occurrence of almost pure $J_c l$-coupling in the nf configurations. Upon the identification of a few of the nf levels, the rest could easily be calculated and identified. We could then safely regard all odd levels left over as belonging to excited np configurations.

[7] It should also be mentioned that a factor of 2/3 is missing from this equation in Slater's work, Vol. II, p. 266.

With the exception of the $(^3P_1)8p$ group, which is predicted to center around 94675 K, all np levels for $n=5, 6, 7, 8, 9$ that fall below the $(^3P_2)$ limit have been found. Two levels belonging to $(^3P_2)10p$ have been identified also. Of the levels based on the $(^1D_2, ^1S_0)$ parents, only the $(^1D_2)5p$ levels are below the $(^3P_2)$ limit. As in the ns and nd configurations, the np levels fall into groups that reflect the structure of the Br II p^4 parents. The coupling of the higher np configurations is between the $J_c l$ and $J_c j$ schemes, but apparently closer to $J_c l$. Happily, configuration interaction of the np set of levels with the nf set is extremely small. The very different coupling exhibited by these two sets of odd levels may partly account for this minimal interaction.

The matrices of spin-orbit interaction for a p^4p configuration have been calculated in an LS basis and are presented in the following paper in this issue of the Journal of Research. A study of the Br I np configurations by means of these matrices has not yet been completed. The results of the calculations will appear later, together with the results of Zeeman observations in progress.

It may be mentioned that the electrostatic [18] and spin-orbit [19] elements of the p^4l matrices for pair-coupling have just been published, as well as the p^4l matrices for J_cj-coupling [19], calculated by Källén. The assignment of K-values to the Br I np levels is based on intensities and approximate calculations with the J_cl diagonal energy expressions given in reference [19]. The LS symbols are based on the intensities of $5p$—$5s$, $6s$, $4d$ transitions.

The Br I $5p$ configuration is rather isolated and except for a few small interactions is regarded as a pure configuration. It should therefore be possible to represent quite accurately in parametric form the distribution of the $5p$ levels. It was for this reason, in fact, that the p^4p matrices in intermediate coupling were calculated. Since the $(^1S_0)\ 5p\ ^2P^\circ$ term is above the $(^3P_2)$ limit and has not been observed, it is not possible to use the diagonal sum rule in the calculation of the parameters. The parameters may, however, be estimated in a variety of ways based on diagonal energy expressions in the several coupling schemes for levels of high J-value, on approximately calculated positions for $(^1S_0)\ 5p\ ^2P^\circ$, and on level differences. The approximate parameters found in this way can be inserted in the energy matrices and improved by iteration.

The most interesting interaction occurring with the $5p$ configuration is perhaps the $(^1D_2)\ 5p\ ^2D^\circ_{5/2,3/2} \times (^3P_2)4f[2]^\circ_{5/2,3/2}$ interaction. The $(^3P_1)6p^2D^\circ$ term lies somewhat higher but may also be involved. Accurate calculations given below show that the two $4f$ levels have been pushed down by 13 K and 21 K for $J=5/2$ and $J=3/2$, respectively. This partly accounts for the surprisingly strong intensity of $(^1D_2)5s\ ^2D - (^3P_2)4f[2]^\circ$ transitions, as pointed out above.

The $(^3P_2)5p\ ^4D^\circ_{3/2}=[1]^\circ_{3/2}$ level seems to lie abnormally high, judging from the diagonal J_cl energy

expressions. This same behavior was noticed in the case of I I by Minnhagen [19], who calculated the I I $6p$ levels by use of the $F^2(5p, 6p)$ parameter only. It was suggested that configuration interaction might be responsible for the high position of the level in question. As evidence for such an interaction, Minnhagen cited the fact that the intensity of the I I line classified as $(^3P_2)6s[2]_{5/2}-(^3P_2)6p[1]^\circ_{3/2}(=8044$ Å) is much stronger than that of the line $(^3P_2)6s[2]_{5/2}-(^3P_2)6p[3]^\circ_{7/2}$ (=9058 Å) whereas the latter line should be stronger for all unperturbed couplings. The only $J=3/2$ level below I I $(^3P_2)6p$ is the ground level $5p^5\ ^2P^\circ_{3/2}$, which renders perturbation difficult to accept. It seems reasonable that the intensity ratio of I I lines just mentioned is, rather, a result of the fact that 8044 Å falls at the wavelength of peak sensitivity of EK—"N" photographic plates, while 9058 Å was undoubtedly photographed on "Q" or "Z" plates, which are less sensitive than "N" plates by about a factor of 10. In Br I, the corresponding lines both occur in the "N" region, and the relative intensities are in the expected order. It is felt that the high position of the level in question, both in I I and Br I, is to be explained by the magnitude of the G^0 $(np, n'p)$ integral, which contributes sizeably to the Br I $5p$ and I I $6p$ energies and should not be neglected. The J_d p^4p diagonal energy expressions for $(^3P_2)np$ $[2]^\circ$, $[1]^\circ$ are, except for an additive constant:

$$[2]^\circ_{5/2} \quad -\frac{7}{50}F^2 \qquad +\frac{18}{600}G^2+\frac{1}{6}\zeta_{n'p}$$

$$[2]^\circ_{3/2} \quad -\frac{7}{50}F^2+\frac{45}{24}G^0+\frac{153}{600}G^2-\frac{1}{4}\zeta_{n'p}$$

$$[1]^\circ_{3/2} \quad +\frac{7}{50}F^2+\frac{5}{24}G^0+\frac{17}{600}G^2-\frac{1}{4}\zeta_{n'p}$$

$$[1]^\circ_{1/2} \quad +\frac{7}{50}F^2+\frac{20}{24}G^0+\frac{50}{600}G^2+\frac{1}{2}\zeta_{n'p}$$

where all integrals refer to the $(np, n'p)$ interaction. Approximate Br I $5p$ parameters, derived as described above, indicate that the effect of G^0 on $[2]^\circ_{3/2}$ brings its diagonal energy very close to that of $[1]^\circ_{3/2}$. Since the two levels are connected by G^0, G^2, and $\zeta_{n'p}$, they repel each other in such a way, neglecting the action of the other levels in the configuration, as to make $[1]^\circ_{3/2}$ appear high and the $K=2$ levels appear as a closer pair. The $[1]^\circ_{1/2}$ level is pushed down by all $5p$ $J=1/2$ levels above it. This same type of effect is probably operating also in the case of the high Br I $(^3P_2)4d[2]$ pair, as mentioned previously.

A qualitative picture of the run of Br I np levels and perturbations can be obtained from figure 7, in which the quantum defect is plotted against absolute level value. The points representing the $(^3P_2)np\ ^4D_{7/2}$ series are very nearly linear for $n=6$, 7, 9, 10. The slight depression at $n=8$ is due to the interaction with $(^3P_1)4f[3]^\circ_{7/2}$. An application of the Ritz formula with $\alpha=2.57410$, $\beta=+3.190\times10^{-6}$ derived by least squares from $(^3P_2)$ 7, 9, $10p\ ^4D^\circ_{7/2}$,

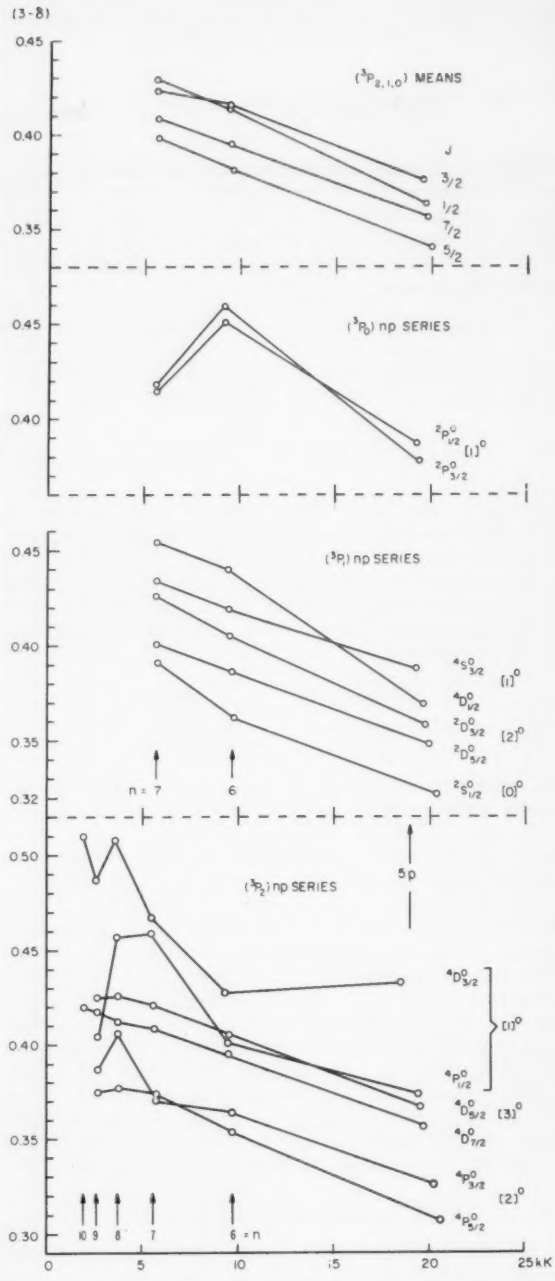

FIGURE 7. *The* $(^3P)np$ *series:* $(3-\delta)$ *plotted against* T.

reproduces these levels almost exactly and shows that the level at $8p$ is depressed by about 2.6 K, its "unperturbed" position being 91540.9 K. The same Ritz formula predicts $(^3P_2)5p\ ^4D^\circ_{7/2}$ to fall 114 K higher than observed, the departure being a result of the regular coupling change along the series.

The great deviation from linearity exhibited in figure 7 by the early members of the $(^3P_2)np\ ^4D^o_{3/2}$, $^4P^o_{1/2}$ and $(^3P_0)np\ ^2P^o_{3/2,1/2}$ series is probably not entirely due to perturbations, since the plots of mean term energies for each J-value are much more regular. However, the possibility of a configuration interaction affecting these levels in such a way as approximately to cancel out in the means should not be overlooked. It seems fairly certain that there is a $(^3P_0)6p \times (^3P_2)7p$ interaction, and the $(^3P_2)6p\ ^4D^o_{3/2}$, $^4P^o_{1/2}$ levels may be influenced by $(^1D_2)5p\ ^2P^o_{3/2,1/2}$. The $(^3P_2)7p$, $8p$, $^4P^o_{3/2}$ levels seem to have been pushed down and up, respectively, through interaction with $(^3P_0)6p\ ^2P^o_{3/2}$, which lies between them.

The most obvious wholesale mutual interactions in the np configurations affect the close $(^3P_1)7p$ and $(^3P_2)9p$ groups, the levels of the first group being higher than expected and those of the second group (except $9p\ ^4D^o_{7/2}$) lower.

(b) $4p^5nf$: All the 67 levels ascribed to nf configurations in table 5 are new. The pronounced J_cl coupling prevailing in these configurations permits the levels to be calculated very exactly by the theoretical expressions of electrostatic energy given by Möller [18]. The J_cl designations of the levels as presented in table 5 are therefore, with one or two exceptions discussed below, definite. The pair structure of these levels is very marked, as can be seen by examining the pair splittings in table 5. All nf levels based on limits other than $(^3P_2)$ and predicted to lie below the $(^3P_2)$ limit have been found. These are the 16 levels of the $(^3P_{1,0})4f$, $5f$ groups. All $(^1D_2, {}^1S_0)nf$ levels lie above the $(^3P_2)$ limit.

Most of the observed transitions involving the Br I nf levels occur in the $(^3P_2)4d-(^3P)nf$ arrays. As mentioned above, $5s-nf$ transitions are also observed, primarily as a result of a $5s \times 4d$ interaction, but nearly all other lines involving nf levels would be difficult to observe since they fall in a very unfavorable region of the spectrum, the far infrared and radiometric regions. The $(^3P_2)4d-(^3P_2)nf$ arrays are similar for each value of n as regards the intensity relationships of the various lines in the array, but the intensity of any particular transition decreases as a rule with increasing n. In general, for transitions between two pair-coupled configurations the lines will be stronger when l, K, and J change by unity in the same direction, or, with a given $\Delta l(=\pm 1)$, when $\Delta J = \Delta K(=\pm 1, 0)$. As usual, also, the stronger lines involve the higher J-values. The representative $(^3P_2)4d-(^3P_2)5f$ array is shown in table 13.

In this table, the adopted K-values of the $(^3P_2)4d$ levels are found together with the corresponding LS designations. The only rigorous selection rule here seems to be that on J. It will be noticed, however, that three transitions from $5f$ in this table that would be allowed by the selection rule on J, but not by the selection rule on K in pure J_cl coupling have not been observed. The same is true in the case of these three transitions for other nf, except that $(^3P_2)4d[3]_{7/2}-(^3P_2)4f[5]^o_{5/2}$ occurs weakly, owing to the "mixing" of the two $(^3P_2)4d$ levels having $J=7/2$. On the other hand, for the $5f$ case in table 13 as well as for other nf, there appear strongly two lines that do "violate" the $\Delta K = 0, \pm 1$ rule. These are the $(^3P_2)4d\ ^4D_{3/2}-(^3P_2)\ nf\ [3]^o_{5/2}$ and $(^3P_2)4d\ ^4F_{5/2}-(^3P_2)nf[4]^o_{7/2}$ transitions. For no value of n have the two $(^3P_2)4d\ ^4F_{5/2,3/2}-(^3P_2)nf[2]^o_{3/2}$ lines been ob-

TABLE 13. *Wavenumbers and intensities of the observed* $(^3P_2)4d-(^3P_2)5f$ *transitions in* Br I

$4d\rightarrow$ / $5f\downarrow$	[4] $^4F_{9/2}$ 80587.61	[4] $^4F_{7/2}$ 81081.10	[3] $^4D_{7/2}$ 79044.50	[3] $^4D_{5/2}$ 79260.91	[2] $^4F_{5/2}$ 81672.28	[2] $^4F_{3/2}$ 81842.02	[1] $^4D_{3/2}$ 79630.67	[1] $^4D_{1/2}$ 80026.40	[0] $^4P_{1/2}$ 81429.97
$[5]^o_{11/2}$ 90873.70	(600) 10286.09								
$[5]^o_{9/2}$ 90873.78		(300) 9792.68	——						
$[4]^o_{9/2}$ 90845.55	(100) 10257.95	——	(500) 11801.03						
$[4]^o_{7/2}$ 90846.78	——	(75) 9765.68	(100) 11802.27	(200) 11585.86	(200) 9174.50				
$[3]^o_{7/2,5/2}$ 90851.30	(15) 10263.69	(15) 9770.21	(300) 11806.78	(100) 11590.39	(250) 9179.02	(20) 9009.31	(300) 11220.60		
$[2]^o_{5/2}$ 90869.64		——	(75) 11825.12	(250) 11608.72	(100) 9197.37	(40) 9027.62	(20) 11238.92		
$[2]^o_{3/2}$ 90868.76				(75) 11607.87	——	——	(150) 11238.09	(200) 10842.35	——
$[1]^o_{3/2}$ 90891.56				(ə0) 11630.57	(2w) 9219.28	(10) 9049.58	(90) 11260.85	(80w) 10865.15	(250) 9461.59
$[1]^o_{1/2}$ 90890.88						——	(90) 11260.20	(80) 10864.48	(100) 9460.95

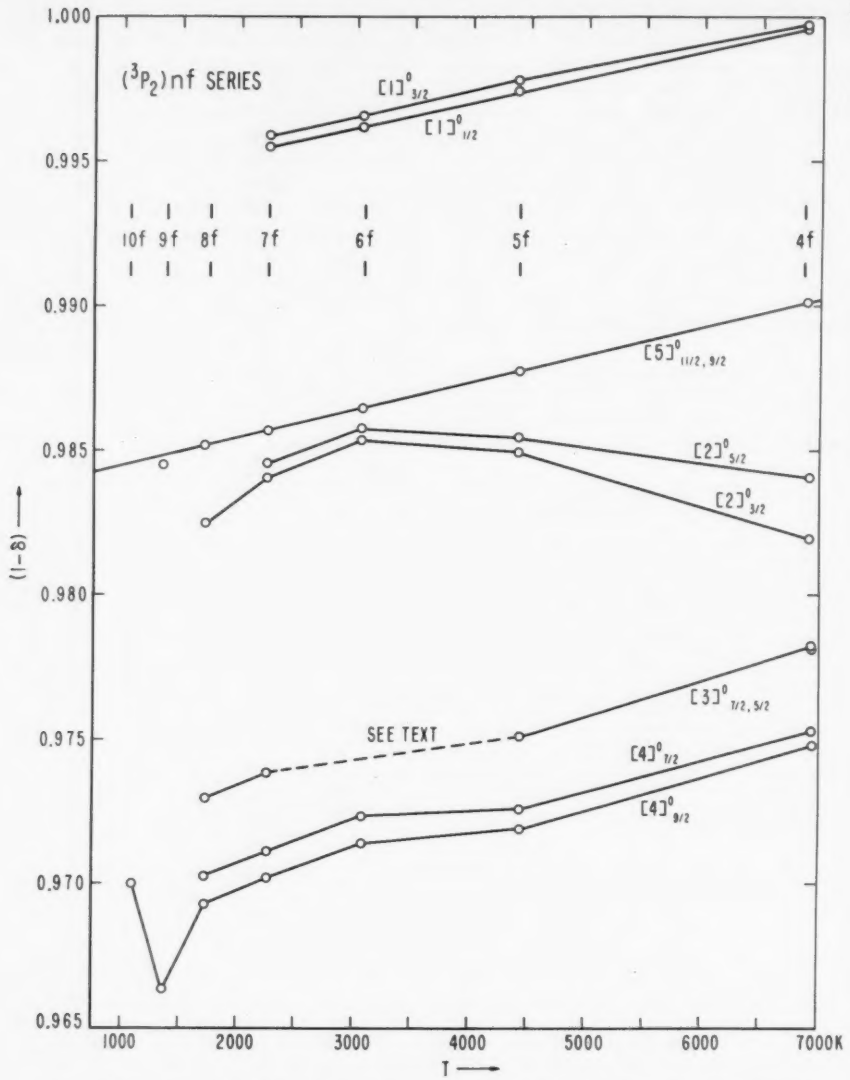

FIGURE 8. *The* $(^3P_2)nf$ *series plotted on a very expanded* $(1-\delta)$ *scale to exhibit small perturbations.*

served. The perturbations that affect the $(^3P_2)4d$ levels having $J=5/2$, 3/2 and the difficulty at present of appraising the quantum significance of the K-values assigned these levels, as mentioned in another section, render premature any detailed correlation of intensity characteristics in the arrays under discussion.

The several perturbations that afflict the $(^3P_2)nf$ series are vividly revealed by a plot of quantum defects against relative term values for these series (fig. 8). In examining this figure, one should bear in mind that the ordinate scale is greatly expanded, and the irregularities in the plots are caused by level perturbations of only a few kaysers and less. An idea of the vertical scale in kaysers can be gained for each value of n by noting the separation of the various pairs. For example, at $n=7$, the vertical separation between $7f[4]^0_{9/2}$ and $7f[4]^0_{7/2}$ corresponds to only 0.57 K, an amount that is probably greater than that by which either level is perturbed. The perturbations in the Br I nf configurations are most conveniently discussed in terms of the J_cl non-diagonal matrix components. We shall therefore consider first the energy matrices and the theoretical calculation of the nf energy level distribution.

The matrices of electrostatic energy are diagonal in J. The diagonal elements of the matrices for p^4f have the form $E=E$ (parent level) $-2F^0-$

$2\bar{f}_2'F^2+2\bar{g}_2'G^2+2\bar{g}_4'G^4$, where $\bar{f}_2'$, $\bar{g}_2'$, $\bar{g}_4'$ are numerical coefficients whose values can be found in Möller's paper, and F^2, G^2, G^4 are the familiar integrals defined in TAS. Levels of a given K-pair have a common $\bar{f}_2'$ coefficient; the pair splitting with respect to J arises from different $\bar{g}_2'$ and $\bar{g}_4'$ coefficients. Small pair splittings, therefore, imply small G^2 and G^4 integrals. In the Br I nf configurations, the contribution to the level energies by the F^2 integral is much greater than that by the G^2 and G^4 integrals. Nondiagonal F^2 is found only between levels with equal K-value and based on the different parents, $^1S_0-{}^1D_2$, $^3P_0-{}^3P_2$, and $^3P_1-{}^3P_2$. Also appearing off the diagonal are G^2 and G^4, connecting levels whose K-values are equal or are different by ± 1. In order that K be a good quantum number, it is thus essential that G^2 and G^4 be small compared with F^2.

In the actual calculation of the nf level distribution, it is convenient and suitable to make certain approximations. All $(^1S_0,{}^1D_2)nf$ levels fall above the principal ionization limit and none was observed. But since these levels are distant and are connected to the levels based on (^3P) only through nondiagonal G^2 and G^4 (and ζ_{4p}), the effect of omitting these levels from the energy matrices will cause negligible error in the calculated $(^3P)nf$ energies. Furthermore, greater accuracy in the calculated distribution of these $(^3P)nf$ levels (18 levels for each n) can be expected if we employ the observed positions of the Br II (^3P) levels rather than adopting the parametric form for these parents. We thus replace the term E (parent level) $-2F^0$ in the above diagonal expression by the quantities: B, $B+3136.4$, and $B+3837.5$, for levels based on $(^3P_2)$, $(^3P_1)$, and $(^3P_0)$, respectively, where B is a constant for any given n. This procedure automatically accounts for nondiagonal ζ_{4p}, which may then be disregarded.

We thus have 18 levels for each n to be represented in parametric form by four parameters, B, F^2, G^2, and G^4. The determination of meaningful parameters cannot be accomplished by a simple application of the diagonal sum rule, because every observed Br I nf level, with the exception of members of the $(^3P_2)nf[5]^\circ$ series, suffers interaction with other configurations. The extent of this interaction can be reasonably well estimated only in the case of the $(^3P_2)nf[4]^5_{9/2}$ levels, because almost the entire interconfigurational contribution to these must come from $(^3P_1)nf[4]^5_{9/2}$ levels, there being no possibility of a $J=9/2$ in the np configurations. After G^4 has been estimated as described below, F^2 can be found from the $(^3P_2)nf$ $[5]^\circ_{11/2}-[4]^5_{9/2}=\frac{1}{6}F^2-\frac{1}{36}G^4$ diagonal interval, provided the nondiagonal intraconfigurational contribution to $[4]^5_{9/2}$, as well as the interconfigurational contribution, have first been removed from the energies as observed. The first of these contributions can be determined by performing a preliminary diagonalization of the $J=9/2$ matrix with a good estimate of F^2. The second contribution can be obtained if a reasonable "unperturbed" $(^3P_2)$ $nf[4]^5_{9/2}$ series can be deduced. If an interaction parameter (see ref. [22], p. 141) $\gamma=23$ K is assumed between the $(^3P_2)nf$ $[4]^5_{9/2}$ and $(^3P_1)nf$ $[4]^5_{9/2}$ series, the former series becomes satisfactorily Ritzian, and after an additional "smoothing" of the series, unperturbed level energies can be estimated to sufficient accuracy, and then F^2 can be derived.

Since nondiagonal contribution to the $(^3P_2)nf[5]^\circ$ pair is negligible, the G^4 parameter can be obtained directly from the observed separation of this pair, whose diagonal energy expressions, including the spin-orbit interaction energy of the f-electron, are

$$[5]^\circ_{11/2}: B+\frac{1}{15}F^2 \qquad +\frac{3}{2}\zeta_f$$

$$[5]^\circ_{9/2}: B+\frac{1}{15}F^2+\frac{11}{54}G^4-\frac{9}{5}\zeta_f.$$

The fact that for $n\geqq 5$, the $[5]^5_{9/2}$ falls higher than $[5]^\circ_{11/2}$ confirms the dominance of $\frac{11}{54}G^4$ over $\frac{33}{10}\zeta_f$ and partially justifies the omission of ζ_f in our calculations. The G^4 parameter for $4f$ has been extrapolated from those for higher n, since the observed coincidence of the $4f$ pair, suggesting an equality of $\frac{11}{54}G^4$ and $\frac{33}{10}\zeta_f$, does not permit a direct calculation of G^4.

If the $(^3P_2)nf[1]^\circ$ levels were unperturbed, G^2 could be calculated fairly accurately from the pair splitting, $\frac{9}{50}G^2$. Even though this series as plotted in figure 8 appears Ritzian, there is some evidence that the series members have all been perturbed upwards in such a way that linearity of the plot was preserved. Nevertheless, G^2 was crudely taken as given by the pair splittings for $n\geqq 5$ and extrapolated for $n=4$, since any other procedure meets with equivalent uncertainty. The remaining parameter, B, was adjusted so as to predict the $(^3P_2)$ $nf[5]^\circ_{11/2}$ levels exactly.

The levels as calculated by use of the parameters found above are compared with the observed positions in table 14 for $4f$, $5f$ and in table 15 for $6f$, $7f$. The B and F^2 parameters are given in table 16, along with the almost constant products $F^2\times n^3$. The agreement between observed and calculated energies is seen to be very good, and it is probably significant that the departures in almost every case agree with the direction of perturbation one might expect on the basis of the plots in figure 8. The calculations predict the observed ordering of K-pairs with respect to energy for all except the perturbed $(^3P_2)4f[3]^\circ$ and $(^3P_1)4f[3]^\circ$ pairs.

The perturbations of the Br I nf levels arise from $nf\times np$ as well as $nf\times n'f$ interactions. Considering first the latter type, we remember that since the coefficients of the Slater integrals in the nf energy matrices are based entirely upon the angular parts of the eigenfunctions, these same coefficients are

TABLE 14. *Comparison between observed and calculated* (^{3}P) 4f *and* 5f *levels*

Level design.	4f		5f	
	Calc.	Obs.	Calc.	Obs.
(^{3}P$_2$) $[5]^\circ_{11/2}$	88392. 2	88392. 2	90873. 7	90873. 7
$[5]^\circ_{9/2}$	392. 3	392. 2	873. 8	873. 8
$[4]^\circ_{9/2}$	339. 3	339. 2	846. 4	845. 6
$[4]^\circ_{7/2}$	340. 4	340. 7	847. 3	846. 8
$[3]^\circ_{7/2}$	347. 9	351. 1	851. 1	851. 3
$[3]^\circ_{5/2}$	348. 5	350. 8	851. 5	
$[2]^\circ_{5/2}$	383. 6	371. 3	869. 7	869. 6
$[2]^\circ_{3/2}$	383. 4	364. 0	869. 5	868. 8
$[1]^\circ_{3/2}$	422. 3	425. 5	889. 6	891. 6
$[1]^\circ_{1/2}$	421. 5	424. 9	888. 9	890. 9
(^{3}P$_1$) $[4]^\circ_{9/2}$	91497. 7	91496. 2	93994. 0	93994. 0
$[4]^\circ_{7/2}$	498. 4	497. 1	994. 5	994. 7
$[3]^\circ_{7/2}$	539. 3	545. 7	94015. 6	94017. 8
$[3]^\circ_{5/2}$	539. 9	542. 4	016. 1	018. 2
$[2]^\circ_{5/2}$	484. 4	483. 0	93987. 3	93998. 4
$[2]^\circ_{3/2}$	483. 7	482. 3	986. 7	987. 6
(^{3}P$_0$) $[3]^\circ_{7/2}$	92209. 5	92228. 3	94700. 7	94700. 2
$[3]^\circ_{5/2}$	209. 9	228. 6	701. 0	700. 4

TABLE 15. *Comparison between observed and calculated* (^{3}P$_2$) 6f *and* 7f *levels*

Level design.	6f		7f	
	Calc.	Obs.	Calc.	Obs.
(^{3}P$_2$) $[5]^\circ_{11/2}$	92222. 7	92222. 7	93036. 1	93036. 1
$[5]^\circ_{9/2}$	222. 8	222. 8	036. 1	036. 1
$[4]^\circ_{9/2}$	206. 9	207. 3	026. 1	026. 1
$[4]^\circ_{7/2}$	207. 4	208. 3	026. 4	026. 7
$[3]^\circ_{7/2}$	209. 6	187. 9	027. 8	028. 4
$[3]^\circ_{5/2}$	209. 9		028. 0	
$[2]^\circ_{5/2}$	220. 5	222. 0	034. 7	035. 4
$[2]^\circ_{3/2}$	220. 4	221. 6	034. 6	035. 0
$[1]^\circ_{3/2}$	232. 0	233. 1	041. 9	042. 6
$[1]^\circ_{1/2}$	231. 6	232. 7	041. 7	042. 4

TABLE 16. *The* B *and* F^2 *parameters for* 4f, 5f, 6f, *and* 7f *configurations, calculated as explained in the text*

Conf.	B	F^2	F$^2\times n^3$
4f	88371. 24	314. 1	201×10^2
5f	90862. 84	162. 9	204
6f	92216. 42	94. 8	205
7f	93032. 09	59. 9	205

valid in the discussion of $nf\times n'f$ interaction. Since this interaction is expected to be greater if a nondiagonal $\bar{f}_2$ is involved, we should expect that the strongest interactions would be of the types $(^3P_1)nf[K]^\circ\times(^3P_2)n'f[K']^\circ$, where $K=K'=2$, 3, or 4, and $(^3P_0)nf[3]^\circ\times(^3P_2)n'f[3]^\circ$. Indeed, the plots in figure 8 show quite clearly that $(^3P_1)4f$ falls just between $(^3P_2)5f$ and $6f$ and pushes $(^3P_2)4f,5f$ levels down and $(^3P_2)6f,7f$ . . . levels up, for $K=2$, 3, 4. Also, the $(^3P_0)4f[3]^\circ\times(^3P_2)6f[3]^\circ$ interaction is, comparatively, very strong, owing to their almost identical unperturbed positions, as indicated by the calculations. It is possible that the designations of these levels should be interchanged. The points corresponding to $(^3P_2)6f[3]^\circ$ fall outside the range of figure 8 and have been omitted. Another striking feature of this figure is that it suggests, correctly, that $(^3P_1)5f[4]^\circ_{9/2}$ falls between $(^3P_2)9f,10f[4]^\circ_{9/2}$.

Superposed on the above interactions are those of the type $nf\times np$, which also seem to be stronger if the interacting levels have the same K-value.

The $(^1D_2)5p$ group appears to interact with nf levels having the appropriate K- and J-values, the largest such interaction being $(^1D_2)5p\,^2D^\circ_{5/2,3/2}\times(^3P_2)4f[2]^\circ_{5/2,3/2}$, owing to the proximity of the levels. The several interactions affecting $(^3P_2)nf[3]^\circ$ pairs make the levels for $n\geqq5$ coincide within the experimental error. Since it is not possible to decide with certainty from which level of the pair a particular line arises, when that line is classifiable by either of the levels, the two levels are represented by a single energy in table 5.

The calculations suggest that the observed $(^3P_2)$ $nf[1]^\circ$ pair is uniformly high. Since a $K=1$ is not possible from the $(^3P_1)$ and $(^3P_0)$ parents, we should expect the observed $[1]^\circ$ series to be almost Ritzian in the absence of interaction with np levels. Now the series *is* almost Ritzian, so that if the series is perturbed, it must be of a complicated sort, involving several np levels, since a single interaction with $(^1D_2)5p\,^2P^\circ_{3/2,1/2}$ would not account for the preservation of the rather strict linearity found in figure 8.

The $(^3P_2)8p\ ^4D^\circ_{5/2}\times(^3P_1)4f[3]^\circ_{7/2}$ interaction, complicated by additional influences on these levels, should also be mentioned, since it is possible that the two designations should be interchanged. It is not entirely clear what causes the $(^3P_1)4f,5f[3]^\circ$ levels to be observed so "much" higher than their calculated positions.

7. Conclusion

Since the Br I line list has now been essentially exhausted—only 26 of 1253 lines remain unclassified—it is clear that any significant additions to the analysis of Br I will demand a thorough, new observation of the spectrum, made with a much stronger source for reasonable exposure times in the red, and one that produces Br_2 emission of much less intensity than the source used in this investigation. Even without making accurate calculations, one can predict very closely, barring strong interactions, the positions of the remaining unknown *ns*, *np*, *nd*,

and *nf* levels that fall below the principal ionization limit. This can be done almost by inspection of tables 5 and 6. One can, then, make educated guesses as to the wavelength region where the stronger lines involving the unknown levels will lie. Of course many of the new lines that would be included in any augmented line list would be accounted for by transitions predicted in the present square array, and might help us in a possible revision of the more insecure level designations mentioned above. A study of the Zeeman effect in Br I is possibly the only and certainly the best method of resolving a few difficulties of interpretation, such as that of the $J=1/2$ levels lying in the vicinity of $(^1S_0)5s\ ^2S_{1/2}$ as discussed above.

Perhaps the most demanding study that could be initiated on Br I is an extensive analysis of the *nd* configurations and their coupling and perturbations. If some of the levels still missing from the $(^3P_2)9d$-$11d$ configurations could be found, a more definite decision could possibly be reached as to whether some levels presently assigned to $(^3P_1)6d$ might not more properly belong to $(^3P_2)9d$.

Of the 26 lines in our list that have defied classification, one has intensity 50, one intensity 15 *w*, and the rest have intensities 10 and less. It is probable that as many as one-half of these lines actually do not arise from neutral atomic bromine. For example, since the six unclassified lines of wavelengths less than 4100 Å would have to result from transitions to the even $(^3P)5s$ levels in order for the upper levels to lie below the $(^3P_2)$ limit, and since no new odd levels predictable on this basis fall in acceptable positions, it is doubtful that these six lines belong to Br I.

There seems to be little hope of finding any Br I levels above the $(^3P_2)$ limit unless autoionization from these levels is somehow avoided. Although we have predicted and looked in our list for many lines that we thought most likely to appear from such levels, none could be established definitely.

The unknown *ng* levels falling below the $(^3P_2)$ limit are predicted to lie in the range 90890 to 95285. Their stronger combinations will generally be with *nf* levels. Since these latter levels are in the range 88300 to 95285 K combinations with *ng* will produce lines that fall in the infrared beyond the region accessible by photography.

For suggesting this problem and offering advice throughout, I thank C. C. Kiess. His interest in the bromine spectrum has lasted over 30 years, and his excitement and enthusiasm as he watched our analysis progress was a constant source of encouragement.

I also express my indebtedness to C. Moore-Sitterly and W. F. Meggers for generously allowing me to draw so persistently upon their great experience and knowledge of atomic spectra.

R. E. Trees examined and improved upon the discussion of the sp^6 configuration. W. R. Bozman frequently advised and instructed me in the various computations by the electronic computer and also took charge of the preparation of prints for the figures in this paper. W. C. Martin critically read the manuscript and offered many useful suggestions. Mrs. Ruth Peterson patiently and accurately carried out some of the final hand calculations, and Mrs. Sylvia Shure carefully typed the manuscript. It is a pleasure to thank each of these colleagues for his or her contribution to this paper.

Finally, and especially, I want to record my gratitude to C. H. Corliss, who provided advisory and, more often, active assistance in all phases of the experimental work that followed our earlier collaboration in obtaining the first series of wavelength observations.

8. References

[1] C. C. Kiess and C. H. Corliss, J. Res. NBS **63A** (Phys. and Chem.) No. 1, 1 (1959).
[2] W. C. Martin and C. H. Corliss, J. Res. NBS **64A** (Phys. and Chem.) No. 6, 443 (1960).
[3] C. H. Corliss, W. R. Bozman, and F. O. Westfall, J. Opt. Soc. Am. **43,** 398 (1953).
[4] C. C. Kiess and T. L. de Bruin, J. Res. NBS **4,** 667 (1930).
[5] C. E. Moore, Atomic Energy Levels, NBS Circ. 467, Vol. II (1952).
[6] P. Lacroute, Ann. Phys. (11) **3,** 5 (1935).
[7] S. Tolansky and S. A. Trivedi, Proc. Roy. Soc. (London) **175,** 366 (1940).
[8] P. G. Wilkinson, J. Opt. Soc. Am. **45,** 862 (1955).
[9] S. Avellén, Ark. f. Fys. **8,** 211 (1954).
[10] J. L. Tech and C. H. Corliss, J. Res. NBS **65A** (Phys. and Chem.) No. 3, 159 (1961).
[11] C. J. Humphreys and H. J. Kostkowski, J. Res. NBS **49,** 73 (1952) RP2345.
[12] E. K. Plyler, L. R. Blaine, and E. D. Tidwell, J. Res. NBS **55,** 279 (1955) RP2630.
[13] C. J. Humphreys and E. Paul, Jr., J. Opt. Soc. Am. **49,** 1180 (1959).
[14] W. C. Martin and J. L. Tech, J. Opt. Soc. Am. **51,** 591 (1961).
[15] E. U. Condon and G. H. Shortley, *The Theory of Atomic Spectra* (Cambridge University Press, London, 1959), hereinafter referred to as TAS.
[16] K. Lidén, Ark. f. Fys. **1,** 229 (1949).
[17] L. Minnhagen, Ark. f. Fys. **18,** 97 (1960).
[18] N. H. Möller, Ark. f. Fys. **18,** 135 (1960).
[19] L. Minnhagen, Ark. f. Fys. **21,** 415 (1962).
[20] G. Racah, Phys. Rev. **61,** 537 (1942).
[21] M. A. Catalán and F. R. Rico, Anales de Fisica y Quimica **54A,** 301 (1958).
[22] B. Edlén, Atomic Spectra, Handb. d. Physik **27,** 80 (Springer-Verlag, Heidelberg, 1963).
[23] J. C. Slater, Quantum Theory of Atomic Structure, Vol. II (McGraw-Hill Book Co., Inc., New York, 1960).
[24] R. E. Watson and A. J. Freeman, Phys. Rev. **124,** 1117 (1961).
[25] J. W. M. DuMond and E. R. Cohen, Handbook of Physics, pt. 7, ch. 10, p. 170 (ed. by E. U. Condon and H. Odishaw, McGraw-Hill Book Co., Inc., New York, 1958).

9. Appendix

TABLE A1. *Wavelengths of* Br I *in the vacuum ultraviolet*

Observed wavelength	Calc. wavelength	Intensity	Observed wave number	Classification
Å			K	
1067.559	0.556	10	93671.6	$4p^5\,^2P^o_{3/2}$—$(^1D_2)4d\,^2F_{5/2}$
1067.805	.802	15	93650.1	$4p^5\,^2P^o_{3/2}$—$(^1D_2)4d\,^2P_{1/2}$
1068.256	.263	10	93610.5	$4p^5\,^2P^o_{3/2}$—$(^1D_2)4d\,^2P_{3/2}$
1068.849	.856	3	93558.6	$4p^5\,^2P^o_{3/2}$—$11s\,^4P_{3/2}$
1073.912	.916	70	93117.5	$4p^5\,^2P^o_{3/2}$—$6d'\,^2P_{3/2}$
1074.243	.245	70	93088.8	$4p^5\,^2P^o_{3/2}$—$(^1D_2)4d\,^2D_{5/2}$
1074.803	.815	10	93040.3	$4p^5\,^2P^o_{3/2}$—$10s\,^4P_{3/2}$
1075.345	.317	15	92993.4	$4p^5\,^2P^o_{3/2}$—$10s\,^4P_{5/2}$
	.354			$4p^5\,^2P^o_{3/2}$—$6d'\,^2P_{1/2}$
1076.964	.964	20	92853.6	$4p^5\,^2P^o_{3/2}$—$8d\,^4F_{3/2}$
1077.873	.878	15	92775.3	$4p^5\,^2P^o_{3/2}$—$8d\,^4D_{3/2}$
1078.124	.124	15	92753.7	$4p^5\,^2P^o_{3/2}$—$8d\,^4D_{5/2}$
1078.242	.247	30	92743.6	$4p^5\,^2P^o_{3/2}$—$8d\,^4F_{5/2}$
1079.320	.326	30	92650.9	$4p^5\,^2P^o_{3/2}$—$8d\,^4D_{1/2}$
1080.882	.883	50	92517.0	$4p^5\,^2P^o_{3/2}$—$(^1D_2)4d\,^2D_{3/2}$
1084.810	.807	10	92182.0	$4p^5\,^2P^o_{3/2}$—$9s\,^4P_{3/2}$
1085.050	.052	15	92161.6	$4p^5\,^2P^o_{3/2}$—$9s\,^4P_{5/2}$
1085.896	.899	5	92089.8	$4p^5\,^2P^o_{3/2}$—$7s''\,^2P_{1/2}$
1087.468	.470	30	91956.7	$4p^5\,^2P^o_{3/2}$—$7d\,^4F_{5/2}$
1087.687	.690	40	91938.2	$4p^5\,^2P^o_{3/2}$—$(^1S_0)5s\,^2S_{1/2}$
1087.819	.821	20	91927.1	$4p^5\,^2P^o_{3/2}$—$7d\,^4F_{3/2}$
1089.039	.040	30	91824.1	$4p^5\,^2P^o_{3/2}$—$7d\,^4P_{1/2}$
1089.203	.203	15	91810.2	$4p^5\,^2P^o_{3/2}$—$7d\,^4D_{5/2}$
1089.322	.323	20	91800.2	$4p^5\,^2P^o_{3/2}$—$7d\,^4D_{3/2}$
1090.623	.620	85	91690.7	$4p^5\,^2P^o_{3/2}$—$7d\,^4D_{1/2}$
1094.722	.719	100	91347.4	$4p^5\,^2P^o_{3/2}$—$7s'\,^4P_{1/2}$
1095.481	.482	100	91284.1	$4p^5\,^2P^o_{3/2}$—$7s'\,^2P_{3/2}$
1096.788	.790	100	91175.3	$4p^5\,^2P^o_{3/2}$—$5d''\,^2D_{5/2}$
1098.881	.885	100	91001.7	$4p^5\,^2P^o_{3/2}$—$5d''\,^2D_{3/2}$
1101.347	.351	50	90797.9	$4p^5\,^2P^o_{3/2}$—$8s\,^4P_{3/2}$
[a] 1101.456			90788.9	$4p^5\,^2P^o_{3/2}$—$8s\,^4P_{5/2}$
1101.498		250	90785.5	$4p^5\,^2P^o_{1/2}$—$(^1D_2)6s\,^2D_{3/2}$
1103.924	.932	60	90585.9	$4p^5\,^2P^o_{3/2}$—$5d'\,^4P_{5/2}$
1104.168	.169	60	90565.9	$4p^5\,^2P^o_{3/2}$—$5d'\,^2F_{5/2}$
1105.460	.464	50	90460.1	$4p^5\,^2P^o_{3/2}$—$5d'\,^2P_{3/2}$
1105.844	.846	50	90428.7	$4p^5\,^2P^o_{3/2}$—$6d\,^4P_{1/2}$
1105.994	.994	70	90416.4	$4p^5\,^2P^o_{3/2}$—$6d\,^4F_{3/2}$
1107.442	.445	50	90298.2	$4p^5\,^2P^o_{1/2}$—$8s'\,^4P_{1/2}$
1107.512	.514	50	90292.5	$4p^5\,^2P^o_{3/2}$—$5d'\,^2P_{1/2}$
1109.422	.432	20	90137.0	$4p^5\,^2P^o_{1/2}$—$10d\,^4D_{3/2}$
1110.904	.911	100	90016.8	$4p^5\,^2P^o_{1/2}$—$(^1D_2)4d\,^2S_{1/2}$
[b] 1111.579	.542	50	89962.1	$4p^5\,^2P^o_{1/2}$—$(^1D_2)4d\,^2P_{1/2}$
1111.751	.754	40	89948.2	$4p^5\,^2P^o_{3/2}$—$6d\,^4D_{5/2}$
1112.743	.747	20	89868.0	$4p^5\,^2P^o_{3/2}$—$6d\,^4D_{3/2}$
1115.448	.448	30	89650.1	$4p^5\,^2P^o_{1/2}$—$9d\,^4D_{3/2}$
1116.105	.105	40	89597.3	$4p^5\,^2P^o_{1/2}$—$9d\,^4D_{1/2}$
1118.173	.169	90	89431.6	$4p^5\,^2P^o_{1/2}$—$6d'\,^2P_{3/2}$
1119.140	.143	60	89354.3	$4p^5\,^2P^o_{1/2}$—$10s\,^4P_{3/2}$
1119.725	.728	90	89307.6	$4p^5\,^2P^o_{1/2}$—$6d'\,^2P_{1/2}$
1121.473	.474	120	89168.4	$4p^5\,^2P^o_{1/2}$—$8d\,^4F_{3/2}$
1121.839	.842	80	89139.4	$4p^5\,^2P^o_{1/2}$—$8d\,^4P_{1/2}$
1124.038	.035	120	88965.0	$4p^5\,^2P^o_{1/2}$—$8d\,^4D_{1/2}$
1125.728	.725	200	88831.4	$4p^5\,^2P^o_{1/2}$—$(^1D_2)4d\,^2D_{3/2}$
1129.979	.981	35	88497.2	$4p^5\,^2P^o_{1/2}$—$9s\,^4P_{3/2}$
1131.171	.166	80	88404.0	$4p^5\,^2P^o_{1/2}$—$7s''\,^2P_{1/2}$
1132.822	.817	100	88275.1	$4p^5\,^2P^o_{3/2}$—$7s\,^4P_{3/2}$

See footnotes at end of table.

TABLE A1. *Wavelengths of* Br I *in the vacuum ultraviolet*—Con.

Observed wavelength	Calc. wavelength	Intensity	Observed wave number	Classification
Å			K	
1133.116	0.110	200	88252.2	$4p^5\,^2P^o_{1/2}$—$(^1S_0)5s\,^2S_{1/2}$
1133.251	.252	80	88241.7	$4p^5\,^2P^o_{1/2}$—$7d\,^4F_{3/2}$
1134.588	.575	300	88137.7	$4p^5\,^2P^o_{1/2}$—$7d\,^4P_{1/2}$
	.622			$4p^5\,^2P^o_{3/2}$—$7s\,^4P_{5/2}$
1134.888	.882	200	88114.4	$4p^5\,^2P^o_{1/2}$—$7d\,^4D_{3/2}$
1136.294	.290	250	88005.4	$4p^5\,^2P^o_{1/2}$—$7d\,^4D_{1/2}$
1139.350	.342	100	87769.3	$4p^5\,^2P^o_{3/2}$—$5d\,^4F_{3/2}$
1139.544	.537	120	87754.4	$4p^5\,^2P^o_{3/2}$—$5d\,^4F_{5/2}$
	.547			$4p^5\,^2P^o_{3/2}$—$5d\,^4P_{1/2}$
1140.732	.739	20	87663.0	$4p^5\,^2P^o_{1/2}$—$7s'\,^4P_{1/2}$
1141.564	.568	25	87599.1	$4p^5\,^2P^o_{1/2}$—$7s'\,^2P_{3/2}$
1145.268	.264	80	87315.8	$4p^5\,^2P^o_{1/2}$—$5d''\,^2D_{3/2}$
1145.854	.846	60	87271.2	$4p^5\,^2P^o_{3/2}$—$5d\,^4D_{1/2}$
1147.689	.689	80	87131.6	$4p^5\,^2P^o_{3/2}$—$5d\,^4D_{3/2}$
1147.943	.943	60	87112.3	$4p^5\,^2P^o_{1/2}$—$8s\,^4P_{3/2}$
1150.312	.307	80	86932.9	$4p^5\,^2P^o_{3/2}$—$5d\,^4D_{5/2}$
1151.381	.380	100	86852.2	$4p^5\,^2P^o_{1/2}$—$5d'\,^4P_{3/2}$
1152.418	.412	100	86774.1	$4p^5\,^2P^o_{1/2}$—$5d'\,^2P_{3/2}$
1152.833	.827	40	86742.8	$4p^5\,^2P^o_{1/2}$—$6d\,^4P_{1/2}$
1152.989	.988	60	86731.1	$4p^5\,^2P^o_{1/2}$—$6d\,^4F_{3/2}$
1154.640	.640	15	86607.1	$4p^5\,^2P^o_{1/2}$—$5d'\,^2P_{1/2}$
1159.030	.025	80	86279.0	$4p^5\,^2P^o_{3/2}$—$6s''\,^2P_{1/2}$
1160.332	.329	100	86182.2	$4p^5\,^2P^o_{1/2}$—$6d\,^4D_{3/2}$
1168.542	.539	150	85576.7	$4p^5\,^2P^o_{3/2}$—$6s'\,^4P_{1/2}$
1170.479	.476	150	85435.1	$4p^5\,^2P^o_{3/2}$—$6s'\,^2P_{3/2}$
1173.827	.825	175	85191.4	$4p^5\,^2P^o_{3/2}$—$4d''\,^2D_{3/2}$
1177.233	.230	250	84945.0	$4p^5\,^2P^o_{3/2}$—$4d''\,^2D_{5/2}$
1178.895	.889	400	84825.2	$4p^5\,^2P^o_{3/2}$—$4s4p^6\,^2S_{1/2}$
1182.171	.169	150	84590.1	$4p^5\,^2P^o_{1/2}$—$7s\,^4P_{3/2}$
1186.161	.159	150	84305.6	$4p^5\,^2P^o_{3/2}$—$4d'\,^4P_{5/2}$
1189.279	.277	1000	84084.6	$4p^5\,^2P^o_{1/2}$—$5d\,^4F_{3/2}$
1189.378	.379	250	84077.6	$4p^5\,^2P^o_{3/2}$—$4d'\,^4P_{3/2}$
1189.498	.500	1000	84069.1	$4p^5\,^2P^o_{1/2}$—$5d\,^4P_{1/2}$
1194.413	.414	200	83723.1	$4p^5\,^2P^o_{3/2}$—$4d'\,^2F_{5/2}$
1196.370	.366	200	83586.2	$4p^5\,^2P^o_{1/2}$—$5d\,^4D_{1/2}$
1196.477	.480	200	83578.7	$4p^5\,^2P^o_{3/2}$—$4d'\,^2P_{3/2}$
1198.371	.374	500	83446.6	$4p^5\,^2P^o_{1/2}$—$5d\,^4D_{3/2}$
1203.353	.354	200	83101.1	$4p^5\,^2P^o_{3/2}$—$4d'\,^2P_{1/2}$
1209.756	.752	800	82661.3	$4p^5\,^2P^o_{3/2}$—$6s\,^4P_{3/2}$
1210.734	.739	1000	82594.5	$4p^5\,^2P^o_{1/2}$—$6s''\,^2P_{1/2}$
1216.006	.010	750	82236.4	$4p^5\,^2P^o_{3/2}$—$6s\,^4P_{5/2}$
1221.128	.125	1000	81891.5	$4p^5\,^2P^o_{1/2}$—$6s'\,^4P_{1/2}$
1221.870	.866	900	81841.8	$4p^5\,^2P^o_{3/2}$—$4d\,^4F_{3/2}$
1223.240	.240	1000	81750.1	$4p^5\,^2P^o_{1/2}$—$6s'\,^2P_{3/2}$
1224.408	.406	1200	81672.1	$4p^5\,^2P^o_{3/2}$—$4d\,^4F_{5/2}$
1226.899	.898	1200	81506.3	$4p^5\,^2P^o_{1/2}$—$4d''\,^2D_{3/2}$
1228.049	.049	750	81430.0	$4p^5\,^2P^o_{3/2}$—$4d\,^4P_{1/2}$
1232.431	.432	7500	81140.4	$4p^5\,^2P^o_{1/2}$—$4s4p^6\,^2S_{1/2}$
1243.897	.901	1200	80392.5	$4p^5\,^2P^o_{1/2}$—$4d'\,^4P_{3/2}$
1249.589	.588	800	80026.3	$4p^5\,^2P^o_{3/2}$—$4d\,^4D_{1/2}$
1251.664	.670	1500	79893.6	$4p^5\,^2P^o_{1/2}$—$4d'\,^2P_{3/2}$
1255.799	.798	1000	79630.6	$4p^5\,^2P^o_{3/2}$—$4d\,^4D_{3/2}$
1259.199	.194	1500	79415.6	$4p^5\,^2P^o_{1/2}$—$4d'\,^2P_{1/2}$
1261.658	.656	1200	79260.8	$4p^5\,^2P^o_{3/2}$—$4d\,^4D_{5/2}$
1266.200	.202	1200	78976.5	$4p^5\,^2P^o_{1/2}$—$6s\,^4P_{3/2}$
1279.477	.480	1000	78156.9	$4p^5\,^2P^o_{1/2}$—$4d\,^4F_{3/2}$
1286.259	.261	1000	77744.8	$4p^5\,^2P^o_{1/2}$—$4d\,^4P_{1/2}$

TABLE A1. *Wavelengths of* Br I *in the vacuum ultraviolet*—Con.

Observed wavelength	Calc. wavelength	Intensity	Observed wave number	Classification
Å			K	
1309.908	0.909	3000	76341.2	$4p^5\ ^2P^\circ_{1/2}$—$4d\ ^4D_{1/2}$
1316.735	.735	3000	75945.4	$4p^5\ ^2P^\circ_{1/2}$—$4d\ ^4D_{3/2}$
1317.372	.375	1000	75908.7	$4p^5\ ^2P^\circ_{3/2}$—$(^1D_2)5s\ ^2D_{3/2}$
1317.695	.691	2000	75890.1	$4p^5\ ^2P^\circ_{3/2}$—$(^1D_2)5s\ ^2D_{5/2}$
1384.598	.595	12000	72223.1	$4p^5\ ^2P^\circ_{1/2}$—$(^1D_2)5s\ ^2D_{3/2}$
1449.903	.901	3000	68970.1	$4p^5\ ^2P^\circ_{3/2}$—$5s''\ ^2P_{1/2}$
1488.452	.459	50000	67183.9	$4p^5\ ^2P^\circ_{3/2}$—$5s'\ ^2P_{3/2}$
1495.132	.129	5	66883.7	$4p^5\ ^2P^\circ_{3/2}$—$5s'\ ^4P_{1/2}$
1531.743	.746	30000	65285.1	$4p^5\ ^2P^\circ_{1/2}$—$5s''\ ^2P_{1/2}$
1540.654	.661	25000	64907.5	$4p^5\ ^2P^\circ_{3/2}$—$5s\ ^4P_{3/2}$
1574.841	0.844	30000	63498.5	$4p^5\ ^2P^\circ_{1/2}$—$5s'\ ^2P_{3/2}$
1576.387	.381	20000	63436.2	$4p^5\ ^2P^\circ_{3/2}$—$5s\ ^4P_{5/2}$
1582.312	.313	25000	63198.7	$4p^5\ ^2P^\circ_{1/2}$—$5s'\ ^4P_{1/2}$
1633.404	.401	75000	61221.8	$4p^5\ ^2P^\circ_{1/2}$—$5s\ ^4P_{5/2}$

[a] λ1101.456 computed wavelength. The line is masked by λ1101.498.

[b] λ1111.579 this may be a Br II line.

TABLE A2. *Observed lines of* Br I

Wavelength	Intensity	Wave number	Classification
Å		K	
3325.307	10*w*	30063.76	$5s\ ^4P_{5/2}$—$7p''\ ^2P^\circ_{3/2}$
3348.566	15	29854.95	$5s\ ^4P_{5/2}$—$10p\ ^4D^\circ_{7/2}$
3400.030	25	29403.07	$5s\ ^4P_{5/2}$—$7p'\ ^4S^\circ_{3/2}$
3400.060	20	29402.81	
3402.411	15	29382.49	$5s\ ^4P_{5/2}$—$7p'\ ^2D^\circ_{3/2}$
3402.436	10	29382.28	
3409.728	15	29319.44	$5s\ ^4P_{5/2}$—$7p'\ ^2D^\circ_{5/2}$
3409.753	10	29319.23	
3418.888	15*w*	29240.89	$5s\ ^4P_{5/2}$—$9p\ ^4D^\circ_{3/2}$
3425.577	60	29183.79	$5s\ ^4P_{5/2}$—$9p\ ^4D^\circ_{7/2}$
3428.605	15	29158.02	$5s\ ^4P_{5/2}$—$9p\ ^4P^\circ_{3/2}$
3429.809	8	29147.79	$5s\ ^4P_{5/2}$—$9p\ ^4P^\circ_{5/2}$
3472.188	20	28792.04	$5s\ ^4P_{5/2}$—$4f''\ [3]^\circ_{7/2}$
3472.216	10	28791.81	
3496.366	5	28592.94	$5s\ ^4P_{3/2}$—$7p''\ ^2P^\circ_{3/2}$
3497.433	1	28584.22	$5s\ ^4P_{3/2}$—$7p''\ ^2P^\circ_{1/2}$
3516.144	40	28432.12	$5s\ ^4P_{3/2}$—$10p\ ^4D^\circ_{3/2}$
3541.173	100	28231.16	$5s\ ^4P_{5/2}$—$8p\ ^4D^\circ_{5/2}$
3556.518	40	28109.36	$5s\ ^4P_{5/2}$—$4f'\ [3]^\circ_{7/2}$
3556.540	30	28109.19	
3557.461	250	28101.91	$5s\ ^4P_{5/2}$—$8p\ ^4D^\circ_{7/2}$
3558.616	75	28092.79	$5s\ ^4P_{5/2}$—$8p\ ^4P^\circ_{5/2}$
3563.706	50	28052.66	$5s\ ^4P_{5/2}$—$8p\ ^4P^\circ_{3/2}$
3564.468	15*w*	28046.67	$5s\ ^4P_{5/2}$—$4f'\ [2]^\circ_{5/2}$
3564.498	10	28046.43	
3579.081	40	27932.16	$5s\ ^4P_{3/2}$—$7p'\ ^4S^\circ_{3/2}$
3581.712	15	27911.64	$5s\ ^4P_{3/2}$—$7p'\ ^2D^\circ_{3/2}$
3589.818	100	27848.62	$5s\ ^4P_{3/2}$—$7p'\ ^2D^\circ_{5/2}$
3599.962	100	27770.15	$5s\ ^4P_{3/2}$—$9p\ ^4D^\circ_{5/2}$
3606.518	20	27719.67	$5s\ ^4P_{3/2}$—$9p\ ^4D^\circ_{5/2}$
3608.864	7	27701.65	$5s\ ^4P_{3/2}$—$9p\ ^4P^\circ_{1/2}$
3644.165	15	27433.31	$5s\ ^4P_{5/2}$—$5f\ [2]^\circ_{5/2}$
3644.198	10	27433.06	
3646.605	100	27414.96	$5s\ ^4P_{5/2}$—$5f\ [3]^\circ_{7/2,5/2}$
3646.626	80	27414.80	
3658.486	2*h*	27325.93	$5s\ ^4P_{3/2}$—$6f\ [1]^\circ_{3/2}$
3659.970	20	27314.85	$5s\ ^4P_{3/2}$—$6f\ [2]^\circ_{5/2}$
3735.800	500	26760.42	$5s\ ^4P_{3/2}$—$8p\ ^4D^\circ_{3/2}$
3745.419	50	26691.70	$5s\ ^4P_{3/2}$—$8p\ ^4P^\circ_{1/2}$
3751.287	10	26649.94	$5s\ ^4P_{3/2}$—$8p\ ^4D^\circ_{5/2}$

TABLE A2. *Observed lines of* Br I—Continued

Wavelength	Intensity	Wave number	Classification
Å		K	
3753. 351	5	26635. 29	$5s\ ^4P_{3/2}$—$4f'\ [3]^o_{5/2}$
3756. 032	30	26616. 28	$5s'\ ^4P_{1/2}$—$7p''\ ^2P^o_{3/2}$
3757. 265	5	26607. 54	$5s'\ ^4P_{1/2}$—$7p''\ ^2P^o_{1/2}$
3761. 746	2	26575. 85	$5s\ ^4P_{3/2}$—$4f'\ [2]^o_{5/2}$
3761. 847	1	26575. 14	$5s\ ^4P_{3/2}$—$4f'\ [2]^o_{3/2}$
3770. 88	150c	26511. 48	$5s\ ^4P_{5/2}$—$6p''\ ^2P^o_{3/2}$
3794. 03	900c	26349. 72	$5s\ ^4P_{5/2}$—$7p\ ^4D^o_{3/2}$
3798. 805	5w	26316. 60	$5s'\ ^2P_{3/2}$—$7p''\ ^2P^o_{3/2}$
3810. 95	1h	26232. 73	$5s\ ^4P_{5/2}$—$7p\ ^4D^o_{5/2}$
3815. 650	1200	26200. 42	$5s\ ^4P_{5/2}$—$7p\ ^4D^o_{7/2}$
3828. 505	700	26112. 45	$5s\ ^4P_{5/2}$—$7p\ ^4P^o_{5/2}$
3829. 75	200c	26103. 96	$5s\ ^4P_{5/2}$—$7p\ ^4P^o_{3/2}$
3844. 035	100	26006. 95	$5s'\ ^4P_{1/2}$—$7p'\ ^4D^o_{1/2}$
3847. 37	5h	25984. 41	$5s\ ^4P_{3/2}$—$5f\ [1]^o_{3/2}$
3850. 619	10	25962. 49	$5s\ ^4P_{3/2}$—$5f\ [2]^o_{3/2}$
3850. 740	1	25961. 67	$5s\ ^4P_{3/2}$—$5f\ [2]^o_{3/2}$
3851. 654	3	25955. 51	$5s'\ ^4P_{1/2}$—$7p'\ ^4S^o_{3/2}$
3854. 702	90	25934. 99	$5s'\ ^4P_{1/2}$—$7p'\ ^2D^o_{3/2}$
3896. 653	200	25655. 78	$5s'\ ^2P_{3/2}$—$7p'\ ^4S^o_{3/2}$
3899. 767	25	25635. 29	$5s'\ ^2P_{3/2}$—$7p'\ ^2D^o_{3/2}$
3905. 823	25w	25595. 55	$5s\ ^4P_{5/2}$—$6p'\ \ ^4S^o_{3/2}$
3905. 858	20	25595. 32	
3909. 385	175	25572. 23	$5s'\ ^2P_{3/2}$—$7p'\ ^2D^o_{5/2}$
3913. 560	12	25544. 95	$5s'\ ^2P_{3/2}$—$7p'\ ^2S^o_{1/2}$
3917. 775	200	25517. 47	$5s\ ^4P_{5/2}$—$6p'\ ^2D^o_{3/2}$
3917. 819	150	25517. 18	
3929. 196	5	25443. 30	$5s'\ ^2P_{3/2}$—$9p\ ^4D^o_{5/2}$
3934. 068	60	25411. 79	$5s\ ^4P_{5/2}$—$6p'\ ^2D^o_{5/2}$
3934. 084	80	25411. 68	
3934. 119	100	25411. 46	
3942. 026	2h	25360. 49	
3943. 776	2	25349. 23	$5s'\ ^4P_{1/2}$—$6f\ [1]^o_{3/2}$
3943. 835	8	25348. 86	$5s'\ ^4P_{1/2}$—$6f\ [1]^o_{1/2}$
3945. 565	4	25337. 74	$5s'\ ^4P_{1/2}$—$6f\ [2]^o_{3/2}$
3969. 416	1	25185. 50	
3969. 434	1	25185. 38	
3973. 967	5	25156. 66	
3991. 363	300	25047. 01	$5s\ ^4P_{5/2}$—$(^1D_2)5p\ ^2D^o_{3/2}$
3992. 363	1500	25040. 74	$5s\ ^4P_{3/2}$—$6p''\ ^2P^o_{3/2}$
3993. 177	5	25035. 64	
3998. 492	35	25002. 36	$5s\ ^4P_{5/2}$—$(^1D_2)5p\ ^2D^o_{3/2}$
3999. 070	200	24998. 75	$5s\ ^4P_{3/2}$—$6p''\ ^2P^o_{1/2}$
a 4000. 599	2w	24989. 19	$5s\ ^4P_{5/2}$—$4f\ [1]^o_{3/2}$
4009. 296	2w	24934. 99	$5s\ ^4P_{5/2}$—$4f\ [2]^o_{5/2}$
4009. 325	2	24934. 81	
4012. 548	60s	24914. 78	$5s\ ^4P_{5/2}$—$4f\ [3]^o_{7/2}$
4012. 580	50	24914. 58	
4016. 453	1h	24890. 55	
4018. 316	200	24879. 01	$5s\ ^4P_{3/2}$—$7p\ ^4D^o_{3/2}$
4021. 772	250	24857. 64	$5s\ ^4P_{3/2}$—$7p\ ^4P^o_{1/2}$
4033. 762	1h	24783. 75	$5s'\ ^4P_{1/2}$—$8p\ ^4D^o_{3/2}$
4037. 324	500	24761. 89	$5s\ ^4P_{3/2}$—$7p\ ^4D^o_{5/2}$
4056. 404	30s	24645. 42	$5s'\ ^4P_{1/2}$—$8p\ ^4P^o_{3/2}$
4056. 425	25	24645. 29	
4057. 020	30	24641. 67	$5s\ ^4P_{3/2}$—$7p\ ^4P^o_{5/2}$
4058. 406	75	24633. 26	$5s\ ^4P_{3/2}$—$7p\ ^4P^o_{3/2}$
4064. 150	4	24598. 44	$5s'\ ^4P_{1/2}$—$4f'\ [2]^o_{3/2}$
4075. 503	50	24529. 92	$5s''\ ^2P_{1/2}$—$7p''\ ^2P^o_{3/2}$
4076. 956	75	24521. 18	$5s'\ ^2P_{1/2}$—$7p''\ ^2P^o_{1/2}$
4083. 149	50	24483. 99	$5s'\ ^2P_{3/2}$—$8p\ ^4D^o_{3/2}$

See footnotes at end of table.

TABLE A2. *Observed lines of* Br I—Continued

Wavelength	Intensity	Wave number	Classification
Å		K	
4094. 643	35	24415. 26	$5s'\ ^2P_{3/2}—8p\ ^4P^\circ_{1/2}$
4106. 352	25	24345. 65	$5s'\ ^2P_{3/2}—8p\ ^4P^\circ_{3/2}$
4113. 132	4	24305. 52	$5s'\ ^2P_{3/2}—8p\ ^4P^\circ_{5/2}$
4114. 165	25	24299. 41	$5s'\ ^2P_{3/2}—4f'\ [2]^\circ_{5/2}$
4124. 233	75	24240. 09	$5s\ ^4P_{3/2}—6p'\ ^4D^\circ_{1/2}$
4143. 974	600	24124. 62	$5s\ ^4P_{3/2}—6p'\ ^4S^\circ_{3/2}$
4157. 425	250	24046. 57	$5s\ ^4P_{3/2}—6p'\ ^2D^\circ_{3/2}$
4164. 158	4	24007. 69	$5s'\ ^4P_{1/2}—5f\ [1]^\circ_{3/2}$
4164. 270	15	24007. 04	$5s'\ ^4P_{1/2}—5f\ [1]^\circ_{1/2}$
4168. 115	10	23984. 90	$5s'\ ^4P_{1/2}—5f\ [2]^\circ_{3/2}$
4175. 786	50	23940. 84	$5s\ ^4P_{3/2}—6p'\ ^2D^\circ_{5/2}$
4179. 322	100	23920. 58	$5s''\ ^2P_{1/2}—7p'\ ^4D^\circ_{1/2}$
4191. 935	50	23848. 61	$5s''\ ^2P_{1/2}—7p'\ ^2D^\circ_{3/2}$
4196. 468	50	23822. 85	$5s\ ^4P_{5/2}—(^1D_2)5p\ ^3P^\circ_{3/2}$
4199. 473	35	23805. 80	$5s\ ^4P_{3/2}—6p'\ ^2S^\circ_{1/2}$
4202. 487	450	23788. 73	$5s\ ^4P_{5/2}—(^1D_2)5p\ ^2F^\circ_{7/2}$
4220. 701	5*h*	23686. 08	$5s'\ ^2P_{3/2}—5f\ [2]^\circ_{5/2}$
4220. 859	2	23685. 19	$5s'\ ^2P_{3/2}—5f\ [2]^\circ_{3/2}$
4231. 643	4	23624. 83	$5s\ ^4P_{5/2}—(^1D_2)5p\ ^2F^\circ_{5/2}$
4240. 366	40	23576. 23	$5s\ ^4P_{3/2}—(^1D_2)5p\ ^2D^\circ_{5/2}$
4248. 414	50	23531. 57	$5s\ ^4P_{3/2}—(^1D_2)5p\ ^2D^\circ_{3/2}$
4250. 818	40	23518. 26	$5s\ ^4P_{3/2}—4f\ [1]^\circ_{3/2}$
4250. 924	15	23517. 68	$5s\ ^4P_{3/2}—4f\ [1]^\circ_{1/2}$
4260. 625	40	23464. 13	$5s\ ^4P_{3/2}—4f\ [2]^\circ_{5/2}$
4261. 964	3	23456. 76	$5s\ ^4P_{3/2}—4f\ [2]^\circ_{3/2}$
4334. 54	20	23064. 01	$5s'\ ^4P_{1/2}—6p''\ ^2P^\circ_{3/2}$
4342. 45	2	23022. 00	$5s'\ ^4P_{1/2}—6p''\ ^2P^\circ_{1/2}$
4365. 14	2000	22902. 34	$5s'\ ^4P_{1/2}—7p\ ^4D^\circ_{3/2}$
4369. 22	75	22880. 95	$5s'\ ^4P_{1/2}—7p\ ^4P^\circ_{1/2}$
4391. 60	800	22764. 35	$5s'\ ^2P_{3/2}—6p''\ ^2P^\circ_{3/2}$
4399. 73	450	22722. 28	$5s'\ ^2P_{3/2}—6p''\ ^2P^\circ_{1/2}$
4404. 57	10	22697. 32	$5s''\ ^2P_{1/2}—8p\ ^4D^\circ_{3/2}$
4412. 49	100	22656. 58	$5s'\ ^4P_{1/2}—7p\ ^4P^\circ_{3/2}$
4423. 03	200	22602. 59	$5s'\ ^2P_{3/2}—7p\ ^4D^\circ_{3/2}$
4425. 14	1500	22591. 81	$5s\ ^4P_{3/2}—(^1D_2)5p\ ^2P^\circ_{1/2}$
4427. 20	40	22581. 30	$5s'\ ^2P_{3/2}—7p\ ^4P^\circ_{1/2}$
4431. 59	1	22558. 93	$5s''\ ^2P_{1/2}—8p\ ^4P^\circ_{3/2}$
4441. 74	10000	22507. 38	$5s\ ^4P_{5/2}—6p\ ^4D^\circ_{3/2}$
[b]4446. 08	15	22485. 41	$5s'\ ^2P_{3/2}—7p\ ^4D^\circ_{5/2}$
4466. 21	200	22384. 07	$5s\ ^4P_{5/2}—6p\ ^4D^\circ_{5/2}$
4469. 98	150	22365. 19	$5s'\ ^2P_{3/2}—7p\ ^4P^\circ_{5/2}$
4471. 67	80	22356. 74	$5s'\ ^2P_{3/2}—7p\ ^4P^\circ_{3/2}$
4472. 61	10000	22352. 04	$5s\ ^4P_{3/2}—(^1D_2)5p\ ^2P^\circ_{3/2}$
4477. 72	20000	22326. 53	$5s\ ^4P_{5/2}—6p\ ^4D^\circ_{7/2}$
4490. 42	1000	22263. 39	$5s'\ ^4P_{1/2}—6p'\ ^4D^\circ_{1/2}$
4513. 44	3000	22149. 84	$5s\ ^4P_{5/2}—6p\ ^4P^\circ_{3/2}$
4513. 82	150	22147. 97	$5s'\ ^4P_{1/2}—6p'\ ^4S^\circ_{3/2}$
4525. 59	15000	22090. 37	$5s\ ^4P_{5/2}—6p\ ^4P^\circ_{5/2}$
4529. 79	600	22069. 89	$5s'\ ^4P_{1/2}—6p'\ ^2D^\circ_{3/2}$
4575. 74	3000	21848. 27	$5s'\ ^2P_{3/2}—6p'\ ^4S^\circ_{3/2}$
4592. 16	200	21770. 15	$5s'\ ^2P_{3/2}—6p'\ ^2D^\circ_{3/2}$
4614. 58	2500	21664. 38	$5s'\ ^2P_{3/2}—6p'\ ^2D^\circ_{5/2}$
4640. 92	40	21541. 42	$5s'\ ^4P_{1/2}—4f\ [1]^\circ_{3/2}$
4641. 02	70	21540. 96	$5s'\ ^4P_{1/2}—4f\ [1]^\circ_{1/2}$
4643. 52	900	21529. 36	$5s'\ ^2P_{3/2}—6p'\ ^2S^\circ_{1/2}$

See footnotes at end of table.

TABLE A2. *Observed lines of* Br I—Continued

Wavelength	Intensity	Wave number	Classification
Å		K	
[b]4654. 18	25	21480. 05	$5s'\ ^4P_{1/2}—4f\ [2]^\circ_{3/2}$
4693. 56	300	21299. 83	$5s'\ ^2P_{3/2}—(^1D_2)5p\ ^2D^\circ_{5/2}$
4703. 42	50	21255. 18	$5s'\ ^2P_{3/2}—(^1D_2)5p\ ^2D^\circ_{3/2}$
4706. 36	12*h*	21241. 90	$5s'\ ^2P_{3/2}—4f\ [1]^\circ_{3/2}$
4720. 03	100	21180. 38	$5s'\ ^2P_{3/2}—4f\ [2]^\circ_{3/2}$
4722. 97	9	21167. 20	$5s'\ ^2P_{3/2}—4f\ [3]^\circ_{5/2}$
4752. 28	2500	21036. 65	$5s\ ^4P_{3/2}—6p\ ^4D^\circ_{3/2}$
4765. 63	250	20977. 72	$5s''\ ^2P_{1/2}—6p''\ ^2P^\circ_{3/2}$
4775. 20	750	20935. 68	$5s''\ ^2P_{1/2}—6p''\ ^2P^\circ_{1/2}$
4780. 31	4000	20913. 30	$5s\ ^4P_{3/2}—6p\ ^4D^\circ_{5/2}$
4785. 19	1600	20891. 97	$5s\ ^4P_{3/2}—6p\ ^4P^\circ_{1/2}$
4802. 67	250	20815. 93	$5s''\ ^2P_{1/2}—7p\ ^4D^\circ_{3/2}$
4807. 61	350	20794. 54	$5s''\ ^2P_{1/2}—7p\ ^4P^\circ_{1/2}$
4834. 46	500	20679. 06	$5s\ ^4P_{3/2}—6p\ ^4P^\circ_{3/2}$
4848. 39	25	20619. 64	$5s\ ^4P_{3/2}—6p\ ^4P^\circ_{5/2}$
4860. 04	250	20570. 22	$5s''\ ^2P_{1/2}—7p\ ^4P^\circ_{3/2}$
4906. 49	10	20375. 48	$5s'\ ^4P_{1/2}—(^1D_2)5p\ ^2P^\circ_{3/2}$
4920. 98	300	20315. 48	$5s'\ ^2P_{3/2}—(^1D_2)5p\ ^2P^\circ_{1/2}$
4921. 80	10*w*	20312. 10	
4954. 73	300	20177. 10	$5s''\ ^2P_{1/2}—6p'\ ^4D^\circ_{1/2}$
4979. 76	4000	20075. 69	$5s'\ ^2P_{3/2}—(^1D_2)5p\ ^2P^\circ_{3/2}$
4983. 25	75	20061. 63	$5s''\ ^2P_{1/2}—6p'\ ^4S^\circ_{3/2}$
5002. 72	500	19983. 55	$5s''\ ^2P_{1/2}—6p'\ ^2D^\circ_{3/2}$
5029. 37	200	19877. 66	$5s'\ ^2P_{3/2}—(^1D_2)5p\ ^2F^\circ_{5/2}$
5063. 74	40	19742. 75	$5s''\ ^2P_{1/2}—6p'\ ^2S^\circ_{1/2}$
5092. 60	4	19630. 86	
5138. 55	10	19455. 32	$5s''\ ^2P_{1/2}—4f\ [1]^\circ_{3/2}$
5139. 47	10*w*	19451. 84	
5148. 78	10	19416. 67	$5p\ ^4P^\circ_{5/2}—6d''\ ^2D_{5/2}$
5150. 47	6*h*	19410. 30	$5p\ ^4P^\circ_{5/2}—6d''\ ^2D_{3/2}$
5220. 71	8	19149. 15	$5p\ ^4P^\circ_{5/2}—10d\ ^4D_{3/2}$
5222. 32	12	19143. 25	$5p\ ^4P^\circ_{5/2}—10d\ ^4D_{5/2}$
5226. 91	20	19126. 44	$5p\ ^4P^\circ_{5/2}—10d\ ^4D_{7/2}$
5241. 43	5	19073. 45	$5p\ ^4P^\circ_{5/2}—6d''\ ^2D_{3/2}$
5245. 12	350	19060. 04	$5s'\ ^4P_{1/2}—6p\ ^4D^\circ_{3/2}$
5261. 80	5	18999. 62	$5p\ ^4P^\circ_{5/2}—(^1D_2)4d\ ^2F_{5/2}$
5285. 23	50	18915. 39	$5s'\ ^4P_{1/2}—6p\ ^4P^\circ_{1/2}$
5297. 32	15	18872. 22	$5p\ ^4P^\circ_{5/2}—11s\ ^4P_{5/2}$
5314. 18	10	18812. 34	$5p\ ^4P^\circ_{5/2}—10d\ ^4D_{3/2}$
5315. 85	8	18806. 44	$5p\ ^4P^\circ_{5/2}—10d\ ^4D_{5/2}$
5317. 25	20	18801. 48	$5p\ ^4P^\circ_{5/2}—6d'\ ^4P_{5/2}$
5318. 83	7	18795. 90	$5p\ ^4D^\circ_{7/2}—12d\ ^4F_{9/2}$
5323. 20	12	18780. 47	$5p\ ^4P^\circ_{5/2}—6d'\ ^4P_{3/2}$
5328. 92	200	18760. 31	$5s'\ ^2P_{1/2}—6p\ ^4D^\circ_{3/2}$
5329. 30	12	18758. 97	$5p\ ^4P^\circ_{5/2}—9d\ ^4F_{7/2}$
5337. 10	40	18731. 56	$5p\ ^4P^\circ_{5/2}—9d\ ^4D_{7/2}$
5345. 42	600	18702. 40	$5s'\ ^4P_{1/2}—6p\ ^4P^\circ_{3/2}$
5348. 29	10	18692. 37	$5p\ ^4P^\circ_{5/2}—(^1D_2)4d\ ^2S_{1/2}$
5354. 67	120	18670. 09	$5p\ ^4P^\circ_{5/2}—6d'\ ^2F_{5/2}$
5356. 74	12*w*	18662. 88	$5p\ ^4P^\circ_{3/2}—(^1D_2)4d\ ^2F_{5/2}$
5364. 19	300	18636. 96	$5s'\ ^2P_{3/2}—6p\ ^4D^\circ_{5/2}$
5370. 34	300	18615. 62	$5s'\ ^2P_{3/2}—6p\ ^4P^\circ_{1/2}$
5379. 13	15	18585. 20	$5p\ ^4D^\circ_{7/2}—11d\ ^4F_{9/2}$
5382. 96	120	18571. 98	$5p\ ^4P^\circ_{5/2}—6d'\ ^2F_{7/2}$
5384. 27	8	18567. 46	$5p\ ^4D^\circ_{7/2}—6d''\ ^2D_{5/2}$

See footnotes at end of table.

TABLE A2. *Observed lines of* Br I—Continued

Wavelength	Intensity	Wave number	Classification
Å		K	
5393. 58	7	18535. 41	$5p\ ^4P^3_{3/2}$—$11s\ ^4P_{5/2}$
5395. 48	1200	18528. 88	$5s''\ ^2P_{1/2}$—$(^1D_2)5p\ ^2P^1_{1/2}$
5395. 55	900	18528. 64	
5414. 26	4	18464. 61	$5p\ ^4P^3_{3/2}$—$6d'\ ^4P_{5/2}$
5420. 43	13	18443. 59	$5p\ ^4P^3_{5/2}$—$6d'\ ^4P_{3/2}$
5420. 80	18	18442. 33	$5p\ ^4P^3_{3/2}$—$9d\ ^4P_{1/2}$
5424. 61	8*h*	18429. 38	$5p\ ^4D^3_{3/2}$—$11d\ ^4F_{7/2}$
5432. 47	60	18402. 72	$5s'\ ^2P_{3/2}$—$6p\ ^4P^3_{3/2}$
5434. 22	7	18396. 79	$5p\ ^4P^3_{3/2}$—$9d\ ^4D_{5/2}$
5450. 09	550	18343. 22	$5s'\ ^2P_{3/2}$—$6p\ ^4P^3_{5/2}$
5453. 03	90	18333. 33	$5p\ ^4P^3_{3/2}$—$6d'\ ^2F_{5/2}$
5455. 16	60	18326. 17	$5p\ ^4P^3_{3/2}$—$9d\ ^4D_{3/2}$
5455. 96	70	18323. 49	$5p\ ^4P^3_{3/2}$—$10s\ ^4P_{5/2}$
5463. 72	80	18297. 46	$5p\ ^4D^3_{7/2}$—$10d\ ^4F_{9/2}$
5466. 22	1200	18289. 10	$5s''\ ^2P_{1/2}$—$(^1D_2)5p\ ^2P^3_{3/2}$
5469. 76	15	18277. 26	$5p\ ^4D^3_{7/2}$—$10d\ ^4D_{7/2}$
5470. 90	5	18273. 45	$5p\ ^4P^3_{3/2}$—$9d\ ^4D_{1/2}$
5504. 46	35*h*	18162. 04	$5p\ ^4D^3_{5/2}$—$10d\ ^4F_{7/2}$
5520. 86	20	18108. 09	$5p\ ^4P^3_{5/2}$—$6d'\ ^2P_{3/2}$
5522. 53	90	18102. 61	$5p\ ^4P^3_{5/2}$—$8d\ ^4D_{3/2}$
5529. 01	175	18081. 40	$5p\ ^4P^3_{5/2}$—$8d\ ^4D_{5/2}$
5532. 22	100	18070. 91	$5p\ ^4P^3_{5/2}$—$8d\ ^4F_{5/2}$
5536. 37	300	18057. 36	$5p\ ^4P^3_{5/2}$—$8d\ ^4D_{7/2}$
5544. 72	6	18030. 17	$5p\ ^4P^3_{3/2}$—$10s\ ^4P_{3/2}$
5546. 90	20	18023. 08	$5p\ ^4D^3_{7/2}$—$11s\ ^4P_{5/2}$
5558. 13	40	17986. 67	$5p\ ^4P^3_{3/2}$—$10s\ ^4P_{5/2}$
5558. 40	10	17985. 79	$5p\ ^4D^3_{5/2}$—$(^1D_2)4d\ ^2F_{7/2}$
5588. 17	160	17889. 98	$5p\ ^4D^3_{7/2}$—$9d\ ^4F_{9/2}$
5590. 56	50	17882. 33	$5p\ ^4D^3_{7/2}$—$9d\ ^4D_{7/2}$
5597. 26	15	17860. 93	$5p\ ^4D^3_{5/2}$—$11s\ ^4P_{3/2}$
5602. 41	8*h*	17844. 51	$5p\ ^4P^3_{3/2}$—$8d\ ^4F_{3/2}$ $5p\ ^4P^3_{5/2}$—$(^1D_2)4d\ ^2D_{3/2}$
5604. 96	4	17836. 39	$5p\ ^4P^1_{1/2}$—$(^1D_2)4d\ ^2P_{1/2}$
5609. 83	10*h*	17820. 91	$5p\ ^4D^3_{7/2}$—$6d'\ ^2F_{5/2}$
5611. 62	125	17815. 22	$5p\ ^4P^3_{3/2}$—$8d\ ^4P_{1/2}$
5627. 24	200	17765. 77	$5p\ ^4P^3_{3/2}$—$8d\ ^4D_{3/2}$
5633. 97	140	17744. 55	$5p\ ^4P^3_{3/2}$—$8d\ ^4D_{5/2}$
5637. 27	130	17734. 16	$5p\ ^4D^3_{5/2}$—$9d\ ^4F_{7/2}$
5640. 86	35	17722. 87	$5p\ ^4D^3_{7/2}$—$6d'\ ^2F_{7/2}$
5645. 31	30	17708. 90	$5p\ ^4D^3_{5/2}$—$9d\ ^4D_{5/2}$
5645. 97	45	17706. 83	$5p\ ^4D^3_{5/2}$—$9d\ ^4D_{7/2}$
5667. 75	9	17638. 79	$5p\ ^4P^1_{1/2}$—$6d'\ ^4P_{3/2}$
5667. 92	8	17638. 26	$5p\ ^4D^3_{3/2}$—$9d\ ^4D_{3/2}$
5685. 77	15*W*	17582. 89	$(^1D_2)5s\ ^2D_{3/2}$—$7p''\ ^2P^1_{1/2}$
5697. 29	18	17547. 34	$5p\ ^4D^3_{3/2}$—$6d'\ ^2F_{7/2}$
5705. 74	85	17521. 35	$5p\ ^4P^1_{1/2}$—$9d\ ^4D_{3/2}$
5709. 44	9	17509. 99	$5p\ ^4P^3_{5/2}$—$9s\ ^4P_{3/2}$
5716. 26	225	17489. 10	$5p\ ^4P^3_{5/2}$—$9s\ ^4P_{5/2}$
5721. 11	100	17474. 28	$5p\ ^4D^3_{7/2}$—$10s\ ^4P_{5/2}$
5722. 97	40*h*	17468. 60	$5p\ ^4P^1_{1/2}$—$9d\ ^4D_{1/2}$
5764. 66	45	17342. 27	$5p\ ^4D^3_{5/2}$—$10s\ ^4P_{3/2}$
5771. 30	5	17322. 31	$5p\ ^4D^3_{7/2}$—$8d\ ^4F_{7/2}$
5777. 69	10	17303. 16	$5p\ ^4P^1_{1/2}$—$6d'\ ^2P_{3/2}$
5779. 97	4	17296. 33	
5783. 32	500	17286. 31	$5p\ ^4D^3_{7/2}$—$8d\ ^4F_{9/2}$
5784. 02	30	17284. 22	$5p\ ^4P^3_{5/2}$—$7d\ ^4F_{5/2}$

TABLE A2. *Observed lines of* Br I—Continued

Wavelength	Intensity	Wave number	Classification
Å		K	
5793. 98	100	17254. 51	$5p\ ^4P^3_{3/2}$—$7d\ ^4F_{3/2}$
5801. 50	40	17232. 14	$5p\ ^4D^2_{7/2}$—$8d\ ^4D_{5/2}$
5803. 82	30	17225. 26	$5p\ ^4P^1_{1/2}$—$10s\ ^4P_{3/2}$
5805. 04	30	17221. 64	$5p\ ^4D^2_{3/2}$—$8d\ ^4F_{5/2}$
5809. 59	250	17208. 15	$5p\ ^4D^2_{7/2}$—$8d\ ^4D_{7/2}$
5819. 56	80	17178. 67	$5p\ ^4P^1_{1/2}$—$6d'\ ^2P_{1/2}$
5821. 45	12	17173. 09	$5p\ ^4P^3_{3/2}$—$9s\ ^4P_{3/2}$
5826. 07	5	17159. 47	
5827. 08	10	17156. 50	$5p\ ^4D^3_{5/2}$—$8d\ ^4F_{3/2}$
5828. 51	150	17152. 29	$5p\ ^4P^3_{3/2}$—$9s\ ^4P_{5/2}$
5828. 89	7	17151. 17	
5830. 39	400	17146. 76	$5p\ ^4D^3_{5/2}$—$8d\ ^4F_{7/2}$
5833. 39	900	17137. 94	$5p\ ^4P^3_{5/2}$—$7d\ ^4D_{5/2}$
5836. 84	150	17127. 81	$5p\ ^4P^3_{5/2}$—$7d\ ^4D_{3/2}$
5852. 08	1800	17083. 21	$5p\ ^4P^3_{5/2}$—$7d\ ^4D_{7/2}$
5861. 20	120	17056. 62	$5p\ ^4D^3_{5/2}$—$8d\ ^4D_{5/2}$
5864. 82	90	17046. 10	$5p\ ^4D^3_{5/2}$—$8d\ ^4F_{5/2}$
5867. 05	60	17039. 62	$5p\ ^4P^1_{1/2}$—$8a\ ^4F_{3/2}$
5869. 47	18	17032. 59	$5p\ ^4D^3_{5/2}$—$8d\ ^4D_{7/2}$
5877. 15	50*w*	17010. 34	$5p\ ^4P^1_{1/2}$—$8d\ ^4P_{1/2}$
5886. 87	60*cw*	16982. 25	$(^1D_2)5s\ ^2D_{3/2}$—$7p'\ ^4D^1_{1/2}$
5889. 87	60	16973. 60	$5s''\ ^2P_{1/2}$—$6p\ ^4D^3_{3/2}$
5894. 28	18	16960. 90	$5p\ ^4P^1_{1/2}$—$8d\ ^4D_{3/2}$
5898. 32	8	16949. 28	$(^1D_2)5s\ ^2D_{5/2}$—$7p'\ ^4S^3_{3/2}$
5898. 51	8*d*	16948. 74	
5898. 96	90	16947. 44	$5p\ ^4P^3_{3/2}$—$7d\ ^4F_{5/2}$
5905. 45	900	16928. 82	$5p\ ^4P^3_{5/2}$—$(^1S_0)5s\ ^2S_{1/2}$; $5p\ ^4D^3_{3/2}$—$(^1D_2)4d\ ^2F_{5/2}$
[c] 5905. 66	80	16928. 22	$(^1D_2)5s\ ^2D_{5/2}$—$7p'\ ^2D^3_{3/2}$
5909. 31	250	16917. 76	$5p\ ^4P^3_{3/2}$—$7d\ ^4F_{3/2}$
5937. 85	90	16836. 45	$5p\ ^4P^1_{1/2}$—$8d\ ^4D_{1/2}$
5940. 48	1600	16828. 99	$5s''\ ^2P_{1/2}$—$6p\ ^4P^1_{1/2}$
5943. 71	140	16819. 85	$5p\ ^4D^3_{3/2}$—$(^1D_2)4d\ ^2D_{3/2}$
5945. 50	600	16814. 78	$5p\ ^4P^3_{3/2}$—$7d\ ^4P_{1/2}$
5950. 32	750	16801. 16	$5p\ ^4P^3_{3/2}$—$7d\ ^4D_{5/2}$
5953. 92	750	16791. 01	$5p\ ^4P^3_{3/2}$—$7d\ ^4D_{3/2}$
5982. 90	12	16709. 67	$5p\ ^4D^3_{3/2}$—$6d'\ ^4P_{3/2}$
5983. 35	5	16708. 42	$5p\ ^4D^3_{3/2}$—$9a\ ^4P_{1/2}$
5985. 32	125	16702. 92	$5p\ ^4P^1_{1/2}$—$(^1D_2)4d\ ^2D_{3/2}$
5992. 89	100	16681. 82	$5p\ ^4P^5_{5/2}$—$7d\ ^4D_{1/2}$
5999. 73	95	16662. 80	$5p\ ^4D^3_{3/2}$—$9d\ ^4D_{5/2}$
6007. 96	200	16639. 98	$5p\ ^4D^2_{7/2}$—$9s\ ^4P_{5/2}$
6018. 17	200	16611. 75	$5p\ ^4P^5_{3/2}$—$7s'\ ^2P_{3/2}$
6022. 66	30	16599. 36	$5p\ ^4D^3_{3/2}$—$6d'\ ^2F_{5/2}$
6025. 24	10*h*	16592. 25	$5p\ ^4D^3_{3/2}$—$9d\ ^4D_{3/2}$
6057. 87	200	16502. 88	$5p\ ^4P^5_{5/2}$—$5d''\ ^2D_{5/2}$
6064. 35	200	16485. 25	$5p\ ^4D^3_{5/2}$—$9s\ ^4P_{3/2}$
6067. 36	5	16477. 07	$5p\ ^4D^2_{7/2}$—$(^1D_2)4d\ ^2G_{7/2}$
6095. 74	700	16400. 36	$5p\ ^4D^2_{7/2}$—$(^1D_2)4d\ ^2G_{9/2}$
6107. 69	125	16368. 27	$5p\ ^4P^1_{1/2}$—$9s\ ^4P_{3/2}$
6111. 10	80	16359. 14	$5p\ ^4D^2_{7/2}$—$7d\ ^4F_{7/2}$
6116. 19	60	16345. 52	$5p\ ^4D^3_{3/2}$—$(^1D_2)4d\ ^2D_{5/2}$
6118. 80	300	16338. 55	$5p\ ^4P^3_{3/2}$—$7s'\ ^4P_{1/2}$
6122. 14	2400	16329. 64	$5p\ ^4D^2_{7/2}$—$7d\ ^4F_{9/2}$
6122. 35	100	16329. 08	$5p\ ^4P^3_{5/2}$—$5d''\ ^2D_{3/2}$
6126. 53	30*W*	16317. 94	$(^1D_2)5s\ ^2D_{5/2}$—$6f\ [4]^1_{7/2}$

See footnotes at end of table.

TABLE A2. *Observed lines of* Br I—Continued

Wavelength	Intensity	Wave number	Classification
Å		K	
6132.71	800	16301.49	$5p\ ^4D^o_{5/2}$—$(^1D_2)4d\ ^2G_{7/2}$
6134.71	75	16296.18	$5p\ ^4D^o_{3/2}$—$10s\ ^4P_{3/2}$
6137.49	150	16288.80	$5p\ ^4D^o_{7/2}$—$7d\ ^4D_{5/2}$
6141.04	100*w*	16279.38	$(^1D_2)5s\ ^2D_{3/2}$—$6f\ [3]^o_{5/2}$
6142.73	100	16274.90	$5p\ ^4P^o_{3/2}$—$7s'\ ^2P_{3/2}$
6148.60	40000	16259.37	$5s\ ^4P_{5/2}$—$5p''\ ^2P^o_{3/2}$
[d] 6151.10	50*d*	16252.76	$5p\ ^4D^o_{3/2}$—$10s\ ^4P_{5/2}$
6158.19	750	16234.05	$5p\ ^4D^o_{7/2}$—$7d\ ^4D_{7/2}$
6177.39	2000	16183.59	$5p\ ^4D^o_{5/2}$—$7d\ ^4F_{7/2}$
6184.09	200	16166.05	$5p\ ^4P^o_{3/2}$—$5d''\ ^2D_{5/2}$
6199.74	50	16125.25	$5p\ ^4P^o_{5/2}$—$8s\ ^4P_{3/2}$
6203.08	900	16116.56	$5p\ ^4P^o_{3/2}$—$8s\ ^4P_{5/2}$
6204.35	90	16113.27	$5p\ ^4D^o_{5/2}$—$7d\ ^4D_{5/2}$
6204.49	90	16112.90	$5p\ ^4P^o_{1/2}$—$7d\ ^4F_{3/2}$
6205.40	120	16110.54	$5p\ ^4D^o_{5/2}$—$8d\ ^4F_{3/2}$
6208.26	100	16103.12	$5p\ ^4D_{5/2}$—$7d\ ^4D_{3/2}$
6216.71	5	16081.23	$5p\ ^4D^o_{3/2}$—$8d\ ^4P_{1/2}$
6225.51	65	16058.50	$5p\ ^4D^o_{3/2}$—$7d\ ^4D_{7/2}$
6235.87	10	16031.82	$5p\ ^4D^o_{3/2}$—$8d\ ^4D_{3/2}$
6244.39	400	16009.95	$5p\ ^4P^o_{1/2}$—$7d\ ^4P_{1/2}$
6248.24	200	16000.08	$5p\ ^4D^o_{3/2}$—$8d\ ^4F_{5/2}$
6251.32	300	15992.20	$5p\ ^4P^o_{3/2}$—$5d''\ ^2D_{3/2}$
6253.69	400	15986.14	$5p\ ^4P^o_{1/2}$—$7d\ ^4D_{3/2}$
6282.46	600	15912.93	$5p\ ^4P^o_{5/2}$—$5d'\ ^4P_{5/2}$
6284.69	8	15907.28	$5p'\ ^2S^o_{1/2}$—$8s'\ ^4P_{1/2}$ $5p\ ^4D^o_{3/2}$—$8d\ ^4D_{1/2}$
6290.13	550	15893.53	$5p\ ^4P^o_{5/2}$—$5d'\ ^2F_{5/2}$
6296.71	700	15876.92	$5p\ ^4P^o_{1/2}$—$7d\ ^4D_{1/2}$
6301.36	275	15865.20	$5p\ ^4P^o_{5/2}$—$5d'\ ^4P_{3/2}$
6315.12	5	15830.63	$5p'\ ^2S^o_{1/2}$—$8s'\ ^2P_{3/2}$
6331.99	300	15788.46	$5p\ ^4P^o_{3/2}$—$8s\ ^4P_{3/2}$
6335.48	1500	15779.76	$5p\ ^4P^o_{3/2}$—$8s\ ^4P_{5/2}$
6336.39	300	15777.49	$(^1D_2)5s\ ^2D_{5/2}$—$8p\ ^4D^o_{3/2}$
6336.56	500	15777.07	
6337.85	60	15773.86	$5p\ ^4D^o_{3/2}$—$(^1D_2)4d\ ^2D_{3/2}$
6343.79	35*w*	15759.09	$(^1D_2)5s\ ^2D_{3/2}$—$8p\ ^4D^o_{3/2}$
6345.30	500	15755.34	$5p\ ^4P^o_{5/2}$—$5d'\ ^2F_{7/2}$
6349.82	500	15744.12	$5p\ ^4P^o_{5/2}$—$6d\ ^4F_{3/2}$
6350.73	60000	15741.87	$5s\ ^4P_{5/2}$—$5p'\ ^4S^o_{3/2}$
6371.60	200*W*	15690.31	$(^1D_2)5s\ ^2D_{3/2}$—$8p\ ^4P^o_{1/2}$
6392.57	35*W*	15638.84	$(^1D_2)5s\ ^2D_{5/2}$—$8p\ ^4P^o_{3/2}$
6398.03	30	15625.49	$5p'\ ^2S^o_{1/2}$—$(^1D_2)4d\ ^2S_{1/2}$
6399.99	10*w*	15620.71	$(^1D_2)5s\ ^2D_{3/2}$—$8p\ ^4P^o_{3/2}$
6405.52	3	15607.22	
6405.58	4	15607.07	
6405.68	6	15606.83	$(^1D_2)5s\ ^2D_{5/2}$—$4f'\ [4]^o_{7/2}$
6405.80	8	15606.54	
6410.32	2500	15595.53	$5p\ ^4P^o_{5/2}$—$6d\ ^4F_{7/2}$
6418.29	45	15576.17	$5p\ ^4P^o_{3/2}$—$5d'\ ^4P_{5/2}$
6418.96	15*s*	15574.54	$(^1D_2)5s\ ^2D_{3/2}$—$4f''\ [2]^o_{5/2}$
6419.03	15	15574.37	
6426.30	500	15556.75	$5p\ ^4P^o_{5/2}$—$5d'\ ^2F_{5/2}$
6435.81	15	15533.77	$5p\ ^4P^o_{1/2}$—$7s'\ ^4P_{1/2}$
6436.60	10	15531.86	
6438.02	600	15528.43	$5p\ ^4P^o_{3/2}$—$5d'\ ^4P_{3/2}$
6458.92	25*h*	15478.19	$5p\ ^4D^o_{3/2}$—$5d''\ ^2D_{3/2}$

See footnotes at end of table.

TABLE A2. *Observed lines of* Br I—Continued

Wavelength	Intensity	Wave number	Classification
Å		K	
6462. 32	500	15470. 04	$5p\ ^4P^{\circ}_{1/2}$—$7s'\ ^2P_{3/2}$
6470. 41	200	15450. 70	$5p\ ^4P^{\circ}_{3/2}$—$5d'\ ^2P_{3/2}$
6475. 23	100*h*	15439. 20	$5p\ ^4D^{\circ}_{3/2}$—$9s\ ^4P_{3/2}$
6483. 56	1800	15419. 36	$5p\ ^4P^{\circ}_{3/2}$—$6d\ ^4P_{1/2}$
6483. 96	35	15418. 41	$5p\ ^4D^{\circ}_{5/2}$—$9s\ ^4P_{5/2}$
6488. 62	800	15407. 34	$5p\ ^4P^{\circ}_{5/2}$—$6d\ ^4F_{3/2}$
6493. 80	20*h*	15395. 05	$5p'\ ^2D^{\circ}_{5/2}$—$8s'\ ^2P_{3/2}$
6501. 51	4	15376. 79	$5p'\ ^2S^{\circ}_{1/2}$—$6d'\ ^4P_{3/2}$
6514. 32	12	15346. 56	$5p\ ^4D^{\circ}_{3/2}$—$7s''\ ^2P_{1/2}$
6514. 62	1000	15345. 85	$5p\ ^4P^{\circ}_{3/2}$—$6d\ ^4F_{5/2}$
[b] 6531. 39	70	15306. 45	$5p'\ ^2D^{\circ}_{3/2}$—$8s'\ ^4P_{1/2}$
6532. 29	600	15304. 34	$5p\ ^4D^{\circ}_{5/2}$—$5d''\ ^2D_{3/2}$
6541. 30	600	15283. 26	$5p\ ^4P^{\circ}_{3/2}$—$5d'\ ^2P_{1/2}$
6544. 57	20000	15275. 62	$5p\ ^4P^{\circ}_{5/2}$—$6d\ ^4D_{5/2}$
6548. 09	1500	15267. 41	$5p\ ^4D^{\circ}_{7/2}$—$8s\ ^4P_{5/2}$
6551. 57	12	15259. 30	$5p'\ ^2S^{\circ}_{1/2}$—$9d\ ^4D_{3/2}$
6559. 80	50000*cw*	15240. 16	$5s\ ^4P_{5/2}$—$5p'\ ^2D^{\circ}_{3/2}$
6571. 31	1000	15213. 46	$5p\ ^4D^{\circ}_{3/2}$—$7d\ ^4F_{5/2}$
6574. 29	15	15206. 57	$5p'\ ^2S^{\circ}_{1/2}$—$9d\ ^4D_{1/2}$
6576. 24	10*W*	15202. 06	
6579. 14	1800	15195. 36	$5p\ ^4P^{\circ}_{5/2}$—$6d\ ^4D_{3/2}$
6579. 36	300	15194. 85	$5p\ ^4D^{\circ}_{3/2}$—$(^1S_0)5s\ ^2S_{1/2}$
6582. 17	20000	15188. 36	$5p\ ^4P^{\circ}_{5/2}$—$6d\ ^4D_{7/2}$
6582. 62	35	15187. 32	$5p\ ^4P^{\circ}_{1/2}$—$5d''\ ^2D_{3/2}$
6584. 14	600	15183. 82	$5p\ ^4D^{\circ}_{3/2}$—$7d\ ^4F_{3/2}$
6589. 62	10*w*	15171. 19	$5p'\ ^2D^{\circ}_{5/2}$—$(^1D_2)4d\ ^2F_{7/2}$
6604. 80	15	15136. 32	$4d\ ^4D_{7/2}$—$10f\ [4]^{\circ}_{9/2}$
6613. 05	4	15117. 44	$5p'\ ^4D^{\circ}_{7/2}$—$8s'\ ^4P_{1/2}$
6620. 47	1500	15100. 50	$5p\ ^4D^{\circ}_{5/2}$—$8s\ ^4P_{3/2}$
6621. 44	8	15098. 29	$5p'\ ^2D^{\circ}_{5/2}$—$(^1D_2)4d\ ^2P_{3/2}$
6624. 26	20	15091. 86	$5p\ ^4D^{\circ}_{5/2}$—$8s\ ^4P_{5/2}$
6629. 09	20	15080. 86	$5p\ ^4D^{\circ}_{3/2}$—$7d\ ^4P_{1/2}$
6631. 62	50000*cw*	15075. 11	$5s\ ^4P_{5/2}$—$5p'\ ^2D^{\circ}_{5/2}$
6635. 10	60	15067. 20	$5p\ ^4D^{\circ}_{3/2}$—$7d\ ^4D_{5/2}$
6636. 62	150	15063. 75	$5p\ ^4D^{\circ}_{7/2}$—$5d'\ ^4P_{5/2}$
6639. 57	40	15057. 06	$5p\ ^4D^{\circ}_{3/2}$—$7d\ ^4D_{3/2}$
6645. 17	40	15044. 37	$5p\ ^4D^{\circ}_{7/2}$—$5d'\ ^2F_{5/2}$
6646. 59	120	15041. 16	$5p'\ ^2S^{\circ}_{1/2}$—$6d'\ ^2P_{3/2}$
6653. 82	15	15024. 81	$5p'\ ^2D^{\circ}_{3/2}$—$(^1D_2)4d\ ^2S_{1/2}$
6666. 93	150	14995. 27	$5p'\ ^2D^{\circ}_{3/2}$—$(^1D_2)4d\ ^2F_{5/2}$
6672. 15	600	14983. 54	$5p\ ^4P^{\circ}_{1/2}$—$8s\ ^4P_{3/2}$
6676. 54	15	14973. 68	$4d\ ^4D_{7/2}$—$5f'\ [3]^{\circ}_{5/2}$ $5p'\ ^2D^{\circ}_{3/2}$—$(^1D_2)4d\ ^2P_{1/2}$
6676. 72	8	14973. 28	$4d\ ^4D_{7/2}$—$5f'\ [3]^{\circ}_{7/2}$
6681. 71	15	14962. 10	$5p'\ ^2D^{\circ}_{5/2}$—$6d'\ ^4P_{5/2}$
6682. 28	20000	14960. 82	$5s\ ^4P_{3/2}$—$5p''\ ^2P^{\circ}_{1/2}$
6684. 17	50	14956. 59	$(^1D_2)5s\ ^2D_{5/2}$—$5f\ [4]^{\circ}_{5/2}$
6684. 23	50	14956. 46	
6684. 33	70	14956. 23	
6687. 33	90	14949. 52	$4d\ ^4D_{7/2}$—$5f'\ [4]^{\circ}_{9/2}$
6688. 08	90	14947. 85	$5p\ ^4D^{\circ}_{3/2}$—$7d\ ^4D_{1/2}$
6690. 35	120*cw*	14942. 78	$(^1D_2)5s\ ^2D_{3/2}$—$5f\ [3]^{\circ}_{7/2}$
6692. 13	10000	14938. 80	$5p\ ^4P^{\circ}_{3/2}$—$6d\ ^4D_{5/2}$
6694. 62	10	14933. 24	$5p'\ ^2D^{\circ}_{3/2}$—$(^1D_2)4d\ ^2P_{3/2}$
6700. 71	60*h*	14919. 67	$5p'\ ^2D^{\circ}_{5/2}$—$9d\ ^4F_{7/2}$
6702. 07	110	14916. 65	$5p'\ ^2S^{\circ}_{1/2}$—$6d'\ ^2P_{1/2}$

See footnotes at end of table.

TABLE A2. *Observed lines of* Br I—Continued

Wavelength	Intensity	Wave number	Classification
Å		K	
6706. 79	60	14906. 15	$5p\ ^4D^{\frac{9}{2}}_{7/2}$—$5d'\ ^2F_{7/2}$
6712. 12	30	14894. 31	$5p'\ ^2D^{\frac{5}{2}}_{5/2}$—$9d\ ^4D_{5/2}$
6713. 06	125	14892. 23	$5p'\ ^2D^{\frac{5}{2}}_{5/2}$—$9d\ ^4D_{7/2}$
6714. 86	90	14888. 23	$5p\ ^4D^{\frac{3}{2}}_{3/2}$—$5d'\ ^4P_{5/2}$
6719. 97	8	14876. 91	
6720. 68	75*h*	14875. 34	$4d\ ^4D_{7/2}$—$9f\ [4]^{\frac{9}{2}}_{5/2}$
6723. 65	400	14868. 77	$5p\ ^4D^{\frac{5}{2}}_{5/2}$—$5d'\ ^2F_{5/2}$
6728. 28	8000	14858. 54	$5p\ ^4P^{\frac{3}{2}}_{3/2}$—$6d\ ^4D_{3/2}$
6738. 61	100	14835. 76	$5p'\ ^4D^{\frac{1}{2}}_{1/2}$—$(^1D_2)4d\ ^2S_{1/2}$
6739. 66	8	14833. 45	$5p\ ^4D^{\frac{7}{2}}_{7/2}$—$6d\ ^4F_{5/2}$
6740. 83	5	14830. 87	$5p'\ ^2D^{\frac{5}{2}}_{5/2}$—$6d'\ ^2F_{5/2}$
6752. 67	6	14804. 87	$5p'\ ^4S^{\frac{3}{2}}_{3/2}$—$8s'\ ^4P_{1/2}$
6760. 06	2000	14788. 69	$5s\ ^4P_{3/2}$—$5p''\ ^2P^{\frac{3}{2}}_{3/2}$
6761. 92	25	14784. 62	$5p'\ ^4D^{\frac{1}{2}}_{1/2}$—$(^1D_2)4d\ ^2P_{1/2}$
6765. 12	8	14777. 62	$5p'\ ^2S^{\frac{1}{2}}_{1/2}$—$8d\ ^4F_{3/2}$
6771. 95	175	14762. 72	$5p\ ^4D^{\frac{3}{2}}_{3/2}$—$5d'\ ^2P_{3/2}$
6774. 63	30*h*	14756. 88	$4d\ ^4D_{5/2}$—$5f'\ [3]^{\frac{7}{2}}_{7/2}$
6778. 57	60	14748. 30	$5p'\ ^2S^{\frac{1}{2}}_{1/2}$—$8d\ ^4P_{1/2}$
6779. 48	2000	14746. 32	$5p\ ^4D^{\frac{9}{2}}_{7/2}$—$6d\ ^4F_{7/2}$
6785. 23	10	14733. 83	$4d\ ^4D_{5/2}$—$5f'\ [4]^{\frac{9}{2}}_{7/2}$
6785. 74	900	14732. 72	$5p'\ ^2D^{\frac{5}{2}}_{5/2}$—$6d'\ ^2F_{7/2}$
6786. 74	2200	14730. 55	$5p\ ^4D^{\frac{5}{2}}_{5/2}$—$5d'\ ^2F_{7/2}$
6787. 34	175	14729. 25	$5p'\ ^2D^{\frac{3}{2}}_{3/2}$—$9d\ ^4D_{5/2}$
6787. 77	8	14728. 31	$5p'\ ^4S^{\frac{3}{2}}_{3/2}$—$8s'\ ^2P_{3/2}$
6790. 04	6500	14723. 39	$5p\ ^4D^{\frac{7}{2}}_{7/2}$—$6d\ ^4F_{9/2}$
6791. 48	1600*c*	14720. 27	$5p\ ^4P^{\frac{3}{2}}_{3/2}$—$6d\ ^4D_{1/2}$
6801. 35	60	14698. 91	$5p'\ ^2S^{\frac{1}{2}}_{1/2}$—$8d\ ^4D_{3/2}$
6816. 72	50	14665. 76	$5p'\ ^2D^{\frac{3}{2}}_{3/2}$—$6d'\ ^2F_{5/2}$
6820. 04	6*h*	14658. 63	$5p'\ ^2D^{\frac{3}{2}}_{3/2}$—$9d\ ^4D_{3/2}$
6820. 39	800	14657. 87	$5p\ ^4D^{\frac{5}{2}}_{5/2}$—$6d\ ^4F_{5/2}$
6826. 02	400	14645. 78	$5p\ ^4P^{\frac{1}{2}}_{1/2}$—$5d'\ ^2P_{3/2}$
6840. 62	175	14614. 53	$5p\ ^4P^{\frac{1}{2}}_{1/2}$—$6d\ ^4P_{1/2}$
6844. 82	5	14605. 56	$5p'\ ^2D^{\frac{5}{2}}_{5/2}$—$6d'\ ^2P_{3/2}$
6845. 27	40*c*	14604. 60	$5p\ ^4D^{\frac{3}{2}}_{3/2}$—$7s'\ ^4P_{1/2}$
6846. 27	150	14602. 46	$5p\ ^4P^{\frac{1}{2}}_{1/2}$—$6d\ ^4F_{3/2}$
6853. 51	3	14587. 04	$5p'\ ^4D^{\frac{1}{2}}_{1/2}$—$6d'\ ^4P_{3/2}$
6858. 22	45	14577. 02	$5p'\ ^2D^{\frac{5}{2}}_{5/2}$—$(^1D_2)4d\ ^2D_{5/2}$
6859. 43	20	14574. 45	$5p'\ ^2S^{\frac{1}{2}}_{1/2}$—$8d\ ^4D_{1/2}$
6861. 15	1800	14570. 80	$5p\ ^4D^{\frac{5}{2}}_{5/2}$—$6d\ ^4F_{7/2}$
6875. 22	20*w*	14540. 98	$5p\ ^4D^{\frac{3}{2}}_{3/2}$—$7s'\ ^2P_{3/2}$
6887. 99	12*h*	14514. 02	$4d\ ^4D_{7/2}$—$8f\ [3]^{\frac{7}{2}}_{7/2,\ 5/2}$
6888. 73	80½	14512. 46	$4d\ ^4D_{7/2}$—$8f\ [4]^{\frac{9}{2}}_{5/2}$
6904. 95	400	14478. 37	$5p\ ^4P^{\frac{1}{2}}_{1/2}$—$5d'\ ^2P_{1/2}$
6922. 86	30	14440. 91	$5p'\ ^2S^{\frac{1}{2}}_{1/2}$—$(^1D_2)4d\ ^2D_{3/2}$
6923. 04	1	14440. 54	$5p'\ ^2D^{\frac{3}{2}}_{3/2}$—$6d'\ ^2P_{3/2}$
6927. 10	2	14432. 07	$5p\ ^4D^{\frac{3}{2}}_{3/2}$—$5d''\ ^2D_{5/2}$
6927. 34	8	14431. 57	$5p'\ ^4S^{\frac{3}{2}}_{3/2}$—$(^1D_2)4d\ ^2P_{3/2}$
6929. 78	400	14426. 49	$5p\ ^4D^{\frac{9}{2}}_{7/2}$—$6d\ ^4D_{5/2}$
6936. 76	20	14411. 98	$5p'\ ^2D^{\frac{3}{2}}_{3/2}$—$(^1D_2)4d\ ^2D_{5/2}$
6962. 99	10	14357. 69	$4d\ ^4D_{3/2}$—$5f'\ [2]^{\frac{5}{2}}_{5/2}$
6971. 96	250	14339. 21	$5p\ ^4D^{\frac{9}{2}}_{7/2}$—$6d\ ^4D_{7/2}$
6992. 25	5	14297. 60	$4d\ ^4D_{5/2}$—$8f\ [3]^{\frac{7}{2}}_{7/2,\ 5/2}$
6992. 83	5	14296. 42	$4d\ ^4D_{5/2}$—$8f\ [4]^{\frac{9}{2}}_{7/2}$
6993. 31	20	14295. 44	$5p'\ ^4S^{\frac{3}{2}}_{3/2}$—$6d'\ ^4P_{5/2}$
7005. 19	10000	14271. 19	$5s\ ^4P_{3/2}$—$5p'\ ^4S^{\frac{3}{2}}_{3/2}$

TABLE A2. *Observed lines of* Br I—Continued

Wavelength	Intensity	Wave number	Classification
Å		K	
7011. 53	50	14258. 29	$5p\ ^4D^\circ_{3/2}$—$5d''\ ^2D_{3/2}$
7015. 15	75	14250. 93	$5p\ ^4D^\circ_{3/2}$—$6d\ ^4D_{5/2}$
7024. 70	20	14231. 56	$5p'\ ^2D^\circ_{3/2}$—$8d\ ^4F_{5/2}$
7026. 53	2	14227. 85	
7031. 36	15	14218. 08	$5p'\ ^2D^\circ_{3/2}$—$8d\ ^4D_{7/2}$
7054. 88	50	14170. 68	$5p\ ^4D^\circ_{5/2}$—$6d\ ^4D_{3/2}$
7058. 38	200	14163. 65	$5p\ ^4D^\circ_{3/2}$—$6d\ ^4D_{7/2}$
7061. 71	1	14156. 97	$5p'\ ^4S^\circ_{3/2}$—$9d\ ^4D_{3/2}$
7066. 33	4	14147. 72	$5p'\ ^2D^\circ_{3/2}$—$8d\ ^4P_{1/2}$
7076. 71	5	14126. 97	$5p'\ ^4D^\circ_{1/2}$—$6d'\ ^2P_{1/2}$
7082. 63	3	14115. 16	$5p''\ ^2P^\circ_{1/2}$—$8s'\ ^4P_{1/2}$
7091. 12	4	14098. 26	$5p'\ ^2D^\circ_{3/2}$—$8d\ ^4D_{3/2}$
7101. 80	5*h*	14077. 06	$5p'\ ^2D^\circ_{3/2}$—$8d\ ^4D_{5/2}$
7107. 14	1	14066. 48	$5p'\ ^2D^\circ_{3/2}$—$8d\ ^4F_{5/2}$
7111. 50	100	14057. 86	$(^1D_2)5s\ ^2D_{5/2}$—$6p''\ ^2P^\circ_{3/2}$
7111. 62	100	14057. 62	
7111. 73	150	14057. 40	
7113. 22	50	14054. 46	$5p\ ^4D^\circ_{3/2}$—$8s\ ^4P_{3/2}$
7113. 60	100	14053. 71	$5p\ ^4P^\circ_{1/2}$—$6d\ ^4D_{3/2}$
7117. 59	15	14045. 83	$5p\ ^4D^\circ_{3/2}$—$8s\ ^4P_{5/2}$
7120. 78	10	14039. 54	$(^1D_2)5s\ ^2D_{3/2}$—$6p''\ ^2P^\circ_{3/2}$
7120. 88	15	14039. 34	
7133. 95	5	14013. 62	$5p''\ ^2S^\circ_{1/2}$—$7s''\ ^2P_{1/2}$
7138. 05	2	14005. 57	$5p''\ ^2P^\circ_{3/2}$—$(^1D_2)4d\ ^2S_{1/2}$
7138. 19	4	14005. 29	$5p'\ ^2D^\circ_{5/2}$—$(^1D_2)4d\ ^2D_{3/2}$
7142. 17	300	13997. 49	$(^1D_2)5s\ ^2D_{3/2}$—$6p''\ ^2P^\circ_{1/2}$
7142. 30	400	13997. 23	
7145. 56	2	13990. 85	$4d\ ^4D_{7/2}$—$7f\ [2]^\circ_{3/2}$
7147. 07	4	13987. 89	$5p'\ ^4D^\circ_{1/2}$—$8d\ ^4F_{3/2}$
7149. 08	15	13983. 96	$4d\ ^4D_{7/2}$—$7f\ [3]^\circ_{7/2,\ 9/2}$
7150. 00	8	13982. 16	$4d\ ^4D_{7/2}$—$7f\ [4]^\circ_{7/2}$
7150. 30	75	13981. 57	$4d\ ^4D_{7/2}$—$7f\ [4]^\circ_{9/2}$
7153. 13	5*h*	13976. 04	$5p''\ ^2P^\circ_{3/2}$—$(^1D_2)4d\ ^2F_{5/2}$
7160. 74	15	13961. 19	$4d\ ^4D_{1/2}$—$5f'\ [2]^\circ_{3/2}$
7162. 10	750	13958. 54	$5s\ ^4P_{3/2}$—$5p'\ ^4D^\circ_{1/2}$
7172. 22	25	13938. 84	$5p'\ ^4S^\circ_{3/2}$—$6d'\ ^2P_{3/2}$
7175. 74	5*H*	13932. 00	$4d\ ^4D_{3/2}$—$8f\ [2]^\circ_{3/2}$
7177. 89	5*h*	13927. 83	$4d\ ^4D_{5/2}$—$8f\ [3]^\circ_{5/2}$
7184. 30	300	13915. 41	$5p\ ^4P^\circ_{1/2}$—$6d\ ^4D_{1/2}$
7194. 24	3	13896. 18	$(^1D_2)5s\ ^2D_{5/2}$—$7p\ ^4D^\circ_{3/2}$
7194. 30	5	13896. 06	
7194. 41	7	13895. 85	
7194. 53	15	13895. 62	
7214. 95	5*c*	13856. 29	$(^1D_2)5s\ ^2D_{3/2}$—$7p\ ^4P^\circ_{1/2}$
7217. 78	20	13850. 86	$5p'\ ^2S^\circ_{1/2}$—$7d\ ^4F_{3/2}$
7222. 31	50	13842. 17	$5p\ ^4D^\circ_{3/2}$—$5d'\ ^4P_{5/2}$
7232. 45	100	13822. 76	$5p\ ^4D^\circ_{3/2}$—$5d'\ ^2F_{5/2}$
7236. 86	7	13814. 34	$5p'\ ^4S^\circ_{3/2}$—$6d'\ ^2P_{1/2}$
7247. 29	5*h*	13794. 46	$5p\ ^4D^\circ_{3/2}$—$5d'\ ^4P_{3/2}$
7255. 56	15*cw*	13778. 74	$(^1D_2)5s\ ^2D_{5/2}$—$7p\ ^4D^\circ_{5/2}$
7257. 82	10*h*	13774. 45	$4d\ ^4D_{5/2}$—$7f\ [2]^\circ_{5/2}$
7260. 45	2000	13769. 46	$5s\ ^4P_{3/2}$—$5p'\ ^2D^\circ_{3/2}$
7261. 46	20	13767. 54	$4d\ ^4D_{5/2}$—$7f\ [3]^\circ_{7/2,\ 5/2}$
7262. 40	25	13765. 76	$4d\ ^4D_{5/2}$—$7f\ [4]^\circ_{7/2}$
7265. 16	5	13760. 53	$(^1D_2)5s\ ^2D_{3/2}$—$7p\ ^4D^\circ_{3/2}$

TABLE A2. *Observed lines of* Br I—Continued

Wavelength	Intensity	Wave number	Classification
Å		K	
7272. 58	3*w*	13746. 49	$(^1D_2)5s\ ^2D_{5/2}$—$7p\ ^4D^0_{7/2}$
7284. 41	5	13724. 17	$5p'\ ^2S^0_{1/2}$—$7d\ ^4D_{3/2}$
7288. 40	150	13716. 65	$5p\ ^4D^0_{3/2}$—$5d'\ ^2P_{3/2}$
7291. 92	1	13710. 03	$5p''\ ^2P^0_{3/2}$—$9d\ ^4D_{5/2}$
7305. 03	75	13685. 43	$5p\ ^4D^0_{3/2}$—$6d\ ^4P_{1/2}$
7310. 45	4	13675. 28	$5p'\ ^4S^0_{3/2}$—$8d\ ^4F_{3/2}$
7311. 48	100*d*	13673. 35	$5p\ ^4D^0_{3/2}$—$6d\ ^4F_{3/2}$
7319. 31	20	13658. 73	
7319. 41	25	13658. 54	$(^1D_2)5s\ ^2D_{5/2}$—$7p\ ^4P^0_{5/2}$
7319. 53	30	13658. 32	
7323. 35	10	13651. 19	$5p'\ ^4D^0_{7/2}$—$(^1D_2)4d\ ^2D_{3/2}$
7329. 20	10*hw*	13640. 30	$(^1D_2)5s\ ^2D_{3/2}$—$7p\ ^4P^0_{3/2}$
7329. 68	1	13639. 40	$5p''\ ^2P^0_{3/2}$—$9d\ ^4D_{3/2}$
7333. 65	20*s*	13632. 02	
7333. 77	25	13631. 80	$(^1D_2)5s\ ^2D_{3/2}$—$7p\ ^4P^0_{3/2}$
7342. 85	10	13614. 94	$5p'\ ^2S^0_{1/2}$—$7d\ ^4D_{1/2}$
7344. 53	100	13611. 83	$5p\ ^4D^0_{3/2}$—$6d\ ^4F_{5/2}$
7348. 51	10000	13604. 45	$5s\ ^4P_{3/2}$—$5p'\ ^2D^0_{5/2}$
7378. 43	20*d*	13549. 29	$5p\ ^4D^0_{3/2}$—$5d'\ ^2P_{1/2}$
7383. 69	5	13539. 63	$4d\ ^4D_{7/2}$—$9p\ ^4P^0_{5/2}$
7385. 54	4*h*	13536. 24	$4d\ ^4D_{1/2}$—$8f\ [2]^0_{3/2}$
7420. 69	2	13472. 13	$5p'\ ^4S^0_{3/2}$—$8d\ ^4D_{1/2}$
7425. 85	750	13462. 76	$5p\ ^4P^0_{5/2}$—$7s\ ^4P_{5/2}$
7452. 13	60	13415. 29	$5p'\ ^2D^0_{3/2}$—$7d\ ^4F_{3/2}$
7453. 43	70	13412. 95	$5p'\ ^2D^0_{3/2}$—$7s''\ ^2P_{1/2}$
7458. 23	50*h*	13404. 32	$4d\ ^4D_{3/2}$—$7f\ [2]^0_{3/2}$
7461. 86	70	13397. 79	$4d\ ^4D_{3/2}$—$7f\ [3]^0_{5/2}$
7464. 68	8	13392. 73	$5p''\ ^2P^0_{3/2}$—$(^1D_2)4d\ ^2D_{5/2}$
7495. 46	15*hw*	13337. 74	$4d\ ^4F_{9/2}$—$9f\ [5]^0_{11/2}$
7497. 81	5	13333. 56	$4d\ ^4D_{5/2}$—$9p\ ^4P^0_{3/2}$
7512. 96	40000	13306. 67	$5s\ ^4P_{5/2}$—$5p\ ^4D^0_{3/2}$
7532. 77	50	13271. 67	$5p'\ ^2S^0_{1/2}$—$7s'\ ^4P_{1/2}$
7535. 79	400	13266. 36	$5p\ ^4P^0_{3/2}$—$7s\ ^4P_{3/2}$
7545. 60	1	13249. 11	$5p''\ ^2P^0_{1/2}$—$6d'\ ^2P_{3/2}$
7551. 40	100	13238. 93	
7551. 48	125	13238. 79	$(^1D_2)5s\ ^2D_{3/2}$—$6p'\ ^4D^0_{1/2}$
7551. 60	175	13238. 58	
7559. 99	70	13223. 89	$5p'\ ^4D^0_{1/2}$—$7s''\ ^2P_{1/2}$
7569. 08	500	13208. 01	$5p'\ ^2S^0_{1/2}$—$7s'\ ^2P_{3/2}$
7570. 87	550	13204. 89	$5p\ ^4D^0_{3/2}$—$6d\ ^4D_{5/2}$
7575. 23	15*w*	13197. 29	
7582. 56	10*h*	13184. 53	
7582. 98	100*h*	13183. 80	$4d\ ^4D_{7/2}$—$4f''\ [3]^0_{7/2}$
7586. 60	25	13177. 51	$4d\ ^4D_{7/2}$—$6f\ [2]^0_{5/2}$
7591. 61	1600	13168. 81	$5s\ ^4P_{3/2}$—$5p'\ ^2S^0_{1/2}$
7594. 52	25	13163. 77	$4d\ ^4D_{7/2}$—$6f\ [4]^0_{7/2}$
7595. 07	1800	13162. 81	$4d\ ^4D_{7/2}$—$6f\ [4]^0_{9/2}$
7598. 00	4	13157. 74	$5p''\ ^2P^0_{3/2}$—$8d\ ^4F_{3/2}$
7604. 03	70	13147. 30	$5p'\ ^2D^0_{3/2}$—$7d\ ^4P_{1/2}$
7606. 28	120	13143. 41	$4d\ ^4D_{7/2}$—$6f\ [3]^0_{7/2,\ 5/2}$
7607. 15	100	13141. 91	
7607. 25	150	13141. 74	
7607. 38	200	13141. 51	$(^1D_2)5s\ ^2D_{3/2}$—$6p'\ ^4S^0_{3/2}$
7607. 54	300	13141. 24	
7616. 41	2000	13125. 93	$5p\ ^4P^0_{3/2}$—$7s\ ^4P_{5/2}$

TABLE A2. *Observed lines of* Br I—Continued

Wavelength	Intensity	Wave number	Classification
Å		K	
7617.82	3	13123.50	$(^1D_2)5s\ ^2D_{3/2}$—$6p'\ ^4S^0_{3/2}$
7617.90	5	13123.36	
7618.03	10	13123.14	
7632.87	50	13097.63	$5p\ ^4P^0_{3/2}$—$5d\ ^4F_{3/2}$
7641.64	600	13082.59	$5p\ ^4P^0_{5/2}$—$5d\ ^4F_{5/2}$
7647.70	40	13072.23	$5p'\ ^4D^0_{1/2}$—$(^1S_0)5s\ ^2S_{1/2}$
7652.60	30	13063.86	$(^1D_2)5s\ ^2D_{3/2}$—$6p'\ ^2D^0_{3/2}$
7652.70	40	13063.69	
7652.85	60	13063.43	
7653.02	120	13063.14	
7663.39	40	13045.46	$(^1D_2)5s\ ^2D_{3/2}$—$6p'\ ^2D^0_{3}$
7663.50	50	13045.28	
7663.63	80	13045.06	
7680.56	5*h*	13016.30	$4d\ ^4D_{1/2}$—$7f\ [1]^0_{3/2}$
7680.74	10*h*	13016.00	$4d\ ^4D_{1/2}$—$7f\ [1]^0_{1/2}$
7681.75	20	13014.29	$5p'\ ^2D^0_{3/2}$—$7d\ ^4D_{1/2}$
7685.11	50	13008.60	$4d\ ^4D_{1/2}$—$7f\ [2]^0_{3/2}$
7698.72	35	12985.60	$5p''\ ^2P^0_{1/2}$—$8d\ ^4F_{3/2}$
7699.58	80	12984.15	$5s'\ ^4P_{1/2}$—$5p''\ ^2P^0_{1/2}$
7703.17	2	12978.10	$4d\ ^4D_{3/2}$—$9p\ ^4P^0_{1/2}$
7704.32	60*h*	12976.16	$4d\ ^4F_{9/2}$—$8f\ [5]^0_{11/2}$
7706.69	15*hw*	12972.17	$4d\ ^4D_{5/2}$—$6f\ [1]^0_{3/2}$
7708.39	8	12969.31	$4d\ ^4F_{9/2}$—$8f\ [4]^0_{9/2}$
7709.35	15*h*	12967.69	$4d\ ^4D_{3/2}$—$4f''\ [3]^0_{5/2}$
7709.55	15*h*	12967.36	$4d\ ^4D_{5/2}$—$4f''\ [3]^0_{7/2}$
7711.68	5	12963.78	$4d\ ^4D_{3/2}$—$9p\ ^4P^0_{3/2}$
7713.27	200	12961.10	$4d\ ^4D_{5/2}$—$6f\ [2]^0_{5/2}$
7713.54	45	12960.65	$4d\ ^4D_{5/2}$—$6f\ [2]^0_{3/2}$
7715.06	100	12958.10	$(^1D_2)5s\ ^2D_{3/2}$—$6p'\ ^2D^0_{5/2}$
7715.16	150	12957.93	
7715.31	200	12957.68	
7715.48	400	12957.39	
7717.18	2	12954.54	$5p'\ ^2P^0_{3/2}$—$8d\ ^4D_{1/2}$
7721.45	300	12947.37	$4d\ ^4D_{5/2}$—$6f\ [4]^0_{7/2}$
7726.02	60	12939.71	$(^1D_2)5s\ ^2D_{3/2}$—$6p'\ ^2D^0_{5/2}$
7726.13	80	12939.53	
7726.26	110	12939.31	
7729.19	1	12934.41	$5p'\ ^4D^0_{1/2}$—$7d\ ^4D_{3/2}$
7733.61	900	12927.01	$4d\ ^4D_{5/2}$—$6f\ [3]^0_{7/2,\ 5/2}$
7734.61	25	12925.34	$5p'\ ^2S^0_{1/2}$—$5d''\ ^2D_{3/2}$
7742.05	1	12912.92	$4d\ ^4F_{7/2}$—$5f'\ [4]^0_{9/2}$
7783.44	9*w*	12844.26	$4d\ ^4F_{7/2}$—$9f\ [5]^0_{9/2}$
7795.01	15	12825.19	$5p'\ ^4D^0_{1/2}$—$7d\ ^4D_{1/2}$
7803.02	30000	12812.03	$5s'\ ^4P_{1/2}$—$5p''\ ^2P^0_{3/2}$
7807.52	50	12804.64	$(^1D_2)5s\ ^2D_{3/2}$—$6p'\ ^2S^0_{1/2}$
7807.64	60	12804.44	
7807.78	100	12804.21	
7821.10	30	12782.41	$5p''\ ^2P^0_{1/2}$—$8d\ ^4D_{1/2}$
7827.23	1200	12772.40	$5p'\ ^2D^0_{5/2}$—$7s'\ ^2P_{3/2}$
7835.08	30	12759.60	$5p'\ ^4S^0_{3/2}$—$(^1S_0)5s\ ^2S_{1/2}$
7841.87	30	12748.55	$5p'\ ^4S^0_{3/2}$—$7d\ ^4F_{3/2}$
7843.58	600	12745.77	$5p\ ^4P^0_{3/2}$—$5d\ ^4F_{5/2}$
7844.01	80	12745.07	$5p\ ^4P^0_{3/2}$—$5d\ ^4P_{1/2}$
7844.10	80	12744.93	
7869.53	10	12703.74	$4d\ ^4F_{9/2}$—$10p\ ^4D^0_{7/2}$

See footnotes at end of table.

TABLE A2. *Observed lines of* Br I—Continued

Wavelength	Intensity	Wave number	Classification
Å		K	
7881.45	2500*s*	12684.53	$5s'\ ^2P_{3/2}$—$5p''\ ^2P^{\circ}_{1/2}$
7881.57	2500	12684.34	
7889.85	600	12671.03	$5p'\ ^2D^{\circ}_{3/2}$—$7s'\ ^4P_{1/2}$
7903.66	50	12648.89	$5p''\ ^2P^{\circ}_{1/2}$—$(^1D_2)4d\ ^2D_{3/2}$
7905.70	50	12645.62	$5p'\ ^4S^{\circ}_{3/2}$—$7d\ ^4P_{1/2}$
7925.81	2500	12613.54	$5p\ ^4D^{\circ}_{7/2}$—$7s\ ^4P_{5/2}$
7929.69	250	12607.37	$5p'\ ^2D^{\circ}_{3/2}$—$7s'\ ^2P_{3/2}$
7932.99	30*W*	12602.12	$4d\ ^4D_{3/2}$—$6f\ [1]^{\circ}_{3/2}$ $4d\ ^4D_{3/2}$—$6f\ [1]^{\circ}_{1/2}$
7938.68	30000*c*	12593.09	$(^1D_2)5s\ ^2D_{5/2}$—$(^1D_2)5p\ ^2D^{\circ}_{3/2}$
7940.07	60	12590.88	$4d\ ^4D_{3/2}$—$6f\ [2]^{\circ}_{3/2}$
7947.94	3000	12578.42	$5p\ ^4D^{\circ}_{3/2}$—$7s\ ^4P_{3/2}$
7950.18	3000	12574.87	$(^1D_2)5s\ ^2D_{3/2}$—$(^1D_2)5p\ ^2D^{\circ}_{3/2}$
7961.33	350	12557.26	$4d\ ^4D_{3/2}$—$6f\ [3]^{\circ}_{3/2}$
7966.84	600	12548.58	$(^1D_2)5s\ ^2D_{5/2}$—$(^1D_2)5p\ ^2D^{\circ}_{3/2}$
7967.03	750	12548.28	
7975.11	10	12535.56	
7975.23	20	12535.38	$(^1D_2)5s\ ^2D_{5/2}$—$4f\ [1]^{\circ}_{3/2}$
7975.39	15	12535.12	
7975.62	35	12534.76	
7978.44	8000	12530.33	$(^1D_2)5s\ ^2D_{3/2}$—$(^1D_2)5p\ ^2D^{\circ}_{3/2}$
7978.57	10000	12530.13	
7989.94	30000	12512.30	$5s'\ ^2P_{3/2}$—$5p''\ ^2P^{\circ}_{3/2}$
7997.02	80	12501.22	$4d\ ^4D_{7/2}$—$4f'\ [3]^{\circ}_{7/2}$
7998.75	175	12498.52	$5p'\ ^2D^{\circ}_{3/2}$—$5d''\ ^2D_{5/2}$
8004.36	25	12489.76	$5p'\ ^2D^{\circ}_{3/2}$—$5d''\ ^2D_{3/2}$
8008.87	30*h*	12482.72	$4d\ ^4F_{7/2}$—$8f\ [5]^{\circ}_{9/2}$
8009.36	75	12481.96	$5p'\ ^4D^{\circ}_{1/2}$—$7s'\ ^4P_{1/2}$
8009.77	100	12481.32	
8009.86	150	12481.18	$(^1D_2)5s\ ^2D_{5/2}$—$4f\ [2]^{\circ}_{5/2}$
8010.00	200	12480.96	
8010.17	400	12480.70	
8013.03	1	12476.24	$4d\ ^4F_{7/2}$—$8f\ [4]^{\circ}_{7/2}$
8014.51	100	12473.94	
8014.60	150	12473.80	$(^1D_2)5s\ ^2D_{5/2}$—$4f\ [2]^{\circ}_{5/2}$
8014.74	175	12473.58	
8014.89	200	12473.35	
8021.57	100	12462.96	
8021.67	150	12462.80	$(^1D_2)5s\ ^2D_{3/2}$—$4f\ [2]^{\circ}_{5/2}$
8021.80	200	12462.60	
8022.52	800	12461.48	$5p\ ^4P^{\circ}_{1/2}$—$7s\ ^4P_{3/2}$ $5p'\ ^2S^{\circ}_{1/2}$—$5d'\ ^4P_{3/2}$
8022.83	15	12461.00	
8022.98	15	12460.77	$(^1D_2)5s\ ^2D_{5/2}$—$4f\ [3]^{\circ}_{7/2}$
8023.14	20	12460.52	
8023.91	900	12459.33	$5p\ ^4P^{\circ}_{5/2}$—$5d\ ^4D_{3/2}$
8026.35	2000	12455.54	$(^1D_2)5s\ ^2D_{3/2}$—$4f\ [2]^{\circ}_{3/2}$
8026.54	2500	12455.24	
8028.22	18	12452.64	$4d\ ^4D_{7/2}$—$4f'\ [4]^{\circ}_{7/2}$
8028.80	400	12451.74	$4d\ ^4D_{7/2}$—$4f'\ [4]^{\circ}_{9/2}$
8029.48	100	12450.68	
8029.53	150	12450.60	$(^1D_2)5s\ ^2D_{5/2}$—$4f\ [4]^{\circ}_{7/2}$
8029.67	200	12450.39	
8029.81	250	12450.17	
8030.91	250*h*	12448.47	$4d\ ^4F_{9/2}$—$7f\ [5]^{\circ}_{11/2}$
8033.40	40	12444.61	$4d\ ^4D_{7/2}$—$8p\ ^4P^{\circ}_{5/2}$

TABLE A2. *Observed lines of* Br I—Continued

Wavelength	Intensity	Wave number	Classification
Å		K	
8034. 83	75	12442. 39	$(^1D_2)\,5s\ ^2D_{3/2}$—$4f\ [3]^5_{5/2}$
8034. 91	100	12442. 27	
8035. 03	150	12442. 08	
8037. 34	40	12438. 51	$4d\ ^4D_{7/2}$—$4f'\ [2]^5_{5/2}$ $4d\ ^4F_{9/2}$—$7f\ [4]^5_{5/2}$
8037. 65	60	12438. 03	$5p\ ^4D^5_{5/2}$—$7s\ ^4P_{5/2}$
8050. 41	15	12418. 31	$5p'\ ^4D^1_{1/2}$—$7s'\ ^2P_{3/2}$
8066. 38	200	12393. 73	$5p''\ ^2P^3_{3/2}$—$7s''\ ^2P_{1/2}$
8072. 89	300	12383. 73	$5p'\ ^2S^1_{1/2}$—$5d'\ ^2P_{3/2}$
8101. 21	150	12340. 44	$5p'\ ^2S^1_{1/2}$—$6d\ ^4F_{3/2}$
8111. 56	50	12324. 70	$5p'\ ^2D^3_{3/2}$—$5d''\ ^2D_{3/2}$
8113. 04	20*h*	12322. 45	$4d\ ^4F_{5/2}$—$5f'\ [4]^5_{7/2}$
8131. 52	30000	12294. 44	$5s'\ ^4P_{1/2}$—$5p'\ ^4S^3_{3/2}$
8137. 89	150	12284. 82	$4d\ ^4D_{5/2}$—$4f'\ [3]^5_{7/2}$
8142. 80	40*h*	12277. 41	$4d\ ^4D_{5/2}$—$8p\ ^4D^5_{7/2}$ $5p'\ ^2D^3_{5/2}$—$8s\ ^4P_{5/2}$
8148. 84	20	12268. 31	$4d\ ^4D_{5/2}$—$8p\ ^4P^5_{3/2}$
8152. 65	1000*c*	12262. 58	$5p\ ^4P^3_{3/2}$—$5d\ ^4D_{1/2}$
8153. 75	10000	12260. 92	$5p\ ^4P^3_{3/2}$—$5d\ ^4D_{5/2}$
8154. 00	25000	12260. 55	$5s\ ^4P_{5/2}$—$5p\ ^4D^5_{5/2}$
8166. 32	175	12242. 05	$5p''\ ^2P^3_{3/2}$—$(^1S_0)\,5s\ ^2S_{1/2}$
8170. 21	200*d*	12236. 22	$4d\ ^4D_{5/2}$—$4f'\ [4]^5_{7/2}$
8172. 09	200	12233. 41	$5p\ ^4D^5_{7/2}$—$5d\ ^4F_{5/2}$
8173. 71	20	12230. 98	$5p''\ ^2P^3_{3/2}$—$7d\ ^4F_{3/2}$
8175. 58	25	12228. 19	$4d\ ^4D_{5/2}$—$8p\ ^4P^5_{3/2}$
8179. 65	40	12222. 10	$4d\ ^4D_{5/2}$—$4f'\ [2]^5_{5/2}$
8180. 01	100	12221. 56	$5p''\ ^2P^1_{1/2}$—$7s''\ ^2P_{1/2}$
8183. 52	450	12216. 32	$5p'\ ^2S^1_{1/2}$—$5d'\ ^2P_{1/2}$
8189. 93	1*hw*	12206. 76	$4d\ ^4D_{1/2}$—$6f\ [1]^3_{3/2}$
8190. 08	1*hw*	12206. 54	
8190. 28	40	12206. 24	$4d\ ^4D_{1/2}$—$6f\ [1]^1_{1/2}$
8197. 73	175*h*	12195. 15	$4d\ ^4D_{1/2}$—$6f\ [2]^3_{3/2}$
8210. 49	3*h*	12176. 19	$4d\ ^4F_{3/2}$—$5f''\ [3]^5_{5/2}$
8215. 12	200	12169. 33	$5p'\ ^4S^3_{3/2}$—$7s'\ ^4P_{1/2}$
8237. 96	500	12135. 59	$5p'\ ^4D^1_{1/2}$—$5d''\ ^2D_{3/2}$
8246. 86	5000	12122. 50	$5p\ ^4P^3_{3/2}$—$5d\ ^4D_{3/2}$
8247. 97	30	12120. 86	$5p'\ ^2D^3_{3/2}$—$8s\ ^4P_{3/2}$
8252. 38	30	12114. 39	$5p''\ ^2P^3_{3/2}$—$7d\ ^4D_{5/2}$
8253. 87	35	12112. 20	$5p'\ ^2D^3_{3/2}$—$8s\ ^4P_{5/2}$
8258. 32	300	12105. 67	$5p'\ ^4S^3_{3/2}$—$7s'\ ^2P_{3/2}$
8264. 96	15000	12095. 95	$5p\ ^4P^5_{3/2}$—$5d\ ^4D_{7/2}$
8272. 44	75000*c*	12085. 01	$5s\ ^4P_{5/2}$—$5p\ ^4D^5_{7/2}$
8280. 24	100	12073. 63	$5p'\ ^2D^5_{5/2}$—$5d'\ ^4P_{5/2}$
8280. 75	100*w*	12072. 88	$5p\ ^4D^5_{5/2}$—$5d\ ^4F_{3/2}$
8291. 06	900	12057. 87	$5p\ ^4D^5_{5/2}$—$5d\ ^4F_{5/2}$
8293. 57	100	12054. 22	$5p'\ ^2D^5_{5/2}$—$5d'\ ^2F_{5/2}$
8308. 49	20	12032. 57	$4d\ ^4F_{9/2}$—$9p\ ^4D^5_{7/2}$
8313. 09	10	12025. 92	$5p'\ ^2D^5_{5/2}$—$5d'\ ^4P_{3/2}$
8334. 70	20000	11994. 74	$5s'\ ^2P_{3/2}$—$5p'\ ^4S^3_{3/2}$
8343. 70	10000	11981. 80	$5s'\ ^4P_{1/2}$—$5p'\ ^4D^1_{1/2}$
8361. 71	300	11955. 99	$5p\ ^4P^1_{1/2}$—$5d\ ^4F_{3/2}$
8362. 38	100*h*	11955. 03	$4d\ ^4F_{7/2}$—$7f\ [5]^5_{5/2}$
8367. 20	15	11948. 15	$5p'\ ^2D^5_{5/2}$—$5d'\ ^2P_{3/2}$
8369. 00	20	11945. 58	$4d\ ^4F_{7/2}$—$7f\ [4]^5_{7/2}$
8372. 79	150	11940. 17	$5p\ ^4P^1_{1/2}$—$5d\ ^4P_{1/2}$
8378. 65	100*w*	11931. 82	$5p'\ ^4D^1_{1/2}$—$8s\ ^4P_{3/2}$
8382. 42	5	11926. 45	$4d\ ^4D_{3/2}$—$8p\ ^4D^5_{5/2}$
8384. 04	1200	11924. 15	$5p\ ^4P^3_{3/2}$—$5d\ ^4D_{5/2}$
8387. 99	100	11918. 53	$5p\ ^4D^5_{7/2}$—$5d\ ^4F_{7/2}$

TABLE A2. *Observed lines of* Br I—Continued

Wavelength	Intensity	Wave number	Classification
Å		K	
8389. 75	300	11916. 03	$5p'\ ^2D^o_{5/2}$—$5d'\ ^2F_{7/2}$
8392. 76	75	11911. 76	$4d\ ^4D_{3/2}$—$4f'\ [3]^o_{5/2}$
8397. 62	50	11904. 86	$5p'\ ^2D^o_{5/2}$—$6d\ ^4F_{3/2}$
8402. 08	20	11898. 55	$4d\ ^4D_{3/2}$—$8p\ ^4P^o_{3/2}$
8408. 68	250	11889. 21	$5p'\ ^2D^o_{3/2}$—$5d'\ ^2F_{5/2}$
8410. 79	10*w*	11886. 22	$4d\ ^4F_{5/2}$—$8f\ [3]^o_{7/2,5/2}$
8411. 61	5*w*	11885. 06	$4d\ ^4F_{5/2}$—$8f\ [4]^o_{7/2}$
8421. 88	4	11870. 57	
8428. 77	75	11860. 87	$5p'\ ^2D^o_{3/2}$—$5d'\ ^4P_{3/2}$
8430. 51	50	11858. 42	$4d\ ^4D_{3/2}$—$8p\ ^4P^o_{5/2}$
8434. 83	150	11852. 35	$4d\ ^4D_{3/2}$—$4f'\ [2]^o_{5/2}$
8435. 34	75	11851. 63	$4d\ ^4D_{3/2}$—$4f'\ [2]^o_{3/2}$
8441. 26	100	11843. 32	$5p'\ ^2D^o_{5/2}$—$6d\ ^4F_{5/2}$
8446. 55	40000	11835. 90	$5s\ ^4P_{3/2}$—$5p\ ^4D^o_{3/2}$
8454. 25	75	11825. 12	$4d\ ^4D_{7/2}$—$5f\ [2]^o_{5/2}$
8467. 38	300	11806. 78	$4d\ ^4D_{7/2}$—$5f\ [3]^o_{7/2,5/2}$
8470. 62	100	11802. 27	$4d\ ^4D_{7/2}$—$5f\ [4]^o_{7/2}$
8471. 51	500	11801. 03	$4d\ ^4D_{7/2}$—$5f\ [4]^o_{9/2}$
8477. 45	4000	11792. 76	$5s'\ ^4P_{1/2}$—$5p'\ ^2D^o_{3/2}$
8484. 40	30	11783. 10	$5p'\ ^2D^o_{3/2}$—$5d'\ ^2P_{3/2}$
8503. 78	400	11756. 25	$5p'\ ^2D^o_{5/2}$—$6d\ ^4F_{7/2}$
8513. 38	1500	11742. 99	$5p\ ^4D^o_{5/2}$—$5d\ ^4F_{7/2}$
8515. 69	100	11739. 80	$5p'\ ^2D^o_{3/2}$—$6d\ ^4F_{3/2}$
8529. 38	8*h*	11720. 96	
8557. 73	1000	11682. 13	$5s'\ ^2P_{3/2}$—$5p'\ ^4D^o_{1/2}$
8560. 57	300	11678. 26	$5p'\ ^2D^o_{3/2}$—$6d\ ^4F_{5/2}$
8565. 30	200	11671. 81	$5p'\ ^4D^o_{1/2}$—$5d'\ ^4P_{3/2}$
8566. 28	1000	11670. 47	$5p\ ^4D^o_{7/2}$—$5d\ ^4F_{9/2}$
8578. 84	400	11653. 39	$5p'\ ^2S^o_{1/2}$—$6d\ ^4D_{1/2}$
8580. 00	20	11651. 81	$5p''\ ^2P^o_{3/2}$—$7s'\ ^4P_{1/2}$
8592. 30	250	11635. 13	$4d\ ^4F_{9/2}$—$6f\ [5]^o_{11/2}$
8595. 50	50	11630. 80	
8595. 67	50	11630. 57	$4d\ ^4D_{5/2}$—$5f\ [1]^o_{3/2}$
8603. 00	2	11620. 66	$4d\ ^4F_{9/2}$—$6f\ [4]^o_{7/2}$
8603. 69	100	11619. 73	$4d\ ^4F_{9/2}$—$6f\ [4]^o_{9/2}$
8604. 06	20*hw*	11619. 23	$5p'\ ^4S^o_{3/2}$—$8s\ ^4P_{3/2}$
8606. 68	20	11615. 69	$5p'\ ^2D^o_{3/2}$—$5d'\ ^2P_{1/2}$
8608. 98	30*hw*	11612. 59	$4d\ ^4P_{1/2}$—$7f\ [1]^o_{3/2}$ $4d\ ^4P_{1/2}$—$7f\ [1]^o_{1/2}$
8610. 49	100	11610. 55	$5p'\ ^4S^o_{3/2}$—$8s\ ^4P_{5/2}$
8611. 85	250	11608. 72	$4d\ ^4D_{5/2}$—$5f\ [2]^o_{5/2}$
8612. 48	75	11607. 87	$4d\ ^4D_{5/2}$—$5f\ [2]^o_{3/2}$
8625. 38	750c	11590. 51	$(^1D_2)5s\ ^2D_{3/2}$—$(^1D_2)5p\ ^2P^o_{1/2}$
8625. 47	100	11590. 39	$4d\ ^4D_{5/2}$—$5f\ [3]^o_{7/2,\ 5/2}$
8628. 84	200	11585. 86	$4d\ ^4D_{5/2}$—$5f\ [4]^o_{7/2}$
8638. 66	20000	11572. 69	$5s\ ^4P_{3/2}$—$5p\ ^4P^o_{3/2}$
8655. 11	100	11550. 70	$5p'\ ^4D^o_{1/2}$—$6d\ ^4F_{3/2}$
8658. 84	10	11545. 72	$4d\ ^4F_{7/2}$—$9p\ ^4D^o_{5/2}$
8668. 84	300	11532. 40	$5p\ ^4D^o_{3/2}$—$7s\ ^4P_{3/2}$
8698. 53	4000	11493. 04	$5s'\ ^2P_{3/2}$—$5p'\ ^2D^o_{3/2}$
8708. 68	75	11479. 64	$5p''\ ^2P^o_{1/2}$—$7s'\ ^4P_{1/2}$
8708. 96	100	11479. 27	$5p''\ ^2P^o_{3/2}$—$5d''\ ^2D_{5/2}$
8725. 33	500	11457. 74	$5p\ ^4P^o_{1/2}$—$5d\ ^4D_{1/2}$
8726. 75	100c	11455. 87	$4d\ ^4D_{1/2}$—$4f'\ [2]^o_{3/2}$
8741. 64	50	11436. 36	$5p'\ ^2D^o_{5/2}$—$6d\ ^4D_{5/2}$
8742. 99	75	11434. 59	$5p\ ^4D^o_{5/2}$—$5d\ ^4D_{3/2}$

TABLE A2. *Observed lines of* Br I—Continued

Wavelength	Intensity	Wave number	Classification
A		*K*	
8749. 10	10	11426. 61	$5p'\ ^4D^0_{7/2}$—$5d'\ ^2P_{1/2}$
8757. 24	10	11415. 99	$5p''\ ^2P^0_{1/2}$—$7s'\ ^2P_{3/2}$
8760. 46	700	11411. 79	$5p\ ^4D^0_{7/2}$—$5d\ ^4D_{5/2}$
8764. 20	500	11406. 92	$5p'\ ^4S^0_{3/2}$—$5d'\ ^4P_{5/2}$
8775. 71	250	11391. 96	$5p\ ^4D^0_{3/2}$—$7s\ ^4P_{5/2}$
8779. 15	50	11387. 50	$5p'\ ^4S^0_{3/2}$—$5d'\ ^2F_{5/2}$
8793. 47	10000c	11368. 95	$(^1D_2)5s\ ^2D_{5/2}$—$(^1D_2)5p\ ^2P^0_{3/2}$
8798. 04	6	11363. 05	$4d\ ^4F_{5/2}$—$7f\ [2]^0_{5/2}$
8801. 03	150	11359. 19	$5p'\ ^4S^0_{3/2}$—$5d'\ ^4P_{3/2}$
8803. 41	100	11356. 12	$4d\ ^4F_{5/2}$—$7f\ [3]^0_{7/2,\ 5/2}$ $5p'\ ^2D^0_{3/2}$—$6d\ ^4D_{3/2}$
8804. 76	20	11354. 38	$4d\ ^4F_{5/2}$—$7f\ [4]^0_{7/2}$
8807. 44	600	11350. 92	$(^1D_2)5s\ ^2D_{3/2}$—$(^1D_2)5p\ ^2P^0_{3/2}$
8807. 68	800	11350. 61	
8808. 85	500	11349. 10	$5p'\ ^2D^0_{5/2}$—$6d\ ^4D_{7/2}$
8819. 96	15000	11334. 81	$(^1D_2)5s\ ^2D_{5/2}$—$(^1D_2)5p\ ^2F^0_{7/2}$
8825. 22	25000	11328. 05	$5s'\ ^2P_{3/2}$—$5p'\ ^2D^0_{5/2}$
8833. 33	175	11317. 65	$5p\ ^4P^0_{1/2}$—$5d\ ^4D_{3/2}$
8842. 85	125	11305. 47	$5p''\ ^2P^0_{3/2}$—$5d''\ ^2D_{3/2}$
8861. 69	85	11281. 43	$5p'\ ^4S^0_{3/2}$—$5d'\ ^2P_{3/2}$
8869. 64	300	11271. 32	$5p'\ ^2D^0_{3/2}$—$6d\ ^4D_{5/2}$
8870. 46	200	11270. 28	$5p\ ^4P^0_{3/2}$—$6s''\ ^2P_{1/2}$
8875. 43	3	11263. 97	$6s\ ^4P_{5/2}$—$7p''\ ^2P^0_{3/2}$
8877. 89	90	11260. 85	$4d\ ^4D_{3/2}$—$5f\ [1]^0_{3/2}$
8878. 40	90	11260. 20	$4d\ ^4D_{3/2}$—$5f\ [1]^0_{1/2}$
8886. 34	40	11250. 14	$5p'\ ^4S^0_{3/2}$—$6d\ ^4P_{1/2}$
8888. 98	4000	11246. 80	$5p\ ^4D^0_{7/2}$—$5d\ ^4D_{7/2}$
8895. 21	20	11238. 92	$4d\ ^4D_{3/2}$—$5f\ [2]^0_{5/2}$
8895. 87	150	11238. 09	$4d\ ^4D_{3/2}$—$5f\ [2]^0_{3/2}$ $5p'\ ^4S^0_{3/2}$—$6d\ ^4F_{3/2}$
8897. 62	30000	11235. 88	$5s\ ^4P_{5/2}$—$5p\ ^4P^0_{5/2}$
8909. 73	300	11220. 60	$4d\ ^4D_{3/2}$—$5f\ [3]^0_{5/2}$
8925. 64	15	11200. 60	$4d\ ^4F_{3/2}$—$7f\ [1]^0_{3/2}$
8932. 40	6000	11192. 13	$5s'\ ^4P_{1/2}$—$5p'\ ^2S^0_{1/2}$
8933. 29	25	11191. 01	$5p'\ ^2D^0_{3/2}$—$6d\ ^4D_{3/2}$
8936. 96	15	11186. 42	$4d\ ^4F^0_{3/2}$—$7f\ [3]^0_{5/2}$
8944. 83	50	11176. 57	$5p'\ ^4S^0_{3/2}$—$6d\ ^4F_{5/2}$
8949. 39	1800	11170. 88	$(^1D_2)5s\ ^2D_{5/2}$—$(^1D_2)5p\ ^2F^0_{5/2}$
8964. 00	9000	11152. 67	$(^1D_2)5s\ ^2D_{3/2}$—$(^1D_2)5p\ ^2F^0_{5/2}$
8972. 83	350	11141. 70	$4d\ ^4F_{7/2}$—$6f\ [5]^0_{9/2}$
8979. 59	200	11133. 31	$5p''\ ^2P^0_{1/2}$—$5d''\ ^2D_{3/2}$
8984. 56	100	11127. 15	$4d\ ^4F_{7/2}$—$6f\ [4]^0_{7/2}$
8985. 32	1	11126. 21	$4d\ ^4F_{7/2}$—$6f\ [4]^0_{5/2}$
8995. 21	50	11113. 98	$5p'\ ^4S^0_{3/2}$—$5d'\ ^2P_{1/2}$
9000. 99	2*h*	11106. 84	$4d\ ^4F_{7/2}$—$6f\ [3]^0_{7/2,\ 5/2}$
9005. 20	50*h*	11101. 65	$5p''\ ^2P^0_{3/2}$—$8s\ ^4P_{3/2}$
9012. 23	20	11092. 99	$5p''\ ^2P^0_{3/2}$—$8s\ ^4P_{5/2}$
9029. 94	300	11071. 23	$5p\ ^4D^0_{5/2}$—$5d\ ^4D_{7/2}$
9045. 06	40	11052. 72	$5p'\ ^2D^0_{3/2}$—$6d\ ^4D_{1/2}$
9066. 28	400	11026. 86	$5p\ ^4D^0_{3/2}$—$5d\ ^4F_{3/2}$
9078. 64	700	11011. 84	$5p\ ^4D^0_{3/2}$—$5d\ ^4F_{5/2}$
9079. 29	125	11011. 05	$5p\ ^4D^0_{3/2}$—$5d\ ^4P_{1/2}$
9084. 29	25	11004. 99	$4d\ ^4F_{5/2}$—$9p\ ^4D^0_{3/2}$
9086. 80	100	11001. 95	$5p'\ ^4D^0_{1/2}$—$6d\ ^4D_{3/2}$
9107. 37	10	10977. 11	$4d'\ ^2F_{5/2}$—$5f''\ [3]^0_{7/2}$
9123. 17	50	10958. 09	$4d\ ^4F_{9/2}$—$4f'\ [3]^0_{7/2}$
9126. 14	4	10954. 53	$4d\ ^4F_{5/2}$—$9p\ ^4D^0_{5/2}$

TABLE A2. *Observed lines of* Br I—Continued

Wavelength	Intensity	Wave number	Classification
Å		K	
9129.31	70	10950.72	$4d\ ^4F_{9/2}$—$8p\ ^4D^\circ_{7/2}$
9147.04	75*h*	10929.50	$5p''\ ^2P^\circ_{1/2}$—$8s\ ^4P_{3/2}$
9166.06	30000	10906.82	$5s\ ^4P_{5/2}$—$5p\ ^4P^\circ_{1/2}$
9173.63	15000	10897.82	$5s''\ ^2P_{1/2}$—$5p''\ ^2P^\circ_{1/2}$
9178.16	20000	10892.44	$5s'\ ^2P_{3/2}$—$5p'\ ^2S^\circ_{1/2}$
9183.14	30	10886.53	$4d\ ^4F_{3/2}$—$7p'\ ^2S^\circ_{1/2}$ $4d'\ ^2P_{1/2}$—$5f'\ [2]^\circ_{3/2}$
9197.16	50	10869.94	$5p''\ ^2P^\circ_{3/2}$—$5d'\ ^2F_{5/2}$
9201.21	80*w*	10865.15	$4d\ ^4D_{1/2}$—$5f\ [1]^\circ_{3/2}$
9201.78	80	10864.48	$4d\ ^4D_{1/2}$—$5f\ [1]^\circ_{1/2}$
9202.47	80	10863.67	$5p'\ ^4D^\circ_{1/2}$—$6d\ ^4D_{1/2}$
9220.56	200	10842.35	$4d\ ^4D_{1/2}$—$5f\ [2]^\circ_{3/2}$
9221.19	35	10841.61	$5p''\ ^2P^\circ_{3/2}$—$5d'\ ^4P_{3/2}$
9226.57	15	10835.29	$4d\ ^4F_{3/2}$—$9p\ ^4D^\circ_{3/2}$
9254.06	70	10803.10	$4d\ ^4P_{1/2}$—$6f\ [1]^\circ_{3/2}$
9254.39	30	10802.72	$4d\ ^4P_{1/2}$—$6f\ [1]^\circ_{1/2}$
9265.42	40000	10789.86	$5s\ ^4P_{3/2}$—$5p\ ^4D^\circ_{5/2}$
9282.80	100	10769.66	$5p'\ ^4S^\circ_{3/2}$—$6d\ ^4D_{5/2}$
9287.82	2	10763.84	$5p''\ ^2P^\circ_{3/2}$—$5d'\ ^2P_{3/2}$
9288.52	200	10763.02	$5p\ ^4P^\circ_{5/2}$—$6s'\ ^2P_{3/2}$
9314.85	30	10732.60	$5p''\ ^2P^\circ_{3/2}$—$6d\ ^4P_{1/2}$
9320.86	15000	10725.68	$5s''\ ^2P_{1/2}$—$5p''\ ^2P^\circ_{3/2}$
9325.32	20	10720.55	$5p''\ ^2P^\circ_{3/2}$—$6d\ ^4F_{3/2}$
9352.55	175	10689.34	$5p'\ ^4S^\circ_{3/2}$—$6d\ ^4D_{3/2}$
9354.56	15	10687.04	$4d\ ^4D_{5/2}$—$6p''\ ^2P^\circ_{3/2}$
9369.94	100	10669.50	$5p''\ ^2P^\circ_{1/2}$—$5d'\ ^4P_{3/2}$
9378.84	1	10659.37	$4d'\ ^2F_{7/2}$—$5f'\ [3]^\circ_{5/2}$
9379.21	30	10658.95	$4d'\ ^2F_{7/2}$—$5f'\ [3]^\circ_{7/2}$
9399.55	5	10635.89	$4d'\ ^2F_{7/2}$—$5f'\ [4]^\circ_{7/2}$
9400.19	90	10635.17	$4d'\ ^2F_{7/2}$—$5f'\ [4]^\circ_{9/2}$
9409.56	20	10624.57	$4d\ ^4D_{7/2}$—$7p\ ^4D^\circ_{5/2}$
9428.58	3	10603.14	$6s\ ^4P_{5/2}$—$7p'\ ^4S^\circ_{3/2}$
9434.51	3	10596.48	$5p''\ ^2P^\circ_{3/2}$—$5d'\ ^2P_{1/2}$
9438.20	80	10592.33	$4d\ ^4D_{7/2}$—$7p\ ^4D^\circ_{7/2}$
9460.14	500*d*	10567.77	$5p\ ^4P^\circ_{5/2}$—$6s'\ ^4P_{1/2}$
9466.45	2*w*	10560.73	$4d\ ^4F_{5/2}$—$6f\ [1]^\circ_{3/2}$
9470.67	20*h*	10556.02	$4d\ ^4F_{5/2}$—$4f''\ [3]^\circ_{7/2}$
9475.11	80	10551.07	$5p'\ ^4S^\circ_{3/2}$—$6d\ ^4D_{1/2}$
9476.32	30	10549.73	$4d\ ^4F_{5/2}$—$6f\ [2]^\circ_{5/2}$
9477.50	60	10548.41	$5p''\ ^2P^\circ_{1/2}$—$6d\ ^4F_{3/2}$
9488.66	120	10536.01	$4d\ ^4F_{5/2}$—$6f\ [4]^\circ_{7/2}$
9495.30	50	10528.64	$5p\ ^4D^\circ_{3/2}$—$5d\ ^4D_{1/2}$
9498.32	20	10525.29	$4d\ ^4D_{5/2}$—$7p\ ^4D^\circ_{3/2}$
9503.78	6*w*	10519.24	$5p\ ^4P^\circ_{5/2}$—$4d'''\ ^2D_{3/2}$
9507.03	75	10515.65	$4d\ ^4F_{5/2}$—$6f\ [3]^\circ_{7/2,\ 5/2}$
9517.27	100	10504.33	$4d\ ^4D_{7/2}$—$7p\ ^4P^\circ_{5/2}$
9543.03	40	10475.98	$4d\ ^4F_{7/2}$—$8p\ ^4D^\circ_{5/2}$
9552.67	175	10465.41	$5p\ ^4P^\circ_{3/2}$—$6s''\ ^2P_{1/2}$
9556.43	2*h*	10461.29	$4d\ ^4F_{7/2}$—$4f'\ [3]^\circ_{5/2}$
9560.17	6	10457.20	$4d\ ^4F_{7/2}$—$8p\ ^4D^\circ_{7/2}$
9576.17	1	10439.72	$4d'\ ^2P_{3/2}$—$5f'\ [3]^\circ_{5/2}$
9588.61	300	10426.18	$5p\ ^4P^\circ_{5/2}$—$6s'\ ^2P_{3/2}$
9590.33	20	10424.31	$5p''\ ^2P^\circ_{1/2}$—$5d'\ ^2P_{1/2}$
9597.98	2	10416.00	$4d\ ^4F_{7/2}$—$4f'\ [4]^\circ_{7/2}$
9598.79	60	10415.12	$4d\ ^4F_{7/2}$—$4f'\ [4]^\circ_{9/2}$
9603.62	35	10409.89	$4d'\ ^2P_{3/2}$—$5f'\ [2]^\circ_{5/2}$

TABLE A2. *Observed lines of* Br I—Continued

Wavelength	Intensity	Wave number	Classification
$\bar{A}$		K	
9604.30	6	10409.15	$4d'\ ^2P_{3/2}$—$5f'\ [2]^0_{3/2}$
9605.34	1	10408.02	$4d\ ^4F_{7/2}$—$8p\ ^4P^0_{5/2}$
9621.02	35*h*	10391.06	$4d\ ^4F_{3/2}$—$6f\ [1]^0_{3/2}$
9623.33	15	10388.56	$5p\ ^4D^0_{3/2}$—$5d\ ^4D_{3/2}$
9625.17	8	10386.58	$4d\ ^4F_{3/2}$—$4f''\ [3]^0_{5/2}$
9627.54	4	10384.02	$6s\ ^4P_{5/2}$—$9p\ ^4D^0_{7/2}$
9631.30	60	10379.97	$4d\ ^4F_{3/2}$—$6f\ [2]^0_{5/2}$
9635.05	20	10375.93	$4d\ ^4D_{3/2}$—$7p\ ^4D^0_{7/2}$
9661.08	1	10347.97	$6s\ ^4P_{5/2}$—$9p\ ^4P^0_{5/2}$
9662.99	20	10345.93	$4d\ ^4F_{3/2}$—$6f\ [3]^0_{5/2}$
9710.68	12	10295.12	$4d'\ ^2F_{5/2}$—$5f'\ [3]^0_{5/2}$
9717.48	40	10287.91	$4d\ ^4D_{3/2}$—$7p\ ^4P^0_{5/2}$
9719.20	600	10286.09	$4d\ ^4F_{9/2}$—$5f\ [5]_{11/2}$
9725.42	40	10279.51	$4d\ ^4D_{5/2}$—$7p\ ^4P^0_{3/2}$
9731.76	350	10272.82	$5p\ ^4P^0_{5/2}$—$4d''\ ^2D_{5/2}$
9732.90	50	10271.61	$4d'\ ^2F_{5/2}$—$5f'\ [4]^0_{7/2}$
9740.41	15	10263.69	$4d\ ^4F_{9/2}$—$5f\ [3]^0_{7/2}$
9745.86	100	10257.95	$4d\ ^4F_{9/2}$—$5f\ [4]^0_{9/2}$
9751.45	90	10252.07	$5p''\ ^2P^0_{3/2}$—$6d\ ^4D_{5/2}$
9793.48	6000	10208.08	$5s''\ ^2P_{1/2}$—$5p'\ ^4S^0_{3/2}$
9810.67	60	10190.19	$5p\ ^4D^0_{3/2}$—$5d\ ^4D_{5/2}$
9818.04	60	10182.54	$5p\ ^4P^0_{3/2}$—$4d''\ ^2D_{3/2}$
9818.21	70	10182.36	
9828.40	15	10171.81	$5p''\ ^2P^0_{3/2}$—$6d\ ^4D_{3/2}$
9831.25	2	10168.86	$4d\ ^4P_{1/2}$—$8p\ ^4P^0_{1/2}$
9844.17	7	10155.51	$4d\ ^4D_{3/2}$—$7p\ ^4D^0_{3/2}$
9864.95	2	10134.12	$4d\ ^4D_{3/2}$—$7p\ ^4P^0_{1/2}$
9896.40	10000	10101.91	$5s\ ^4P_{3/2}$—$5p\ ^4P^0_{3/2}$
9943.85	250	10053.71	$(^1D_2)5s\ ^2D_{5/2}$—$6p\ ^4D^0_{3/2}$
9944.18	250	10053.38	
9945.22	1	10052.33	$4d\ ^4P_{1/2}$—$4f'\ [2]^0_{3/2}$
9959.04	1	10038.38	$4d\ ^4D_{3/2}$—$7p\ ^4D^0_{5/2}$
9961.92	20	10035.47	$(^1D_2)5s\ ^2D_{3/2}$—$6p\ ^4D^0_{5/2}$
9962.13	30	10035.26	
9963.89	1	10033.49	$5p''\ ^2P^0_{3/2}$—$6d\ ^4D_{1/2}$
10001.96	10	9995.30	$4d\ ^4F_{5/2}$—$8p\ ^4D^0_{3/2}$
10025.23	4*h*	9972.10	$6s\ ^4P_{5/2}$—$6f\ [4]^0_{7/2}$
10045.71	3*h*	9951.77	$6s\ ^4P_{5/2}$—$6f\ [3]^0_{7/2,\ 5/2}$
10056.87	15	9940.73	$4d'\ ^4P_{3/2}$—$5f'\ [3]^0_{5/2}$
10061.53	25	9936.12	$5p\ ^4P^0_{3/2}$—$4d''\ ^2D_{5/2}$
10061.68	25	9935.97	
10079.75	10	9918.16	$4d\ ^4D_{3/2}$—$7p\ ^4P^0_{5/2}$
10085.99	35	9912.03	$(^1D_2)5s\ ^2D_{3/2}$—$6p\ ^4D^0_{5/2}$
10087.94	1	9910.11	$4d'\ ^4P_{3/2}$—$5f'\ [2]^0_{3/2}$
10088.31	10	9909.75	$4d\ ^4D_{3/2}$—$7p\ ^4P^0_{3/2}$
10102.82	12	9895.51	$5s''\ ^2P_{1/2}$—$5p'\ ^4D^0_{1/2}$
10107.60	100	9890.83	$(^1D_2)5s\ ^2D_{3/2}$—$6p\ ^4P^0_{1/2}$
10107.86	150	9890.58	
10113.74	2	9884.83	$4d\ ^4F_{5/2}$—$8p\ ^4D^0_{5/2}$
10119.19	3	9879.51	$4d\ ^4D_{1/2}$—$6p''\ ^2P^0_{1/2}$
10128.79	4	9870.14	$4d\ ^4F_{5/2}$—$4f'\ [3]^0_{5/2}$
10133.00	5	9866.04	$4d\ ^4F_{5/2}$—$8p\ ^4D^0_{7/2}$
10140.08	3000	9859.15	$5s'\ ^4P_{1/2}$—$5p\ ^4D^0_{3/2}$
10174.75	12	9825.56	$4d\ ^4F_{3/2}$—$8p\ ^4D^0_{3/2}$
10175.47	20	9824.86	$4d\ ^4F_{5/2}$—$4f'\ [4]^0_{7/2}$

TABLE A2. *Observed lines of* Br I—Continued

Wavelength	Intensity	Wave number	Classification
A		*K*	
10184. 02	300	9816. 61	$5p\ {}^4P^o_{3/2}$—$4s4p^6\ {}^2S_{1/2}$
10184. 49	200	9816. 16	
10197. 61	18	9803. 53	$4d\ {}^4D_{7/2}$—$6p'\ {}^2D^o_{5/2}$
10208. 91	300	9792. 68	$4d\ {}^4F_{7/2}$—$5f\ [5]^o_{9/2}$
10225. 23	1	9777. 05	$4d'\ {}^2F_{5/2}$—$7p''\ {}^2P^o_{3/2}$
10231. 61	8	9770. 95	$4d\ {}^4D_{5/2}$—$6p'\ {}^4S^o_{3/2}$
10232. 39	15	9770. 21	$4d\ {}^4F_{7/2}$—$5f\ [3]^o_{7/2,\ 5/2}$
10237. 14	75	9765. 68	$4d\ {}^4F_{7/2}$—$5f\ [4]^o_{7/2}$
10237. 74	6000	9765. 10	$5s\ {}^4P_{3/2}$—$5p\ {}^4P^o_{3/2}$
10243. 31	3	9759. 79	$4d\ {}^4D_{1/2}$—$7p\ {}^4D^o_{3/2}$
10248. 27	3	9755. 07	$4d''\ {}^2D_{5/2}$—$5f''\ [3]^o_{7/2}$
10265. 89	15*h*	9738. 33	$5p\ {}^4D^o_{5/2}$—$6s'\ {}^2P_{3/2}$
10293. 23	1	9712. 46	$4d'\ {}^4P_{5/2}$—$5f'\ [3]^o_{5/2}$
10293. 65	50	9712. 07	$4d'\ {}^4P_{5/2}$—$5f'\ [3]^o_{7/2}$
10299. 62	1000	9706. 44	$5s''\ {}^2P_{1/2}$—$5p'\ {}^2D^o_{3/2}$
10305. 99	10	9700. 44	$4d\ {}^4F_{3/2}$—$4f'\ [3]^o_{5/2}$
10310. 62	600*s*	9696. 08	$(^1D_2)5s\ {}^2D_{5/2}$—$6p\ {}^4P^o_{3/2}$
10310. 92	700	9695. 80	
10312. 90	40	9693. 94	$5p'\ {}^2S^o_{1/2}$—$5d\ {}^4F_{3/2}$
10314. 03	8	9692. 87	$4d\ {}^4D_{5/2}$—$6p'\ {}^2D^o_{5/2}$
10320. 09	15	9687. 18	$4d\ {}^4F_{3/2}$—$8p\ {}^4P^o_{3/2}$
10324. 96	3	9682. 61	$4d'\ {}^4P_{5/2}$—$5f'\ [2]^o_{5/2}$
10329. 74	80*s*	9678. 13	$(^1D_2)5s\ {}^2D_{3/2}$—$6p\ {}^4P^o_{3/2}$
10330. 17	100	9677. 73	
10370. 29	1	9640. 29	$4d\ {}^4F_{3/2}$—$4f'\ [2]^o_{3/2}$
10374. 37	12*cw*	9636. 50	$(^1D_2)5s\ {}^2D_{5/2}$—$6p\ {}^4P^o_{5/2}$
10377. 65	1500	9633. 45	$5p\ {}^4P^o_{3/2}$—$4d'\ {}^4P_{5/2}$
10384. 15	2	9627. 42	$4d'\ {}^2P_{1/2}$—$7p'\ {}^2S^o_{1/2}$
10388. 40	1	9623. 48	$5p'\ {}^2D^o_{3/2}$—$7s\ {}^4P_{5/2}$
10390. 74	175	9621. 32	$5p\ {}^4P^o_{1/2}$—$6s'\ {}^2P_{3/2}$
10414. 97	8	9598. 93	$5p'\ {}^2D^o_{3/2}$—$7s\ {}^4P_{3/2}$
10415. 10	8	9598. 81	
10457. 96	30000	9559. 47	$5s'\ {}^2P_{3/2}$—$5p\ {}^4D^o_{3/2}$
10483. 35	8	9536. 32	$5p\ {}^4D^o_{3/2}$—$6s''\ {}^2P_{1/2}$
10505. 05	8	9516. 62	$4d\ {}^4D_{3/2}$—$6p'\ {}^4D^o_{1/2}$
10507. 91	12	9514. 03	$4d\ {}^4D_{1/2}$—$7p\ {}^4P^o_{3/2}$
10513. 67	1	9508. 82	$4d''\ {}^2D_{3/2}$—$5f''\ [3]^o_{5/2}$
10529. 40	3	9494. 62	$5p\ {}^4D^o_{5/2}$—$4d''\ {}^2D_{3/2}$
10529. 58	3	9494. 45	
10554. 72	1	9471. 84	
10566. 15	250	9461. 59	$4d\ {}^4P_{1/2}$—$5f\ [1]^o_{3/2}$
10566. 87	100	9460. 95	$4d\ {}^4P_{1/2}$—$5f\ [1]^o_{1/2}$
10569. 67	2*d*	9458. 44	$5p'\ {}^2D^o_{3/2}$—$7s\ {}^4P_{5/2}$
10591. 51	10*w*	9438. 94	$4d\ {}^4D_{7/2}$—$(^1D_2)5p\ {}^2D^o_{5/2}$
10599. 94	1	9431. 43	$6s\ {}^4P_{5/2}$—$8p\ {}^4D^o_{3/2}$
10608. 66	40	9423. 68	$5p\ {}^4D^o_{7/2}$—$4d''\ {}^2D_{5/2}$
10616. 31	1	9416. 89	
10619. 65	1	9413. 93	$4d'\ {}^4P_{3/2}$—$7p''\ {}^2P^o_{1/2}$
10624. 34	1	9409. 77	$5p'\ {}^4D^o_{1/2}$—$7s\ {}^4P_{3/2}$
10629. 45	18	9405. 25	$5p\ {}^4P^o_{5/2}$—$4d'\ {}^4P_{3/2}$
10634. 08	1	9401. 15	$4d\ {}^4D_{3/2}$—$6p'\ {}^4S^o_{3/2}$
10638. 82	15	9396. 96	$4d'\ {}^2F_{7/2}$—$7p'\ {}^2D^o_{5/2}$
10660. 80	3	9377. 59	$5p\ {}^4P^o_{1/2}$—$4d''\ {}^2D_{3/2}$
10694. 91	12	9347. 68	$4d\ {}^4D_{7/2}$—$4f\ [5]^o_{9/2}$
10718. 84	100	9326. 81	$4d\ {}^4D_{7/2}$—$4f\ [2]^o_{5/2}$

TABLE A2. *Observed lines of* Br I—Continued

Wavelength	Intensity	Wave number	Classification
A		*K*	
10723. 10	15	9323. 11	$4d\ ^4D_{3/2}—6p'\ ^2D^\circ_{3/2}$
10742. 14	1000	9306. 58	$4d\ ^4D_{7/2}—4f\ [3]^\circ_{7/2}$
10742. 48	100	9306. 29	$6s\ ^4P_{5/2}—4f'\ [3]^\circ_{5/2}$ $4d\ ^4D_{7/2}—4f\ [3]^\circ_{5/2}$
10747. 20	20	9302. 20	$6s\ ^4P_{5/2}—8p\ ^4D^\circ_{7/2}$
10753. 58	150	9296. 68	$5p\ ^4P^\circ_{3/2}—4d'\ ^4P_{5/2}$
10754. 13	200	9296. 21	$4d\ ^4D_{7/2}—4f\ [4]^\circ_{7/2}$
10755. 92	3000	9294. 66	$4d\ ^4D_{7/2}—4f\ [4]^\circ_{9/2}$
10757. 77	6	9293. 06	$6s\ ^4P_{5/2}—8p\ ^4P^\circ_{3/2}$
10794. 92	5	9261. 08	$6s\ ^4P_{5/2}—4f'\ [4]^\circ_{7/2}$
10795. 10	10	9260. 93	
10798. 09	25	9258. 36	$5p'\ ^2D^\circ_{5/2}—5d\ ^4F_{3/2}$
10804. 40	3	9252. 95	$6s\ ^4P_{5/2}—8p\ ^4P^\circ_{5/2}$
10810. 05	300	9248. 12	$5p\ ^4D^\circ_{5/2}—4d''\ ^5D_{5/2}$
10811. 47	1*w*	9246. 90	$6s\ ^4P_{5/2}—4f'\ [2]^\circ_{5/2}$
10815. 65	6	9243. 33	$5p'\ ^2D^\circ_{5/2}—5d\ ^4F_{5/2}$
10840. 05	500*d*	9222. 52	$4d\ ^4D_{5/2}—(^1D_2)5p\ ^2D^\circ_{5/2}$
10843. 86	2*w*	9219. 28	$4d\ ^4F_{5/2}—5f\ [1]^\circ_{3/2}$
10846. 12	10	9217. 36	$4d\ ^4D_{3/2}—6p'\ ^2D^\circ_{3/2}$
10869. 70	100	9197. 37	$4d\ ^4F_{5/2}—5f\ [2]^\circ_{5/2}$
10871. 62	90	9195. 74	$5p'\ ^2S^\circ_{1/2}—5d\ ^4D_{1/2}$
10891. 43	250	9179. 02	$4d\ ^4F_{5/2}—5f\ [3]^\circ_{7/2,5/2}$
10892. 79	100	9177. 87	$4d\ ^4D_{5/2}—(^1D_2)5p\ ^2D^\circ_{5/2}$
10896. 79	200	9174. 50	$4d\ ^4F_{5/2}—5f\ [4]^\circ_{7/2}$
10908. 62	60*d*	9164. 55	$4d\ ^4D_{5/2}—4f\ [1]^\circ_{3/2}$
10947. 50	1	9132. 00	$4d'\ ^2P_{1/2}—6f\ [1]^\circ_{3/2}$
10947. 89	1	9131. 68	$4d'\ ^2P_{1/2}—6f\ [1]^\circ_{1/2}$
10960. 83	2*w*	9120. 90	$4d\ ^4D_{1/2}—6p'\ ^4D^\circ_{1/2}$
10961. 30	3	9120. 51	$4d'\ ^2P_{1/2}—6f\ [2]^\circ_{3/2}$
10973. 48	500	9110. 38	$4d\ ^4D_{5/2}—4f\ [2]^\circ_{5/2}$
10979. 00	300	9105. 80	$5s''\ ^2P_{1/2}—5p'\ ^2S^\circ_{1/2}$
10982. 30	100	9103. 07	$4d\ ^4D_{5/2}—4f\ [2]^\circ_{5/2}$
10989. 51	1	9097. 10	$5p'\ ^4S^\circ_{3/2}—7s\ ^4P_{3/2}$
10991. 12	2	9095. 76	$4d'\ ^2F_{5/2}—7p'\ ^2D^\circ_{5/2}$
10997. 85	600	9090. 20	$4d\ ^4D_{5/2}—4f\ [3]^\circ_{7/2}$
10998. 28	400	9089. 84	$4d\ ^4D_{5/2}—4f\ [3]^\circ_{5/2}$
11007. 42	10	9082. 29	$4d\ ^4D_{3/2}—6p'\ ^2S^\circ_{1/2}$
11010. 45	600	9079. 79	$4d\ ^4D_{5/2}—4f\ [4]^\circ_{7/2}$
11012. 31	5	9078. 26	$5p'\ ^2D^\circ_{3/2}—5d\ ^4F_{5/2}$
11013. 22	20	9077. 51	$5p'\ ^2D^\circ_{3/2}—5d\ ^4P_{1/2}$
11018. 55	1	9073. 12	$4d''\ ^2D_{3/2}—5f'\ [3]^\circ_{5/2}$
11024. 25	10	9068. 43	$5p\ ^4P^\circ_{3/2}—4d'\ ^4P_{3/2}$
11039. 80	60	9055. 66	$5p\ ^2S^\circ_{1/2}—5d\ ^4D_{3/2}$
11045. 74	800*d*	9050. 79	$5p\ ^4P^\circ_{5/2}—4d'\ ^2F_{5/2}$
11047. 21	10	9049. 58	$4d\ ^4F_{3/2}—5f\ [1]^\circ_{5/2}$ $4d''\ ^2D_{3/2}—5f'\ [4]^\circ_{7/2}$
11047. 62	17	9049. 25	$4d\ ^4F_{9/2}—7p\ ^4D^\circ_{7/2}$
11074. 08	40	9027. 62	$4d\ ^4F_{3/2}—5f\ [2]^\circ_{5/2}$
11093. 51	250	9011. 81	$5p\ ^4P^\circ_{1/2}—4s4p^6\ ^2S_{1/2}$
11094. 24	100	9011. 22	
11096. 59	20	9009. 31	$4d\ ^4F_{3/2}—5f\ [3]^\circ_{5/2}$
11100. 65	1	9006. 02	$6s\ ^4P_{3/2}—8p\ ^4D^\circ_{5/2}$

TABLE A2. *Observed lines of* Br I—Continued

Wavelength	Intensity	Wave number	Classification
A		*K*	
11101.36	1	9005.44	$4d\ ^4D_{1/2}$—$6p'\ ^4S^o_{3/2}$
11161.72	1*w*	8956.74	$5p'\ ^4S^o_{3/2}$—$7s\ ^4P_{5/2}$
11194.99	100	8930.12	$5s'\ ^4P_{1/2}$—$5p\ ^4P^o_{1/2}$
11197.14	3	8928.41	$5p'\ ^2D^o_{5/2}$—$5d\ ^4F_{7/2}$
11225.08	250	8906.18	$5p\ ^4P^o_{5/2}$—$4d'\ ^2P_{3/2}$
11247.50	2	8888.43	$5p'\ ^4D^o_{1/2}$—$5d\ ^4P_{1/2}$
11292.69	2	8852.86	$4d\ ^4D_{3/2}$—$(^1D_2)5p\ ^2D^o_{5/2}$
11316.93	10*w* (8)	8833.90	$5p\ ^4D^o_{3/2}$—$6s'\ ^4P_{1/2}$
11325.97	1 (—)	8826.85	
11350.04	65 (27)	8808.13	$4d\ ^4D_{3/2}$—$(^1D_2)5p\ ^2D^o_{3/2}$
11367.25	4*w* (7)	8794.79	$4d\ ^4D_{3/2}$—$4f\ [1]^o_{3/2}$
11367.97	4*w*	8794.24	$4d\ ^4D_{3/2}$—$4f\ [1]^o_{1/2}$
11437.61	9 (11)	8740.69	$4d\ ^4D_{3/2}$—$4f\ [2]^o_{5/2}$
11447.27	18 (36)	8733.32	$4d\ ^4D_{3/2}$—$4f\ [2]^o_{3/2}$
11464.58	35 (100)	8720.13	$4d\ ^4D_{3/2}$—$4f\ [3]^o_{5/2}$
11501.31	1 (*m*)	8692.28	$5p\ ^4D^o_{3/2}$—$6s'\ ^2P_{3/2}$
11508.77	30 (85)	8686.65	$4d\ ^4D_{1/2}$—$6p'\ ^2S^o_{1/2}$
11583.71	10 (8)	8630.45	$5s'\ ^2P_{3/2}$—$5p\ ^4P^o_{1/2}$
11597.64	1 (4)	8620.08	$5p'\ ^2D^o_{5/2}$—$5d\ ^4D_{3/2}$
11631.33	2 (2)	8595.12	$5p'\ ^2D^o_{3/2}$—$5d\ ^4D_{1/2}$
11636.08	1 (—)	8591.61	$5p'\ ^4S^o_{3/2}$—$5d\ ^4F_{3/2}$
11640.94	1 (10)	8588.02	$4d\ ^4F_{7/2}$—$7p\ ^4D^o_{3/2}$
11666.20	20*d* (169)	8569.43	$5p\ ^4P^o_{3/2}$—$4d'\ ^2P_{3/2}$
11742.85	400 (219)	8513.49	$5s'\ ^2P_{3/2}$—$5p\ ^4D^o_{5/2}$
11810.29	1 (1)	8464.88	$4d'\ ^2F_{5/2}$—$6f\ [3]^o_{7/2,\ 5/2}$
11819.40	2 (—)	8458.35	
11833.14	1 (—)	8448.53	$5p\ ^4D^o_{3/2}$—$4d''\ ^2D_{3/2}$
11870.77	4 (5)	8421.75	$5p'\ ^2D^o_{5/2}$—$5d\ ^4D_{5/2}$
11883.95	4 (6)	8412.41	$4d\ ^4D_{1/2}$—$(^1D_2)5p\ ^2D^o_{3/2}$
11902.79	5 (19)	8399.09	$4d\ ^4D_{1/2}$—$4f\ [1]^o_{3/2}$
11903.61	8 (16)	8398.51	$4d\ ^4D_{1/2}$—$4f\ [1]^o_{1/2}$
11928.11	8 (13)	8381.26	$4d'\ ^2P_{1/2}$—$4f'\ [2]^o_{3/2}$
11990.57	15 (38)	8337.61	$4d\ ^4D_{1/2}$—$4f\ [2]^o_{3/2}$
12088.15	2 (—)	8270.30	
12285.57	2 (*m*)	8137.40	$4d'\ ^2F_{7/2}$—$4f'\ [4]^o_{9/2}$
12303.89	35 (275)	8125.29	$5s'\ ^4P_{1/2}$—$5p\ ^4P^o_{3/2}$
12354.43	1 (40)	8092.05	$5p\ ^4P^o_{3/2}$—$4d'\ ^2P_{1/2}$
12368.95	1*w* (170)	8082.55	$5p\ ^4D^o_{3/2}$—$4s4p^6\ ^2S_{1/2}$
12809.50	1 (400)	7804.57	$4d\ ^4F_{9/2}$—$4f\ [5]^o_{11/2}$

[a] λ4000.599 If this line itself is not of molecular origin, it is probably the blended hfs components of shorter wavelength for this transition, the long wavelength component having been lost in the molecular background.

[b] λλ4446.08, 4654.18, 6531.39. There are Cl lines of almost these same wavelengths.

[c] λ5905.66 This line appears to be the long wavelength hfs component of this transition, the other components having been obscured by the wing of the adjacent line.

[d] λ6151.10 Blended with ghost of adjacent strong line.

[e] λ7617.82 The transition $5p'\ ^2D^o_{3/2}$—$7d\ ^4D_{3/2}$ probably contributes to this component.

TABLE A3. *Lines of* Br I *observed radiometrically*

Computed wavelength	Intensity	Computed wave number	Classification
Å		K	
11806.31	1	8467.73	$4d\ ^4F_{7/2}—7p\ ^4P^o_{5/2}$
12094.54	3	8265.93	$5p'\ ^4D^o_{1/2}—5d\ ^4D_{3/2}$
12108.09	14	8256.68	$5p'\ ^2D^o_{5/2}—5d\ ^4D_{7/2}$
12108.16		8256.63	$5p'\ ^2D^o_{3/2}—5d\ ^4D_{5/2}$
12303.93	275	8125.26	$5s'\ ^4P_{1/2}—5p\ ^4P^o_{3/2}$
12354.56	40	8091.96	$5p\ ^4P^o_{3/2}—4d'\ ^2P_{1/2}$
12368.99	170	8082.52	$5p\ ^4D^o_{3/2}—4s4p^6\ ^2S_{1/2}$
12513.40	20	7989.25	$5p\ ^4P^o_{5/2}—6s\ ^4P_{3/2}$
12647.55	10	7904.51	$4d'\ ^2P_{3/2}—4f'\ [2]^o_{5/2}$
12755.94	60	7837.34	$5p\ ^4D^o_{7/2}—4d'\ ^2F_{7/2}$
12809.50	400	7804.57	$4d\ ^4F_{9/2}—4f\ [5]^o_{11/2}$
12859.77	30	7774.06	$4d'\ ^2F_{5/2}—4f'\ [4]^o_{7/2}$
12861.74	30	7772.87	$5s''\ ^2P_{1/2}—5p\ ^4D^o_{3/2}$
12897.12	48	7751.55	$4d\ ^4F_{9/2}—4f\ [4]^o_{9/2}$
13048.21	38	7661.79	$5p\ ^4D^o_{3/2}—4d'\ ^2F_{7/2}$
13064.15	110	7652.44	$5p\ ^4P^o_{3/2}—6s\ ^4P_{3/2}$
13217.17	1700	7563.85	$5p\ ^4P^o_{5/2}—6s\ ^4P_{5/2}$
13328.04	10	7500.93	$5p'\ ^2S^o_{1/2}—6s'\ ^4P_{1/2}$
13349.73	36	7488.74	$5s'\ ^2P_{3/2}—5p\ ^4P^o_{5/2}$
13392.33	20	7464.92	$4d'\ ^4P_{3/2}—4f'\ [3]^o_{5/2}$
13484.87	9	7413.69	$5p'\ ^4D^o_{1/2}—6s''\ ^2P_{1/2}$
13584.48	30	7359.33	$5p'\ ^2S^o_{1/2}—6s'\ ^2P_{3/2}$
13674.13	300	7311.08	$4d\ ^4F_{7/2}—4f\ [5]^o_{9/2}$
13808.19	23	7240.10	$6p\ ^4P^o_{1/2}—10s\ ^4P_{3/2}$
13808.45		7239.96	$4d'\ ^4P_{5/2}—4f'\ [3]^o_{7/2}$
13821.95	9	7232.89	$4d\ ^4D_{1/2}—(^1D_2)5p\ ^2P^o_{3/2}$
13822.07		7232.83	$6p\ ^4D^o_{3/2}—10s\ ^4P_{5/2}$
13822.56		7232.57	$4d'\ ^4P_{5/2}—8p\ ^4D^o_{7/2}$
13833.14	750	7227.04	$5p\ ^4P^o_{3/2}—6s\ ^4P_{5/2}$
14078.51	10	7101.08	$5p'\ ^4S^o_{3/2}—6s''\ ^2P_{1/2}$
14290.98	68	6995.51	$4d\ ^4P_{1/2}—4f\ [1]^o_{3/2}$
14292.20		6994.91	$4d\ ^4P_{1/2}—4f\ [1]^o_{1/2}$
14354.57	1800	6964.52	$5p\ ^4D^o_{5/2}—6s\ ^4P_{3/2}$
14439.14	344	6923.73	$5p'\ ^2D^o_{5/2}—6s'\ ^2P_{3/2}$
14488.21	105	6900.28	$5p'\ ^2D^o_{3/2}—6s'\ ^4P_{1/2}$
14599.73	338	6847.57	$5p\ ^4P^o_{1/2}—6s\ ^4P_{3/2}$
14607.80	21	6843.79	$5s''\ ^2P_{1/2}—5p\ ^4P^o_{1/2}$
14888.70	1250	6714.67	$5p\ ^4D^o_{7/2}—6s\ ^4P_{5/2}$
14896.37	55	6711.21	$5p'\ ^4D^o_{1/2}—6s'\ ^4P_{1/2}$
14923.43	12	6699.04	$4d\ ^4F_{5/2}—4f\ [2]^o_{5/2}$
14968.61	85	6678.82	$4d\ ^4F_{5/2}—4f\ [3]^o_{7/2}$
14969.33		6678.50	$4d\ ^4F_{5/2}—4f\ [3]^o_{5/2}$
14991.94	89	6668.43	$4d\ ^4F_{5/2}—4f\ [4]^o_{7/2}$
15003.82	35	6663.15	$5p\ ^4P^o_{3/2}—4d\ ^4F_{5/2}$
15052.95	10	6641.40	$4d\ ^4F_{3/2}—(^1D_2)5p\ ^2D^o_{5/2}$
15146.09	30	6600.56	$4d''\ ^2D_{5/2}—4f'\ [3]^o_{7/2}$
15185.29	188	6583.52	$5p''\ ^2P^o_{3/2}—6s''\ ^2P_{1/2}$
15185.43		6583.46	$4d\ ^4F_{3/2}—4f\ [1]^o_{3/2}$
15186.82		6582.86	$4d\ ^4F_{3/2}—4f\ [1]^o_{1/2}$
15258.39	10	6551.98	$4d''\ ^2D_{5/2}—4f'\ [4]^o_{7/2}$
15311.39	63	6529.30	$4d\ ^4F_{3/2}—4f\ [2]^o_{5/2}$
15359.71	22	6508.76	$4d\ ^4F_{3/2}—4f\ [3]^o_{5/2}$
15422.36	28	6482.32	$4d\ ^4D_{7/2}—6p\ ^4P^o_{5/2}$
15539.25	3	6433.56	$5p'\ ^2D^o_{5/2}—4d''\ ^2D_{5/2}$
15570.03	219	6420.84	$5p\ ^4P^o_{3/2}—4d\ ^4P_{1/2}$
15593.01	37	6411.38	$5p''\ ^2P^o_{1/2}—6s''\ ^2P_{1/2}$
15599.33	18	6408.78	$5p\ ^4P^o_{5/2}—4d\ ^4F_{7/2}$
15624.15	24	6398.60	$5p'\ ^4S^o_{3/2}—6s'\ ^4P_{1/2}$
15624.47		6398.47	$6p\ ^4D^o_{7/2}—9s\ ^4P_{5/2}$
15804.98	7	6325.39	$4d\ ^4D_{3/2}—6p\ ^4P^o_{3/2}$
15890.32	2	6291.42	$4d''\ ^2D_{3/2}—4f'\ [2]^o_{5/2}$
15948.40	20	6268.51	$5p'\ ^2D^o_{3/2}—4d''\ ^2D_{5/2}$
15955.01	8	6265.91	$4d\ ^4D_{3/2}—6p\ ^4P^o_{5/2}$
15977.73	47	6257.00	$5p'\ ^4S^o_{3/2}—6s'\ ^2P_{3/2}$
16253.66	90	6150.78	$5p\ ^4D^o_{7/2}—4d\ ^4F_{5/2}$
16584.66	250	6028.02	$5p\ ^4P^o_{1/2}—4d\ ^4F_{3/2}$
16625.37	10	6013.26	$5p'\ ^4S^o_{3/2}—4d''\ ^2D_{3/2}$
16657.89	10	6001.52	$5p'\ ^2S^o_{1/2}—4d'\ ^4P_{3/2}$
16731.19	1800	5975.23	$5p\ ^4D^o_{5/2}—4d\ ^4F_{5/2}$
17254.05	105	5794.16	$5p'\ ^2D^o_{3/2}—4d'\ ^4P_{5/2}$
17335.81	25	5766.83	$5p'\ ^4S^o_{3/2}—4d''\ ^2D_{5/2}$
17801.50	330	5615.97	$5p\ ^4P^o_{1/2}—4d\ ^4P_{1/2}$
17982.00	40	5559.60	$5p\ ^4D^o_{7/2}—4d\ ^4F_{7/2}$
18191.08	60	5495.70	$5p''\ ^2P^o_{3/2}—4d''\ ^2D_{3/2}$
18212.72	10	5489.17	$4d'\ ^2F_{7/2}—6p'\ ^2D^o_{5/2}$
18510.48	180	5400.87	$5p'\ ^2D^o_{3/2}—4d'\ ^4P_{3/2}$
18568.31	500	5384.05	$5p\ ^4D^o_{5/2}—4d\ ^4F_{7/2}$
18779.29	313	5323.56	$5p''\ ^2P^o_{1/2}—4d''\ ^2D_{3/2}$
19045.07	547	5249.27	$5p''\ ^2P^o_{3/2}—4d''\ ^2D_{5/2}$
19181.99	266	5211.80	$5p'\ ^4D^o_{1/2}—4d'\ ^4P_{3/2}$
19183.17		5211.48	$5p'\ ^2D^o_{5/2}—4d'\ ^2F_{5/2}$
19317.02	120	5175.37	$4d\ ^4F_{9/2}—6p\ ^4D^o_{7/2}$
19497.52	313	5127.43	$5p'\ ^4S^o_{3/2}—4d'\ ^4P_{5/2}$
19606.57	263	5098.94	$5p\ ^4D^o_{3/2}—4d\ ^4F_{3/2}$
19733.62	3450	5066.11	$5p\ ^4D^o_{7/2}—4d\ ^4F_{9/2}$
19810.58	452	5046.43	$5p'\ ^2D^o_{3/2}—4d'\ ^2F_{5/2}$
19894.71	68	5025.09	$5p'\ ^2S^o_{1/2}—4d'\ ^2P_{1/2}$
19925.72	138	5017.27	$5p\ ^4P^o_{5/2}—4d\ ^4D_{1/2}$
20073.55	7	4980.32	$4d'\ ^2F_{7/2}—4f\ [4]^o_{9/2}$
20162.50	138	4958.35	$5p\ ^4P^o_{5/2}—4d\ ^4D_{3/2}$
20248.38	8	4937.32	$(^1D_2)5p\ ^2F^o_{5/2}—(^1D_2)4d\ ^2G_{7/2}$
20281.73	500	4929.20	$5p\ ^4D^o_{3/2}—4d\ ^4F_{5/2}$
20405.97	7	4899.19	$5p'\ ^4S^o_{3/2}—4d'\ ^4P_{3/2}$
20624.67	547	4847.24	$5p'\ ^2D^o_{5/2}—4d'\ ^2F_{7/2}$
21093.83	43	4739.43	$4d\ ^4F_{7/2}—6p\ ^4D^o_{5/2}$
21213.11	14	4712.78	$5p'\ ^4D^o_{1/2}—4d'\ ^2P_{3/2}$
21285.74	17	4696.70	$(^1D_2)5p\ ^2F^o_{7/2}—(^1D_2)4d\ ^2G_{9/2}$
21330.29	37	4686.89	$5p\ ^4D^o_{3/2}—4d\ ^4P_{1/2}$
21631.91	359	4621.54	$5p\ ^4P^o_{3/2}—4d\ ^4D_{3/2}$
21743.98	14	4597.72	$6s\ ^4P_{3/2}—(^1D_2)5p\ ^2P^o_{3/2}$
21787.24	469	4588.59	$5p\ ^4P^o_{5/2}—4d\ ^4D_{5/2}$
21801.59	6	4585.57	$5p'\ ^2S^o_{1/2}—6s\ ^4P_{3/2}$
22720.19	60	4400.17	$5p'\ ^4S^o_{3/2}—4d'\ ^2P_{3/2}$
22865.65	950	4372.18	$5p\ ^4P^o_{5/2}—4d\ ^4D_{7/2}$
23404.15	12	4271.58	$4d\ ^4F_{5/2}—6p\ ^4D^o_{5/2}$
23513.15	206	4251.78	$5p\ ^4P^o_{3/2}—4d\ ^4D_{5/2}$
23732.96	40	4212.40	$5p\ ^4P^o_{1/2}—4d\ ^4D_{1/2}$
24099.97	2	4148.25	$4d\ ^4F_{5/2}—6p\ ^4D^o_{5/2}$

(Paper 67A6–238)

JOURNAL OF RESEARCH of the National Bureau of Standards—A. Physics and Chemistry
Vol. 67A, No. 6, November—December 1963

Matrices of Spin-Orbit Interaction in the Electron Configurations $np^2\ n'\ p$ and $np^4\ n'\ p$

Jack L. Tech

(November 2, 1962)

The matrices of spin-orbit interaction in the $p^2\ p$ and $p^4\ p$ electron configurations have been calculated. The matrices have been checked by showing that their eigenvalues, calculated by use of an IBM 7090, agree with the correct eigenvalues known from the theory of jj-coupling. For the sake of completeness, the matrices of electrostatic interaction for these configurations are also given.

1. Introduction

In connection with our analysis of the first spectrum of bromine, reported in the preceding paper, it became desirable to know the energy matrices in intermediate coupling for the configuration $np^4\ n'\ p$. Since the matrices of spin-orbit interaction for this configuration have not appeared in the literature it was decided, at the suggestion of Professor Racah, to calculate them. The primary use of such interaction matrices is to obtain approximate predicted values for the energy levels of atomic systems. The eigenvalues and eigenvectors of the matrices represent, respectively, the energy levels and wave functions of the atomic system.

The predicted levels are a great aid in the problem of locating and identifying the observed energy levels. Until recently, most comparisons with observations were carried out in the approximation of pure Russell-Saunders coupling, employing in the theoretical calculations only the matrices of the electrostatic interaction. But the availability of electronic digital computers now renders it practical to include the effects of spin-orbit interaction in the calculations.

2. Spin-Orbit Interaction

The matrices of spin-orbit interaction for the configuration $np^2\ n'\ p$ are given in table 3. Since the energy matrix is diagonal in J, the nondiagonal elements occur only between levels with the same J value. There is thus one matrix for each possible value of J. The rows and columns of the matrices are specified by the name of the term in LS-coupling notation, the terms in parentheses denoting the parent terms in np^2. The elements of these matrices are linear combinations of the spin-orbit integrals ζ and ζ', where ζ is written for ζ_{np} and ζ' for $\zeta_{n'p}$. Both these integrals are positive. Their coefficients were calculated following the methods outlined by Fano and Racah [1].[1] Values of the $\overline{W}$-coefficients, or 6-j symbols, needed for these calculations were obtained from the compilation of Rotenberg et al. [2]. The matrices have been checked by using an IBM 7090 to determine their eigenvalues and showing them to agree with the correct eigenvalues known from the theory of jj-coupling [cf. 3, ch. 10].

The matrices for the $np^4\ n'\ p$ configuration are identical to the above except that in this case the sign of the spin-orbit coupling parameter ζ_{np} is reversed [3, p. 299].

3. Electrostatic Interaction

To obtain the complete energy matrices in intermediate coupling, the electrostatic matrices must be added to the spin-orbit matrices of table 3. The matrices of electrostatic interaction in Russell-Saunders coupling are well-known for the $np^2\ n'\ p$ and $np^4\ n'\ p$ configurations, and we give them here in tables 1 and 2 for the sake of completeness. The elements of the matrices are expressed as linear combinations of the usual parameters F_k and G_k, which are defined as certain integrals over radial wave functions [3, p. 177]. We calculated the coefficients of these parameters from the general tables given by Slater [4, vol. II, appendix 21]. Terms of a kind that occur only once in these configurations have no matrix elements connecting them to other terms; the diagonal components give the energies directly. Since there are two $^2D^\circ$ terms, however, there are matrix components between them, and the electrostatic energies of the

[1] Figures in brackets indicate the literature references at the end of this paper

two terms are found as the eigenvalues of the corresponding matrix. The same holds also for the three $^2P^\circ$ terms.

Following Slater, the energies are stated in terms of the average energy, $E_{av} \equiv E$, which represents the center of gravity of the terms of the configuration, each term being assigned the weight $(2S+1)(2L+1)$. The energy expressions can easily be converted, if desired, so as to conform to the usage of Condon and Shortley. In this case, E is replaced in the energy expressions by the following quantities:

Configuration	E
$np^2n'p$	$(F_0+2F_0')-2F_2-\frac{1}{3}G_0'-\frac{10}{3}G_2'$
$np^4n'p$	$(6F_0+4F_0')-12F_2-\frac{2}{3}G_0'-\frac{20}{3}G_2'$

Here, as in tables 1 and 2, the parameters without primes refer to the (np, np) interactions while those with primes refer to the $(np, n'p)$ interactions. In accordance with TAS, the subscripted parameters are defined in terms of the corresponding superscripted parameters as follows:

$$F_2(p,p) = \frac{1}{25} F^2(p,p)$$

$$F_2(p,p') = \frac{1}{25} F^2(p,p')$$

$$G_0(p,p') = G^0(p,p')$$

$$G_2(p,p') = \frac{1}{25} G^2(p,p')$$

TABLE 1. *Electrostatic energies for $np^2n'p$*

Parent	Term	Energy
(^3P)	$^4D^\circ$	$E-3F_2-F_2'-\frac{2}{3}G_0'-\frac{2}{3}G_2'$
	$^4P^\circ$	$E-3F_2+5F_2'-\frac{2}{3}G_0'-\frac{20}{3}G_2'$
	$^4S^\circ$	$E-3F_2-10F_2'+\frac{7}{3}G_0'-\frac{20}{3}G_2'$
	$^2S^\circ$	$E-3F_2-10F_2'-\frac{2}{3}G_0'+\frac{25}{3}G_2'$
(^1D)	$^2F^\circ$	$E+3F_2+2F_2'-\frac{2}{3}G_0'+\frac{7}{3}G_2'$

	$(^3P)^2D^\circ$	$(^1D)^2D^\circ$
$(^3P)^2D^\circ$	$E-3F_2-F_2'+\frac{5}{6}G_0'+\frac{16}{3}G_2'$	$-\frac{3}{2}G_0'+3G_2'$
$(^1D)^2D^\circ$	$-\frac{3}{2}G_0'+3G_2'$	$E+3F_2-7F_2'+\frac{5}{6}G_0'-\frac{2}{3}G_2'$

	$(^3P)^2P^\circ$	$(^1D)^2P^\circ$	$(^1S)^2P^\circ$
$(^3P)^2P^\circ$	$E-3F_2+5F_2'+\frac{5}{6}G_0'+\frac{25}{3}G_2'$	$+\frac{\sqrt{5}}{2}G_0'+2\sqrt{5}G_2'$	$-G_0'+5G_2'$
$(^1D)^2P^\circ$	$+\frac{\sqrt{5}}{2}G_0'+2\sqrt{5}G_2'$	$E+3F_2+7F_2'+\frac{1}{6}G_0'-\frac{13}{3}G_2'$	$+4\sqrt{5}F_2'-\frac{\sqrt{5}}{3}G_0'-\frac{\sqrt{5}}{3}G_2'$
$(^1S)^2P^\circ$	$-G_0'+5G_2'$	$+4\sqrt{5}F_2'-\frac{\sqrt{5}}{3}G_0'-\frac{\sqrt{5}}{3}G_2'$	$E+12F_2$

4. Summary

The matrices of spin-orbit interaction for the configurations $np^2n'p$ and $np^4n'p$ have been calculated and are presented in table 3. The matrices of electrostatic interaction are also given, in tables 1 and 2. The complete energy matrices for these configurations can thus be formed in the approximation that neglects spin-spin and spin-other-orbit interactions as well as configuration mixing.

The configurations under discussion occur in a number of important neutral and ionized atoms, including the halogens and Bi, Sb, As, P, N, and their isoelectronic sequences. The sets of energy levels associated with these configurations are known to different stages of completeness for the various atoms. A systematic, comparative study of these atoms is being launched. A similar study is contemplated for the $np^2n'd$ and $np^4n'd$ configurations, whose spin-orbit matrices are presently being calculated and will be reported at a later time.

TABLE 2. *Electrostatic energies for $np^4n'p$*

Parent	Term	Energy
(^{3}P)	^{4}D°	$E-3F_2+F_2'-\frac{1}{3}G_0'-\frac{10}{3}G_2'$
	^{4}P°	$E-3F_2-5F_2'-\frac{1}{3}G_0'-\frac{10}{3}G_2'$
	^{4}S°	$E-3F_2+10F_2'-\frac{1}{3}G_0'-\frac{10}{3}G_2'$
	^{2}S°	$E-3F_2+10F_2'-\frac{1}{3}G_0'-\frac{10}{3}G_2'$
(^{1}D)	^{2}F°	$E+3F_2-2F_2'-\frac{1}{3}G_0'+\frac{8}{3}G_2'$

	(^{3}P)^{2}D°	(^{1}D)^{2}D°
(^{3}P)^{2}D°	$E-3F_2+F_2'-\frac{1}{3}G_0'+\frac{61}{6}G_2'$	$-\frac{9}{2}G_2'$
(^{1}D)^{2}D°	$-\frac{9}{2}G_2'$	$E+3F_2+7F_2'-\frac{1}{3}G_0'-\frac{11}{6}G_2'$

	(^{3}P)^{2}P°	(^{1}D)^{2}P°	(^{1}S)^{2}P°
(^{3}P)^{2}P°	$E-3F_2-5F_2'+\frac{8}{3}G_0'+\frac{25}{6}G_2'$	$+\sqrt{5}G_0'-\frac{\sqrt{5}}{2}G_2'$	$+G_0'-5G_2'$
(^{1}D)^{2}P°	$+\sqrt{5}G_0'-\frac{\sqrt{5}}{2}G_2'$	$E+3F_2-7F_2'+\frac{4}{3}G_0'-\frac{19}{6}G_2'$	$-4\sqrt{5}F_2'+\frac{\sqrt{5}}{3}G_0'+\frac{\sqrt{5}}{3}G_2'$
(^{1}S)^{2}P°	$+G_0'-5G_2'$	$-4\sqrt{5}F_2'+\frac{\sqrt{5}}{3}G_0'+\frac{\sqrt{5}}{3}G_2'$	$E+12F_2$

TABLE 3. *Matrices of spin-orbit interaction for the configuration $np^2n'p$*

$J=\frac{7}{2}$	$(^1D)^2F^\circ$	$(^3P)^4D^\circ$
$(^1D)^2F^\circ$	$+\frac{1}{2}\zeta'$	$+\frac{\sqrt{2}}{2}\zeta$
$(^3P)^4D^\circ$	$+\frac{\sqrt{2}}{2}\zeta$	$+\frac{1}{2}(\zeta+\zeta')$

$J=\frac{5}{2}$	$(^1D)^2F^\circ$	$(^3P)^4D^\circ$	$(^3P)^2D^\circ$	$(^1D)^2D^\circ$	$(^3P)^4P^\circ$
$(^1D)^2F^\circ$	$-\frac{2}{3}\zeta'$	$+\frac{1}{3}\zeta$	$-\frac{\sqrt{14}}{6}\zeta$	$-\frac{\sqrt{14}}{6}\zeta'$	0
$(^3P)^4D^\circ$	$+\frac{1}{3}\zeta$	$-\frac{1}{12}(\zeta+\zeta')$	$-\frac{\sqrt{14}}{12}(\zeta-2\zeta')$	$+\frac{\sqrt{14}}{12}\zeta$	$+\frac{\sqrt{21}}{12}(\zeta-\zeta')$
$(^3P)^2D^\circ$	$-\frac{\sqrt{14}}{6}\zeta$	$-\frac{\sqrt{14}}{12}(\zeta-2\zeta')$	$+\frac{1}{6}(2\zeta-\zeta')$	$+\frac{1}{6}\zeta$	$+\frac{\sqrt{6}}{12}(\zeta+2\zeta')$
$(^1D)^2D^\circ$	$-\frac{\sqrt{14}}{6}\zeta'$	$+\frac{\sqrt{14}}{12}\zeta$	$+\frac{1}{6}\zeta$	$+\frac{1}{6}\zeta'$	$+\frac{\sqrt{6}}{4}\zeta$
$(^3P)^4P^\circ$	0	$+\frac{\sqrt{21}}{12}(\zeta-\zeta')$	$+\frac{\sqrt{6}}{12}(\zeta+2\zeta')$	$+\frac{\sqrt{6}}{4}\zeta$	$+\frac{1}{4}(\zeta+\zeta')$

$J=\frac{3}{2}$	$(^3P)^4D^\circ$	$(^3P)^2D^\circ$	$(^1D)^2D^\circ$	$(^3P)^4P^\circ$	$(^3P)^2P^\circ$	$(^1D)^2P^\circ$	$(^1S)^2P^\circ$	$(^3P)^4S^\circ$
$(^3P)^4D^\circ$	$-\frac{1}{2}(\zeta+\zeta')$	$-\frac{1}{4}(\zeta-2\zeta')$	$+\frac{1}{4}\zeta$	$+\frac{1}{3}(\zeta-\zeta')$	$-\frac{\sqrt{5}}{12}(\zeta+2\zeta')$	$+\frac{1}{12}\zeta$	$-\frac{\sqrt{5}}{3}\zeta$	0
$(^3P)^2D^\circ$	$-\frac{1}{4}(\zeta-2\zeta'$	$-\frac{1}{4}(2\zeta-\zeta')$	$-\frac{1}{4}\zeta$	$+\frac{1}{12}(\zeta+2\zeta')$	$+\frac{\sqrt{5}}{12}(2\zeta+\zeta')$	$+\frac{1}{12}\zeta$	$-\frac{\sqrt{5}}{3}\zeta$	0
$(^1D)^2D^\circ$	$+\frac{1}{4}\zeta$	$-\frac{1}{4}\zeta$	$-\frac{1}{4}\zeta'$	$+\frac{1}{4}\zeta$	$-\frac{\sqrt{5}}{4}\zeta$	$-\frac{3}{4}\zeta'$	0	0
$(^3P)^4P^\circ$	$+\frac{1}{3}(\zeta-\zeta')$	$+\frac{1}{12}(\zeta+2\zeta')$	$+\frac{1}{4}\zeta$	$-\frac{1}{6}(\zeta+\zeta')$	$-\frac{\sqrt{5}}{12}(\zeta-2\zeta')$	$+\frac{5}{12}\zeta$	$+\frac{\sqrt{5}}{3}\zeta$	$+\frac{\sqrt{10}}{6}(\zeta-\zeta')$
$(^3P)^2P^\circ$	$-\frac{\sqrt{5}}{12}(\zeta+2\zeta')$	$+\frac{\sqrt{5}}{12}(2\zeta+\zeta')$	$-\frac{\sqrt{5}}{4}\zeta$	$-\frac{\sqrt{5}}{12}(\zeta-2\zeta')$	$+\frac{1}{12}(2\zeta-\zeta')$	$+\frac{\sqrt{5}}{12}\zeta$	$+\frac{1}{3}\zeta$	$+\frac{\sqrt{2}}{6}(\zeta+2\zeta')$
$(^1D)^2P^\circ$	$+\frac{1}{12}\zeta$	$+\frac{1}{12}\zeta$	$-\frac{3}{4}\zeta'$	$+\frac{5}{12}\zeta$	$+\frac{\sqrt{5}}{12}\zeta$	$-\frac{1}{4}\zeta'$	0	$+\frac{\sqrt{10}}{6}\zeta$
$(^1S)^2P^\circ$	$-\frac{\sqrt{5}}{3}\zeta$	$-\frac{\sqrt{5}}{3}\zeta$	0	$+\frac{\sqrt{5}}{3}\zeta$	$+\frac{1}{3}\zeta$	0	$+\frac{1}{2}\zeta'$	$-\frac{\sqrt{2}}{3}\zeta$
$(^3P)^4S^\circ$	0	0	0	$+\frac{\sqrt{10}}{6}(\zeta-\zeta')$	$+\frac{\sqrt{2}}{6}(\zeta+2\zeta')$	$+\frac{\sqrt{10}}{6}\zeta$	$-\frac{\sqrt{2}}{3}\zeta$	0

TABLE 3. *Matrices of spin-orbit interaction for the configuration $np^2n'p$*—Continued

$J=\frac{1}{2}$	$(^3P)^4D^\circ$	$(^3P)^4P^\circ$	$(^3P)^2P^\circ$	$(^1D)^2P^\circ$	$(^1S)^2P^\circ$	$(^3P)^2S^\circ$
$(^3P)^4D^\circ$	$-\frac{3}{4}(\zeta+\zeta')$	$+\frac{\sqrt{5}}{12}(\zeta-\zeta')$	$-\frac{\sqrt{10}}{12}(\zeta+2\zeta')$	$+\frac{\sqrt{2}}{12}\zeta$	$-\frac{\sqrt{10}}{3}\zeta$	0
$(^3P)^4P^\circ$	$+\frac{\sqrt{5}}{12}(\zeta-\zeta')$	$-\frac{5}{12}(\zeta+\zeta')$	$-\frac{\sqrt{2}}{12}(\zeta-2\zeta')$	$+\frac{\sqrt{10}}{12}\zeta$	$+\frac{\sqrt{2}}{3}\zeta$	$-\frac{1}{3}(\zeta+2\zeta')$
$(^3P)^2P^\circ$	$-\frac{\sqrt{10}}{12}(\zeta+2\zeta')$	$-\frac{\sqrt{2}}{12}(\zeta-2\zeta')$	$-\frac{1}{6}(2\zeta-\zeta')$	$-\frac{\sqrt{5}}{6}\zeta$	$-\frac{2}{3}\zeta$	$+\frac{\sqrt{2}}{6}(2\zeta+\zeta')$
$(^1D)^2P^\circ$	$+\frac{\sqrt{2}}{12}\zeta$	$+\frac{\sqrt{10}}{12}\zeta$	$-\frac{\sqrt{5}}{6}\zeta$	$+\frac{1}{2}\zeta'$	0	$-\frac{\sqrt{10}}{6}\zeta$
$(^1S)^2P^\circ$	$-\frac{\sqrt{10}}{3}\zeta$	$+\frac{\sqrt{2}}{3}\zeta$	$-\frac{2}{3}\zeta$	0	$-\zeta'$	$+\frac{\sqrt{2}}{3}\zeta$
$(^3P)^2S^\circ$	0	$-\frac{1}{3}(\zeta+2\zeta')$	$+\frac{\sqrt{2}}{6}(2\zeta+\zeta')$	$-\frac{\sqrt{10}}{6}\zeta$	$+\frac{\sqrt{2}}{3}\zeta$	0

5. References

[1] U. Fano and G. Racah, Irreducible Tensorial Sets (Academic Press, Inc., New York, N.Y., 1959).

[2] M. Rotenberg, R. Bivins, N. Metropolis, and J. K. Wooten, Jr., The $3-j$ and $6-j$ Symbols (The Technology Press, MIT, Cambridge, Mass., 1959).

[3] E. U. Condon and G. H. Shortley, The Theory of Atomic Spectra (Cambridge University Press, London, 1951) referred to as TAS.

[4] J. C. Slater, Quantum Theory of Atomic Structure, vol. I and II (McGraw-Hill Book Co., New York, N.Y., 1960).

(Paper 67A6–239)

JOURNAL OF RESEARCH of the National Bureau of Standards—A. Physics and Chemistry
Vol. 67A, No. 6, November-December 1963

A Study of the Gas-Stabilized Arc as an Emission Source for the Measurement of Oscillator Strengths. Determination of Some Relative *gf*-Values for Fe I*

Marvin Margoshes and Bourdon F. Scribner

(July 23, 1963)

A study has been made of the application of the gas-stabilized arc source to the determination of oscillator strengths in atomic spectra. In this source, a solution of salts of one or more elements may be injected and the elements excited directly in an arc plasma with steady emission of spectral intensities. The source can be taken to be characterized by local thermal equilibrium, but with a large radial temperature gradient. An experiment indicates that when two elements are introduced into the arc in a solution, the relative concentrations of the elements in the discharge are the same as in the solution within the probable experimental error. This experiment indicates one way that the arc may be used for the determination of absolute oscillator strengths. New measurements are reported of the *gf*-values of 105 lines of Fe I between 2900 and 4150 Å, and the new values are compared with the results of earlier measurements.

1. Introduction

The gas-stabilized arc source was developed initially for the spectrographic analysis of solutions [1].[1] The source is an arc between a graphite anode and a thoriated tungsten cathode. The arc is stabilized in position by a stream of argon, and samples are introduced into the arc column as solutions in the form of a fine spray. In the course of studies of the properties of this discharge, it became apparent that the stability of emission intensities and the ease of introduction of the elements in a controlled manner might make the source applicable to the measurement of oscillator strengths in atomic spectra.

The intensity, I_{ij}, of a line resulting from transitions between an upper energy level, i, and a lower energy level, j, can be related to the transition probability, A_{ij}, when the source is at thermal equilibrium and when self-absorption and induced transitions can be neglected:

$$I_{ij}=D(N/u)h\nu_{ij}g_iA_{ij}\exp(-E_i/kT), \qquad (1)$$

where D is the depth of the emitting vapor, N is the number of atoms or ions per unit volume, h is Planck's constant, g_i is the statistical weight of the excited state, E_i is the energy of the upper level of the transition, k is Boltzmann's constant, T is the absolute temperature, and u is the partition function, equal to $\Sigma_n g_n \exp(-E_n/kT)$. A similar equation may be written in terms of the oscillator strength f_{ij}:

$$I_{ij}=-D(N/u)(8\pi^2\epsilon^2h\nu_{ij}^3/mc^3)g_if_{ij}\exp(-E_i/kT), \quad (2)$$

where ϵ and m are the charge and mass of an electron, and c is the velocity of light. There is a simple relation between the oscillator strengths for emission and absorption, $g_if_{ij}=-g_jf_{ji}$, while the relation between the emission and absorption transition probabilities is more complex.

If atomic oscillator strengths or transition probabilities are known, it is possible to derive considerable information from the study of the intensities of emission or absorption spectra. For example, rewriting eq (2) in logarithmic form, rearranging, and substituting c/λ for ν, gives

$$\log(I_{ij}\lambda_{ij}^3/g_if_{ij})=\log K-0.4343E_i/kT, \qquad (3)$$

where K includes those constants of eq (2) not explicitly included in eq (3). If the emitting atomic vapor is in thermal equilibrium, a plot of the left-hand side of eq (3) versus E_i will give a straight line with a slope equal to $-0.4343/kT$. In this way, the temperature of the atomic vapor may be determined. The temperature may also be measured from the intensity ratio of only two lines. For this purpose, eq (2) should be written in the form

$$I_{ij}/I_{mn}=(\nu_{ij}^3g_if_{ij}/\nu_{mn}^3g_mf_{mn})\exp[(E_m-E_i)/kT]. \quad (4)$$

Equations similar to (3) and (4) can also be written in terms of the transition probabilities.

If the vapor is not in thermal equilibrium, the intensities of the emission lines can be used to determine the numbers of atoms in individual energy levels, and these data can provide some indication of the mechanisms of energy transfer. Transition probabilities and oscillator strengths are of extreme importance in astrophysics, where their knowledge makes it possible to obtain information from solar and stellar spectra, including chemical composition, that could not be obtained in any other way.

*Presented in part at the Xth Colloquium Spectroscopicum Internationale, College Park, Maryland, June 18–22, 1962.

[1] Figures in brackets indicate the literature references at the end of this paper.

Oscillator strengths or transition probabilities may be measured from the absorption or emission spectra of atomic vapor having a uniform, known composition and temperature. The King furnace [2] can provide such a vapor suitable for absorption measurements. However, measurements with the King furnace normally provide information only on lines for which the lower energy level is at or near the ground state, since the temperatures attainable with this furnace are not high enough to give any significant concentration of atoms in the higher energy levels. Measurements of atomic transition probabilities and oscillator strengths have been made from emission spectra in flames and arcs. Flames can be made reasonably homogeneous in temperature and composition, but they are too cool to excite many atomic lines, and even fewer ion lines. Arcs are not usually homogeneous in composition and temperature, but if they are stable it may be possible to study their composition and temperature as a function of position in the arc column. The studies described here were designed to investigate the applicability of the gas-stabilized arc source to the measurement of oscillator strengths.

2. Description of the Source

A complete description of the source has been given previously [1], and only a summary is given here. Figure 1 is a schematic diagram of the gas-stabilized arc source. The anode is a graphite disk with an opening in the center. The atomizer is located just below the anode, and it is held in a water-cooled brass cylinder by a poly(tetrafluoroethylene) collar which keeps it electrically insulated from the discharge. The orifice is another graphite disk which is held in a water-cooled brass plate mounted on a Bakelite sleeve fitting snugly over the brass cylinder holding the anode and the atomizer. In this way the orifice is electrically insulated from the rest of the source so that it may take on the local potential of the arc. A stream of argon is introduced tangentially through the Bakelite sleeve to control the position of the arc. The cathode is a thoriated tungsten rod which is held vertically on the axis of the discharge by a water-cooled copper chamber.

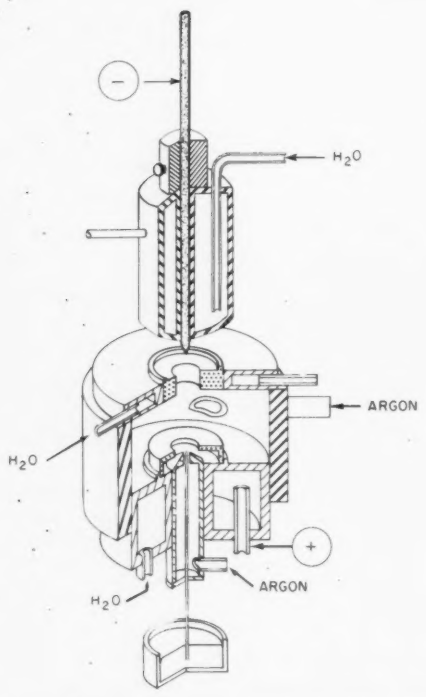

FIGURE 1. *Schematic diagram of the gas-stabilized arc source.*

The electrical power for the discharge may be provided by a d-c arc rectifier power supply or by d-c line power controlled by a ballast resistor. Either type of power supply is satisfactory, but an inductor in the ouput is necessary for stable operation.

When no solution is introduced, the arc burns quietly with very little fluctuation in position. When water or a solution is introduced, the arc becomes somewhat turbulent, but appears to remain stable in position. However, high-speed movies (4000 to 7000 frames/sec) show that, when water is sprayed in, the arc moves about in a random manner and only appears to be stable because the motion is extremely rapid.

The voltage drop between the electrodes is 40 v when no sample is introduced and rises to about 50 v when 0.2 ml/min of water is sprayed in. The arc current and voltage remain stable for extended periods without any adjustment of the power supply. The arc may be operated for 30 min or more at a current of 20 amp and a sample spray rate of 0.2 ml/min; the time of operation is limited by attack by water vapor on the hot tungsten cathode or, in some cases, the deposition of material from the solution onto this electrode. The graphite anode need be replaced only after a few hours of operation, and the orifice requires even less frequent replacement or cleaning.

The spectrum of the discharge shows lines of the elements in the solution and bands of OH and N_2^+, as well as lines of Ar and Ar^+ and diffuse lines of H and N. The spectra of thorium and tungsten are strong at the cathode, but these lines decrease rapidly in intensity toward the orifice and are indistinguishable above background in the lower half of the gap. There is relatively strong continuous radiation from the arc, probably arising from recombination of argon ions and electrons.

The movement of the arc is rapid enough so that the measured emission intensities are quite constant, even with a short time constant in the recording system. When an emission line is recorded with a time constant of ½ sec, the fluctuations in intensity are about 5 percent, peak to peak [1]. Observations over a period of 30 to 40 min, with 30 sec integration of the signal, have shown [1] that the line intensities remain constant to within 1 or 2 percent.

3. Temperature of the Arc

Because of the rapid random motion of the arc, the distribution of temperatures in the discharge could be studied only if the exposure times were made very short. There has been no attempt to do this, and the data reported here represent averages in both space and time. For this reason, all temperatures given here should be considered to be effective excitation temperatures only.

Preliminary studies of the temperature of the arc have been reported previously [1]. These temperatures were determined from the relative intensities of four Cr II lines at 2860.93, 2862.57, 2870.44, and 2875.99 Å using relative transition probabilities given by Zagoryanskaya [3]. The measurements indicated a temperature of 8125 °K, and no systematic changes with temperature were found when the current and sample flow were varied.

The temperature of the arc has also been measured from the relative intensities of 41 lines of Ti II, 24 lines of Ti I, and 95 lines of Fe I. The measurements were based on *gf*-values given by King [4] for Ti II, and by Corliss and Bozman [5] for Ti I and Fe I. The experimental arrangement for these temperature measurements was the same as is described in section 5.1 of this paper.

For each of the thermometric species (Ti I, Fe I, Ti II) a plot was made of log $(I\lambda^3/gf)$ versus the energy of the upper state of the transition. Figure 2 shows the plot obtained in this way for Fe I. The slope of the best straight line for the data points was calculated by the method of least squares, and the temperature of the arc was found from $T=-0.4343/kb$, where b is the slope of the line. The temperatures found were: from Ti II, 7570 °K; from Ti I, 5540 °K; from Fe I, 5510 °K. The exposure for the measurement with Ti II was made with a solution containing both titanium and chromium; a temperature of 7680 °K was found in this exposure from the relative intensities of the four Cr II lines in the 2860 to 2875 Å region. The difference of 400° between the temperature obtained with the Cr II lines in previous experiments and in this exposure may be related to a small difference in the method of recording the spectra. The exposures indicating a temperature of 8125 °K were made with the source focused on the entrance slit of the spectrograph [1], while the exposure giving a temperature of 7680° K was made with the slit evenly illuminated with light passing through a mask on the source (see sec. 5.1). In the latter case, a wider area of the discharge was viewed and a lower temperature was found.

The plots of log $(I\lambda^3/gf)$ versus E were all linear within the precision of the data, which is consistent with an assumption of local thermal equilibrium (LTE). The fact that the measurements with Ti II and Cr II agree, as do those with Ti I and Fe I, is again consistent with LTE. However, this evidence does not establish that the arc is characterized by LTE. In this work, it was found that an effective excitation temperature could be determined

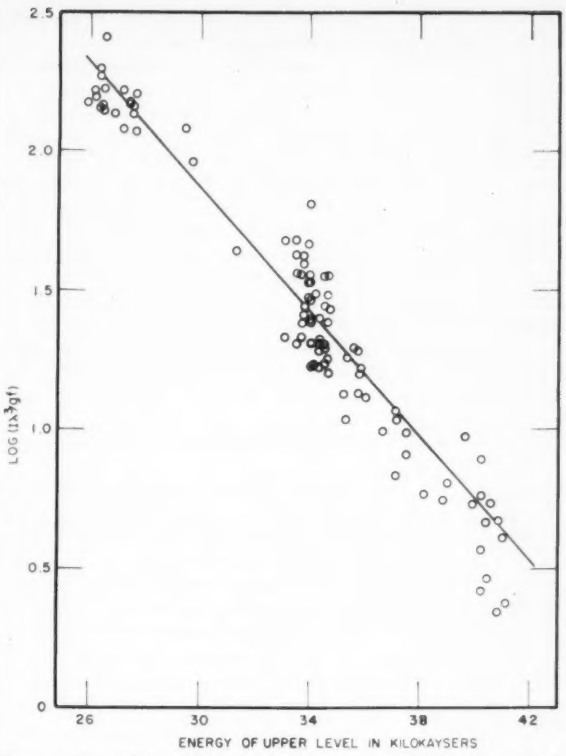

FIGURE 2. *Plot of log* $(I\lambda^3/gf)$ *versus energy of the upper state for lines of* Fe I *in gas-stabilized arc source. gf-Values taken from Corliss and Bozman [5]. Straight line shows least squares fit to points.*

for the arc. In addition, Kitaeva et al. [19] have found that an arc in argon is in LTE over the current range from 10 to 200 amp, which includes the current used in our work. Therefore, the arc was assumed to be characterized by LTE for the purpose of this study. If LTE is assumed, the disparity between the effective excitation temperatures obtained from the spectra of neutral atoms and of ions can be interpreted as indicating a large radial temperature gradiant in the arc.

4. Excitation of Mixed Solutions

Direct measurement of absolute transition probabilities with this source would be difficult because the concentration of an element in the discharge cannot easily be determined. Measured relative transition probabilities can be placed on an absolute scale if an absolute transition probability has been determined by some other method for at least one emission line. In the case of those elements for which no absolute transition probabilities are known, it may be possible to take advantage of the fact that two or more elements can be introduced into the source in known relative proportions. The assumption must then be made that the relative concentrations of the elements in the arc are the same as in the solutions being introduced, or else a

correction must be made for differential volatilization or diffusion of the elements.

The possibility of performing measurements of this kind has been explored by introducing into the discharge a solution containing manganese and lead and measuring the intensity ratio for the line pair Mn 4031/Pb 2833 Å. Absolute *gf*-values for these lines have been determined in the same laboratory and by the same procedure [6, 7]. The expected intensity ratio was calculated assuming that the concentration ratio of the elements in the discharge was the same as in the solution. No attempt was made to correct for any self-absorption that might occur. Ionization in the arc was taken into account.

For a source characterized by local thermal equilibrium, ionization is described by the Saha equation:

$$N^+N_e/N^\circ=[(2\pi mkT)^{3/2}2u^+/h^3u^\circ]\exp(-V/kT), \quad (5)$$

where N^+, N_e, and N° are the concentrations of ions, electrons, and neutral atoms, u^+ and u° are the partition functions for the ion and the neutral atom at the temperature, T, of the discharge, V is the ionization energy of the neutral atom, and the other symbols have the same meaning as before. For the two elements Mn and Pb, eq (5) can be reduced to

$$(N^+_{Mn}/N^\circ_{Mn})/(N^+_{Pb}/N^\circ_{Pb}) =[(u^+_{Mn}/u^\circ_{Mn})/(u^+_{Pb}/u^\circ_{Pb})]\exp[(V_{Pb}-V_{Mn})/kT]. \quad (6)$$

The first ionization energies of lead and manganese are 7.385 and 7.40 ev, so that the exponential term may be taken as equal to one. Substituting partition functions from Corliss and Bozman [5],

$$(N^+_{Mn}/N^\circ_{Mn})/(N^+_{Pb}/N^\circ_{Pb}) =(7.8/6.5)/(2.1/1.6)=0.92. \quad (7)$$

To a reasonably good approximation, the degree of ionization should be the same for both elements, and the ratio of the concentrations of the neutral atoms should be about the same as the ratio of the total concentrations. Corliss [8] found that manganese was 29 percent ionized and lead was 31.5 percent ionized in the copper arc.

Equation (2) of section 1 may be rewritten for the intensity ratio of the Mn/Pb line pair:

$$(I_{Mn}/I_{Pb}) =(N^\circ_{Mn}u^\circ_{Pb}\lambda^3_{Pb}g_{Mn}f_{Mn}/N^\circ_{Pb}u^\circ_{Mn}\lambda^3_{Mn}g_{Pb}f_{Pb})\exp[(E_{Pb} -E_{Mn})/kT]. \quad (8)$$

Because the spectra are of neutral atoms, the effective excitation temperature that should apply is the one obtained with the Fe I or Ti I lines. Assuming a temperature of 5510 °K, an intensity ratio of 1.61 was calculated for the ratio of the molar concentrations of lead and manganese in the experiment ($M_{Mn}/M_{Pb}=1.72$). The observed intensity ratios in two exposures were 2.17 and 2.03, average=2.10. The ratio of calculated to observed relative intensities was 0.76.

The difference between the calculated and observed intensities might be due in part to demixing in the arc column [20], although it is to be hoped that the rapid passage of the gas through the excitation zone would limit the extent of demixing. The accuracies of the transition probabilities are also open to question. The precisions of the values, as determined by repeated measurements in the same laboratory and by the same method, are 8 to 10 percent [6, 7], but the accuracies of the values are not known.

These measurements cannot provide positive information on how accurately absolute oscillator strengths can be determined through the introduction of mixed solutions into the gas-stabilized arc source. However, the agreement between the observed and calculated intensity ratios in this one experiment is good enough to indicate that the technique will be of value.

5. Measurement of *gf*-Values for Fe I

As a part of this study, new measurements have been made of the oscillator strengths of 105 lines in the first spectrum of iron. Relative *gf*-values for these lines were determined by King and King [9] from furnace absorption measurements. Relative *gf*-values for a few of the lines were redetermined by Sobolev [10] from the spectrum of an arc between copper electrodes containing a small percentage of iron. More recent measurements of transition probabilities for most of these lines were made by Crosswhite [11] with a number of emission and absorption sources. Finally, Corliss and Bozman [5] have tabulated *gf*-values for most of these lines, based on measurements of spectra from an arc between copper electrodes containing 0.1 atomic percent of iron. The data of Crosswhite and those of Corliss and Bozman are relative values which have been placed on an absolute scale by means of conversion factors derived from absolute measurements.

Sobolev observed that his *gf*-values did not agree with those of King and King, and he ascribed the difference to a lack of thermal equilibrium in the King furnace. Crosswhite found a systematic difference between his measurements and those of King and King; when the two sets of data are placed on the same scale at longer wavelengths, the *gf*-values determined by the Kings are low by about a factor of 10 compared to Crosswhite's values at shorter wavelengths. Crosswhite ascribed the wavelength-dependent difference to scattered light in the spectrograph used by the Kings.

5.1 Experimental Procedure

For measurements of the *gf*-values of Fe I, the source was operated at 20 amp and equipped with a mask arranged to pass light from a 1 mm-wide vertical cross-section through the axis of the arc in the lower half of the gap between the orifice and the cathode. The spectra were photographed in the first order of a 21-ft Wadsworth mount grating spectrograph with a 15,000 line/in. grating. The 30-μ entrance slit of the spectrograph was evenly illuminated, and four steps of a 1:2 step sector were employed to permit photometry of lines having widely different intensities. Two 10-in. SA-1 plates were used for each set of exposures in order to include the region from 2900 Å to the long wavelength limit of the emulsion (about 4150 Å). The exposure time was selected to give a transmittance value of about 70 percent for the background in the darkest step. The plates were developed for three minutes in D–19 at 20 °C, and the transmittance values of the lines and the adjacent background were measured on a nonrecording microphotometer. The emulsion calibration was determined for each plate at 50 Å intervals by the two-step method [12].

Two sets of plates were exposed. One set was exposed with a solution containing 1 g/liter of iron (as ferric chloride), and the other with solutions containing 5 and 10 g/liter of iron. An exposure was also made on each set of plates with distilled water introduced into the arc to permit identification of interfering lines and bands. An additional exposure was also made on each set of plates of the continuous radiation from the anode of an 8-amp arc between graphite electrodes, arranged as described by Euler [13]. This permitted a correction to be made for the variation of response with wavelength of the emulsion and the spectrograph, using the temperature and emissivity data for the graphite anode given by Euler. The correction was interpolated through the *CN* band region. Finally an exposure was made on each set of plates of an iron arc for wavelength calibration.

5.2. Results

The effective excitation temperature of the discharge was found for each exposure with the three concentrations of iron, as described in section 3. The temperatures found were 5610, 5420, and 5510 °K, average 5510 °K. These data do not indicate any effect of the concentration of iron in the solution on the temperature of the discharge.

In the three exposures, the intensities of the Fe I lines increased by a larger factor than the increase in the concentration of iron in the solutions. For example, the line intensities increased by a factor of 2.9 when the concentration of iron in the solution was increased by a factor of 2.0, from 5 to 10 g/liter. This effect may be due to a shift in the ionization equilibrium, as has been observed [14] for the excitation of easily ionized elements in flames. If a significant portion of the electron concentration in the discharge is from ionization of iron, then the electron concentration will also increase with increased iron concentration. In accordance with the Saha equilibrium, this will result in a lesser degree of ionization as the total iron concentration is increased. Accordingly, the rise in the concentration of neutral iron atoms, and the intensity of the Fe I lines, can be expected to be greater than the increase in the total concentration of iron.

A total of 105 lines from the list of King and King [9] were observed in the three exposures. Several of the lines were not observed with a measurable intensity in all exposures, being either too light at the lowest concentration or too dark at the highest concentration. A few of the lines which could be observed on one set of plates could not be observed in the other set because they happened to come at the space between the two plates in the camera.

Relative *gf*-values for the 105 lines were calculated from the measured intensities using the relation $gf_r = I_r\lambda^3 \exp(E/kT)$, where I_r and f_r are the relative intensities and oscillator strengths. The three sets of values were normalized to the same scale and an average *gf*-value was found for each line. To take into account the improvement in the precision of photometry with increasing line/background ratio, the *gf*-values from the three individual exposures were weighted approximately in proportion to the square root of the concentrations; the values obtained from the exposure with the most dilute solution were assigned a weight of 1, those from the exposure with the solution containing 5 g/liter of iron were assigned a weight of 2, and the values from the exposure with the most concentrated solution were assigned a weight of 3. The average deviation from the weighted mean of the values was also calculated for each line for which there were two or three measurements. The relative average deviation ranged from 0 to 15 percent, with an average of 4.2 percent. The relative *gf*-values were then normalized to the absolute scale of *gf* (3719.94 Å) = 0.288 [16].

Many of the lines observed in this study are subject to self-absorption, since the lower energy levels of the transitions are at or near the ground level. The extent of self-absorption in the gas-stabilized arc source was investigated by comparing the relative intensities obtained in the exposures with 5 and 10 g/liter of iron. For this purpose, the lines were divided into three groups, according to the degree of self-absorption found by Crosswhite [11] for these lines in a 1 amp d-c arc between iron electrodes. For 25 of these lines, Crosswhite found no significant self-absorption in the 1 amp arc; the ratio of the intensities at the two concentrations in the gas-stabilized arc, I_{10}/I_5, averaged 2.91, with a standard deviation of 0.24. For 31 of these lines, Crosswhite found less than 30 percent self-absorption; for these lines $I_{10}/I_5 = 2.90 \pm 0.11$. For 39 of the lines, Crosswhite found more than 30 percent self-absorption in the 1 amp arc; for these $I_{10}/I_5 = 2.75 \pm 0.20$. The difference in the ratio I_{10}/I_5 for the group of lines which showed more than 30 percent self-absorption in the 1 amp arc and the other two groups of lines

is statistically significant. While the effect of self-absorption is detectable, it has not been a serious cause of error in our work. The ratio I_{10}/I_5 changed by 5.5 percent between the lines which were found by Crosswhite to be not self-absorbed and those that showed more than 30 percent self absorption in the 1 amp arc; this difference is comparable to the photometric error.

Table 1 lists the *gf*-values found in this study. The wavelengths and energy levels are taken from the tables of Meggers, Corliss, and Scribner [15]. The *gf*-values found for these lines by King and King [9], by Crosswhite [11], and by Corliss and Bozman [5] are also listed. (Crosswhite's tables list ϵ-values which are related to the *gf*-values by a wavelength-dependent conversion factor. Crosswhite states that multiplication of the ϵ-values by the conversion factor will give the *f*-values. Actually, this operation gives the *gf*-values.) The *gf*-values given by the Kings and by Crosswhite are also placed on the absolute scale based on $gf(3719.94\ \text{Å})=0.288$ [16]. Crosswhite's values had been normalized to an earlier [17] absolute measurement of the same Fe I line which was lower by about a factor of three.

TABLE 1. *Excitation energies and oscillator strengths for lines of Fe* I

Wavelength[a]	Energy levels[a] Kaysers (cm^{-1})		gf-values			
	Lower	Upper	This work	Corliss & Bozman	Crosswhite [b]	King & King [b]
2912.16	0	34329	0.0459	0.068	0.0513	0.0054
2929.01	416	34547	.0548	.073	.0665	.0073
2936.90	0	34040	.213	.26	.322	.014
2941.34	704	34692	.0331	.050	.0417	.0065
2947.88	416	34329	.222	.28	.324	.015
2953.94	704	34547	.188	.23	.243	.015
2957.36	888	34692	.119	.13	.138	.012
2965.26	978	34692	.0728	.071	.0782	.0092
2966.90	0	33695	.446	.51	.780	.023
2970.10	888	34547	.127	.13	.011	.015
2981.45	416	33947	.0722	.091	.11	.0076
2983.57	0	33507	.318	.40	.469	.020
2994.43	416	33802	.354	.38	.503	.023
2999.51	6928	40257	.669	.71	.85	.19
3000.95	704	34017	.328	.37	.509	.025
3007.28	404	33947	.0344	.033	.045	.0060
3008.14	888	34122	.194	.32	.294	.019
3009.57	7377	40594	.410	.61	.54	.17
3017.63	888	34017	.0462	.069	.0584	.0087
3018.98	7728	40842	.280	.43	.39	.17
3021.07	416	33507	.512	.48	.773	.034
3024.03	888	33947	.0607	.088	.083	.0087
3025.84	978	34017	.195	.13	.268	.018
3031.64	8155	41131	.184	.49	.23	.12
3037.39	888	33802	.292	.31	.437	.024
3040.43	7377	40257	.113	.35	.17	.087
3042.02	8155	41018	.0905	.15	.13	.071
3042.66	7986	40842	.138	.46	.19	.12
3047.60	704	33507	.358	.40	.505	.024
3057.45	6928	39626	1.02	1.1	1	.27
3059.09	416	33096	0.253	0.28	0.368	0.021
3075.72	7728	40231	.476	.72	.7	.27
3083.74	7986	40405	.303	.53	.5	.21
3091.58	8155	40491	.178	.46	.23	.15
3100.30	7986	40231	.236	.56	.4	.21
3100.67	7728	39970	.327	.52	.5	.19
3193.23	0	31307	.0107	.021	.01	.0037
3196.93	19562	50833	3.67	8.5	5.3	[c] .0022
3476.70	978	29733	0.0341	0.050	0.0256	.035
3497.84	888	29469	.0314	.036	.0236	.012
3513.82	6928	35379	.111	.32	.10	.14
3521.26	7377	35768	.164	.32	.14	.17
3558.52	7986	36079	.338	.66	.26	.36
3565.38	7728	35768	1.06	1.5	.71	.98
3570.10	7377	35379	2.09	3.4	1.0	1.4
3585.32	7728	35612	0.231	0.33	0.46	0.26
3585.71	7377	35257	.108	.25	.22	.14
3586.99	7986	35856	.240	.39	.22	.30
3608.86	8155	35856	1.19	2.0	.79	1.1
3618.77	7986	35612	1.38	1.9	1.1	1.6
3647.84	7377	34782	0.918	1.2	0.64	0.87
3649.51	21716	49109	3.31	6.1	7.7	[c] .0015
3679.92	0	27167	0.0272	0.059	0.0226	.033
3687.46	6928	34040	.199	.51	.193	.23
3705.57	416	27395	.0482	.079	.0409	.060
3707.82	704	27666	.0116	.030	------	.0071
3709.25	7377	34329	.298	.59	.285	.39
3719.94	0	26875	.288	.52	.288	.29
3722.56	704	27560	.0525	.084	.0464	.065
3727.62	7728	34547	.307	.57	.292	.41
3733.32	888	27666	0.0410	0.076	0.0354	0.050
3734.87	6928	33695	2.25	4.2	2.51	2.6
3737.13	416	27167	0.220	0.32	0.215	0.24
3743.36	7986	34692	.217	.48	.208	.30
3745.56	704	27395	.152	.24	.15	.18
3745.90	978	27666	0.0476	0.066	0.043	0.060
3748.26	888	27560	.0902	.15	.0829	.10
3749.49	7377	34040	1.59	2.7	1.74	2.0
3758.24	7728	34329	1.08	2.2	1.18	1.5
3763.79	7986	34547	0.686	1.3	0.724	0.98
3767.19	8155	34692	.489	0.97	.526	.71
3787.88	8155	34547	.162	.36	.170	.27
3790.10	7986	34363	.0300	.045	.036	.051
3795.00	7986	34329	.219	.49	.213	.32
3798.51	7377	33695	.102	.20	.0941	.14
3799.55	7728	34040	.160	.33	.178	.27
3812.96	7728	33947	.153	.22	.13	.18
3815.84	11976	38175	1.83	3.6	2.0	2.8
3834.22	7728	33802	0.485	0.86	0.637	0.81
3840.44	7986	34017	.335	.57	.371	.47
3841.05	12969	38996	1.25	2.3	1.4	2.0
3849.97	8155	34122	0.150	0.37	0.20	0.28
3856.37	416	26340	.0433	.070	.0454	.060
3859.91	0	25900	.141	.31	.162	.19
3872.50	7986	33802	.132	.23	.135	.22
3878.02	7728	33507	.136	.32	.143	.23
3878.58	704	26479	.0358	.074	.0464	.048
3886.28	416	26140	.0689	.14	.0690	.087
3887.05	7377	33096	.0748	.20	.112	.15
3888.52	12969	38678	.436	.96	.47	.65
3895.66	888	26550	.0233	.032	.0176	.028
3899.71	704	26340	.0284	.047	.0241	.038
3902.95	12561	38175	.528	1.3	.72	.98
3906.48	888	26479	.00597	0.012	.00628	.010
3920.26	978	26479	.0175	.032	.0204	.026
3922.91	416	25900	.0193	.042	.0194	.031
3927.92	888	26340	.0271	.061	.0241	.038
3930.30	704	26140	.0293	.062	.0241	.042
3969.26	11976	37163	.594	1.0	.59	.81
4005.25	12561	37521	.413	0.87	.47	.65
4045.82	11976	36686	2.48	5.3	2.3	3.3
4063.60	12561	37163	1.51	2.5	1.7	2.3
4071.74	12969	37521	1.32	2.3	1.5	2.1
4132.06	12969	37163	0.237	0.69	0.43	0.60
4143.87	12561	36686	.341	.76	.55	.76

[a] Wavelength and energy level values taken from Meggers, Corliss and Scribner [15].

[b] Relative values given by King and King [9] have been normalized to an absolute scale of gf (3719.94Å) = 0.288 [16]. Absolute values given by Crosswhite [11] have been recalculated to the same absolute scale. See text for details.

[c] The energy levels assigned to these lines in the work of King and King [9] are considerably different from those assigned in the tables of Meggers, Corliss, and Scribner [15].

5.3. Discussion

Figure 3 shows a comparison between the results of this work and the data given by King and King [9]. The ratio of the *gf*-values from the two studies is plotted as a function of the wavelength of each line. The wavelength-dependent error in the values of King and King, first noted by Crosswhite [11], is shown clearly. The points fall low at short wavelengths and they also show increased scatter compared to the points at the longer wavelengths. These data tend to confirm Crosswhite's deduction that the values obtained by the Kings are low at shorter wavelengths apparently because of scattered light in the spectrograph.

Figure 4 is a comparison of the data obtained in this study and the results given by Crosswhite [11]. The ratio of the *gf*-values is plotted as a function of the energy of the upper state of the transition. Although the points are scattered, there appears to be a downward trend of the ratio of the *gf*-values with the excitation energy of the line. This energy-dependent difference reflects a systematic difference between the data of Crosswhite and the values given by Corliss and Bozman [5]. The data listed by Corliss and Bozman are derived from the measurements by Meggers, Corliss, and Scribner [15] of line intensities in a copper arc. Corliss [18] found the temperature of this arc to be 5100 $\pm$110 °K, and this temperature was used by Corliss and Bozman in the calculation of the *gf*-values. With the *gf*-values given by Crosswhite and the line intensities listed by Meggers, Corliss, and Scribner, a temperature of 4750 °K is found for the copper arc. There is, therefore, an energy-dependent bias between the *gf*-values obtained by Crosswhite and those given by Corliss and Bozman.

The present measurements are related to those of Corliss and Bozman in such a way that there can be no systematic differences that are dependent on the excitation energies of the lines. However, a wavelength-dependent difference is possible. Figure 5 is a comparison of the data of this study with those of Corliss and Bozman, plotted as a function of wavelength. These appears to be a slight trend of the ratio of the *gf*-values with wavelength. The same comparison when made between the results of this work and those of Crosswhite shows an indication of a trend in the opposite direction (fig. 6). Figure 5 also shows how the absolute scale of Corliss and Bozman differs from the one adopted in this work.

The *gf*-values resulting from the work described here have a random error of 4.2 percent (see sec. 5.2.) Corliss and Bozman estimate the precision of their *gf*-values at 30 to 35 percent in the range of excitation energies of these lines, and their data agree with the values of the present study within this factor, aside from the difference in the absolute scale. Crosswhite does not give an estimate of the precision of his values, but an indication of the random errors involved in his measurements can be obtained by comparison of the values obtained by him from

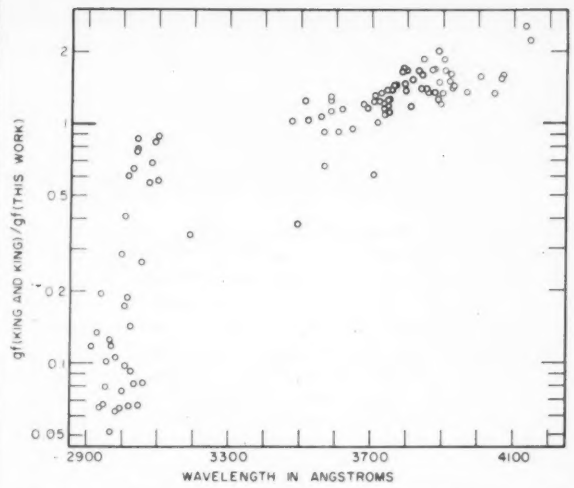

FIGURE 3. *Comparison of* gf*-values from this study with values given by King and King [9], showing wavelength-dependent difference.*

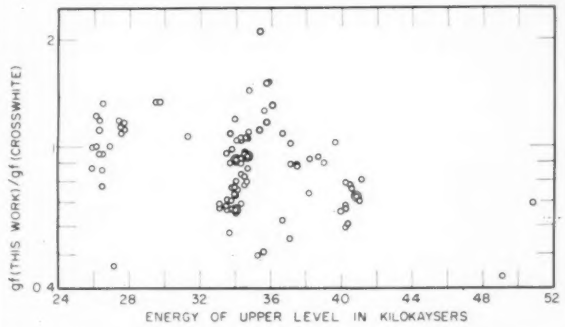

FIGURE 4. *Comparison of* gf*-values from this study with values given by Crosswhite [11], showing energy-dependent difference.*

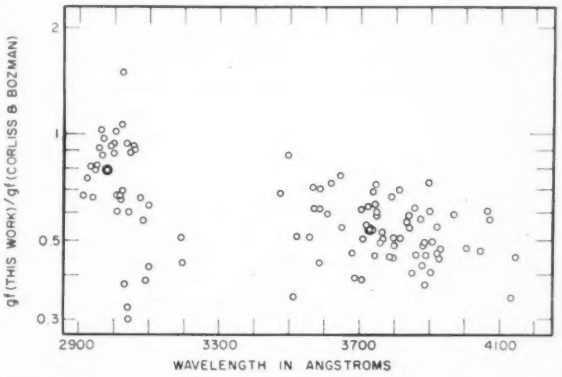

FIGURE 5. *Comparison of* gf*-values from this study with values given by Corliss and Bozman [5], showing wavelength-dependent difference.*

TABLE 2.—*Comparison of* gf*-values measured with different sources*

Data of Crosswhite [11].

Sources*	a/d	a/e	a/f	a/h	d/e	d/f	d/h	e/f	e/h	f/h
Average ratio of *gf*-values	1.86	0.90	0.82	0.96	1.15	1.00	0.65	0.99	0.97	1.01
Standard deviation of ratio	0.94	.32	.27	.73	0.26	0.096	.34	.22	.46	0.094
Number of lines compared	21	22	22	51	11	11	26	24	32	32

*The letters correspond to *gf*-values measured with the following sources:
a—1 amp d-c arc; d—flame in absorption; e—electrodeless discharge; f—flame in emission; h—hollow cathode.

measurements with different sources. Table 2 lists the results of such a comparison. Good agreement between two sets of results is indicated when the ratio of the *gf*-values is near unity and the standard deviation of the ratio is small. Good agreement according to this criterion is found in some instances, but in other cases the average of the ratios is far from unity or the standard deviation is quite large. Overall, the relative standard deviation is 44 percent. The *gf*-values listed in table 1, and compared with the results of this study in figures 4 and 6 have been selected by Crosswhite as being probably the most reliable, so that the random errors may not be as large as the 44 percent relative standard deviation found by the internal comparison. However, it is not unreasonable to assume that much of the scatter of the points in figures 4 and 6 represents random errors in the measurements made by Crosswhite.

6. Conclusions

The results of the present study indicate that the gas-stabilized arc source should be useful for the determination of transition probabilities. The source appears to exhibit local thermal equilibrium but it does have a large radial temperature gradient. The spectral intensities emitted by the arc are remarkably constant even though the arc is not completely stable in position. The absolute concentrations of the elements in the discharge are not known, so that only relative transition probabilities may be determined directly. However, one experiment indicated that when a solution containing a mixture of elements is introduced into the arc the relative concentrations of the elements in the plasma are approximately the same as in the solution. It may therefore be possible to determine absolute transition probabilities by means of measurements with mixed solutions, employing known absolute values for one element to place relative values for another element on an absolute scale. The effects of self-absorption are not large in the gas-stabilized arc source, and they can be studied by varying the composition of the solution that is introduced into the discharge.

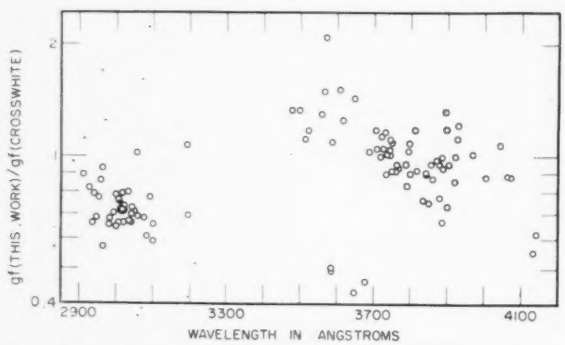

FIGURE 6. *Comparison of* gf*-values from this study with values given by Crosswhite [11], showing wavelength-dependent difference.*

The gas-stabilized arc source has been applied to the redetermination of oscillator strengths for 105 lines in the first spectrum of iron. Systematic differences have been found between the results of this study and those of King and King [9], Crosswhite [11], and Corliss and Bozman [5]. The new data do not make it possible to select any one set of *gf*-values as being more accurate than the others, except that a wavelength-dependent error in the data of King and King, first noted by Crosswhite, has been confirmed. The new measurements are believed to have smaller random errors than any of the previous values.

7. References

[1] B. F. Scribner and M. Margoshes, Actes IX Colloquium Spectroscopicum Internationale, Groupement pour l'Avancement Methodes Spectrographiques, Paris, vol. II, p. 309 (1962).
[2] A. S. King, Astrophys. J. **27,** 353 (1908); **28,** 300 (1908).
[3] E. V. Zagoryanskaya, Zh. Eksperim. i. Teor. Fiz. **19,** 447 (1949).
[4] R. B. King, Astrophys. J. **94,** 27 (1941).
[5] C. H. Corliss and W. R. Bozman, Experimental transition probabilities for spectral lines of seventy elements, NBS Mono. 53, U.S. Government Printing Office, Washington, D.C., (1962).
[6] G. D. Bell, M. H. Davis, R. B. King, and P. M. Routly, Astrophys. J. **129,** 437 (1959).
[7] G. D. Bell and R. B. King, Astrophys. J. **133,** 718 (1961).
[8] C. H. Corliss, J. Research NBS **66A,** 169 (1962).
[9] R. B. King and A. S. King, Astrophys. J. **87,** 24 (1938).
[10] N. N. Sobolev, Zh. Eksperim. i. Teor. Fiz. **13,** 131 (1943).
[11] H. M. Crosswhite, The spectrum of Fe I, Johns Hopkins Spectroscopic Report 13, The Johns Hopkins University, Baltimore, Md. (1958).
[12] J. R. Churchill, Ind. Eng. Chem., Anal. Ed. **16,** 653 (1944).
[13] J. Euler, Ann. Physik, (6) **11,** 203 (1953).
[14] J. A. Dean, Flame photometry, p. 103 McGraw-Hill Book Co., Inc., New York, N.Y., (1960).
[15] W. F. Meggers, C. H. Corliss, and B. F. Scribner, Tables of spectral line intensities, Part I, NBS Mono. 32, U.S. Government Printing Office, Washington, D.C. (1961).
[16] G. D. Bell, M. H. Davis, R. B. King, and P. M. Routly, Astrophys. J. **127,** 775 (1958).
[17] R. B. King, Astrophys. J. **95,** 78 (1942).
[18] C. H. Corliss, J. Res. NBS **66A,** (Phys. and chem.) No. 1, 5 (1962).
[19] V. F. Kitaeva, V. N. Kolesnikov, V. V. Obukhov-Denisov, and N. N. Sobolev, Zh. Tekhn. Fiz. **32,** 1084 (1962).
[20] J. Richter, Z. Astrophys. **53,** 262 (1961).

(Paper 67A6–240)

JOURNAL OF RESEARCH of the National Bureau of Standards—A. Physics and Chemistry
Vol. 67A, No. 6, November–December 1963

Tritium-Labeled Compounds IX. Determination of Isotope Effects in Reactions Yielding Water-*t* from Nonvolatile Reactants. Oxidation of Aldoses-*1-t* With Iodine

Horace S. Isbell and Lorna T. Sniegoski

(June 28, 1963)

A convenient method is presented for estimating isotope effects in reactions which yield water-*t*. The water-*t* is separated by freeze-drying, and k^*/k is calculated from the extent of the reaction and the ratio of the radioactivity of the water-*t* to that of the initial reactant. Application of the method to the oxidation of aldoses-1-*t* at 25 °C with iodine in alkaline solution gives values for k^*/k ranging from 0.12 to 0.17, with an average of 0.14. There are no significant differences in the values of k^*/k obtained for aldoses differing in configuration, or for pentoses and hexoses. The isotope effect corresponds to a ratio of one to seven for the respective rates of reaction of the labeled and unlabeled molecules.

1. Discussion

1.1. Determination of Isotope Effects

Isotope effects, or differences in the rates of reaction for isotopically labeled and unlabeled molecules, provide a tool for study of reaction mechanisms [1].[1] The isotope effect, k^*/k, can be determined by various techniques, some of which have been described in prior publications from this laboratory [2, 3].

A simple method has now been developed for determining k^*/k for reactions in which water-*t* is formed from a nonvolatile reactant. The method is based on the separation and analysis of the water-*t* formed in the reaction. The ratio of k^*/k is then calculated from the equation of Stevens and Attree [4] as modified by Ropp [5]:

$$k^*/k = \log(1-rf)/\log(1-f) \qquad (1)$$

In this equation, f is the fraction of initial reactant that has been consumed, and r is the ratio of the molar specific radioactivity of the accumulated product (of partial reaction) to that of the initial reactant.

In the experimental procedure developed, the reaction is allowed to proceed to the desired extent. The fraction f is estimated from the amount of the reagent used or by other convenient means. The solution containing the products of partial reaction and the residual reactant is diluted with water to a known volume. A portion of this solution is freeze-dried, the water-*t* obtained by sublimation is assayed, and the total activity of the water-*t* (the product of partial reaction) is calculated. The total activity of the initial reactant is obtained from the specific activity and weight of the aldose-*1-t*. The ratio of the activity of the water-*t* to the activity of the initial reactant equals rf. Substituting the values of f and rf in eq (1) gives k^*/k.

[1] Figures in brackets indicate the literature references at the end of this paper.

The method can be applied to a wide variety of reactions which yield water-*t* from nonvolatile reactants; it is illustrated here by a study of the oxidation of aldoses-*1-t* with iodine in alkaline solution.

1.2 Oxidation of Aldoses-*1-t* With Iodine in Alkaline Solution

In a prior investigation, Isbell, Sniegoski, and Frush [2] measured the isotope effect for the oxidation of D-glucose-*1-t* by iodine in alkaline solution by means of their double-label technique. The observed value of k^*/k (0.17) is substantially the same as that (0.15) previously found by Kaplan [6] for the bromine oxidation of ethanol-*1-t*, but differs greatly from that (0.53) found for the bromine oxidation of α-D-glucose-*1-t* [7]. The rate of oxidation of α-D-glucose-*1-t* with bromine in slightly acid solution depends, in part, on the rate of anomerization to the rapidly oxidized β-D-glucose-*1-t* [8]. The anomerization reaction has a weak, secondary isotope-effect, whereas the direct oxidation has a strong, primary isotope-effect. In the oxidation of aldoses with iodine in alkaline solution, equilibrium is maintained throughout the reaction and, consequently, the isotope effect is not influenced by a rate-controlling anomerization. In view of this fact, it seems probable that the value of k^*/k for the reaction is typical of a reaction involving rupture of the C-1 to H bond of an aldose-*1-t* present in a steady-state equilibrium. The value of k^*/k for this type of reaction is needed for interpreting many of the reactions of labeled carbohydrates.

To ascertain whether all aldoses, on oxidation with iodine, give essentially the same value of k^*/k, a series of measurements was made with aldoses-*1-t* of diverse types. The results, summarized in table 1, show that the values of k^*/k are essentially constant and that there are no significant differences in the values for aldoses differing in configuration, or

TABLE 1. *Isotope effects in oxidation of aldoses-1-t with iodine in alkaline solution at 25 °C*

Aldose-*1-t*	Fraction of aldose oxidized	Radioactivity in original reactant	Radioactivity of water-*t* formed	Isotope effect
	f	μc	μc	k^*/k
L-Arabinose	0.100	6.05	0.092	0.15
	.200	6.36	.194	.14
	.300	5.64	.262	.13
				Avg. 0.14
D-Xylose	.165	15.90	.347	.12
	.200	13.78	.411	.17
	.303	13.83	.756	.16
				Avg. 0.15
D-Glucose	.100	7.60	.120	.15
	.200	7.43	.252	.15
	.300	7.56	.409	.16
				Avg. 0.15
D-Mannose	.107	9.82	.143	.13
	.198	7.55	.214	.13
	.313	7.47	.334	.12
				Avg. 0.13
D-Galactose	.101	6.26	.082	.12
	.199	6.35	.186	.13
	.317	6.42	.340	.14
				Avg. 0.13
D-Talose	.100	10.86	.194	.17
	.200	11.26	.340	.14
	.300	10.09	.515	.15
				Avg. 0.15
L-Rhamnose monohydrate	.100	16.71	.239	.14
	.200	11.28	.330	.13
	.300	12.40	.504	.12
				Avg. 0.13

TABLE 2. *Determination of isotope effects in the oxidation of aldoses-1-t with iodine in alkaline solution by the double-label technique [2]*

Fraction of aldose oxidized	Ratio of functional to reference isotope in carrier mixture	Isotope effect
D-Glucose-*6-C*^{14}*-1-t*[a]		
f	*p*	k^*/k
0.0	9.12	
.761	30.89	0.15
.785	30.66	.21
.839	43.05	.15
.882	52.17	.18
		Avg. 0.17
D-Mannose-*2-C*^{14}*-1-t*		
0.0	7.72	
.726	23.43	.14
.756	26.39	.13
		Avg. 0.14

[a] These measurements for D-glucose-*6-C*^{14}*-1-t* were previously reported in [2].

for pentoses and hexoses. The average value of k^*/k (0.14) and the lack of its dependence on the structure of the aldose are in accord with the conclusion that the C-1 to H bond is ruptured in the rate-determining step.

In addition to the measurements of k^*/k given in table 1, measurements were also made for D-mannose-*1-t* (table 2) by means of the double-label technique previously developed [2]. The results obtained by the two methods are in good agreement, considering that the values for the water-*t* method are based on the early part of the reaction period, whereas those for the double-label method are based on the latter part.

2. Experimental Procedure

2.1. Materials and Apparatus

a. Labeled Aldoses

The sugars labeled at C-1 with tritium were prepared by reducing the corresponding lactones with $LiBH_4$-*t* [9]. The purity of each sugar was checked, before use, by paper chromatography. One chromatogram was developed with 1-butanol—acetic acid—water (4:1:5, upper phase), and another with 2-butanone—acetic acid—water saturated with boric acid (9:1:1). The chromatograms were scanned with a gas-flow, windowless counter, and then sprayed with aniline hydrogen phthalate. Whenever either chromatogram showed the presence of more than one substance, the labeled aldose was recrystallized and then rechromatographed. The pure, labeled sugars, generally having an activity of about 1 μc/mg, were assayed with a liquid scintillation counter.

D-Mannose-*2-C*^{14} was prepared by the procedure given in [10], and D-mannose-*2-C*^{14}*-1-t* by recrystallizing a suitable mixture of D-mannose-*2-C*^{14} and D-mannose-*1-t* from water—methanol—2-propanol. The activity of the doubly labeled D-mannose, determined as described in sec. 2.1.c was about 1 μc/mg for tritium and 0.1 μc/mg for carbon-14.

b. Standard Solutions

0.04 *N* Iodine (containing 4 g of potassium iodide per 100 ml of solution) and 0.04 *N* sodium hydroxide were used.

c. Counting Equipment

The counting was done with a Packard Tri-Carb Liquid Scintillation Spectrometer, Series 314E [11]. The counter was operated at 1325 v, with discriminators so adjusted that one scaler (red) counted at 8 to 40 v and the other (green) at 10 to 100 v; the temperature of the counting chamber was +5 °C. The scintillation solution [12] contained, per liter, 7 g of PPO (2,5-diphenyloxazole, scintillation grade), 0.3 g of dimethyl POPOP [2,2′-*p*-phenylenebis(4-methyl-5-phenyloxazole), scintillation grade], and 100 g of naphthalene, in dioxane (Eastman). Aqueous solutions (100 μl, generally containing about 0.02 μc of tritium) were counted in 10 ml of the

scintillation solution. In each instance, duplicate samples were prepared and counted to a total of 10,000 counts, to give a statistical accuracy of ±1 percent.

2.2 Determination of Tritium

The counting efficiency for tritium was determined as described in sec. 2.1.c, by analysis of a standard sample of tritiated water. A factor, expressed as μc of tritium per count per sec, was calculated from the count (red scaler) and the known activity. Samples containing unknown amounts of tritiated water were analyzed in the same way as the standard, and the activity was calculated by means of the factor.

2.3. Determination of Carbon-14 and Tritium in the Same Sample

The determination of carbon-14 and tritium in the same sample was carried out with the scintillation counter so adjusted that each isotope was counted efficiently in one scaler and inefficiently in the other [11]. The efficiencies for carbon-14 and for tritium with each scaler were determined by separately counting standard samples of D-glucose-*1*-C^{14} and D-glucose-*1*-*t*. The activities of unkown samples were then calculated by the following equations:

$$A^T=[R_r-R_g(E_r^C/E_g^C)]/[E_r^T-E_g^T(E_r^C/E_g^C)]$$
$$=k_1R_r-k_2R_g \quad (2)$$

$$A^C=[R_r-R_g(E_r^T/E_g^T)]/[E_r^C-E_g^C(E_r^T/E_g^T)]$$
$$=k_3R_r-k_4R_g \quad (3)$$

where A^T=disintegrations per second due to tritium, A^C=disintegrations per second due to carbon-14, R_r=count rate on the red scaler, R_g=count rate on the green scaler, E_r^C=counting efficiency of carbon-14 on the red scaler, E_g^C=counting efficiency of carbon-14 on the green scaler, E_r^T=counting efficiency of tritium on the red scaler, and E_g^T=counting efficiency of tritium on the green scaler. The combined constants, k_1, k_2, k_3 and k_4, were derived from the experimentally determined counting-efficiencies. Under the conditions described in sec. 2.1.c, a mixture containing carbon-14 and tritium gave values of *0.126*, *0.707*, 0.175, and 0.082 for E_r^C, E_g^C, E_r^T and E_g^T, respectively.

2.4. Determination of k^*/k by the Water-*t* Method

The procedure for studying the oxidation of aldoses-*1*-*t* was as follows: Several weighed samples (approximately 10 mg each) of each aldose-*1*-*t* were oxidized at room temperature by dissolving each in 0.5 ml of water, adding sufficient 0.04 *N* iodine to give a small degree of oxidation (about 10, 20, or 30%), and then adding dropwise 1.5 equivalents of 0.04 *N* sodium hydroxide. After 15 min, each solution was transferred to a 10-ml volumetric flask and diluted to volume. Then, about 2 ml of the solution was transferred to a standard-tapered male-joint, round-bottomed flask containing about 50 mg of sodium carbonate. The solution was frozen, and the ice-*t* was sublimed under vacuum into another flask. The sublimate was warmed to room temperature, and 100-μl samples of the liquid were removed and assayed with the liquid scintillation counter by the procedure given in sec. 2.1.c. In each instance, the amount of tritium in the reaction mixture was calculated from the amount of the aldose-*1*-*t* added; the amount of water-*t* formed was calculated from the volume of the reaction mixture and the specific activity of the sublimed water. The extent of the reaction, *f*, was calculated from the amount of iodine added.

In a typical measurement, a 9.241-mg sample of D-glucose-*1*-*t* containing 7.43 μc of tritium was allowed to react with 0.51 ml of 0.04 *N* iodine and 0.77 ml of 0.04 *N* sodium hydroxide. The reaction mixture was diluted to 10 ml with water, and a 2-ml sample was freeze-dried. A 100-μl sample of the water-*t*, obtained by freeze-drying, assayed 15.36 counts per second, corresponding to 0.00252 μc in the sample or 0.252 μc in 10 ml. Thus, $rf=0.252/7.43=0.0339$. The amount of iodine added corresponded to $f=0.20$. Substitution of these values in eq (1) gives 0.15 for k^*/k.

2.5. Determination of k^*/k by Double-Labeling

A weighed sample (10 mg) of the C^{14}-labeled aldose-*1*-*t* was dissolved in water (0.5 ml) and treated with sufficient 0.04 *N* iodine and 0.04 *N* sodium hydroxide to oxidize between 75 and 90 percent of the aldose. After 15 min, the solution was diluted with 5 ml of water, and 100 mg of the unlabeled aldose was added as carrier. The solution was passed through 20 ml of mixed cation- and anion-exchange resins (Amberlite IR-120 (H^+) and Duolite A4). The effluent was concentrated under reduced pressure to a sirup from which the labeled aldose was crystallized; it was recrystallized twice from methanol—2-propanol. After being dried, the purified carrier-mixture was assayed for carbon-14 and tritium by the procedure given in section 2.3. A sample of the original C^{14}-labeled aldose-*1*-*t* was also assayed. The amount of the residual reactant was calculated from the equation:

$$w=\frac{s'w'}{s-s'} \quad (4)$$

where w is the weight of the residual reactant, w' is the weight of the nonradioactive carrier added, and s and s' are the specific activities (in carbon-14) of the initial reactant and the carrier mixture, respectively. The fraction of aldose oxidized, f, is the ratio of reactant consumed to initial reactant.

The value of k^*/k was calculated as previously described [2] from the equation:

$$k^*/k=1+[\log(p/p^\circ)/\log(1-f)] \quad (5)$$

where p° is the ratio of tritium to carbon-14 in the initial reactant, and p is the ratio in the residual reactant. The results obtained for D-glucose-*6*-C^{14}-*1*-*t* and D-mannose-*2*-C^{14}-*1*-*t* are givin in table 2.

3. References

[1] L. Melander, Isotope Effects on Reaction Rates (Ronald Press Co., New York, 1960).
[2] H. S. Isbell, L. T. Sniegoski, and H. L. Frush, Anal. Chem. **34**, 982 (1962).
[3] L. T. Sniegoski, H. L. Frush, and H. S. Isbell, J. Res. NBS **65A** (Phys. and Chem.) No. 5, 441 (1961).
[4] W. H. Stevens and R. W. Attree, Can. J. Res. **27B**, 807 (1949).
[5] G. A. Ropp, J. Am. Chem. Soc. **82**, 842 (1960).
[6] L. Kaplan, J. Am. Chem. Soc. **77**, 5469 (1955).
[7] H. S. Isbell and L. T. Sniegoski (unpublished data).
[8] H S Isbell and W. W. Pigman, BS J. Res. **10**, 337 (1933) RP534.
[9] H. S. Isbell, H. L. Frush, N. B. Holt, and J. D. Moyer, J. Res. NBS **64A** (Phys. and Chem.) No. 2, 177 (1960).
[10] H. S. Isbell, H. L. Frush, and R. Schaffer, J. Res. NBS **54**, 201 (1955) RP2581.
[11] Operation Manual, Tri-Carb Liquid Scintillation Spectrometer, Series 314E, Packard Instrument Co., Inc., La Grange, Ill.
[12] F. Newton Hayes, Packard Technical Bulletin (November 1960).

(Paper 67A6–241)

JOURNAL OF RESEARCH of the National Bureau of Standards—A. Physics and Chemistry
Vol. 67A, No. 6, November–December 1963

Buffer Solutions of Potassium Dihydrogen Phosphate and Sodium Succinate at 25 °C

Maya Paabo, Roger G. Bates, and Robert A. Robinson

(July 2, 1963)

A buffer mixture consisting of equal molalities (m) of potassium dihydrogen phosphate and sodium succinate is proposed as a useful reference point in the study of acid-base equilibria, bridging the present gap between pH 5.5 and pH 6.8. The $p(a_H\gamma_{Cl})$ at 25 °C has been determined by electromotive-force measurements for five buffer solutions in which m varied from 0.005 to 0.025. The conventional pa_H of each solution has been derived and found to be in good agreement with that calculated from existing data for the two equilibria concerned. The pa_H varies from 6.251 at $m=0.005$ to 6.109 at $m=0.025$. The buffer mixture has been used successfully for the determination of the dissociation constants of 2-nitro-4-chlorophenol and 2,6-dichlorophenol.

1. Introduction

The useful application of the acidity function $-\log(a_H\gamma_{Cl})$ or $p(a_H\gamma_{Cl})$ in the accurate determination of dissociation constants or pK values has been described [1, 2].[1] In the determination of the pK of a weak acid by the spectrophotometric method, a buffer solution is needed with a value of $p(a_H\gamma_{Cl})$ not too far removed from the pK of the acid. For example, in the determination of the dissociation constant of p-nitrophenol at 25 °C [3], $pK=7.156$, a series of equimolar mixtures of potassium dihydrogen phosphate and disodium hydrogen phosphate of different total ionic strengths were used; their $p(a_H\gamma_{Cl})$ values lay between 6.912 and 7.080. For 2-chloro-4-nitrophenol, $pK=5.45$, solutions equimolal with respect to both sodium hydrogen succinate and sodium succinate were used [4]; their $p(a_H\gamma_{Cl})$ values lay between 5.477 and 5.553.

Neither of these buffer systems would be particularly suitable for an acid with pK about 6.2 and we have, therefore, now studied the buffer system consisting of sodium succinate and potassium dihydrogen phosphate at equal molalities (m). The $p(a_H\gamma_{Cl})$ values of five solutions in which m varied from 0.005 to 0.025 have been determined at 25 °C. By the application of a conventional definition of the activity coefficient of chloride ion, conventional pa_H values of these solutions have been calculated.

2. Method

The electromotive-force method by which $p(a_H\gamma_{Cl})$ was determined and values of pa_H assigned has been thoroughly described in earlier publications [2, 5]. It consisted of the following three steps:

1. Measurement of the emf of the following cell:

$$\text{Pt; } H_2(g,1\text{ atm}),\ KH_2PO_4(m),\ Na_2C_4H_4O_4(m),\ KCl(m'),\ AgCl;\ Ag$$

at 25 °C. Five different buffer mixtures consisting of equimolal amounts of potassium dihydrogen phosphate and sodium succinate (m varying from 0.005 to 0.025) were studied. Measurements were made with four concentrations (m') of potassium chloride, namely 0.005, 0.01, 0.015, and 0.02 molal, at each of the five buffer concentrations.

The emf was corrected to a partial pressure of 1 atm hydrogen in the usual way, and $p(a_H\gamma_{Cl})$ was calculated from each value of the emf (E) by the formula

$$p(a_H\gamma_{Cl})=\frac{(E-E^\circ)F}{RT\ln 10}+\log m' \qquad (1)$$

The standard potential (E°) was taken to be 0.22234 v at 25 °C [6], and the coefficient $F/(RT\ln 10)$ has the value 16.9047 v^{-1} at this temperature.

2. The limiting value of $p(a_H\gamma_{Cl})$ in the absence of potassium chloride, termed $p(a_H\gamma_{Cl})^\circ$, was determined for each of the five buffer solutions by plotting $p(a_H\gamma_{Cl})$ as a function of the molality of added potassium chloride and extrapolating to 0.

3. The conventional pa_H was computed from $p(a_H\gamma_{Cl})^\circ$ by the relationship.

$$pa_H=p(a_H\gamma_{Cl})^\circ+\log\gamma_{Cl} \qquad (2)$$

with the use of the convention [7]

$$\log\gamma_{Cl}=\frac{-A\sqrt{I}}{1+1.5\sqrt{I}} \qquad (3)$$

where I is the ionic strength and A, the Debye-Hückel slope, has the value 0.5108 mole $^{-1/2}$ kg $^{1/2}$ at 25 °C.

3. Experimental Procedure

The potassium dihydrogen phosphate was NBS Standard Sample 186Ib. Two different samples of sodium succinate hexahydrate, reagent grade, were used. In addition, a portion of one of the samples

[1] Figures in brackets indicate the literature references at the end of this paper.

was recrystallized and dried to remove its water of hydration. There were no apparent differences among buffers made from the three samples of sodium succinate. Potassium chloride was recrystallized once from water. The conductivity of the distilled water used to prepare the solutions was no greater than 0.8×10^{-6} ohm^{-1} cm^{-1}.

An increase of emf with time, the cause of which has not been determined, was observed. This increase was more rapid with the dilute solutions than with the more concentrated ones. It was therefore found necessary to make the emf measurements on the three most dilute buffer mixtures on the same day the solutions were prepared. However, the same values of the emf were obtained for fresh 0.02 m and 0.025 m buffer solutions on the day of preparation and one day later.

In terms of pa_H units, the 0.025 m buffer solution increased in pa_H by only 0.002 after standing two days and 0.012 after 12 days. However, the 0.01 m solution increased by 0.012 unit in 24 hr and the 0.005 m solution by 0.028 in the same time.

The stability of the primary and secondary phosphates in aqueous solution seems beyond question. Furthermore, no instability of buffer solutions composed of primary and secondary succinates was found in earlier work [8]. Nevertheless, it is advisable, for the greatest accuracy, to use the mixed buffers on the day of their preparation. This procedure was successful in the determination of the dissociation constants of 2-nitro-4-chlorophenol and 2,6-dichlorophenol (see below).

4. Results and Discussion

The results of the emf measurements and the calculations of $p(a_H\gamma_{Cl})$ are summarized in table 1. The average values of $p(a_H\gamma_{Cl})$ corresponding to the four molalities of potassium chloride are plotted as a function of the chloride molality in figure 1. The intercepts at $m'=0$, that is $p(a_H\gamma_{Cl})^\circ$, are given in table 2. The intercepts were determined by the method of least squares; the standard deviation of the intercept, σ_i, is given in the third column of the table. The pa_H values listed in the last column were calculated from $p(a_H\gamma_{Cl})^\circ$ together with the conventional definition of the activity coefficient of chloride ion [see eqs (2) and (3)]. The pa_H of equimolal solutions of potassium dihydrogen phosphate and sodium succinate at 25° is plotted in figure 2 as a function of the molality of each salt.

It is of interest to compare these experimental values of pa_H with the pa_H calculated from the dissociation constants for the two acid-base equilibria which fix the acidity of these buffer solutions. The dissociation constant of dihydrogen phosphate ion is given by $pK_{2P}=7.200$ at 25 °C [9], whereas that for succinate ion is expressed by $pK_{2S}=5.636$ at the same temperature [8]. From the mass law expressions for the two equilibria,

$$2\,pa_H=pK_{2P}+pK_{2S}-\log\frac{m_{P^-}m_{S^-}}{m_{P^=}m_{S^-}}-\log\frac{\gamma_{P^-}}{\gamma_{P^=}}-\log\frac{\gamma_{S^-}}{\gamma_{S^=}} \quad (4)$$

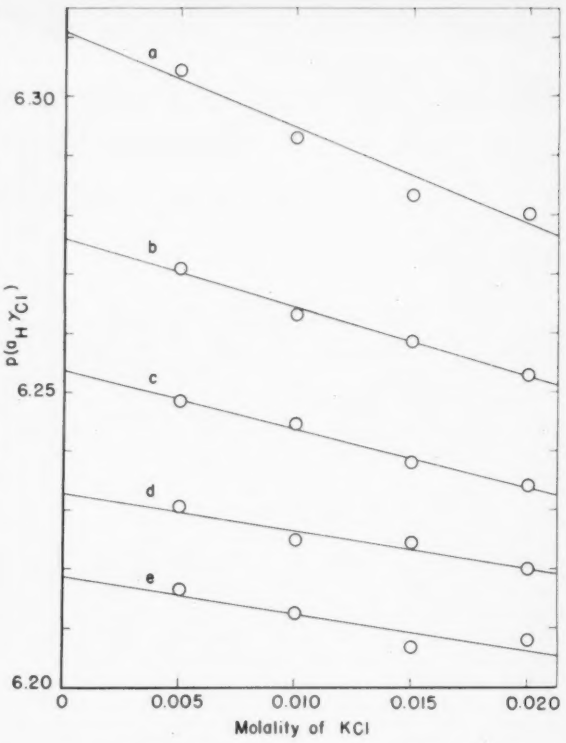

FIGURE 1. *Effect of added potassium chloride on the $p(a_H\gamma_{Cl})$ for equimolal mixtures of potassium dihydrogen phosphate and sodium succinate at 25 °C.*

Molality of each buffer salt: a, 0.005; b, 0.01; c, 0.015, d, 0.02; e, 0.025.

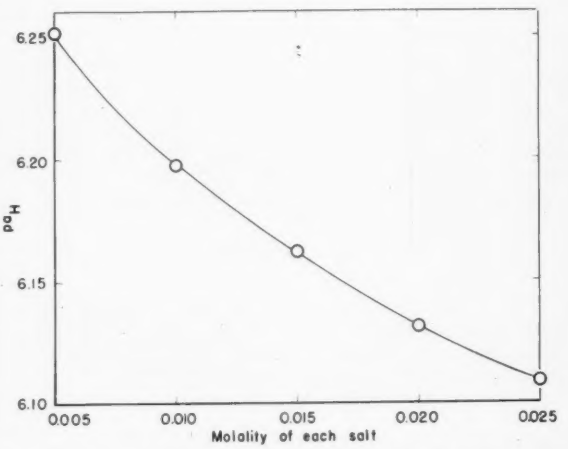

FIGURE 2. *pa_H at 25 °C for equimolal mixtures of potassium dihydrogen phosphate and sodium succinate as a function of the molality of each salt.*

TABLE 1. *Electromotive force of the cell* Pt; $H_2(g, 1\ atm)$, $KH_2PO_4(m)$, Na_2Suc (m), KCl (m'), AgCl; Ag *at 25 °C.*

Values of $p(a_H\gamma_{Cl})$

m	m' = 0.005		0.010		0.015		0.020	
	E	$p(a_H\gamma_{Cl})$	E	$p(a_H\gamma_{Cl})$	E	$p(a_H\gamma_{Cl})$	E	$p(a_H\gamma_{Cl})$
0.025	0.72610	6.215	0.70815	6.212	0.69757	6.210	0.68990	6.205
	.72627	6.218	.70830	6.215	.69751	6.209	.69013	6.209
	.72605	6.214	.70806	6.211	.69724	6.204	.68999	6.206
	.72636	6.219	.70810	6.212	.69723	6.204	.69026	6.211
			.70808	6.211				
.020	.72691	6.229	.70896	6.226	.69833	6.223	.69083	6.221
	.72706	6.231	.70879	6.223	.69835	6.223	.69098	6.223
	.72709	6.232	.70872	6.222	.69861	6.227	.69053	6.216
			.70904	6.228				
.015	.72808	6.248	.71005	6.245	.69923	6.238	.69162	6.234
.010	.72945	6.272	.71121	6.264	.70052	6.260	.69273	6.253
	.72936	6.270	.71108	6.262	.70039	6.257	.69272	6.253
.005	.73136	6.304	.71298	6.294	.70191	6.283	.69430	6.279
	.73140	6.304	.71296	6.294	.70193	6.283	.69439	6.281
			.71279	6.291				

TABLE 2. $p(a_H\gamma_{Cl})^\circ$ *and* pa_H *for equimolal solutions of potassium dihydrogen phosphate and sodium succinate at 25 °C*

m	$p(a_H\gamma_{Cl})^\circ$	σ_i	pa_H
0.025	6.219	0.001	6.109
.020	6.233	.001	6.131
.015	6.254	.001	6.162
.010	6.276	.001	6.197
.005	6.311	.002	6.251

where P and S refer respectively to the phosphate and succinate ions of the indicated charge.

The acid-base reaction taking place when the two buffer salts are mixed in solution may be represented by

$$H_2PO_4^- + Suc^= = HPO_4^= + HSuc^-. \qquad (5)$$

The extent to which this reaction proceeds need not be known, for the concentration term of eq (4) has a value of unity, provided the stoichiometric molalities of potassium dihydrogen phosphate and sodium succinate were equal. Furthermore, the ionic strength (I) is equal to $4m$ regardless of the extent to which reaction (5) proceeds.

The last two terms of eq (4) may be estimated as follows. In the course of the investigations which led to the determination of pK_{2P} and pK_{2S} the quantities log $[\gamma_{P^=}/(\gamma_{P^=}\gamma_{Cl^-})]$ and log $[\gamma_{S^=}/(\gamma_{S^=}\gamma_{Cl^-})]$ in phosphate buffer solutions and succinate buffer solutions, respectively, were evalutated and found to fit the Hückel equation with ion-size parameters of 4.4 Å and 7.0 Å. If these same parameters are used to calculate the ratios of the activity coefficients of the two phosphate anions and of the two succinate anions in the mixed buffer at 25°, eq (4) then becomes

$$pa_H = 1/2\,(pK_{2P} + pK_{2S}) - \frac{1.532\sqrt{m}}{1+2.89\sqrt{m}} - \frac{1.532\sqrt{m}}{1+4.60\sqrt{m}}. \qquad (6)$$

The pa_H values calculated by this equation are compared in table 3 with those derived directly from the emf measurements. The agreement, which is most satisfactory, lends support to the reliability of the experimental data.

TABLE 3. *"Observed" and calculated values of* pa_H *for five aqueous mixtures of* KH_2PO_4 *and* $Na_2C_4H_4O_4$ *at 25 °C*

$m_{KH_2PO_4} = m_{Na_2Suc}$	pa_H (observed)	pa_H (calc., eq (6))
0.025	6.109	6.111
.02	6.131	6.133
.015	6.162	6.160
.01	6.197	6.194
.005	6.251	6.246

The change of pa_H with temperature can be calculated in a similar fashion. Inspection of eq (4) shows that the effect of temperature changes on the pa_H of the phosphate-succinate mixture will be a combination of the change of the mean pK with temperature and of the temperature effect on the activity coefficients. The heats of dilution of completely dissociated electrolytes are neither large nor very different in the dilute range, and it is justifiable for our purpose to replace d log $(\gamma_{P^=}/\gamma_{P^-})/dT$ and d log $(\gamma_{S^=}/\gamma_{S^-})/dT$ by 3 d log $\gamma_\pm/dT$, where $\gamma_\pm$ is the mean ionic activity coefficient of one of the common uni-univalent strong electrolytes and T is the temperature in °K. From eq (4), one may therefore write

$$\frac{d}{dT}pa_H = \frac{1}{2}\frac{d}{dT}\left(pK_{2P} + pK_{2S}\right) - 3\frac{d}{dT}\log\gamma_\pm. \qquad (7)$$

Data in the literature [8, 9] provide the following temperature coefficients:

$$\frac{d\,pK_{2P}}{dT} = 0.020912 - \frac{2073.0}{T^2} \qquad (8)$$

and

$$\frac{d\,pK_{2S}}{dT} = 0.019153 - \frac{1679.13}{T^2}. \qquad (9)$$

Furthermore, it has been shown that d log $\gamma_\pm/dT$ for four common strong electrolytes has the following average values at 25°: -0.00007 deg^{-1} at $I=0.01$, -0.00012 deg^{-1} at $I=0.04$, and -0.0002 deg^{-1} at $I=0.1$.

From these data it may be seen that the contribution of the changes in pK to dpa_H/dT is -0.00180 deg^{-1} at 20 °C, -0.00107 deg^{-1} at 25 °C, and -0.00038 deg^{-1} at 30 °C. The temperature coefficient of pa_H at 25 °C for three of the mixed buffers is as follows:

m	$d\,pa_H/dT$
0.005	-0.00086 deg^{-1}
.01	-0.00071
.025	-0.0004

It is clear that the phosphate-succinate mixture has

a lower pa_H-temperature coefficient than either the phosphate buffer or the succinate buffer at room temperature. This is a considerable advantage when the buffer is used in spectrophotometric measurements where the temperature of the absorption cells is not well controlled.

5. Application to the Determination of Dissociation Constants

To illustrate the use of these buffer solutions in spectrophotometric work and to obtain a further check on their $p(a_H\gamma_{Cl})^\circ$ values, determinations of the dissociation constants of two substituted phenols is aqueous solution at 25 °C have been made.

In the spectrophotometric method [1, 10], the dissociation constant K of a weak uncharged acid HA,

$$K=\frac{a_{H^+}m_{A^-}}{m_{HA}}\frac{\gamma_{A^-}}{\gamma_{HA}}, \qquad (10)$$

is determined by measuring the degree of dissociation in a solution of known $p(a_H\gamma_{Cl})^\circ$ by optical methods. Substitution of α, the degree of dissociation, in eq (10) gives

$$pK=p(a_H\gamma_{Cl})^\circ-\log\frac{\alpha}{1-\alpha}-\log\frac{\gamma_{A^-}}{\gamma^\circ_{Cl^-}\gamma_{HA}}. \qquad (11)$$

A small correction is made to allow for the effect of the weak acid on $p(a_H\gamma_{Cl})^\circ$ [11].

The succinate-phosphate buffer has been used to measure the dissociation constants of two substituted phenols. Details are given in tables 4 and 5. In the case of 2-nitro-4-chlorophenol (table 4), the last term of eq (11) has been neglected in arriving at pK (corr.) The average of the five pK values is 6.45_8. There is a small but regular upward trend of pK with decreasing ionic strength; this may indicate that the last term of eq (11) is not completely negligible, and extrapolation to zero ionic strength, by the method of least squares, gives pK 6.46_5. Either value is in good agreement with that obtained earlier [4].

The value now found for 2,6-dichlorophenol, 6.78_6, (table 5) is also in good agreement with 6.79_1, which has been obtained in some unpublished work, using the potassium dihydrogen phosphate-disodium hydrogen phosphate buffer.

TABLE 4. *Dissociation constant of 2-nitro-4-chlorophenol in water at 25 °C*

Ionic strength [a]	$p(a_H\gamma_{Cl})^\circ$	D [b]	$\log\frac{D-D_1}{D_2-D}$	pK	pK (corr.)
0.10	6.219	0.356	−0.230	6.449	6.448
.08	6.233	.359	−.223	6.456	6.455
.06	6.254	.366	−.206	6.460	6.458
.04	6.276	.374	−.187	6.463	6.460
.02	6.311	.384	−.165	6.476	6.469
				Avg.	6.458
				$K=3.48\times10^{-7}$	

[a] The molar concentration of 2-nitro-4-chlorophenol was 4.80×10^{-5}. The buffer solutions contained equimolar disodium succinate and potassium dihydrogen phosphate.

[b] The absorption cells were 4 cm in length. D_1, the optical density of the undissociated phenol, measured in 0.01 M HCl, was 0.062. D_2, the optical density of the fully ionized phenol, measured in 0.01 M NaOH, was 0.855. Measurements were made at 427 mμ.

TABLE 5. *Dissociation constant of 2,6-dichlorophenol in water at 25 °C*

Ionic strength [a]	$p(a_H\gamma_{Cl})^\circ$	D [b]	$\log\frac{D-D_1}{D_2-D}$	pK	pK (corr.)
0.10	6.219	0.365	−0.572	6.791	6.790
.08	6.233	.376	−.556	6.789	6.787
.06	6.254	.389	−.537	6.791	6.789
.04	6.276	.403	−.509	6.785	6.782
.02	6.311	.431	−.478	6.789	6.783
				Avg.	6.786
				$K=1.64\times10^{-7}$	

[a] The molar concentration of 2,6-dichlorophenol was 8.73×10^{-5}. The buffer solutions contained equimolar disodium succinate and potassium dihydrogen phosphate.

[b] The absorption cells were 4 cm in length. D_1, the optical density of the undissociated phenol, measured in 0.01 M HCl, was 0. D_2, the optical density of the fully ionized phenol, measured in 0.01 M NaOH, was 1.728. Measurements were made at 300 mμ.

6. References

[1] R. G. Bates and G. Schwarzenbach, Helv. Chim. Acta **37,** 1069 (1954).
[2] R. G. Bates and R. Gary, J. Res. NBS **65A,** 495 (1961).
[3] G. F. Allen, R. A. Robinson, and V. E. Bower, J. Phys. Chem. **66,** 171 (1962).
[4] V. E. Bower and R. A. Robinson, J. Phys. Chem. **64,** 1078 (1960).
[5] R. G. Bates, J. Res. NBS **66A,** 179 (1962).
[6] R. G. Bates and V. E. Bower, J. Res. NBS **53,** 283 (1954).
[7] R. G. Bates and E. A. Guggenheim, Pure and Appl. Chem. **1,** 163 (1960).
[8] G. D. Pinching and R. G. Bates, J. Res. NBS **45,** 322 (1950) RP 2142.
[9] R. G. Bates and S. F. Acree J. Res. NBS **34,** 373 (1945); A. K. Grzybowski, J. Phys. Chem. **62,** 555 (1958).
[10] R. A. Robinson and A. I. Biggs, Trans. Faraday Soc. **51,** 901 (1955).
[11] R. A. Robinson and A. K. Kiang, Trans. Faraday Soc. **51,** 1938 (1955).

(Paper 67A6–242)

JOURNAL OF RESEARCH of the National Bureau of Standards—A. Physics and Chemistry
Vol. 67A, No. 6, November–December 1963

Recalibration of the NBS Glass Standards of Spectral Transmittance [1]

Harry J. Keegan, John C. Schleter, and Marion A. Belknap

(July 10, 1963)

In 1934, Gibson, Walker, and Brown developed sets of four colored glass filters to serve as working standards of spectral transmittance for checking the reliability of spectrophotometers. Several sets of these glasses were measured carefully and reserved and designated as future reference standards. Duplicate standards evaluated by comparison with the reference standards are available by purchase to the public. The current set of reference standards was established in the years 1945 to 1947, and one of these reference standards (selenium-red) was recalibrated in 1952. This paper reports a recalibration, made in 1961 and 1962, of all four glasses (selenium-red, carbon-yellow, copper-green, cobalt-blue) on three spectrophotometers (Cary 14, Beckman DU, König-Martens). Except for the cobalt-blue standard, the values of spectral transmittance found differ from those previously assigned by amounts differing at some wavelengths by as much as or slightly more than the uncertainties estimated for the present values, though not by amounts exceeding the combined uncertainties of the present and previous determinations. The indicated changes for these three standards are fairly regular, however, and support the view that the selenium-red and carbon-yellow standards are changing chiefly by formation of a reflectance-reducing film on the surfaces. The indicated rate of upward drift is slow, and suggests that it takes about 10 years for the drift to exceed the assigned uncertainity.

1. Introduction

In 1934, Gibson, Walker, and Brown [1] [2] described a set of four colored glass filters which they had developed to serve as standards of spectral transmittance to check the reliability of spectrophotometers. Several sets of these glasses were carefully measured at a number of wavelengths by using mercury, helium and incandescent sources and were reserved and designated as future reference standards. Duplicate standards evaluated by comparison with the reference standards were made available to the public by purchase. Although nearly nonselective filters are best suited to the detection of errors in the photometric scale, the filters chosen have spectral transmittances that vary markedly with wavelength and thus permit detection of slit-width errors and stray-energy errors as well as photometric-scale errors; thus a single selective filter may afford checks of the photometric scale over a large fraction of the whole scale [2, 3]. Table 1 identifies the glasses that have served as reference standards, and figure 1 shows the approximate spectral transmittances of these filters. The reports issued with the sets of duplicate standards gave the assigned values of transmittance at about 20 wavelengths between 390 and 750 nm [3] together with the estimated uncertainties and the temperature coefficients.

TABLE 1. *Identification of the glasses used as reference standards*

No.	Designation	1934–1940	1945–1947
1	Selenium-red	Jena OG 3-8 Jena OG 3-10	Jena OG 3-21
2	Carbon-yellow	Corning HT Yellow α[4] HT Yellow α[7]	Corning HT Yellow C-14
3	Copper-green	Jena BG 14-1 Jena BG 14-10	Jena BG 14-19
4	Cobalt-blue	Corning G 55A α[11] G 55A α[3]	Corning G 55A β[3]

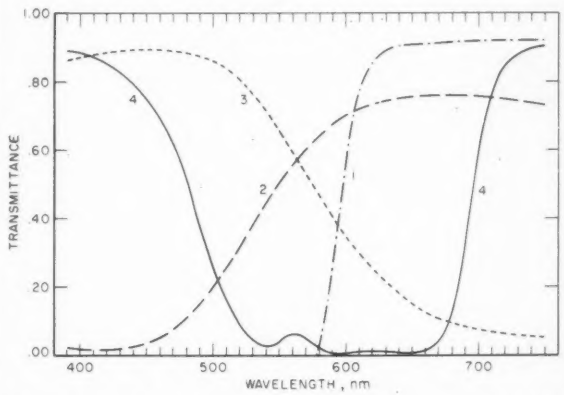

FIGURE 1. *Typical spectral transmittance curves of glass duplicate standards issued by the NBS for checking the reliability of spectrophotometers.*

The four types are: 1. Selenium-red, 2. Carbon-yellow, 3. Copper-green, and 4. Cobalt-blue.

[1] An abridged version of this paper will appear in the J. Opt. Soc. Am. 54 January 1964.
[2] Figures in brackets indicate the literature references at the end of this paper.
[3] Nanometers, 10^{-9} meters, formerly called millimicrons.

TABLE 2. *Estimated uncertainty in the value of absorbance,* U_a, *and the change* d, *in absorbance for temperature change of 15 °C, for the selected wavelengths for incandescent (Inc.) and line (Hg and He) sources used for the four reference standards*

Wavelength	Source	Selenium-red		Carbon-yellow		Copper-green		Cobalt-blue	
λ *in nm*		U_a	d	U_a	d	U_a	d	U_a	d
390	Inc			±0.052	−0.0005	±0.002	0.000	±0.002	0.000
404.7	Hg			.069	−.0025	.002	.000	.002	.000
420	Inc			.046	−.0025				
435.8	Hg			.014	−.0015	.001	.000	.002	.000
471.3	He			.011	+.001	.001	.000	.004	.000
491.6	Hg							.005	+.0005
501.6	He			.006	+.0035	.002	.000	.007	+.001
520	Inc			.004	+.0035			.010	+.0005
530	Inc			.003	+.003	.002	.000		
540	Inc							.008	−.003
546.1	Hg			.003	+.0025	.003	.000	.008	−.004
560	Inc			.002	+.002	.003	.000	.007	−.003
570	Inc	0.000							
578	Hg	±.06	+0.17	.003	+.0015	.004	−.0005	.008	−.004
587.6	He	.04	+.11	.003	+.0015				
600	Inc	.008	+.022	.002	+.001	.006	−.0005	.024	−.005
620	Inc	.003	+.002	.002	+.0005	.005	−.001	.017	−.003
640	Inc	.002	.000	.003	+.0005	.007	−.001	.023	−.005
660	Inc	.002	.000	.003	.000				
667.8	He					.007	−.001	.027	+.004
680	Inc							.033	+.006
690	Inc	.002	.000	.003	.000			.026	+.004
706.5	He							.004	+.002
710	Inc					.012	−.001		
720	Inc	.002	.000	.003	−.0005			.003	+.0005
750	Inc	.002	.000	.003	−.0005	.015	−.0005	002	.000

TABLE 3. *Previously adopted value of transmittance,* T, *and estimated uncertainty in the values of transmittance,* U, *at the respective wavelengths for the four reference standards*

Wave-length	Selenium-red (1952)*		Carbon-yellow (1946)*		Copper-green (1946)*		Cobalt-blue (1946)*	
λ *in nm*	*T*	*U*	*T*	*U*	*T*	*U*	*T*	*U*
390			0.025	±0.003	0.862	±0.003	0.895	±0.004
404.7			.020	.003	.877	.003	.884	.005
420			.019	.002				
435.8			.0240	.0007	.893	.004	.806	.003
471.3			.081	.002	.894	.004	.612	.006
491.6							.344	.004
501.6			.208	.003	.859	.005	.245	.004
520			.316	.003			.091	.002
530			.379	.003	.760	.004		
540							.0308	.0006
546.1			.479	.003	.671	.004	.0335	.0006
560			.557	.003	.585	.004	.064	.001
570	0.000							
578	.0042	±0.0005	.636	.003	.473	.003	.0273	.0005
587.6	.118	.01	.668	.003				
600	.550	.02	.699	.003	.350	.003	.0074	.0002
620	.852	.007	.731	.004	.256	.003	.0100	.0002
640	.904	.005	.747	.005	.187	.003	.0074	.0002
660	.914	.005	.754	.005				
667.8					.122	.002	.034	.002
680							.14	.01
690	.919	.005	.755	.005			.34	.02
706.5							.713	.007
710					.074	.002		
720	.918	.005	.748	.005			.845	.005
750	.917	.005	.730	.005	.057	.002	.901	.005

*Date of adoption of values.

Table 2 gives for each wavelength the light source used and the estimated uncertainties and a multiple of the temperature coefficients of the reference standards expressed on the absorbance scale. Absorbance is defined as the logarithm of the reciprocal of the internal transmittance T_i. Since internal transmittance for these glasses is closely equal to transmittance T multiplied by a constant (about 1/0.9) to correct for reflection losses [8], differences in absorbance are closely equal to differences in the logarithm of the reciprocal of transmittance T uncorrected for reflection losses. Accordingly the uncertainties U_a in absorbance entered in table 2 are computed from the uncertainties U in transmittance as:

$$U_a=[\log_{10}(T+U)-\log_{10}(T-U)]/2$$

Similarly, the temperature coefficients δ of absorbance are computed from the relation:

$$-\log_{10} T_\theta=-\log_{10} T_{25}+b\delta(\theta-25).$$

where θ is the temperature of the glass in degrees C, b is the thickness of the glass in mm, and $-\log_{10}T_{25}$ is the absorbance measurement made at 25 °C. The temperature coefficient δ is thus the change in $-\log_{10}T$ (closely equal to the change in $-\log_{10}T_i$) for a temperature change of 1 °C, and a thickness of 1 mm. These glass reference standards are measured at 25 °C and are used over a temperature range of ±15 °C. For convenience, because the temperature coefficient is relatively small compared with the value of absorbance, a quantity d equal to 15 times the temperature coefficient is used to designate the change in absorbance for a temperature change of 15 °C, as follows:

$$-\log_{10}T_\theta = -\log_{10}T_{25} + bd(\theta - 25)/15.$$

This relationship is considered valid for values of θ between 0 and 50 °C.

The current set of reference standards was measured in the years 1945 to 1947. A detailed analysis of the data obtained for one of the reference standards (cobalt-blue, Corning G 55A β^9) was published by Gibson and Balcom [4] in 1947. The uncertainties, U, were estimated as the huge error (4.9 times the probable error) of the mean values of transmittance. In 1950, Gibson and Belknap [5] published a study of the permanence of samples of the carbon-yellow, the copper-green, and the cobalt-blue glasses exposed under clear glass to south skylight and sunlight for periods up to three years. Expressed in terms of transmittance change ΔT, these samples were found to change but slightly, excepting only the copper-green glass below 500 nm, where there appears to be a definite solarization effect.

No such study was made for ordinary use of these glasses in the laboratory. It was assumed that if the glasses would change only slowly with extensive exposure to sunlight under glass, they would not change significantly in many years of ordinary use. A redetermination of the spectral transmittance of the current reference standard for selenium-red glass was carried out in 1952 and resulted in slight changes in the assigned values, but it could not be determined with certainty that the transmittance had changed. The 1946 and 1952 data are given in table 3.

Meanwhile, interest in the duplicate standards was increasing. Table 4 shows the number of duplicate standards of each type of glass issued in the years 1933–1942, 1943–1946, and 1947–1962.

TABLE 4. *Numbers of duplicate standards issued*

Years	Calibration of duplicate standards in charge of:	Selenium-red	Carbon-yellow	Copper-green	Cobalt-blue	Total
1933–1942	Mabel E. Brown and Geraldine W. Haupt	7	20	10	15	52
1943–1946	Margaret M. Balcom and Lois A. Peterson	0	11	7	16	34
1947–1962	Marion A. Belknap	20	161	113	99	393
	Totals	27	192	130	130	479

A set of these glass standards, issued in 1958 to the Frankford Arsenal, was submitted in October 1961 for recalibration. A routine comparison of them with the same reference standards used in the original calibration showed that the transmittances for each of the four glasses bore a significantly different relation to the corresponding reference standard than in 1958. It was presumed that this changed relation referred primarily to the duplicate standards, whose uses and possible exposure to radiant energy at the Frankford Arsenal were unspecified, rather than to the reference standards known to be irradiated only by incandescent-lamp light for short periods of time at infrequent intervals; and this presumption was subsequently proved to be correct. Nevertheless, check data obtained in 1952, 1953, 1959, and 1960 for the reference standards were reviewed. Although no single set of data proved that any of the reference standards had certainly changed, all four sets of data considered together showed some evidence of a slow continuing drift in spectral transmittance of the selenium-red, the carbon-yellow and the copper-green reference standards. The cobalt-blue glass alone showed no change in spectral transmittance. An extensive recalibration of all four reference standards was then undertaken. It is the purpose of the present paper to describe this recalibration, and to discuss its results.

2. Method of Spectrophotometry

The recalibration of the four reference standards of spectral transmittance was carried out by means of the Cary 14 recording spectrophotometer, the Beckman DU manual spectrophotometer [6], and the König-Martens visual spectrophotometer [7]. Table 5 lists the spectrophotometers used in the several calibrations of reference standards of spectral transmittance. The procedural details of the present recalibration are given below.

2.1. Cary Recording Spectrophotometer

Two sets of measurements of each of the four reference standards of spectral transmittance were made on the Cary recording photoelectric spectrophotometer (Model 14M, Serial No. 173) by means of the absorbance ($-\log T$) scale. At the same time measurements were made of a clear borosilicate crown glass, 1.0 mm thick, of known index of refraction and Abbe value ($n_D=1.517$, $\nu=64.5$).[4] This index and Abbe value are the same as those found for the borosilicate crown glass, 1.0 mm thick, whose spectral transmittances were known from a previous study [8]. These known spectral transmittances were used as a photometric-scale correction for transmittances of the reference standards greater than 40 percent. For each wavelength the ratio R_λ of the reference-standard transmittance to

[4] We are indebted to Irving Malitson for these measurements of index of refraction and Abbe value

TABLE 5. *Spectrophotometers used in the several calibrations of reference standards of spectral transmittance*

Spectrophotometer	Date of calibration			
König-Martens visual	1930–1940	1940–1950	1950–1960	1960–
Gibson photoelectric and thermoelectric.	1930–1940	1940–1950		
Hilger photographic sector-photometer.	1930–1940			
Beckman DU photoelectric ("BQ-1")			1950–1960	1960–
Beckman DU photoelectric ("BQ-2")		1940–1950		
Cary 14M recording photoelectric				1960–

that of the borosilicate crown glass was computed from the absorbance readings. The value T_λ of the transmittance of the reference standard was computed as:

$$T_\lambda = R_\lambda T_{0\lambda},$$

where $T_{0\lambda}$ is the known spectral transmittance of the borosilicate crown glass [8]. For T_λ less than 40 percent the value corresponding to the reading of the absorbance scale was accepted without correction. The wavelength calibration of the instrument was carried out as described by Keegan, Schleter, and Judd [9]. All measurements refer to the specimen at 25 °C.

2.2. Beckman DU Spectrophotometer

The spectral transmittances of the reference standards were measured on the Beckman DU ("BQ–1") spectrophotometer with incandescent source after calibration of wavelength scale at emission lines of mercury, helium, hydrogen, neon, and cesium. Frequent checks of the wavelength calibration were made by means of the mercury line at 546.1 nm. Each standard was measured in two positions in the sample holder for each set of readings. The holder was positioned so as to place the standard near the exit slit and away from the phototube. As recommended by Gibson and Balcom [4], the measurements were made with no lens over the exit slit. The spectral transmittance of each standard was measured at selected wavelengths by ratio to a blank beam set to 100 percent transmittance as a reference. The shift from the blue-sensitive to red-sensitive phototube was made at 620 nm. The selector switch was shifted to 0.1 for transmittance readings below 10 percent to give "times-10" readings at narrower slitwidths. A purple stray-energy filter was used for all measurements taken at 390 nm. The sample compartment was surrounded by a water jacket maintained at 25 °C by a constant-temperature water bath. The numbers of sets of readings made on the reference standards are as follows:

Selenium-red		Carbon-yellow	Copper-green	Cobalt-blue
Below 600nm	Above 600nm	Full spectra	Full spectra	Full spectra
2	3	7	3	2

The extra set of readings above 600 nm for the selenium-red standard was obtained by ratio of readings for the standard to those for a clear glass (Corning 9700).

2.3. König-Martens Spectrophotometer

The spectral transmittances of the four reference standards were measured on the König-Martens visual spectrophotometer [7] by using emission lines of a mercury source and a helium source and, at some wavelengths, by using an incandescent source. As explained on pages 464–465 of reference [5], it was early found advisable, because of the low luminosities of the Hg and He sources at 471.3, 491.6, 667.8, and 706.5 nm, to use the incandescent source at these wavelength settings, and this has been done in all later work on the König-Martens visual spectrophotometer. However, for the present standardization of the NBS reference standards, measurements were made with both incandescent and line sources at these four wavelengths. The wavelength scale was checked by settings on certain of the mercury and helium lines each time the instrument was used and each time the width of the ocular slit was changed. The widths of the collimator and ocular slits were 0.2 mm for the readings taken by means of the incandescent source, and were varied from 0.2 to 0.4, or 0.5 mm for the line sources. Accurately calibrated sector disks (transmittances approximately 1, 10, 50, and 60 percent) were used for measurement of low transmittances or for transmittances near to those of the sectors to increase the accuracy of the readings. Stray-energy filters were used at wavelengths near the two ends of the visible spectrum and at wavelengths of low transmittance. Each set of readings consisted of 20 readings of angle on the Martens photometer; first, 10 for the standard inserted in one beam, and second, 10 for it in the other beam. The transmittance was computed as the cotangent of the first angle multiplied by the tangent of the second. At least two sets of readings were taken for each standard at each selected wavelength between 404.7 and 660 nm and a few additional readings between 660 and 706.5 nm because of the added uncertainty of the settings in this region of low luminosity. All readings were made with the standards in a holder maintained at 25° C by means of a constant-temperature water bath.

3. Reduction of Data and Estimates of Uncertainty

The spectral transmittances assigned to the reference standards are weighted means of the transmittances found individually by the three spectrophotometers used. The weights assigned to the individual values of transmittance for a particular standard at a particular wavelength were based on the known relative capabilities of the three instruments. For example, the values obtained by means of the König-Martens visual spectrophotometer in spectral regions yielding observing fields of low luminance (such as near the extremes of the visible

spectrum) were given less weight because of the resulting unreliability of the visual settings. On the other hand values of spectral transmittance obtained by means of an emission line in a spectral region of rapid variation of transmittance with wavelength were given more weight.

In tables 6, 7, 8, and 9, are given for each of the four reference standards and for each of the three instruments at the respective wavelengths, the average value of the transmittance so measured, the assigned weight, the range in transmittance, the adopted weighted mean, and the estimated uncertainty in the value of transmittance.

The year or years of measurement on the indicated spectrophotometers are shown in the parenthesis under the name of the instrument. The uncertainty of the assigned value of transmittance at a particular wavelength was made the same as that assigned previously (see table 3); with exceptional cases where it was agreed that a change was necessary. In these cases the uncertainty was estimated from the range of the individual values obtained on the three instruments averaged over a spectral region variable in extent from 0 to 50 nm and centered on that wavelength. Some smoothing of these values was resorted to whenever no reason was apparent for a rapid change in uncertainty with wavelength. In no case was the uncertainty allowed to be less than one-half the range of the spectrophotometric data. These ranges correspond roughly to estimates of three times the standard deviation of the adopted value [10].

TABLE 6. *Spectral transmittance,* T, *of selenium-red reference standard Jena OG 3-21, 1.7 mm, as measured on indicated spectrophotometers; assigned weight,* W, *range,* R, *adopted weighted mean, and estimated uncertainty of value of transmittance,* U

Wavelength	König-Martens (1962)*		Beckman DU (1961–1962)*		Cary Model 14 (1962)*		Range	Adopted weighted mean	Estimated uncertainty
λ *in nm*	*T*	*W*	*T*	*W*	*T*	*W*	*R*	*T*	*U*
390 to 570	0.000	-------	0.000	-------	0.000	-------	0.000	0.000	----------
578	.0041	4	.0033	2	.0034	4	.0008	.0037	±0.0005
587.6	.115	4	.102	3	.110	3	.013	.110	.01
600	.564	3	.556	4	.561	3	.008	.560	.01
620	.858	4	.856	4	.861	2	.005	.857	.006
640	.906	4	.903	4	.909	2	.006	.905	.004
660	.913	4	.914	4	.920	2	.007	.915	.004
690	.917	3	.918	5	.925	2	.008	.919	.004
720	.918	2	.919	6	.926	2	.008	.920	.004
750	.919	1	.919	7	.925	2	.006	.920	.004

*Date of measurement.

TABLE 7. *Spectral transmittance,* T, *of carbon-yellow reference standards Corning HT yellow C14, 2.0 mm, as measured on indicated spectrophotometers; assigned weight,* W, *range,* R, *adopted weighted mean and estimated uncertainty of transmittance,* U

Wavelength	König-Martens (1962)*		Beckman DU (1961–1962)*		Cary Model 14 (1962)*		Range	Adopted weighted mean	Estimated uncertainty
λ *in nm*	*T*	*W*	*T*	*W*	*T*	*W*	*R*	*T*	*U*
390	-------	-------	0.025	5	0.025	5	0.000	0.025	±0.003
404.7	0.019	3	.019	4	.019	3	.000	.019	.003
420	-------	-------	.019	5	.019	5	.000	.019	.002
435.8	.0244	4	.0234	2	.0248	4	.0014	.0244	.0008
471.3	.081	2	.080	4	.082	4	.002	.081	.002
501.6	.209	3	.206	4	.209	3	.003	.208	.003
520	.316	3	.318	4	.320	3	.004	.318	.003
530	.381	3	.380	4	.382	3	.002	.381	.003
546.1	.480	3	.480	4	.484	3	.004	.481	.003
560	.558	3	.560	4	.562	3	.004	.560	.003
578	.634	3	.639	4	.642	3	.008	.638	.004
587.6	.671	3	.669	4	.674	3	.005	.671	.004
600	.702	4	.702	4	.704	2	.002	.702	.004
620	.736	4	.734	4	.739	2	.005	.736	.004
640	.750	4	.751	4	.756	2	.006	.752	.005
660	.756	4	.758	4	.763	2	.007	.758	.005
690	.760	3	.759	4	.764	3	.005	.761	.005
720	-------	-------	.752	6	.756	4	.004	.754	.005
750	-------	-------	.733	6	.736	4	.003	.734	.005

*Date of measurement.

TABLE 8. *Spectral transmittance, T, of copper-green reference standard Jena BG 14–19, 2.0 mm, as measured on indicated spectrophotometers; assigned weight, W, range, R, adopted weighted mean, and estimated uncertainty of transmittance, U*

Wavelength	König-Martens (1962)*		Beckman DU (1962)*		Cary Model 14 (1962)*		Range	Adopted weighted mean	Estimated uncertainty
λ *in nm*	*T*	*W*	*T*	*W*	*T*	*W*	*R*	*T*	*U*
390			0.866	6	0.864	4	0.002	0.865	±0.003
404.7	0.876	2	.878	4	.878	4	.002	.878	.003
435.8	.893	3	.891	4	.892	3	.002	.892	.003
471.3	.893	2	.893	4	.892	4	.001	.893	.003
501.6	.862	3	.861	4	.860	3	.002	.861	.003
530	.759	3	.765	4	.762	3	.006	.762	.004
546.1	.672	3	.678	4	.677	3	.006	.676	.004
560	.593	3	.594	4	.589	3	.005	.592	.004
578	.477	3	.481	4	.476	3	.005	.478	.004
600	.348	3	.358	4	.352	3	.010	.353	.005
620	.258	3	.257	4	.258	3	.001	.258	.003
640	.187	3	.188	4	.187	3	.001	.187	003
667.8	.123	3	.123	4	.122	3	.001	.123	002
710	.078	1	.075	5	.075	4	.003	.075	.002
750			.057	5	.057	5	.000	.057	.002

* Date of measurement.

TABLE 9. *Spectral transmittance, T, of cobalt-blue reference standard Corning G 55 Aβ[9], 3.0 mm, as measured on indicated spectrophotometers; assigned weight, W, range, R, adopted weighted mean, and estimated uncertainty of transmittance, U*

Wavelength	König-Martens (1962)*		Beckman DU (1962)*		Cary Model 14 (1962)*		Range	Adopted weighted mean	Estimated uncertainty
λ *in nm*	*T*	*W*	*T*	*W*	*T*	*W*	*R*	*T*	*U*
390			0.894	6	0.892	4	0.002	0.893	±0.004
404.7	0.887	2	.880	4	.880	4	.007	.881	.005
435.8	.808	3	.808	4	.805	3	.003	.807	.003
471.3	.613	2	.618	4	.612	4	.006	.615	.006
491.6	.344	2	.351	4	.342	4	.009	.346	.004
501.6	.248	3	.249	4	.244	3	.005	.247	.004
520	.091	4	.092	3	.089	3	.003	.091	.002
540	.0314	4	.0308	3	.0310	3	.0006	.0311	.0006
546.1	.0339	4	.0334	3	.0344	3	.0010	.0339	.0006
560	.064	4	.064	3	.065	3	.001	.064	.001
578	.0290	4	.0281	3	.0274	3	.0016	.0282	.0008
600	.0073	4	.0072	3	.0073	3	.0001	.0073	.0004
620	.0100	4	.0104	3	.0104	3	.0004	.0102	.0004
640	.0075	6	.0082	2	.0074	2	.0008	.0076	.0004
667.8	.032	4	.032	4	.034	2	.002	.032	.002
680	.127	2	.132	5	.139	3	.012	.133	.01
690	.310	2	.338	5	.352	3	.042	.337	.02
706.5	.708	2	.703	4	.714	4	.011	.708	.007
720			.844	7	.852	3	.008	.846	.005
750			.902	7	.909	3	.007	.904	.005

* Date of measurement.

In table 10 the change in transmittance between the present value and the previously adopted value of spectral transmittance is given for each of the four reference standards at the respective wavelengths.

Figures 2, 3, 4, and 5 show as circles these differences in spectral transmittance assigned by the present recalibration and that assigned by the previous calibration for the selenium-red, the carbon-yellow, the copper-green, and the cobalt-blue standards. They also show as broken lines centered about the abscissa the estimates of the uncertainties of the values of spectral transmittance resulting from the present recalibration.

TABLE 10. *Change in spectral transmittance, ΔT, for the four reference standards between the present adopted weighted mean and the previously adopted values*

Wavelength	Selenium-red	Carbon-yellow	Copper-green	Cobalt-blue
λ *in nm*	ΔT (1962–1952)	ΔT (1962–1946)	ΔT (1962–1946)	ΔT (1962–1946)
390	.....	0.000	+0.003	−0.002
404.7	.....	−.001	+.001	−.003
420	.....	.000	.....	.....
435.8	.....	+.0004	−.001	+.001
471.3	.....	.000	−.001	+.003
491.6	.....	.....	.....	+.002
501.6	.....	.000	+.002	+.002
520	.....	+.002	.....	.000
530	.....	+.002	+.002	.....
540	.....	.....	.....	+.0003
546.1	.....	+.002	+.005	+.0004
560	.....	+.003	+.007	.000
570	0.000	.....	.....	.....
578	−.0005	+.002	+.005	+.0009
587.6	−.008	+.003	.....	.....
600	+.010	+.003	+.003	−.0001
620	+.005	+.005	+.002	+.0002
640	+.001	+.005	.000	+.0002
660	+.001	+.004	.....	.....
667.8	.....	.....	+.001	−.002
680	.....	.....	.....	−.003
690	.000	+.006	.....	−.002
706.5	.....	.....	.....	−.005
710	.....	.....	+.001	.....
720	+.002	+.006	.....	+.001
750	+.003	+.004	.000	+.003

4. Discussion

It will be noted from figure 2 that three of the ten newly assigned values of spectral transmittance for the selenium-red reference standard differ from the previous assigned values by amounts approaching the estimated uncertainty. Because the previously assigned values are uncertain by about the same amount, this recalibration by itself fails to prove that the selenium-red standard has changed since 1952. The results of the two spectrophotometers (König-Martens and Beckman DU "BQ-1") common to the 1952 determination and the present determination, however, both indicate that a change has occurred. Furthermore, comparison of the 1947 with the 1952 determination shows similar changes. It seems likely that indications of increases in transmittance between 620 and 750 nm correspond to formation of a reflectance-reducing film on the surfaces. Several of the duplicates of this reference standard show visible evidence of such films. The decreases in transmittance indicated near the cut-off of the transmittance curve may not be real. (See fig. 2, wavelengths 570 and 587.6 nm). In any case, there is no established cause for such a change.

Figure 3 gives an indication of formation of a reflectance-reducing film on the surfaces of the carbon-yellow reference standard similar to that by figure 2 for the selenium-red standard. Note that the indicated discrepancies between the present and the previous assignments of spectral transmittance are roughly proportional to the spectral transmit-

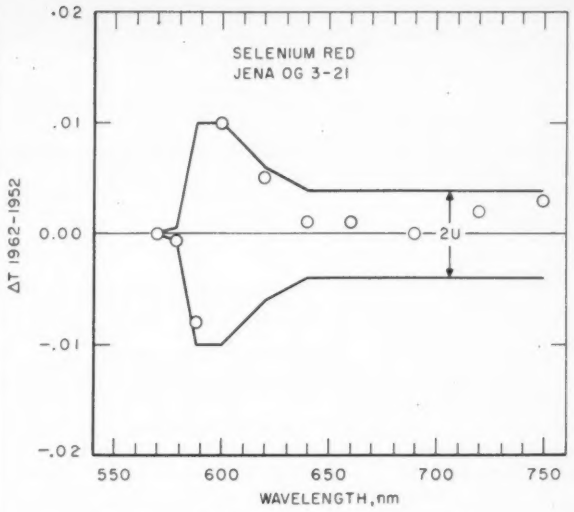

FIGURE 2. *Selenium-red reference standard.*

Differences (shown as circles) between spectral transmittances assigned in 1962 and in 1952 compared to estimates (shown as broken lines) of the uncertainty of the 1962 recalibration.

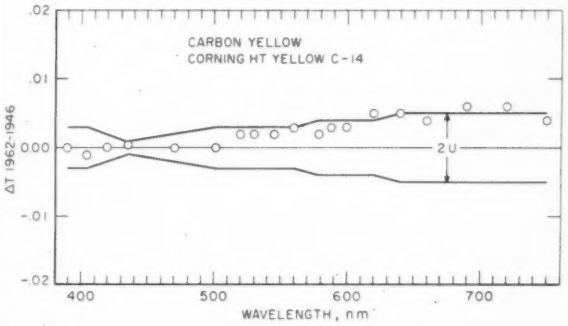

FIGURE 3. *Carbon-yellow reference standard.*

Differences (shown as circles) between spectral transmittances assigned in 1962 and in 1946 compared to estimates (shown as broken lines) of the uncertainty of the 1962 recalibration.

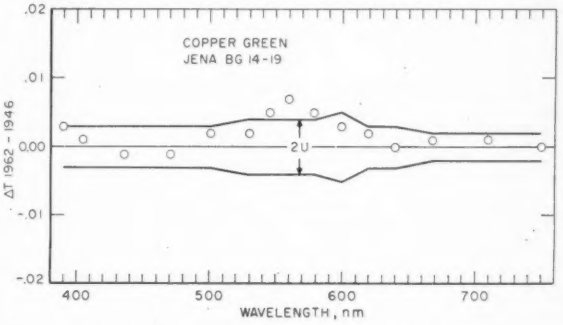

FIGURE 4. *Copper-green reference standard.*

Differences (shown as circles) between spectral transmittances assigned in 1962 and in 1946 compared to estimates (shown as broken lines) of the uncertainty of the 1962 recalibration.

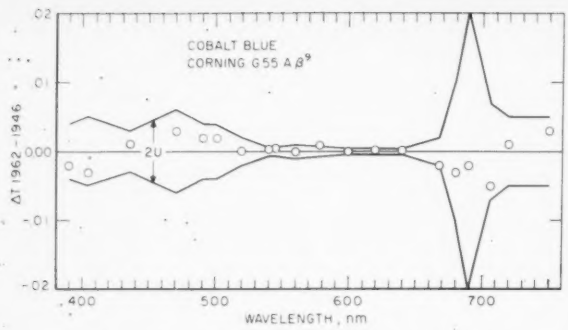

FIGURE 5. *Cobalt-blue reference standard.*

Differences (shown as circles) between spectral transmittances assigned in 1962 and in 1946 compared to estimates (shown as broken lines) of the uncertainty of the 1962 recalibration.

tances themselves, (see fig. 1), as would be expected from the formation of a reflectance-reducing film.

Figure 4 indicates some increases (390, 405, 500–620 nm) and some decreases (436, 471 nm) in assigned values of spectral transmittance. This indicated pattern is not consistent with the hypothesis that a reflectance-reducing film has been forming on the copper-green reference standard. If the indicated changes are real, and this has not been proved, they must be ascribed to a cause other than film formation (such as a slow chemical change in the glass), or to a combination of film formation with other cause or causes unknown.

Figure 5 gives no plausible suggestion that the cobalt-blue reference standard is changing even slowly. In table 10 the indicated changes are either small compared to the estimated uncertainty of the present determinations, or irregular.

In summary, it may be stated that three of the reference standards of spectral transmittance are probably subject to a slight impermanence, the maximum changes in a 10-year period being of the order of magnitude of the uncertainties in their calibration. Owners of duplicate standards not subjected to unusually severe usage (exposure to high-energy particles, ultraviolet energy, high temperatures, or chemical fumes) may find in figures 2 to 5 a reasonably valid basis for revising the adopted transmittance for their duplicate standards. In the absence of information to the contrary, the changes may be assumed as a first approximation to be proportional with time, and the time for recently issued duplicates (1952 to 1961) should be counted from 1952 for the selenium-red standards, and from 1946 for the carbon-yellow, the copper-green, and the cobalt-blue standards.

5. References

[1] K. S. Gibson, G. K. Walker, and M. E. Brown, Filters for testing the reliability of spectrophotometers, J. Opt. Soc. Am. **24,** 58 (1934).

[2] K. S. Gibson, Spectrophotometry (200 to 1,000 millimicrons), NBS Circ. 484, p. 36 (Sept. 15, 1949).

[3] Standards for checking the calibration of spectrophotometers (200 to 1,000 mμ), NBS Circ. LC–1017, pp. 10–12 (Jan. 1955).

[4] K. S. Gibson and M. M. Balcom, Transmission measurements with the Beckman quartz spectrophotometer, J. Res. NBS **38,** 611 (1947) RP1798.

[5] K. S. Gibson and M. A. Belknap, Permanence of glass standards of spectral transmittance, J. Res. NBS, **44,** 463 (1950) RP2093.

[6] H. H. Cary and A. O. Beckman, A quartz photoelectric spectrophotometer, J. Opt. Soc. Am. **31,** 682 (1941).

[7] H. J. McNicholas, Equipment for measuring the reflective and transmissive properties of diffusing media, J. Res. NBS **13,** 211 (1934).

[8] H. J. Keegan, M. A. Belknap, and D. J. Cordrey, Spectral transmissive properties of five selected optical glasses, J. Res. NBS **52,** 305 (1954) RP2505.

[9] H. J. Keegan, J. C. Schleter, and D. B. Judd, Glass filters for checking performance of spectrophotometer-integrator systems of color measurement, J. Res. NBS **66A** (Phys. and Chem.) No. 3, 203 (1962).

[10] W. J. Dixon, and F. J. Massey, Introduction to statistical analysis, 2d ed. (McGraw-Hill Book Co., Inc., New York, 1957).

(Paper 67A6–243

JOURNAL OF RESEARCH of the National Bureau of Standards—A. Physics and Chemistry
Vol. 67A, No. 6, November-December 1963

Thermal Behavior of Muscovite Sheet Mica

Stanley Ruthberg

(July 11, 1963)

The three spectral types of muscovite sheet mica, i.e., very pink ruby, light green, and dark green, were subjected to heat treatments at temperatures up to 600 °C. The changes in the apparent optic axial angle and in the absorption spectra (0.3 to 15 μ) were studied along with color.

The differentiation of muscovite sheet according to these spectral types extends to the behavior of apparent optic axial angle and to certain regions of the spectrum under heat treatment. The pink associated absorption region (0.47 to 0.6 μ) can be enhanced or bleached away by appropriate thermal treatment, although the associated infrared multiplet at 3 to 3.5 μ is little affected. The absorption band at 12 μ increases in intensity with temperature of treatment. It is suspected that the 0.47 to 0.6 μ absorption is the result of color centers.

It has been shown that measurable differences exist in apparent optic axial angle and absorption spectrum, as well as in color, for muscovite sheet micas. These differences indicate that there must be basic chemical and structural variations. They further provide a quantitative, though complex, categorization of the material [1].[1]

The present paper reports the effect of heat treatment on color, apparent optic axial angle, and absorption spectrum for several of the representative categories of the material so established. The treatments were at temperatures of 600 °C and less, usually considered to be below the decomposition point.

1. Experimental Procedures

The details of measurement of apparent optic axial angle, absorption spectrum, and color are as before [1,2].

Comparisons of spectral variations are again made in terms of the resonance absorption coefficient (below background), $\alpha_\lambda(R)$, defined with respect to an appropriately placed base line as

$$\alpha_\lambda(R) = -\frac{1}{t} \ln (T_R/T_b) \qquad (1)$$

where T_R is the transmission at the resonance band center, T_b is the value at the base line for the same wavelength, and t is the specimen thickness.

Color was determined by comparison with the previously selected standard samples.

1.1. Specimens

Three categories of muscovite sheet were chosen. These were very pink ruby, light green, and dark green, which represent the three end-types as defined in the earlier work.

Crystal sheets were all of high quality, V–1 to V–4 [3], with origins in India, Brazil, Tanganyika, and the United States.

As appropriate combination of visual color determination and restriction to magnitude of apparent optic axial angle can assure selection of these end-types, such procedure was used for sample choice. Specimens were first selected according to visual color. They were then picked for magnitude of apparent optic axial angle. The very pink ruby specimens were restricted to angles between 68° and 72.5°. Light greens were restricted to angles greater than 72.5°. Dark greens were taken with angles less than 68°. Selection was further restricted to those specimens for which repeatability was obtained in the measurement of angle to within 5′ of arc.

1.2. Heat Treatment

Specimens were air fired. Several temperature-time schedules were used which employed temperatures of 300, 500, and 600 °C and time intervals ranging from 3 min to 72 hr.

Samples were contained in covered Vycor crucibles to avoid contamination. Crucibles were first chemically cleaned and air fired at 500 °C. Clean procedures of sample handling were employed.

To reduce thermal lag the firebrick supports for the crucibles were first brought to temperature in the muffle furnace. These were then quickly withdrawn, the loaded crucibles were set in, and the assembly moved back into the furnace. Withdrawal was in the reverse order. The interval of treatment was measured from the time when the crucible went into the furnace to that when it was withdrawn and taken out of the firebrick holder. The consequent heating and cooling data for a

[1] Figures in brackets indicate the literature references at the end of this paper.

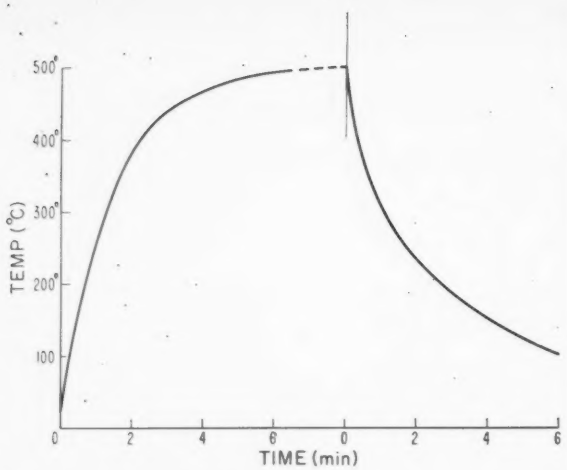

FIGURE 1. *Heating and cooling curves for a representative sample subjected to a heating procedure at 500* °C.

Crucible was thrust into furnace at 0 time on heating curve, and was extracted and removed from firebrick holder at 0 time on cooling curve.

typical sample were as shown in figure 1. For these, temperature was measured with a fine thermocouple inserted between laminae. It is seen that 3 min in the furnace, set at 500 °C, caused the sample temperature to rise to ~430 °C and to be above 400 °C for about ½ min. Ten minutes in the furnace caused the sample temperature to be above 450 °C for over 6 min.

To lessen the number of runs, many samples were placed in each crucible. As a control procedure appropriate mixing of sample categories in these crucibles was used. In some runs samples from each end-type were mixed together. In other runs samples were grouped according to one type only.

Both sequential and individual temperature times were utilized, i.e., some samples were heated to a series of temperatures, for varying times, other samples received a single temperature-time treatment. Specific treatments were as follows:

1. Various time intervals at 300 and 500 °C, mixed samples—Crystal sheets were sectioned and distributed into a number of crucibles. Each crucible had three samples, one of each of the end-types, so placed within it as to be separated from each other, and each crucible received one particular temperature-time treatment. A temperature of 300 °C was used for time intervals of 90 min and 5, 24, 48, and 72 hr. A temperature of 500 °C was used for time intervals of 3, 10, 30, and 90 min, 5 and 24 hr.

2. Fixed interval of 24 hr at several temperatures, no mixing—Samples were sectioned and distributed into the crucibles so that only one type was in each crucible. Three crucibles, one for each type, were heated together for a specific time and temperature. The period of time was 24 hr. Temperatures were 300, 500, and 600 °C.

3. Interval of 90 min at 300 °C, no mixing—Same preparation as (2).

4. Successive treatments for 24 hr at several temperatures, mixed samples—Mixed types of single crystal sheets were heated successively at 300 °C–24 hr, then 500 °C–24 hr, and then 600 °C–24 hr.

When sectioned, a crystal sheet was cut into a number of pieces of small area not less than ½ in.×½ in. Angles and/or spectra were obtained before and after treatment on each individual section.

2. Results

2.1. Spectrum

The spectral changes due to heat treatment are substantial in the 0.3 to 1 μ region. The infrared region of 1 to 15 μ is less affected with little correlation found except in the 3 to 3.5 μ and 12 μ areas.

a. 0.3 to 1μ

Representative results in the 0.3 to 1 μ region for the three end types are shown in figures 2, 3, and 4. Each figure is for a single crystal which had been cut into four sections. Each section received a specific temperature treatment for 24 hr (procedure No. 2). The very pink ruby and dark green types are most affected but with different overall rseponse. Quantitative results are given in figures 5, 6, and 7 in terms of the absorption coefficients for wavelengths of 0.44, 0.49, and 0.58 μ, which coefficients have been used previously to categorize muscovite sheet.

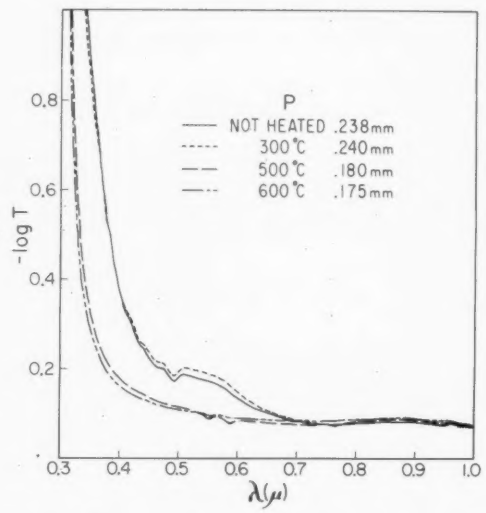

FIGURE 2. *Change in the 0.3 to 1 μ absorption spectrum of a pink ruby with heating for 24 hr at various temperatures (No. 2 schedule).*

Specimen thickness is indicated.

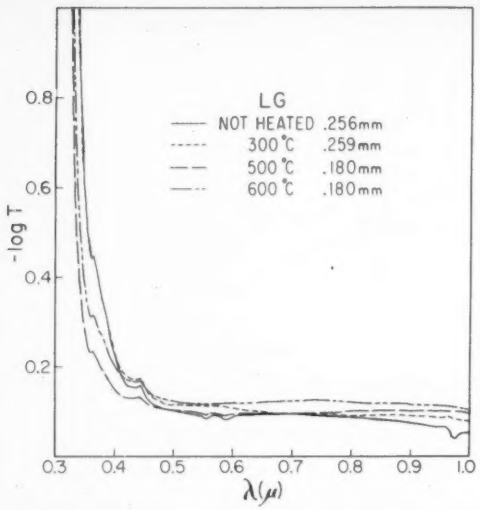

FIGURE 3. *Change in the 0.3 to 1 μ absorption spectrum of a light green with heating for 24 hr at various temperatures (No. 2 schedule).*

Specimen thickness is indicated.

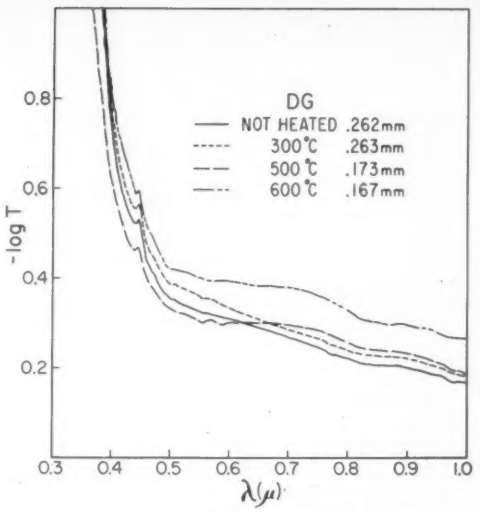

FIGURE 4. *Change in the 0.3 to 1 μ absorption spectrum for a dark green with heating for 24 hr at various temperatures (No. 2 schedule).*

Specimen thickness is indicated.

These data show that the red color of the pink ruby is enhanced by the low temperature (300 °C) treatment, but that bleaching results from the higher temperatures. The color changes from pink to a gray with residual pinkness after 500 °C and to gray after 600 °C. The deep absorption edge shifts to shorter wavelength. Transparency is also increased by 500 °C but tends to diminish after 600 °C.

The 0.47 to 0.6 μ pink associated absorption region is also enhanced in the dark green by 300 °C treatment, which caused the material to become khaki in appearance. The higher temperature again diminished the pink associated absorption and turned color to a very deep green. Opacity increased considerably and the absorption edge shifted strongly to longer wavelengths. Two additional coefficients have been introduced to describe the broad absorption which has appeared at ~0.72 μ as center wavelength. These are $\alpha'_{0\text{-}72}$, the total absorption coefficient at 0.72 μ ($-\frac{1}{l}\ln T$) and $\alpha_{0\text{-}72}$, the resonance absorption coefficient, eq (1). These two coefficients measure height of the absorption as well as the base-to-peak value.

Light green was least affected. This typical specimen took on a slight gray cast after 300 °C treatment with a small increase in the pink associated absorption region at 0.47 to 0.6 μ; however, color returned to light green after the high-temperature treatments.

Pink ruby specimens which had been exposed to 500 °C for 24 hr were subsequently heated at 300 °C for as long as 52 hr. The pink associated absorption region of 0.47 to 0.6 μ was not restored. On the contrary, such treatment then caused a further

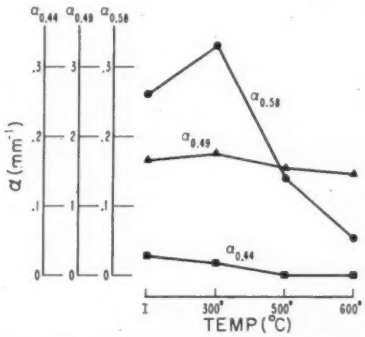

FIGURE 5. *Change in visible spectrum of a pink ruby due to heating (No. 2 schedule) as described by absorption coefficients.*

$\alpha_{0.44}$ is green correlated. $\alpha_{0.49}$ is a measure of band edge absorption. $\alpha_{0.58}$ relates to visible pink associated absorption. *I* is initial untreated value.

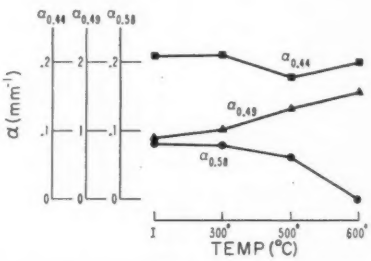

FIGURE 6. *Visible spectrum change due to heating for a light green as described by absorption coefficients (No. 2 schedule).*

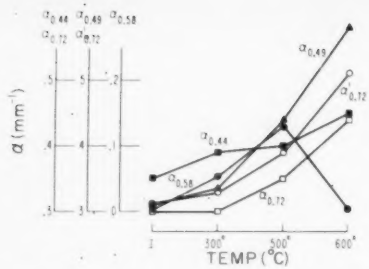

FIGURE 7. *Visible spectrum change due to heating for a dark green as described by absorption coefficients (No. 2 schedule).*

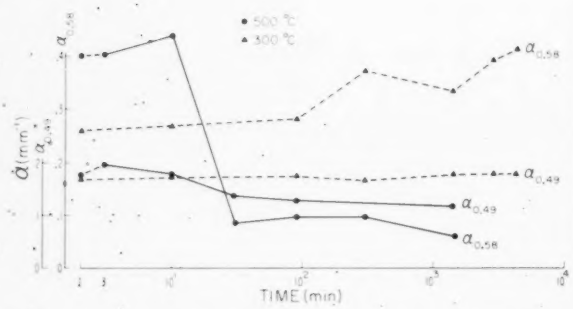

FIGURE 8. *Effect of heating on the visible pink associated absorption region of 0.47 to 0.6 μ and on the height of the absorption edge of a very pink ruby.*

No. 1 procedure for heat treatment. $\alpha_{0.58}$ is a measure of the pink associated absorption. $\alpha_{0.49}$ is a measure of the height of the absorption edge and of transparency.

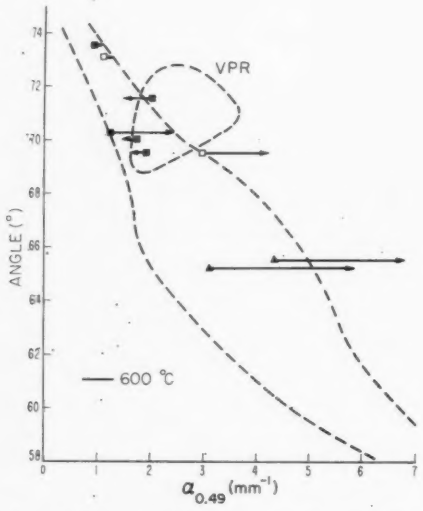

FIGURE 9. *The magnitude and direction of change of $\alpha_{0.49}$ due to heating at 600 °C for 24 hr as a function of initial coordinates.*

☒—very pink ruby, □—ruby, ▲—dark green, ■—pale green.

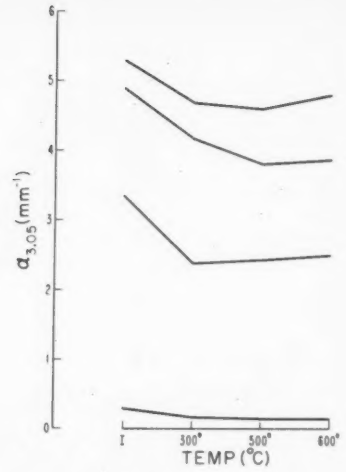

FIGURE 10. *Effect of heat treatment on the infrared pink correlated structure as represented by $\alpha_{3.05}$ for various initial values.*

The upper three traces are for very pink specimens, while the lowest trace is for a green ruby [1].

leveling of the spectral profile. Bleaching does not appear to be spontaniously reversible. Induced visible changes have remained stable at room temperatures for over two years.

The response of the pink associated region is more complex than already shown. Typical kinetics of the reaction are shown in figure 8 for treatments at 300 and 500 °C. Whereas the red color is seen to increase with firing times at 300 °C, 500 °C treatment enhanced the red color after short treatment but bleached it away on longer exposures. At the same time opacity increased slightly with short exposure but diminished on long exposure.

The relationship of the shift in the absorption edge as a result of treatment at 600 °C to the initial value of apparent optic axial angle is shown in figure 9. The two outlined regions denote the general association previously found [1] for untreated samples between the height of the absorption edge, here measured by $\alpha_{0.49}$, and apparent optic axial angle. VPR designates the domain of very pink ruby specimens. The other region represents the general relationship for all specimens other than very pink ruby. The direction of change, as shown by the arrows, and the magnitude of change in $\alpha_{0.49}$, as shown by the length of the arrows, due to treatment are dependent upon the initial coordinates. Those specimens which originated within the VPR domain diminished in value of $\alpha_{0.49}$. All others increased in value.

b. 1 to 15μ

The effect of treatment on the 3 to 3.5 μ pink correlated infrared region is shown in figure 10. Variations are shown for three very pink ruby specimens of different initial values of $\alpha_{3.05}$, and for comparison the results are included for a ruby

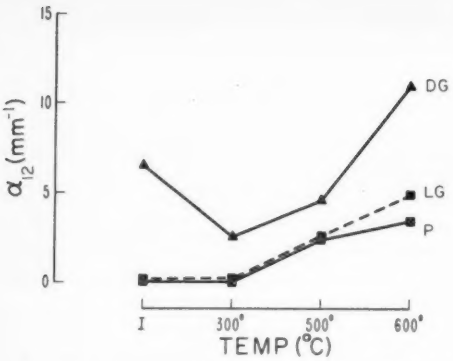

FIGURE 11. *Change in α_{12} with heat treatment (No. 2 thermal schedule), for spectral types.*

Very pink ruby, light green, and dark green.

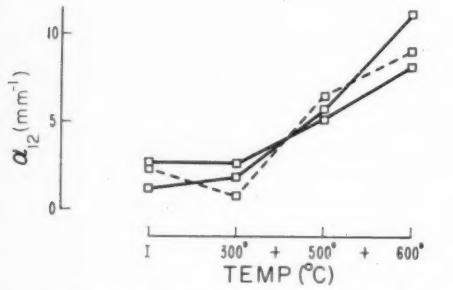

FIGURE 12. *Effect of heat treatment on the 12 μ band of several ruby specimens (No. 4 procedure).*

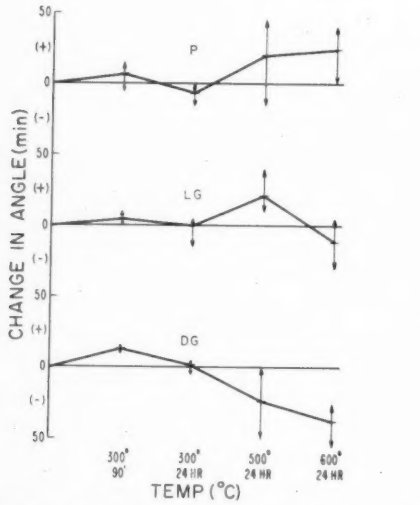

FIGURE 13. *Behavior of apparent optic angle with heat schedule for the three spectral types: pink ruby, light green, and dark green.*

specimen with small initial $\alpha_{3.05}$ (green ruby). Each crystal was subjected to sucessive temperatures of 300, 500, and 600 °C for 24 hr at each temperature (procedure 4). Although decreased by these treatments, the 3 to 3.5 μ absorption does not disappear. This is in contrast to the response of the visible pink associated region of 0.47 to 0.6 μ.

No noticeable increase in absorption was found in the 3 to 3.5 μ region in the light green and dark green types.

Changes in the 12 μ area are given in figures 11 and 12. In general heat treatment causes an increased absorption. Some specimens, as these examples show, decrease in absorption after low temperature heating. Such behavior is similar to that of the visible pink associated absorption; however, a consistent correlation of this effect with the color was not found.

No overall trends were found for the remaining bands of this region, although the thermal behavior of the 13.3 and 14.5 μ bands generally followed that of the 12.5 μ band, just as was the case for untreated specimens.

2.2. Apparent Optic Axial Angle

The apparent optic axial angle changes by fractions of a degree with these low temperature treatments and in a manner distinctive with each spectral type.

The manner in which the apparent optic axial angle varies with the severity of thermal treatment as a function of end type can be seen in figure 13. These data were taken from 21 selected crystal sheets appropriately sectioned and distributed for thermal procedures 1 through 3. Of these crystals eight were very pink ruby, seven were dark green, and six were light green. The complete spread in the data is shown for each temperature-time and average values are joined by the line segments.

It is seen (fig. 13) that the low-temperature (300 °C) behavior is essentially the same for all three types in that the angle is increased to a maximum with short exposure but then diminished by longer exposure. On the average light green has the smallest increase in angle, while dark green has the largest when subjected to 300 °C. However, the high temperatures of 500 and 600 °C cause changes in angle characteristic of each type. Pink ruby and dark green experience changes in angle opposite in sign. The changes in light green show some characteristics of each of the other two.

3. Conclusions

The differentiation of muscovite sheet according to the three end-types of very pink ruby, light green, and dark green appears to be substantiated by their response to thermal treatment.

The changes caused by these relatively low-temperature treatments raise a number of questions about the structure of the material. Particular attention is merited by the effects on the visible and the infrared pink associated absorption regions of 0.47 to 0.6 μ and

3 to 3.5 μ. The 3 to 3.5 μ absorption was only found in ruby specimens along with a direct association with the 0.47 to 0.6 μ absorption [1]. But thermal treatment can both enhance and bleach out the visible absorption while the infrared absorption is relatively little affected. Too, the visible absorption is a weak structure on the edge of a deep absorption edge. These factors point to a defect structure as being responsible for the 0.47 to 0.6 μ absorption, which defect structure is the result of a particular crystal molecular arrangement evidencing the 3 to 3.5 μ absorption.

The author thanks John C. Schleter of Metrology Division for the spectrograms of the 0.3 to 1 μ region.

4. References

[1] S. Ruthberg, Mary W. Barnes, and R. H. Noyce, J. Res. NBS **67A** (Phys. and Chem.), No. 4, 309–324 (July–Aug. 1963).
[2] S. Ruthberg, J. Res. NBS **65C** (Eng. and Instr.), No. 2, 125 (Apr.–June 1961).
[3] American Society for Testing Material D 351–53T, Natural Muscovite Mica Based Upon Visual Quality."

(Paper 67A5–244)

JOURNAL OF RESEARCH of the National Bureau of Standards—A. Physics and Chemistry
Vol. 67A, No. 6, November–December 1963

Absolute Configuration and Chemical Topology

Stephen J. Tauber

(July 15, 1963)

The stereochemistry of catenanes, knotted molecules, and Borromean rings is discussed. An augmentation of the Cahn-Ingold-Prelog convention for designating absolute configuration is proposed. A convention is proposed for designating the absolute configuration of knotted molecules. A suggestion is made concerning the citing of the absolute configuration of molecularly dissymmetric diastereomers.

Proposals of rules for designating absolute configuration have been put forth by Cahn, Ingold, and Prelog [1] and by Terentiev and Potapov.[2] The rules of the latter workers are deliberately linked to nomenclature. Those of the former workers rely entirely on structure and have found wide acceptance among organic chemists. In their closely reasoned paper Cahn, Ingold, and Prelog properly claim to have covered by their rules all known types of dissymmetry deriving from tetracovalent and tricovalent atoms.

Work aiming toward the establishment of a major system for handling chemical information requires the ability precisely to designate chemical structures without recourse to structural formulas. A number of notation systems have been devised for representing chemical structures by linear arrays of symbols,[3] although none of the systems has yet been perfected even for organic compounds.[4] Since an adequate information handling system must accommodate not only all known structural types but also those structural types which have to date been merely speculated on, an examination of more esoteric stereochemistry was undertaken. I now wish to propose an augmentation of the Cahn-Ingold-Prelog (C-I-P) rules and the addition of a new (specialized) set of rules to cover a wider range of molecularly dissymmetric structural types.

The molecularly dissymmetric structures for which further rules are necessary are of two types: (1) substituted catenanes,[5] which are stereochemically related to substituted allenes and spiro compounds, and (2) knots,[6, 7] compounds whose dissymmetry is due entirely to topology, independent of substitution.[6, 7] The C-I-P convention is inapplicable to knots and before being applied to catenanes requires a further convention for defining the "near groups".

Catenanes

Because of free rotation of each ring of a catenane about its own axis, compounds such as [34.34]-catenan-1,18,1′,18′-tetraone 1,1′-dioxime, I, of which two enantiomeric configurations are possible, could exist in any number of conformations related to the angle of rotation about the axes of the rings. Some of the conformations of one of the enantiomers are shown in figure 1. If the two rings are not identical, as in [36.34]-catenan-1,19,1′,18′-tetraone 1,1′-dioxime, II, then some of the conformations of figure 1 correspond to two distinct conformations; e.g., conformation Ia corresponds to conformations IIa and IIb (fig. 2). The choice of an "axis of asymmetry" under section 5.1 of Cahn et al.[1] (such that the dissymmetry element contain the maximum number of atoms, with the widest possible distribution, and most preferred by the sequence rule) would require basing the designation of the configuration of [34.34]-catenan-1,18,1′,18′-tetraone 1,1′-dioxime on conformation Ic, Id, or Ie. Application to these three conformations of the C-I-P sequence rules does *not* lead to assignment of the same absolute configuration (cf. fig. 3).

For a compound such as [36.36]-catenan-1,10,-19,1′,10′,19′-hexaone 10,10′-dioxime, III, an attempt to choose an axis of dissymmetry under section 5.1 of Cahn et al. would be thwarted because the carbonyl oxygen atoms would have to lie on the axis, and the molecule would then have a plane of dissymmetry instead of an axis of dissymmetry (cf. fig. 4). In this case it would be necessary to

[1] R. S. Cahn, C. K. Ingold, and V. Prelog, Experientia **12,** 81 (1956).
[2] A. P. Terentiev and V. M. Potapov, Tetrahedron **1,** 119 (1957).
[3] Cf., e.g.
(a) G. M. Dyson, A new notation and enumeration system for organic compounds, 2d ed., Longmans, Green and Co., Ltd., London (1949)—most recent edition published by International Union of Pure and Applied Chemistry Commission on Codification, Ciphering and Punched Card Techniques as Rules for I.U.P.A.C. notation for organic compounds, Longmans, Green and Co., Ltd., London (1961);
(b) M. Gordon, C. E. Kendall, and W. H. T. Davison, Chemical ciphering—a universal code as an aid to chemical systematics, Royal Institute of Chemistry of Great Britain and Ireland, London (1948);
(c) W. J. Wiswesser, A chemical line-formula notation, Thomas Y. Crowell Co., New York (1954); and
(d) H. W. Hayward, A new sequential enumeration and line formula notation system for organic compounds, Patent Office Research and Development Reports, No. 21, Patent Office, U.S. Department of Commerce, Washington (1961).
[4] Contrary to the claims by partisans of one of the notation systems.
[5] E. Wasserman, J. Am. Chem. Soc. **82,** 4433 (1960).
[6] W. J. Ambs, Mendel Bull. **17,** Spring, 26 (1953).
[7] H. L. Frisch and E. Wasserman, J. Am. Chem. Soc. **83,** 3789 (1961)

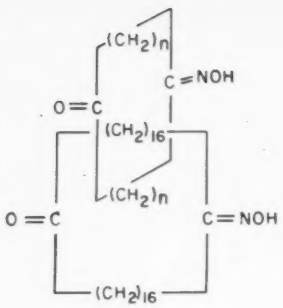

I n = 16
II n = 17

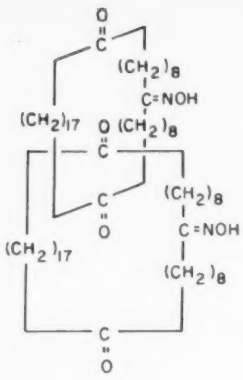

III

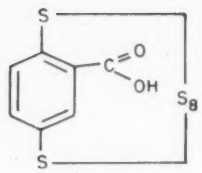

IV

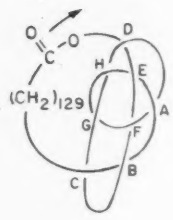

V

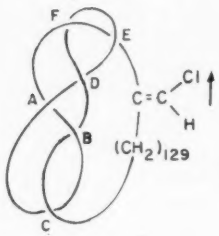

VI

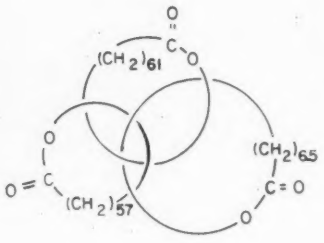

VII

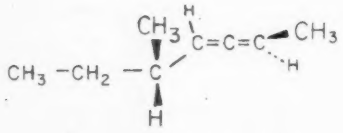

VIII

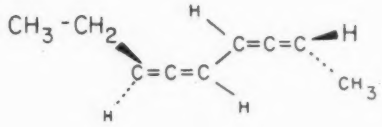

IX

choose not only the appropriate side of the plane of dissymmetry from which to view the molecule but, because the three atoms specified by section 5.3 of Cahn et al.[1] (the oxime C, N, and O—cf., below) lie in a plane perpendicular to the plane of dissymmetry, also the appropriate quadrant on that side. This ought to be the quadrant *nearer* the atom *in* the plane of dissymmetry most senior by the sequence rule. However even for a specific conformation, e.g., IIIb, the designation of absolute configuration would differ according to whether the plane of dissymmetry be chosen to contain ring A or ring B (cf. fig. 5). Note that in [36.36]-catenan-1,10,19,1′,10′,19′-hexaone 10,10′-dioxime the methylene carbon atoms, and the corresponding hydrogen atoms, are pairwise identical (positions 9 and 11, 8 and 12, 2′ and 18′, etc.) under the sequence rule. It is therefore necessary to base the designation of configuration on atoms not bound directly to the plane of dissymmetry. A similar situation obtains when the considerations of section 5.3 (planar asymmetry) of Cahn et al. are applied to a compound having a polysulfide bridge instead of a polymethylene ether bridge lying in the plane of dissymmetry. Thus the atoms determining the configuration of 2,3,4,5,6,7,8,9,10,11-decathiabicyclo-[10.2.2]hexadeca-12,14,15-triene-13-carboxylic acid,[8] IV, are the 13, 14 and carboxyl carbon atoms.

[8] Cf. A.M. Patterson, L. T. Capell, and D. F. Walker, The ring index, 2d ed., American Chemical Society, Washington (1960), RRI 1967.

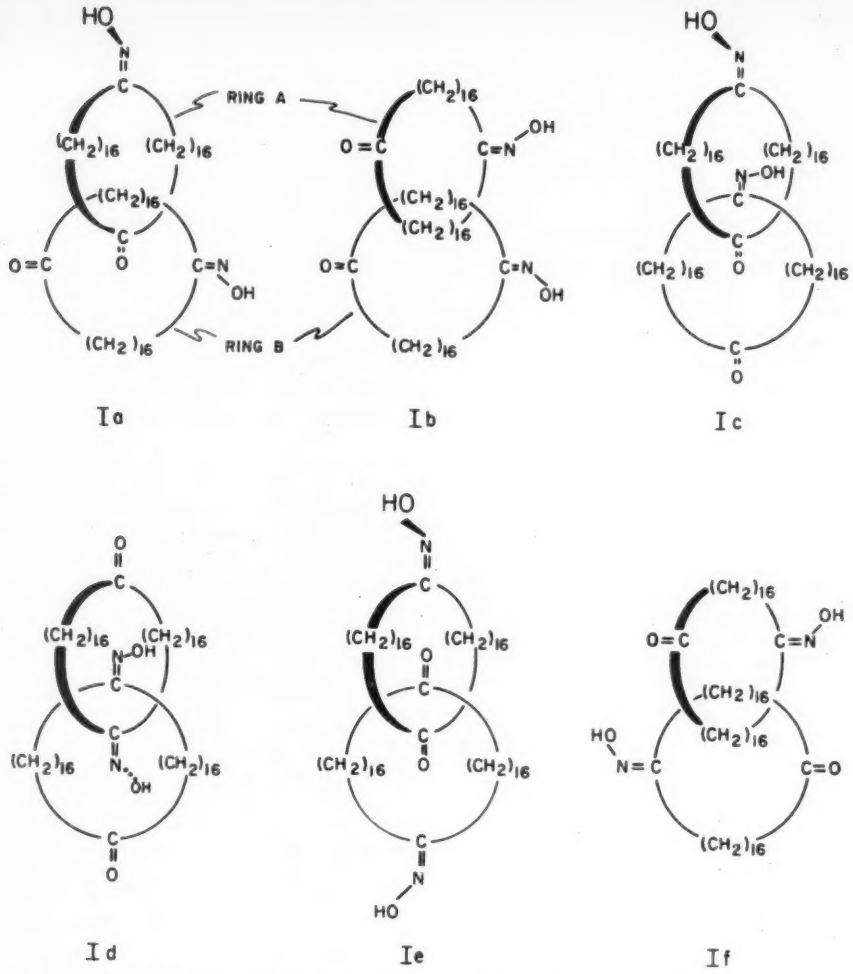

FIGURE 1. *[34.34]-Catenan-1,18,1',18'-tetraone 1,1'-dioxime in various conformations differing in the angles of rotation about the axes of the individual rings.*

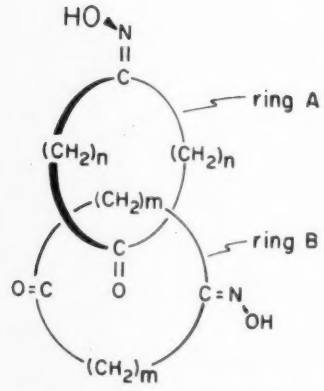

II a n = 16, m = 17

II b n = 17, m = 16

FIGURE 2. *Two conformations of [36.34]-catenan-1,19,1',18'-tetraone 1,1'-dioxime.*

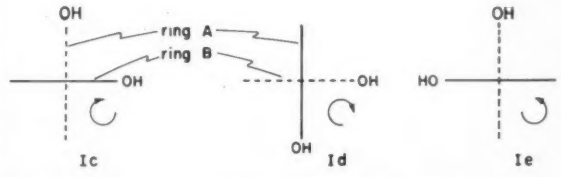

FIGURE 3. *Ends views of [34.34]-catenan-1,18,1',18'-tetraone 1,1'-dioxime in the conformations preferred by the Cahn-Ingold-Prelog convention.*

The curved arrows indicate the directions defined by the conversion rule.

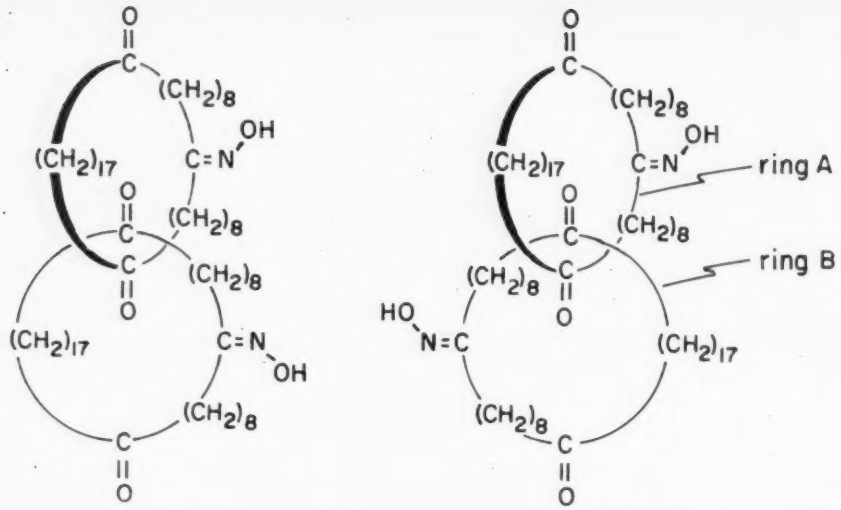

III a III b

FIGURE 4. *[36.36]-Catenan-1,10,19,1',10',19'-hexaone 10,10'-dioxime in the conformations which place the preferred atoms* [1] *on a potential axis of dissymmetry, here occupied by the four carbonyl groups.*

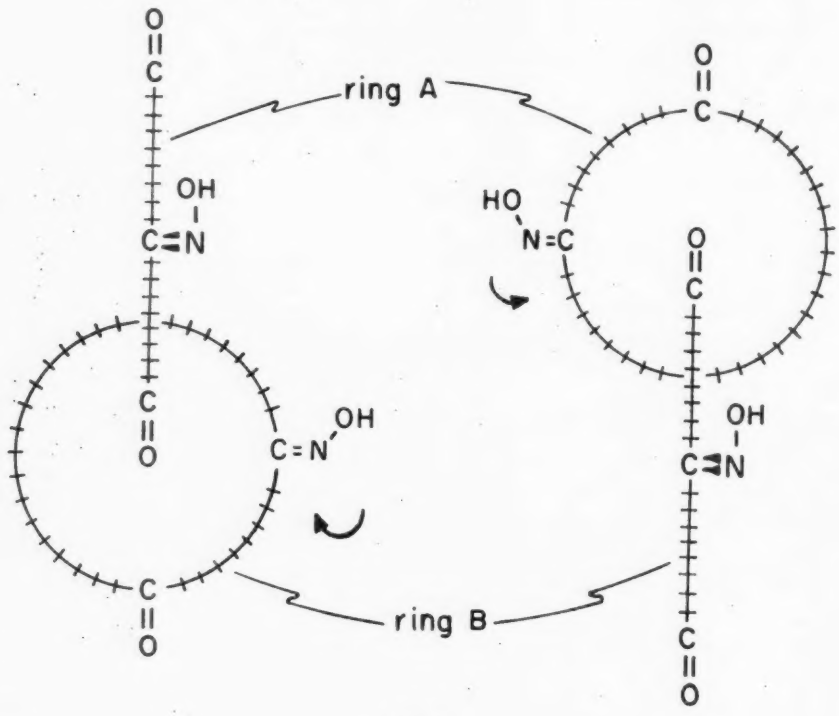

III b

FIGURE 5. *Two views of a single conformation of [36.36]-catenan-1,10,19,1',10',19'-hexaone 10,10'-dioxime.*

The curved arrows indicate the directions defined by the conversion rule. [1]

I therefore propose the following rule to govern the choice of the element of dissymmetry:

Dissymmetry Element Rule. Select an element of dissymmetry by applying in turn the following hierarchy of criteria:

(1) *The element of dissymmetry be of minimum dimensionality;*

(2) It contain a maximum number of atoms;

(3) The atoms have maximum distribution;

(4) The element of dissymmetry contain the atom or set of atoms most senior by the sequence rule; and

(5) *The atoms on the element of dissymmetry most senior by the sequence rule have the maximum separation.*

The philosophy of first difference of the C-I-P convention is maintained; the substantive changes proposed appear in italics.

Application of subrule (5) resolves the ambiguity with respect to compound I, causing conformation Ie to be the proper one from which to determine the absolute configuration and thus causing the enantiomer represented to be the (*S*)-form. Application of subrules (1) and (5) to compound III requires conformation IIIc (fig. 6) to be the basis for determination of the absolute configuration, and the enantiomer shown of compound III is the (*S*)-form.

Knots

It was pointed out at least as early as 1953, by Ambs,[6] that a simple cyclic compound could exist as an enantiomeric pair if it were in the form of a trefoil knot. The same observation may be seen to apply to most other knots. Since such molecular dissymmetry may exist even in molecules all of whose carbon atoms are identical—indeed all of whose atoms are identical—the C-I-P convention cannot be made to apply.

The designation of the absolute configuration of a knotted molecule must necessarily depend on the topology of the corresponding knot. A serviceable convention can be based on the normalized knot projections.[9] For each knot there exists a planar projection [10] having a minimum number of intersections. Normalized projections of the trefoil knot and of the figure-eight knot are shown in figure 7. That which projects as an intersection in the planar projection shall be called a *double point* in the knot. At each double point one segment of the knot passes over another segment of the knot. If a direction is ascribed to the knot, then at each double point two situations are possible (cf. fig. 8). The projection of the upper segment must be rotated either clockwise or counterclockwise through an angle of less than 180° to bring it into coincidence with the projection of the lower segment. A *characteristic* ϵ shall be ascribed to each double point; $\epsilon=+1$ if the pro-

[9] K. Reidemeister, Knotentheorie, Julius Springer, Berlin (1932); republ. Chelsea Publishing Co., New York (1948), p. 18 ff.

[10] Actually a set of equivalent projections.

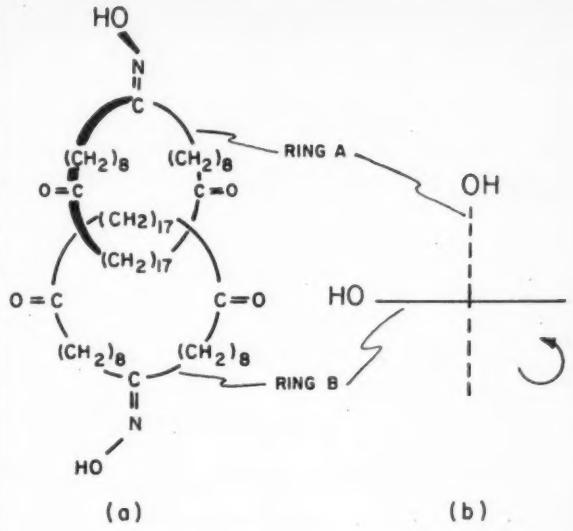

III c

FIGURE 6. *[36.36]-Catenan-1,10,19,1′,10′,19′-hexaone 10,10′-dioxime in the preferred conformation according to the presently proposed convention: (a) perspective and (b) end view.* This conformation has an axis of dissymmetry.

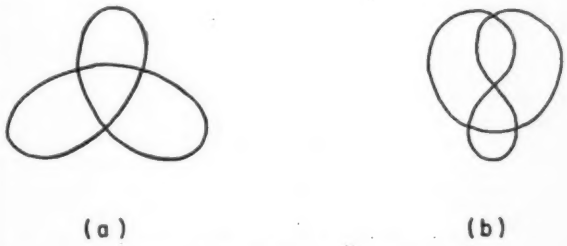

FIGURE 7. *Normalized projections of (a) trefoil and (b) figure-eight knots.*

FIGURE 8. *The two possible relative orientations of directed knot segments at a double point.*

jection of the upper segment must be rotated clockwise to bring it into coincidence with the projection of the lower line segment, and $\epsilon = -1$ if it must be rotated counterclockwise. Examination of figure 8 reveals that the characteristic of a double point is invariant: If the knot is turned over (viewed from the other side) or if the direction ascribed to the knot is reversed, then the value of the characteristic is still *unchanged*.

It is now possible to form the sum $\Sigma\epsilon$ over all double points of the knot. I propose that the absolute configuration of a knot be designated

(R) if $\Sigma\epsilon > 0$

and

(S) if $\Sigma\epsilon < 0$.

By this convention the knots in figure 9 designated as (a), (c), (e), (g), (h), and (i) are in the (R)-form

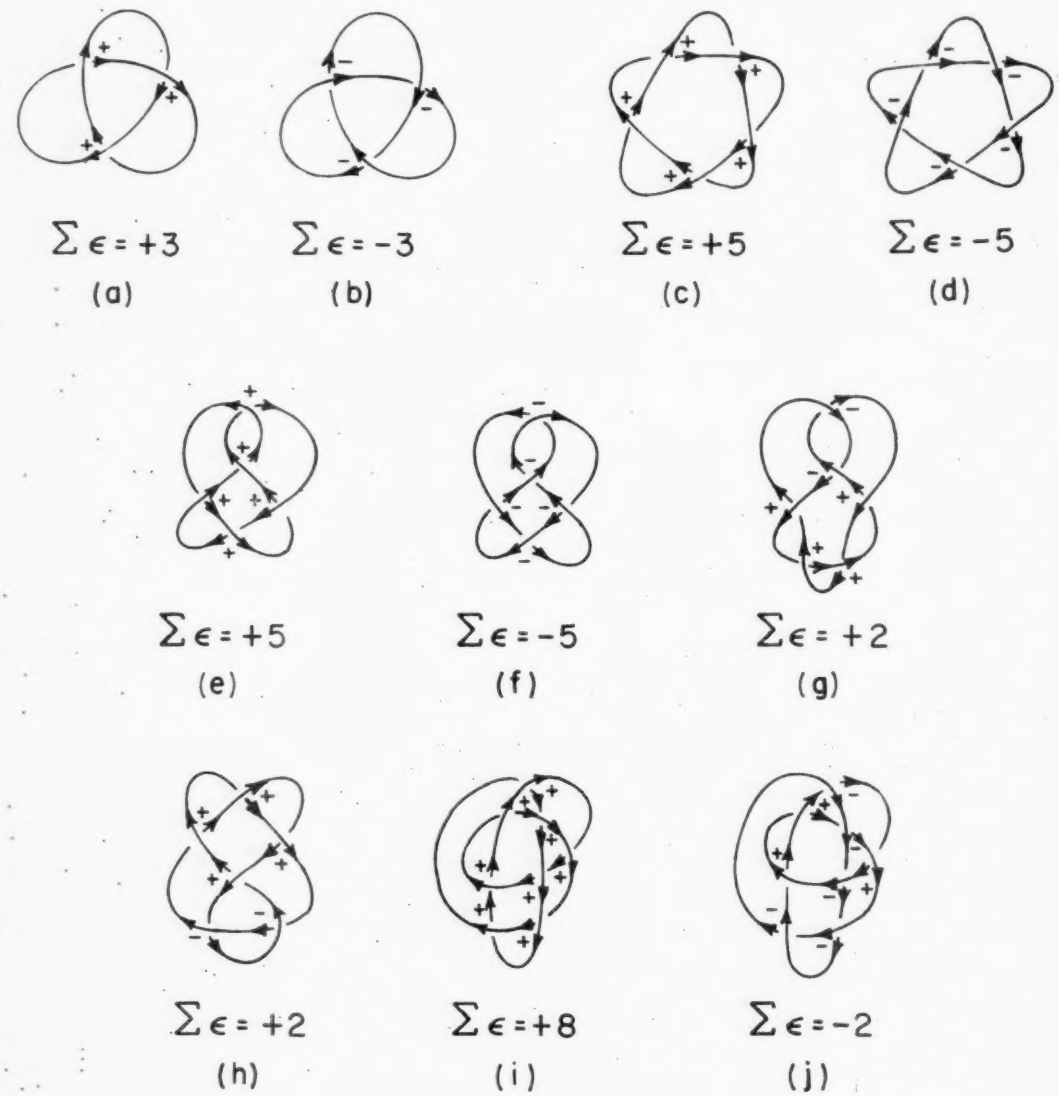

FIGURE 9. *Examples of knots which differ from their mirror images.*

(A ± sign indicates each double point with a value of the characteristic $\epsilon = \pm 1$. The total of the values of the characteristics is indicated under each knot. The arrows superimposed on the knots are for ease of determining the values of the characteristics and are *not* an attribute of the knots.)

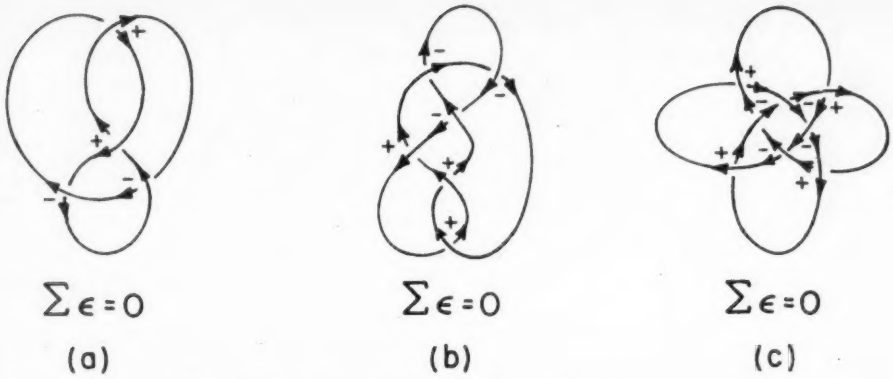

FIGURE 10. *Examples of knots which are identical with their mirror images.*

and knots (b), (d), (f), and (j) are in the (*S*)-form. Knots (a) and (b), (c) and (d), and (e) and (f) are enantiomeric pairs.

For certain knots $\Sigma\epsilon=0$ (cf. fig. 10). This is exactly as it should be, for precisely these knots are identical with their mirror images (cf. fig. 11). Note however that although knot (b) of figure 10 is not per se optically active, if the knot has an intrinsic direction then it exists as an enantiomeric pair (cf. fig. 11B). For this situation a further convention is necessary for assigning an absolute configuration. I propose the following *directed knot convention:*

(1) Assign the positive direction to the knotted molecule such that one proceeds *to* the atom most senior by the sequence rule *from* its more senior neighbor.

(2) Determine the largest possible number of successive double points along the knot in the positive direction which have $\epsilon=+1$. Define the molecule as

(*R*) if an equal number of successive double points follow which have $\epsilon=-1$, and

(*S*) if a smaller number of successive double points follow which have $\epsilon=-1$.

The two atoms under subrule (1) are to be members of the cyclic portion of the molecule when possible, otherwise they are to be the atoms nearest the cyclic portion which can define the direction. Thus the lactone V has its positive direction defined by proceeding from the carbonyl carbon atom to the oxy oxygen atom, and consequently, under subrule (2), it is the (*S*) isomer because after double points A, B, C, and D (with $\epsilon=+1$) only double points E and F follow with $\epsilon=-1$ before double point B is again reached. The positive direction of the chloroolefin VI is defined by proceeding from the terminal hydrogen atom to the chlorine atom, and the molecule shown is the (*R*) isomer since double points A, B, C, and A are followed by D, E, F, and D.

It is worth noting that a set of Borromean rings is identical with its mirror image even if each ring has a direction attributed to it and each ring is different from the others, e.g., in the trilactone VII, 2,2′,2″-triketo-1,1′,1″-trioxa[67.63.59]ballantane. The identity of mirror images is more readily apparent when a set of Borromean rings is represented not as a "well-known brewer's symbol" [11] (fig. 12) but in the alternative representation of figure 13.

Molecularly Dissymmetric Diastereomers

The designation of the absolute configuration of a compound is fixed entirely by the stereochemical structure of the compound. However, for purposes of *citing* the absolute configuration it is generally necessary to couple the symbol (*R*) or (*S*) with the name of the compound and, in the case of compounds having several asymmetric centers, with the designation of the center of asymmetry. Thus we use such names as (2*R*:3*S*)-3-amino-2-butanol or (2*S*:3*R*)-3-hydroxy-2-butylamine. In the case of diastereomers involving molecular dissymmetry and a center of asymmetry, as in (*R*:5*S*)-5-methyl-2,3-heptadiene, VIII, it is readily apparent from the absence of a positional designation which symbol refers to the sense of the molecular dissymmetry. Nor can confusion exist in naming compounds having two similar axes or planes of dissymmetry, which would take the prefix (*R*:*R*)-, (*S*:*S*)-, or *meso*- (or (*R*:*S*)-) to their names.

Possible confusion occurs when the absolute configuration of a molecule having dissimilar axes or planes of dissymmetry is cited. For names of such compounds I urge the following practice:

(1) For compounds named fragment by fragment cite the sense of dissymmetry together with the fragment; e.g., (*R*)-4-methyl-4-((*S*)-4-ketocyclohexyl)cyclohexanone dioxime and (*R*)-4-(2-(*R*:2*S*)-3,4-hexadienyl)cyclohexanone oxime.

(2) For compounds named as a unit cite the senses of dissymmetry in the same order as that in which the parts of the molecule are cited; thus (*S*:*R*)-2,3,

[11] E. Wasserman, Sci. Am. **207,** No. 5, 94 (Nov. 1962).

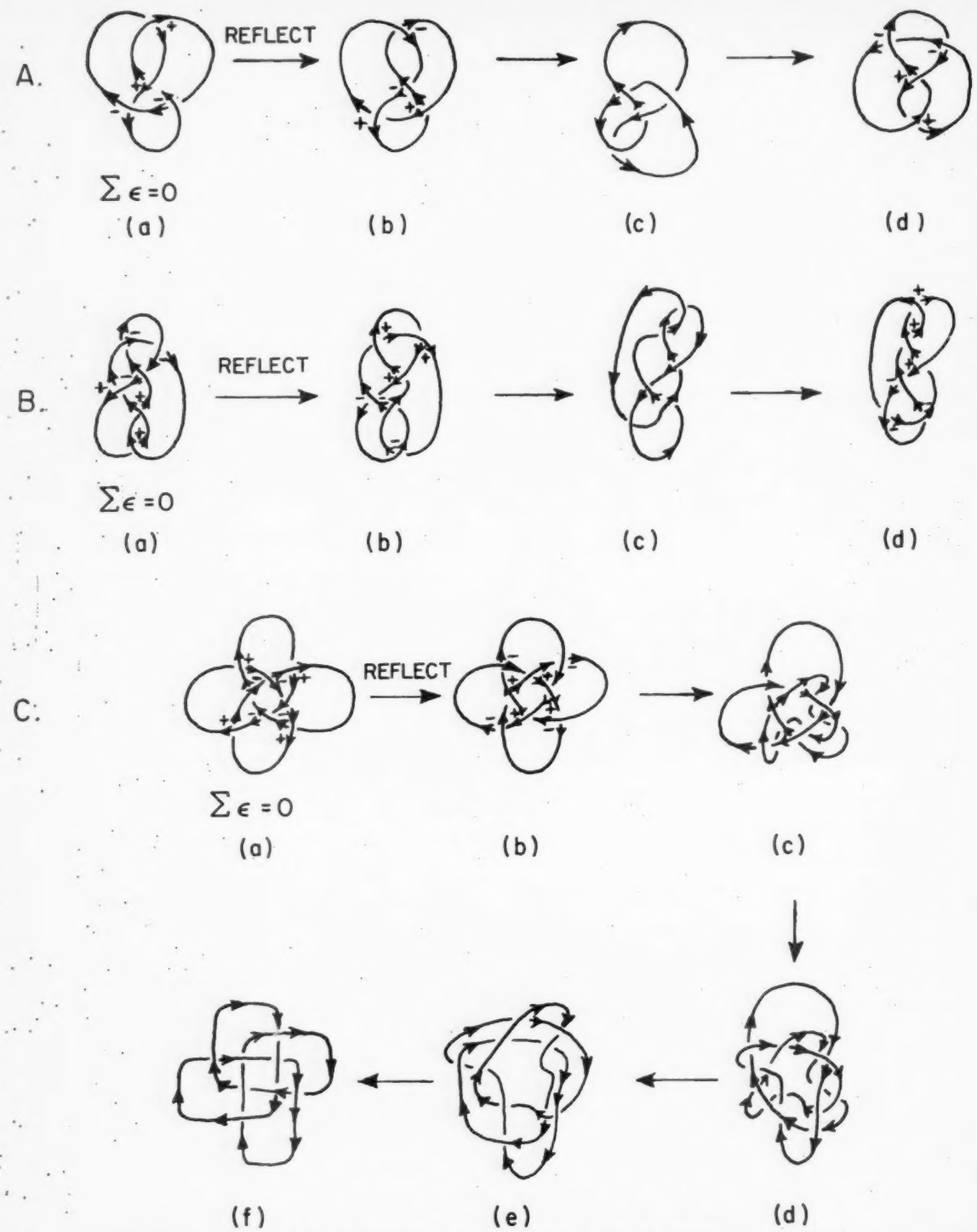

FIGURE 11. *Successive distortions of the mirror images of knots (b) into the original knots (a).**

The knots of figures 11A and 11C are identical with their mirror images regardless of direction attributed to the knots. The knot of figure 11B is identical with its mirror image if and only if no direction is attributed to it.

*A: Rotate (d) 180° about a horizontal axis in the plane of the paper; B: rotate (d) 180° in the plane of the paper; C: rotate (f) 45° in the plane of the paper and smooth the curve.

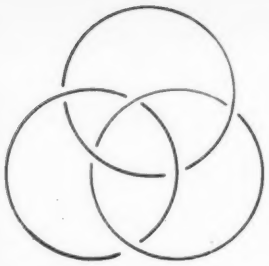

FIGURE 12. *Borromean rings.*

5,6-nonatetraene, but (*R*:*S*)-α-ethyl-ω-methyldiallenyl, for IX. An alternative procedure is to cite the atoms defining the axes or planes of dissymmetry, e.g. (2,4*S*:5,7*R*)-2,3,5,6-nonatetraene, but in the naming of very complex structures this can become excessively cumbersome.

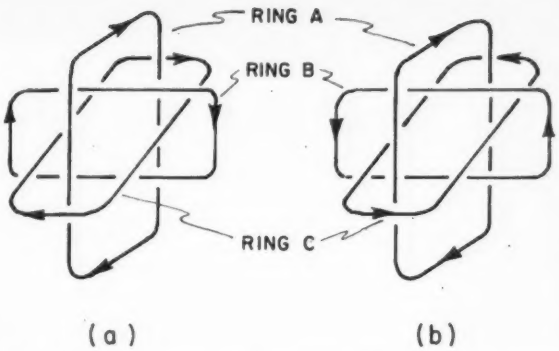

FIGURE 13. *Borromean rings, showing the identity of mirror images.*

Reflection of (a) in a plane parallel to ring A yields (b), which when rotated 180° about the axis of ring A again yields (a).

Paper 67A6–245).

JOURNAL OF RESEARCH of the National Bureau of Standards—A. Physics and Chemistry
Vol. 67A, No. 6, November–December 1963

Reversibility of Polyester Adsorption on Glass [1,2]

Robert R. Stromberg and Warren H. Grant

(July 18, 1963)

The adsorption of poly(ethylene *o*-phthalate) from chloroform solution on glass powder and aluminum oxide was studied. The adsorption of a number of fractions, varying in number average molecular weight from 970 to 6250 showed a decrease in the moles of polymer adsorbed with increase in molecular weight. The results are interpreted to indicate that this polymer molecule lies in a relatively flattened conformation on the glass surface. More polymer was adsorbed on glass powder at 50 °C than at 0 °C. Adsorption on glass powder that had been outgassed to remove adsorbed water was less than on untreated glass. Initial adsorption at one temperature followed by exposure at the other temperature resulted in complete reversibility of sorption on the untreated glass. Decreasing the temperature from 50 to 0 °C resulted in desorption from the outgassed glass, but increasing the temperature did not result in additional adsorption. These differences are ascribed in part to adsorption across an adsorbed water layer on the untreated glass. An explanation for the "one-direction reversibility" observed for the outgassed glass is presented.

1. Introduction

Most studies of polymer adsorption have been concerned with relatively high molecular weight materials. Their behavior is, of course, very different from that of small molecules. Molecules of intermediate molecular weight are also of interest, but have not been extensively investigated. In previous work in this area, the adsorption of a series of relatively low molecular weight poly(ethylene glycols) on a porous carbon [1][3] and of several polyesters with molecular weights of the order of 4000 on glass, silica, and alumina [2] has been studied. The adsorption isotherms for the polyesters were not nearly as steep at low concentrations as were those for higher molecular weight polymers; a plateau was not attained until relatively high solution concentrations were reached.

The adsorption-desorption behavior of polymer molecules has been of interest, in part, because of the information implied regarding the conformation of the polymer molecule and interactions with the surface. Polymer molecules have been reported to adsorb relatively rapidly [2, 3, 4, 5] on nonporous surfaces, although some recent measurements indicate that this is not necessarily so under all conditions [4, 6]. A recent theoretical treatment [7, 8] has concluded that times to equilibrium are long, caused in part by rearrangements of the molecule at the surface. The times required for desorption, using the same solvent, can be of a different order of magnitude from those required for adsorption. For some systems no desorption occurs within practical units of time (see, e.g., ref. [2]), while for others some desorption does occur [3, 5, 6]. In one study, Soxhlet extraction removed only negligible amounts of polystyrene that had been adsorbed on carbon black [9]. In systems in which no desorption occurred with the same solvent used for adsorption, it has been shown that it is possible to remove the adsorbed polymer by using a better solvent [2, 3].

The effect of temperature on the amount of polymer adsorbed is, in general, not very large; both increases and decreases as a result of increasing the temperature have been reported. It also has been shown that it is possible to desorb some polymer by means of changes in temperature. Poly(neopentyl succinate) is for all practical purposes "irreversibly" adsorbed when glass is used as the substrate and the same solvent used for desorption [2]. Adsorbing the polyester at one temperature and changing the temperature demonstrated that polymer could be desorbed by a temperature increase, but that decreasing the temperature did not readsorb the polymer [5]. Similar measurements were made with poly(methyl methacrylate) and poly(vinyl acetate) adsorbed on iron from several solvents [10]. The behavior of these systems was similar. The "reversibility" of the adsorption was dependent upon the direction from which the temperature change was effected.

It has not been clear whether the polymer displaces a molecule such as water from the surface of a solid before it is adsorbed itself, is adsorbed on top of the water molecule, or perhaps is prevented from being adsorbed by the adsorbed water. In the case of polystyrene adsorbed on carbon, it was found that predrying tends to decrease the amount of polymer adsorbed [9, 11].

This paper reports the results of a study of the molecular weight dependence, the reversibility of adsorption as a function of temperature, and the effect of adsorbed water on the adsorption of poly(ethylene *o*-phthalate) on glass surfaces.

[1] Supported in part by funds provided by the Bureau of Naval Weapons.
[2] Presented in part at American Chemical Society Meeting, Chicago, Ill., Sept. 1961.
[3] Figures in brackets indicate the literature references at the end of this paper.

2. Experimental Procedure

2.1 Materials

The polymer used in this study was the linear saturated polyester, poly(ethylene *o*-phthalate). It was prepared by refluxing ethylene glycol and phthalic anhydride in a molar ratio of 1 : 1 for various times to obtain the desired average molecular weights. Four such preparations were made,[4] covering a range of molecular weights. After purification, each of these preparations was individually fractionated from 0.5 percent solutions of polymer in acetone with water as the nonsolvent.

The number average molecular wieghts ($\overline{M}_n$) of the fractions were obtained by end-group analysis. Preparation 1 was fractionated into 10 fractions, from which a fraction with $\overline{M}_n=970$ was selected. Preparation 3 was fractionated into 9 fractions, from which those with $\overline{M}_n=2300$, 3100, and 4300 were selected. Portion 4 was fractionated into 8 fractions, two of which with $\overline{M}_n=5450$ and 6250 were used. After fractionation the polymers were precipitated from chloroform solution with ether and dried in a vacuum oven at 80 °C for approximately 18 hr.

X-ray analysis did not show any evidence of crystallinity. The fraction with the molecular weight of 6250 was used to study the effect of drying and of temperature changes.

Chloroform was the solvent for all adsorption measurements. It was distilled from calcium chloride prior to use. For those experiments in which moisture was to be rigorously excluded, the chloroform was vacuum distilled after drying over calcium hydride.

The principal adsorbent was Pyrex glass power, 325 mesh. The entire quantity of glass powder was mixed to obtain a homogeneous mixture, evacuated for several days in individual tubes, and sealed under vacuum for storage. In this manner the surface of the glass was protected from attack by the atmosphere during storage. Each tube contained approximately enough glass powder to obtain a complete adsorption isotherm. The surface area [5] of the glass as determined by BET nitrogen adsorption was 1.8 m^2/g. The other adsorbent used was aluminum oxide [6] with a surface area (see note 5) of 55 m^2/g.

2.2 Procedure

The amount of polymer adsorbed was determined by measuring the change in the concentration of the polymer solution, using the carbonyl absorption band at approximately 5.8 μ. Measurements were made in a double-beam infrared instrument in a cell approximately 0.4 mm in length.

The experiments in which rigorous drying of the material was not a factor were carried out by pipetting 20 ml of polymer solution that had been maintained at a constant temperature into a tube containing 10 g of glass powder or 0.3 g of Al_2O_3 that had also been maintained at the same temperature. After filling, the tubes were maintained at the same temperature and sealed with a gas torch. The sealed tube was then rotated end over end in a constant temperature bath for a length of time that depended on the specific experiment but was at least 20 hr in all cases. The solution and glass powder, therefore, were at the same temperature both before and during the initial portion of an adsorption experiment. After the elapsed adsorption time, the rotation was stopped, the glass allowed to settle at the same constant temperature, and in the experiments in which drying was not involved, the tubes were opened and a portion of the solution removed for analysis. If the adsorption mixture was to be reexamined or retreated, 1 ml of the solution was removed for analysis and the tube resealed. The small amount of glass powder that remained suspended in the solutions to be analyzed was removed by centrifugation.

For those experiments designed to study the effect of temperature change on the amount of polymer adsorbed, tubes were filled as described above and rotated at a constant temperature of 50 ± 0.5 °C and 0 ± 0.5 °C for approximately 20 hr. The powder was then allowed to settle at constant temperature, the tube opened, 1 ml of solution removed for analysis, and the tube resealed. The adsorption tubes were then placed in a bath at the other temperature and rotated for approximately 44 hr. The glass was again allowed to settle at the constant temperature, the tube reopened and 1 ml of solution again removed for analysis. In some cases the tubes were resealed and rotated at the original temperature for an additional 44 hr, and the solution analyzed again after this time.

Some of the adsorption runs were carried out on glass powder that had been pretreated to remove water and other gases from the surface. The powder was outgassed under a vacuum of about 10^{-5} mm of Hg at a temperature of 250 °C for 48 hr and polymer solution added without exposing either adsorbent or solution to the atmosphere. This was accomplished by connecting, by means of break-off seals, a tube containing polymer solution to each tube containing glass powder. During the time that the adsorbent was outgassed, the tubes containing the polymer solution were evacuated, the solvent distilled from the polymer, dried over calcium hydride and redistilled back into the calibrated polymer tube. In this manner water was removed from the glass, solvent, and polymer. The assembly was removed from the vacuum system and brought to constant temperature (50 or 0 °C) prior to mixing. The adsorption was carried out as described above. In order to remove solution for analyisis without exposure of the glass-solution system to the atmosphere, small calibrated tubes were preattached to each adsorption tube. It was possible, therefore, after one phase of the adsorption experiment, to pour 1 ml of solution into such a tube for analysis, and

[4] Polymer prepared by H. L. Steinberg, National Bureau of Standards.
[5] The surface areas were determined by Dr. C. M. Hunt and Mr. A. W. Woolf, National Bureau of Standards.
[6] Alon C, provided by the Godfrey L. Cabot Corp.

seal it from the system. In this manner the remaining solution was not exposed to the atmosphere prior to rotation at another temperature.

3. Results

The adsorption isotherms at 50 °C of six fractions of poly(ethylene *o*-phthalate) in chloroform solution, ranging in molecular weight from 970 to 6250, are given in figure 1. The largest difference among the curves is between that of the low molecular weight of 970, which represents about 5 repeating units, and that of the molecular weight of 2300. The curves for molecular weights ranging form 2300 to 6250 are grouped relatively close together; there is a definite although small dependence on molecular weight for this range. It is realized, of course, that the surface area determined from nitrogen adsorption is probably not the actual surface area available to the polymer. The molecular weight of the polymer fractions used was not very large, and the actual area available, although probably smaller than that determined by nitrogen adsorption, may not be too different. It is also reasonable to expect that the fraction of surface area available does not change significantly for the range of molecular weights studied.

The adsorption isotherms of poly(ethylene *o*-phthalate) from chloroform solution on the glass powder at 0 and 50 °C and on Al_2O_3 at 50 and 15 °C are shown in figure 2. The adsorbent powders were exposed to air before the adsorption. More polymer is adsorbed as the temperature is increased. When the temperature is changed after adsorption has taken place, as described in the experimental portion, the results shown in figure 3 are obtained. The glass had been exposed to the atmosphere prior to the initial adsorption, and the tubes opened to the atmosphere for sampling prior to being placed in a bath at another temperature. Essentially complete reversibility occurs when the temperature is cycled. When the adsorption is carried out at 50 °C initially and then changed to 0 °C, the isotherm shifts from that of 50 °C, to that of 0 °C. When the temperature is again changed back to 50 °C, the isotherm again shifts back to the original isotherm of 50 °C. The same reversibility occurs when 0 °C is the initial adsorption temperature.

The results of heating and outgassing the glass powder prior to adsorption are shown in figure 4. A decrease in the adsorbance at both 50 and 0 °C was observed as a result of the pretreatment of the glass powder. The effect of the temperature cycling was also altered as a result of the heating and outgassing. Changing the temperature from 50 to 0 °C again resulted in a shift in the isotherm to a lower adsorbance. Changing the temperature back to 50 °C, however, did not result in an increase in the amount adsorbed. When the adsorption was initially carried out at 0 °C and the temperature then changed to 50 °C, the isotherm remained at the same location; no additional polymer was adsorbed to increase the adsorbance to that obtained when the adsorption was initially carried out at 50 °C.

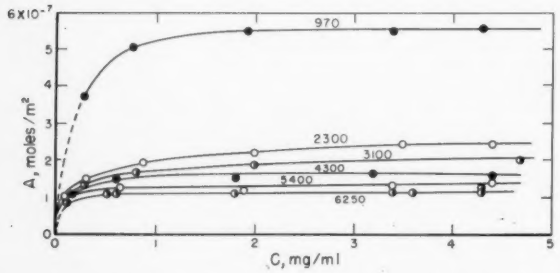

FIGURE 1. *Adsorption isotherms of 6 molecular weight fractions of poly(ethylene o-phthalate) on glass powder.*

The moles adsorbed per m^2 are plotted against the final solution concentration. The molecular weights given are number average; the adsorption temperature was 50 °C, and the solvent chloroform.

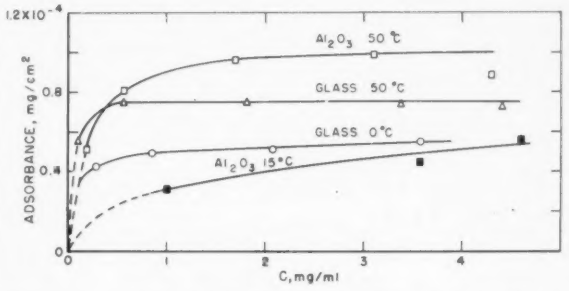

FIGURE 2. *Absorbance of $\overline{M}_n$=6250 fraction at 0 and 50 °C on glass powder, and at 50 and 15 °C on Al_2O_3.*

The powders were exposed to air prior to adsorption.
△ Glass 50 °C
○ Glass 0 °C
□ Al_2O_3 50 °C
■ Al_2O_3 15 °C

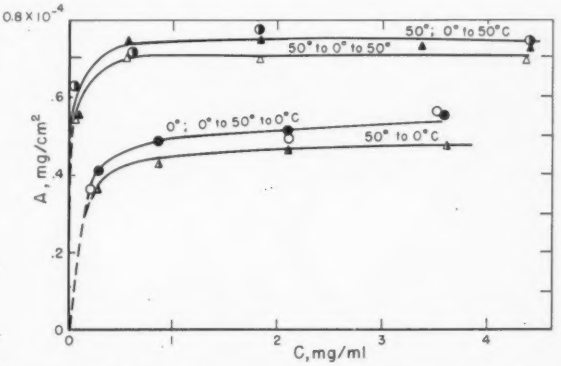

FIGURE 3. *Effect of temperature cycle on adsorption isotherms of $\overline{M}_n$=6250 fraction from chloroform solution on glass powder.*

Glass powder exposed to atmosphere prior to contact with polymer solution.
▲ 50 °C
▲ 50 to 0 °C
△ 50 to 0 to 50 °C
● 0 °C
◑ 0 to 50 °C
○ 0 to 50 to 0 °C

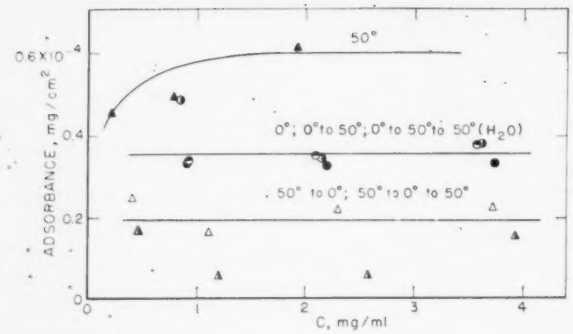

FIGURE 4. *Effect of temperature cycle on adsorption isotherms obtained on glass after pretreating the glass by outgassing and heat.*

Adsorptions and temperature cycles carried out without exposing the glass powder to the atmosphere. Solvent- chloroform; polymer fraction $\bar{M}_n$=6250.

▲ 50 °C
◭ 50 to 0 °C
△ 50 to 0 to 50 °C
● 0 °C
◑ 0 to 50 °C
◓ 0 to 50 to 50 °C in presence of added water

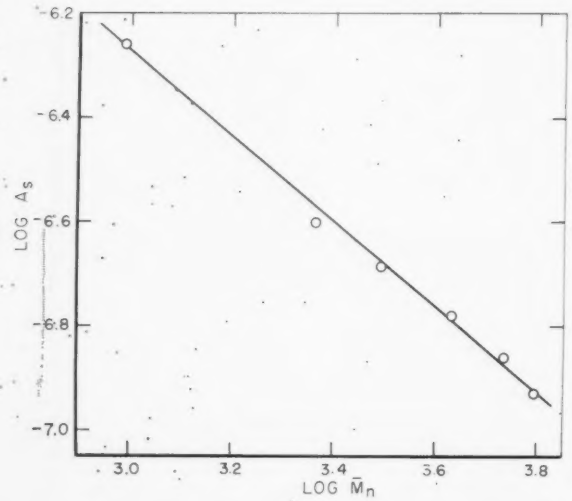

FIGURE 5. *Plot of* log A *versus* log $\overline{M}_n$ *to determine the effect of molecular weight on the amount of polymer adsorbed.*

In order to determine the effect of water added after adsorption had taken place on a "nonreversible system," tubes in which adsorption had initially occurred at 0 °C and which had then been changed to 50 °C were opened, 1 ml of water added, and the tube sealed and rotated at 50 °C for an additional 44 hr. The addition of this water did not cause additional polymer to be adsorbed to equal the absorbance of the 50 °C isotherm, as can be seen from figure 4.

4. Discussion

4.1. Conformation on Adsorbent

The adsorption of polydimethylsiloxanes [12] and poly(methyl methacrylate) [10] has been found to fit the empirical equation $A=KM^a$ where A is the amount of polymer adsorbed at the plateau of the isotherm, M is the molecular weight in relative units, and K and a are constants. If the log of A is plotted against the log of M_n, a straight line is obtained for the fractions of poly(ethylene *o*-phthalate), as shown in figure 5. The values of K and a obtained from a least squares calculation are

$$K=1.38\times10^{-4} \text{ moles/m}^2,$$

$$a=-0.81.$$

These values can be compared with those obtained using the other polymer systems. The size of a is an indication of the conformation of the polymer on the surface. In the case of poly(methyl methacrylate) [10], the values of a were very close to zero for two solvents and two adsorbents. For the polydimethylsiloxanes [12], the values of a varied from 0.23 to 0.40, depending on the solvent and adsorbent. Both of these sets of values of a were obtained for A expressed in the *weight of the polymer*. If A were expressed in moles per unit area, the values for poly(methyl methacrylate) would become close to -1 and those for the polydimethylsiloxanes would vary from -0.77 to -0.60.

As seen in figure 1, the number of moles of polymer adsorbed decreases with increasing molecular weight, giving rise to *negative* values of a. The range of possible values of a, when A is expressed in *moles per unit area* is $-1\leq a\leq 0$. When $a=0$, the empirical equation shows that the number of molecules adsorbed is independent of molecular weight. This can be interpreted [12] to mean that the polymer molecules would be attached at one location only. When $a=-1$, they would be flat on the surface, assuming "monolayer" adsorption.

The values of a for poly(ethylene *o*-phthalate) is between these two limits, but is much closer to the limit -1. The number of moles adsorbed per unit area would be expected, therefore, to be much more sensitive to changes in molecular weight at relatively low molecular weights, and much less sensitive at higher molecular weights. This can be seen from figure 1 to be the case.

These results would indicate, then, that the poly(ethylene *o*-phthalate) molecule lies in a relatively flattened conformation on the glass surface, but nevertheless still has some extension into the solution.

It appears that the conformation of the molecule at the surface is very dependent on the specific system studied if the value of a can be used as a criterion. For poly(methyl methacrylate) [10] the value of a was very close to zero, indicating such a flat array for the systems studied. On the other hand, the polydimethylsiloxanes [12] gave values between 0.23 and 0.43.

In table 1 are listed the degree of polymerization for the different molecular weights studied here and the area available per molecule and per segment, i.e., repeating ester unit. At the lower molecular weights, each repeating unit has available to itself an area of approximately 55 to 60 Å^2. This is only slightly less than the areas determined for a series of polyesters on aqueous surfaces [13, 14]. It would appear then, that at the low molecular weights, the polymer molecule is able to spread on the surface relatively freely, and to lie relatively flat, similar to its conformation on a water surface where a large amount of freedom of motion is possible.

TABLE 1. *Glass surface area available for adsorption of poly(ethylene o-phthalate)*

$\bar{M}_n$	Degree of polymerization	Adsorption	Area	Area
		Moles/m²	*Å²/molecule*	*Å²/segment*
970	5	5.5×10^{-7}	300	60
2300	12	2.4	690	57
3100	16	2.0	850	54
4300	22	1.7	970	44
5400	28	1.3	1260	45
6250	32	1.2	1430	45

In the case of the larger molecular weights studied here, it appears that a limiting surface area of the order of 45 Å^2 is available per segment. This area is still relatively large, implying that the molecule lies relatively flat on the surface with only small loops extending into the solution. It should be noted that these conclusions regarding the flatness of the adsorbed molecule are based on a uniform surface available to the molecule. If the entire surface is not available to the molecule for adsorption, then the loops extending into the solution must be larger, of course.

4.2 Reversibility of Sorption

It was shown in figure 2 that the adsorbance of poly(ethylene *o*-phthalate) from chloroform solution was greater at higher temperatures than at lower temperatures. It had been reported earlier [2] that less polyester was adsorbed from toluene solution at higher temperatures. It is probable that this observed decrease in the adsorbance from toluene, a poor solvent, was caused by a large increase in the polymer-solvent interaction brought about by the higher temperature. Therefore, what was most probably measured was not simply the effect of two different temperatures, but essentially adsorption from what was almost two different solvents, a poor (low-temperature) and a relatively good (high-temperature) solvent. This effect would be negligible for chloroform. Therefore, the larger adsorption at the higher temperature is probably the normal condition to be expected for polyester adsorption on these oxide surfaces. It is realized, of course, that differences in adsorbent-solvent interaction may also be involved.

Work previously reported has shown that cycling the temperature resulted in adsorption that was dependent upon the temperature path followed. It is realized that given sufficient time, equilibrium conditions would be established and the systems discussed below would all be reversible. The dependence upon path, therefore, refers to the observed results and what appears to be "nonreversible" actually means an extremely slow rate of desorption. For a polyester system in which toluene was the solvent, there was a decrease in adsorbance when the temtemperature was raised, but the polymer did not readsorb when the temperature was lowered [5]. A similar behavior was observed for poly(vinyl acetate) and poly(methyl methacrylate) [10]. The three systems were similar in that polymer could be desorbed, but additional polymer could not be readsorbed. The system poly(ethylene *o*-phthalate)-chloroform-glass described in this paper exhibited somewhat different behavior. When the glass powder had been exposed to the atmosphere, the system was completely reversible. However, when the glass was pretreated by drying, the system was no longer completely reversible. In this case also polymer was only desorbed, although the desorption was brought about by decreasing, rather than increasing, the temperature.

The surfaces of amorphous silica and silica gel have been studied by means of infrared spectrophotometry, especially in relation to the nature of the adsorbed water and bound water, and the effect of temperature on this water [15, 16, 17]. Water vapor was found to adsorb physically on the silanol sites only and not on the remainder of the surface [15]. Rehydration of the surface was completely reversible up to 400 °C and a change in the nature of the dehydrated surface was indicated above this temperature. It was also reported [17] that "bound water" in silica gel consists entirely of SiOH groups located on the surface and that the spectrum of physically adsorbed water resembled that of liquid water. Further, outgassing below 300 °C did not change the number of surface silanol groups [16]. Therefore, our outgassing of glass at 250 °C should have removed only the physically adsorbed water layer and should not have appreciably changed the character of the glass surface.

It would appear, then, that the adsorption of the poly(ethylene *o*-phthalate) onto the untreated glass, and the complete reversibility of adsorbance as a result of temperature cycling, as shown in figure 3, could result from adsorption of the polymer, not onto the glass surface directly, but rather onto the preadsorbed water layer. As mentioned earlier, the glass surface area available per segment is not too different from that expected on a water surface. The polymer could be expected to adsorb and desorb relatively readily from such a "water" surface.

As described above, dehydration should remove the adsorbed water layer, leaving a surface consisting, to a large extent, of silanol groups. Adsorbed water interacts with these surface silanol groups through hydrogen bonds [16]. It is reasonable to

suppose that the polyester would also be bound to this dehydrated surface by hydrogen bonds. A different surface, therefore, is available to the polymer after outgassing of the glass powder, and the nature of the adsorptive bond may be somewhat different. As was observed in figures 3 and 4, the outgassing results in a decrease in the adsorbance. This may be a result of fewer adsorption sites available on the glass surface.

In the case of the pretreated glass, it is possible that the total number of sites on the glass occupied by polyester at both temperatures is approximately the same. The differences in the adsorbance are related to the different number of sites occupied per polymer molecule, i.e., the conformation of the polymer molecule. This an oversimplification, of course, and all factors such as differences in solvent-adsorbent interaction, etc., should be considered. When the temperature is lowered, desorption does take place, as required for equilibrium. The remaining polymer molecules rearrange so as to occupy the vacated sites.

When the temperature is again raised, the equilibrium situation calls for a somewhat different polymer conformation. As each polymer molecule now occupies more area than allowed at equilibrium, polymer must be desorbed before additional polymer can be readsorbed. It seems apparent that under these circumstances, the desorption required to achieve the new polymer conformation proceeds at an extremely slow rate, resulting in what appears to be an irreversible condition. Addition of water to the system, figure 4, did not dislodge the adsorbed layer.

It is apparent from the discussion and possibilities presented here that much more knowledge is necessary about the conformation of the polymer molecule. The thickness of adsorbed polymer films *in situ* has been recently investigated using ellipsometry [18]. The system studied was polystyrene of molecular weight 76,000 adsorbed on a chrome-chrome oxide surface from cyclohexane near the theta temperature. For solution concentrations of the order of 1 to 6 mg/ml, it was determined that the polymer was adsorbed as a highly swollen film containing about 12 g/100 ml of polymer and extending about 200 Å into the solution. It is apparent that studies of this nature must be extended to the systems described here, in which both the adsorbent surface and the polymer molecule have more nearly the same polar character.

5. References

[1] W. Heller and W. Tanaka, Phys. Rev. **82,** 302 (1951) (Abstract); W. Tanaka, M.S. Thesis, Wayne University, Detroit, Mich. (1951).
[2] R. R. Stromberg, A. R. Quasius, S. D. Toner, and M.S. Parker, J. Res. NBS **62,** 71 (1959).
[3] J. Koral, R. Ullman, and F. R. Eirich, J. Phys. Chem. **62,** 541 (1958).
[4] C. Peterson and T. K. Kwei, J. Phys. Chem. **65,** 1330 (1961)
[5] R. R. Stromberg and G. M. Kline, Modern Plastics **38,** 123 (Apr.); 241 (May 1961).
[6] R. R. Stromberg, W. H. Grant, and E. Passaglia, "Rate of Adsorption of Polystyrene onto Chrome Surfaces" Abstracts, American Chemical Society Meeting, Los Angeles, Calif., April 1963.
[7] A. Silberberg, J. Phys. Chem. **66,** 1872 (1962).
[8] A. Silberberg, J. Phys. Chem. **66,** 1884 (1962).
[9] H. L. Frisch, M.Y. Hellman, and J. L. Lundberg, J. Polymer Sci. **38,** 441 (1959).
[10] S. Ellerstein and R. Ullman, J. Polymer Sci. **55,** 123 (1961); S. Ellerstein, Ph. D. Dissertation, Polytechnic Institute of Brooklyn (1960).
[11] J. F. Hobden and H. H. G. Jellinek, J. Polymer Sci. **11,** 365 (1953).
[12] R. Perkel and R. Ullman, J. Polymer Sci. **54,** 127 (1961).
[13] W. M. Lee, R. R. Stromberg, and J. L. Shereshefsky, J. Res. NBS **66A** (Phys. and Chem.), 439 (1962).
[14] W. M. Lee, J. L. Shereshefsky, and R. R. Stromberg, J. Res. NBS **65A** (Phys. and Chem.), 51 (1961).
[15] G. J. Young, J. Colliod Sci. **13,** 67 (1958).
[16] R. S. McDonald, J. Phys. Chem. **62,** 1168 (1958).
[17] H. A. Benesi and A. C. Jones, J. Phys. Chem. **63,** 179 (1959).
[18] R. R. Stromberg, E. Passaglia, and D. Tutas, J. Res. NBS **67A** (Phys. and Chem.), 431 (1963).

(Paper 67A6–246)

JOURNAL OF RESEARCH of the National Bureau of Standards—A. Physics and Chemistry
Vol. 67A, No. 6, November–December 1963

Chemical Purity by Dielectric Cryometry

Gaylon S. Ross and Lois J. Frolen

August 5, 1963

A consideration of the deficiencies in standard methods used for the cryometric determination of purity has led to a new approach in which the measurement of an intensive rather than an extensive property is the controlling factor. This method, measurement of the dielectric constant as a function of the fraction melted and correlation with the accompanying change in temperature, allows calculation of purity with high precision. The apparatus used and experimental work performed to ascertain the scope of the method are described. Determination of purity for organic compounds with differing polarizabilities and dipole moments indicate a rather wide applicability of the method. The large change in the dielectric constant of a high purity compound as it passes from solid to liquid state, with an accompanying small change in temperature, may allow automatic control of temperature within extremely narrow limits.

1. Cryometric Method

The well-known method of freezing point depression, $(T_{f0}-T_f)$—where T_{f0} is the freezing point of the pure material and T_f that of the actual sample—provides a sensitive nondestructive measure of impurities. In this method a physical property, ϕ, is determined as a function of temperature, T_x, in the region of the liquid-solid transition. The liquid fraction, F, is presumed to be a linear function of ϕ, that is:

$$F=\frac{\phi_S-\phi_X}{\phi_S-\phi_L}. \tag{1}$$

For nearly pure substances the generalized van't Hoff equation applies:

$$\sum N_i=\frac{\Delta H_f}{RT_{f0}^2}\cdot(T_{f0}-T_x)\cdot F \tag{2}$$

ΣN_i designates the sum of the mole fractions of impurities soluble in the liquid and insoluble in the solid. Conventionally it is written N_2^*. ΔH_f is the molar heat of fusion of the pure material. R is the gas constant. The factor $\Delta H_f/RT_{f0}^2$ is generally referred to as the cryoscopic constant, A, and $(T_{f0}-T_x)$ is equated to ΔT so that eq (2) can be written:

$$1-N_1^*=N_2^*=FA\Delta T \tag{3}$$

Where N_1^* is the mole fraction of the major component.

On rewriting (3) we have the straight line relationship:

$$\frac{1}{F}=\frac{A}{N_2^*}\cdot(T_{f0}-T_x). \tag{4}$$

When $F=1$, $T_x=T_f$, the melting point of the sample by definition. When the line is extrapolated to $\frac{1}{F}=0$, $T_x=T_{f0}$, so that by thermodynamic theory applicable to dilute solutions the melting point of the pure substance can be derived experimentally from a plot of $\frac{1}{F}$ versus T_x. In practice experimenters often derive T_{f0} by extrapolation of the hyperbolic relation (3) to $\frac{1}{F}=0$.

Presently there exist three widely used cryometric techniques. In dilatometry [1, 2] [1] the sample volume is the physical property ϕ. The two other techniques effectively depend on heat content. They are adiabatic calorimetry [3, 4] and time-temperature (thermometric) freezing curves [5, 6]. A carefully conducted comparison [7] has shown that the three techniques, each at its best, can give reliable results. The chief advantage in the calorimetric approach is that one directly obtains accurate values for heats of fusion as well as heat capacity data for both the solid and liquid phases. The same properties can be obtained, if less accurately, from the other two techniques by auxiliary experiments.

In all cryometric techniques the maintenance of good thermal and thermodynamic equilibrium, as well as of good temperature control and measurement, are basic problems. The change in physical property, ϕ, associated with the liquid/solid transformation should be large in terms of measurability.

2. Dielectric Technique

In the dielectric technique the measured variable, ϕ, is the change in electrical capacitance of a capacitor with the sample as dielectric. The technique is applicable to a wide range of compounds but is subject to the following restrictions: (1) The samples must be in the purity range of 98.5 mole percent or greater; (2) the impurities must be closely related in properties to the major component; (3) the sample and impurities must have no interfacial polarization effects; (4) the sample must have high electrical resistivity. The magnitude of the change in capacitance on solid-liquid transformation depends on the

[1] Figures in brackets indicate the literature references at the end of this paper.

polarizability, polarity, and volume changes of the sample. In general the change in capacitance of a sample during fusion is large and can be readily and accurately measured. Since the temperature variation of the dielectric constant of normal liquids and solids is quite small and since the entire melting process of nearly pure materials occurs within a small temperature range, the change in dielectric constant during the phase change ($\phi_S - \phi_L$) can be considered to be temperature independent. The impurities which remain in a carefully purified sample can usually be assumed to be closely related in properties to the major component. Hence, at least in the range of the static dielectric constant determination (100 to 100,000 c/s), the dielectric effects of the impurity molecules may be assumed to be negligible. Under these conditions the change in dielectric constant reflects only the change in phase whereas the temperatures depend only on the impurity.

In principle, data could be obtained from freezing or melting experiments. To approach the true equilibrium curve in a freezing experiment after the inevitable undercooling, the cell would necessarily have to be of low heat capacity. No such stringent limitation exists for apparatus designed for melting experiments. The melting process has herefore been adopted throughout.

Gravitational separation of solid during the final stages of melting may cause gross departures from uniformity in phase distribution. The method is not sensitively dependent on such uniformity but significant departures from the ideal curves occur during the last stages of melting. Glass beads are inserted to prevent the gravitational separation of the two phases.

Since the end effects in the cell are essentially constant, the measured capacitance is primarily due to that portion of the sample which is between the electrodes, and the change in capacitance is proportional to the mole fraction melted. The amount of sample above the electrode is not critical provided it represents the same composition of sample as exists between the two electrodes. However, if the cell were only partially filled, the expanding liquid would displace the air which was formerly between the electrodes, resulting in a nonlinear relationship between the capacitance change and the fraction melted.

The sample is frozen by a quenching technique so that the impurities are dispersed throughout randomly oriented small crystals. If thermodynamic equilibrium is maintained, the crystals should melt at the surfaces which are in contact with the impurities. The shape, volume and the position of the two phases change continuously during melting. Neither the Clausius-Mossotti equation nor a generalized version such as the Wiener equation can be applied. At present, it is impossible to analyze the system mathematically. However, if it is assumed that the capacitor is filled with a homogeneous dielectric whose dielectric constant is continuously changing, the experimental results here presented can be rationalized.

Equation (3) describes the hyperbolic relationship between F and T_x, and, in analyzing the data, Saylor's method [11] of fitting hyperbolae was used. Either the above method or the least-square fitting of the data using (4) permits calculation of T_{fo}. The sample purity is calculated using eq (3) wherein $F=1$ and $T_x=T_f$.

3. Apparatus

Figure 1 shows the construction of the capacitance cell and the auxiliary heating, cooling, and insulating containers. The capacitance cell is constructed of brass throughout. The 3.0 mm spacing between the inner and outer electrodes is uniformaly maintained by fused silica spacers. The capacitance, C_o, of the cell in vacuum has a nominal value of 30 pf. The average temperature of the inner electrode is measured with four glass enclosed thermocouple junctions, which are sealed into holes drilled 90° apart and to different depths. A steel electrode lead is screwed into the central, high-potential electrode and a brass lead is attached to the ground-potential electrode in a similar manner. Two brass shields are used to control the cell temperature.

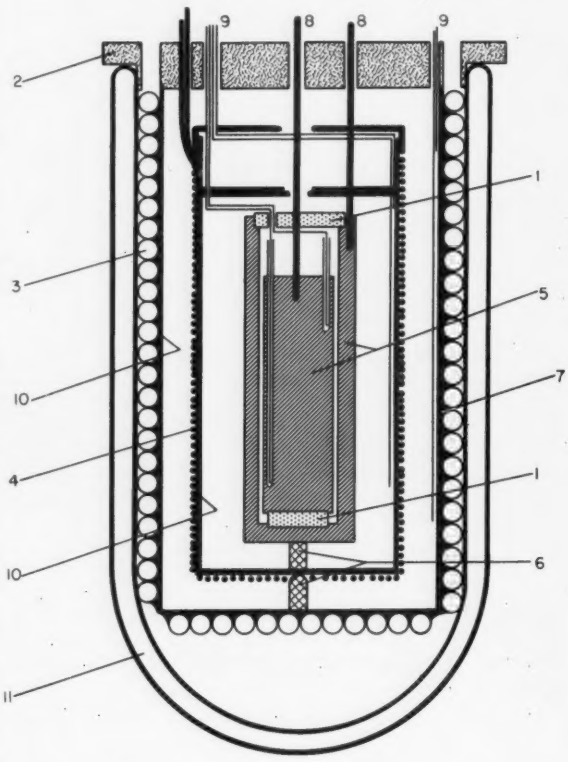

FIGURE 1. *Cell and sheild assembly.*

1, Fused silica
2, Lucite cover
3, Cooling coils
4, Heating wire
5, Cell walls
6, Mycalex spacers
7, Polyurethane insulation
8, Electrode leads
9, Thermocouple leads
10, Brass containers
11, Dewar
Scale, 1 : 2.5

The inner one is wrapped with asbestos-insulated Nichrome wire and the outer one has copper coils soldered to it. Each shield is fitted with a separate, four-junction series thermocouple for monitoring its temperature. The cell and the shields are insulated with carefully machined expanded polyurethane foam and are supported with Mycalex rods. The entire assembly fits in a gallon dewar and all leads protrude through the insulation, containers, and the top of the bakelite cover of the vacuum container. Electrically and thermally insulated leads, held in fixed positions throughout their lengths, are attached above the bakelite cover.

In this work both a General Radio, Type 716–C capacitance bridge and a General Radio impedance comparator have been used to measure capacitance. With the capacitance bridge, the capacitance and the dissipation factor are measured manually and directly. The field strength used is approximately 35 v/cm. The detection limits of this instrument are ± 0.2 pf.

With the impedance comparator the capacitance of the sample can be measure using fixed frequencies of 100, 1000, 10,000, and 100,000 c/s. The impedance comparator has little or no detectable zero drift during a 24-hr period. The field strength is approximately 0.75 v/cm. A measured capacitance difference of 0.01 pf between the cell and a variable precision capacitor can be detected. The impedance comparator displays the phase angle and impedance differences independently on two meters. It also provides a direct current output which can be recorded. When the phase angle is large, it is balanced with a resistance network which has little reactance. A schematic drawing of the system used to measure and record the capacitance and the temperature of the cell is shown in figure 2. Leeds and Northrup, Speedomax, Type G, X-time and X-Y recorders are used.

An ice-water bath is used as a reference for the shield thermocouple systems, and a water-triple point cell is used as a reference for the cell system. The difference in emf between the cell thermocouples and a balancing Leeds and Northrup, Type K–3, Universal potentiometer is amplified with a Leeds and Northrup d-c microvolt indicating amplifier. The output of the amplifier is then recorded. With this system a temperature difference of 0.0001 ° C is detectable.

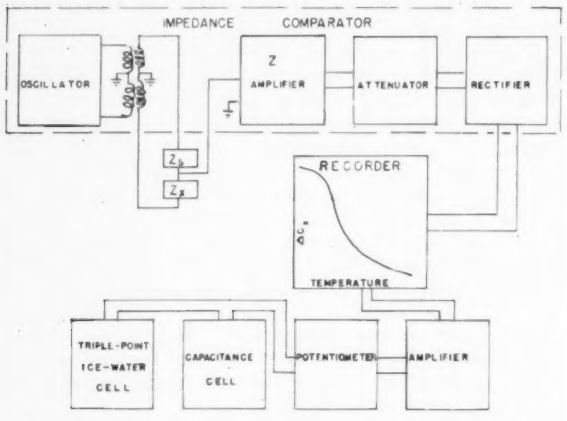

FIGURE 2. *Block diagram of the measuring and recording assembly.*

Other experiments were run to determine the minimum time necessary to insure thermodynamic equilibrium during the melting sequence. Eight hours was found to be sufficient. In still other experiments the melting process was halted and the sample was slowly refrozen. Figure 3 shows a plot of temperature versus capacitance change for one of these experiments. The fact that the two curves are superimposed illustrates one of the important advantages of the dielectric method over the thermometric method, namely that constancy in the melting rate is not necessary and that the melting sequence can even be interrupted by a period of refreezing without appreciably influencing the determination.

Freezing and melting experiments were conducted using all the fixed frequencies of the impedance comparator. No noticeable change was observed in the melting curves as a result of this change. The freezing was also done while using higher electrical field strengths, direct-current fields, and without an electrical field. In all cases the melting curves and the capacitance of the cell, when the sample was completely frozen, remained unaltered.

4. Experimental Detail

4.1 Preliminary Experiments

Series-connected, multiple-junction thermocouple systems were used in order to obtain high sensitivity and to measure temperatures which truly represented the average over the system. The uniformity of the temperature in the cell and in the first, heated shield was determined by differential temperature measurements during the melting sequence. The temperature difference between the

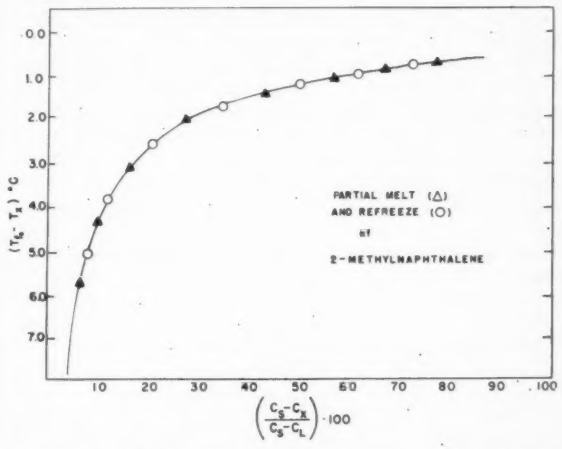

FIGURE 3. *Partial melt and refreeze of 2-methylnaphthalene.*

top and bottom of both the inner electrode and the shield were recorded during preliminary melting experiments. The maximum temperature difference between the top and bottom of the shield was found to be less than 0.1 °C, and the maximum observed difference in the cell was 0.003 °C. 2-Methylnaphthalene was the material used in these experiments.

Approximate calibration of the thermocouples was achieved by immersing the sensing junctions and a calibrated platinum resistance thermometer in a well stirred oil bath whose temperature was slowly changed from 100 to 0 °C. A better calibration was achieved by performing freezing experiments with the various samples while simultaneously using both the junctions and the platinum resistance thermometer as temperature-sensing elements. As a result of this comparison, the absolute temperature of the cell, as measured by the calibrated thermocouples, is known to about 0.05 °C over the entire calibration range, and the temperature difference in the melting ranges of the samples used is accurate to the limit of the sensing equipment (0.0001 °C).

4.2 Experimental Determination of Purity

The liquefied sample is poured into the space between the electrodes with the top fused silica spacer removed. The amount of sample used is such that, when the sample is frozen, the solid extends just over the central electrode. After filling, the top fused silica spacer is replaced, and the cell and shields are assembled as shown in figure 1. The appropriate electrical connections are made and either a temperature-controlled liquid or gas is circulated through the coils surrounding the outer container. After the cell and its contents are cooled below the freezing point of the bulk sample, seeding is spontaneous or initiated by "sparking" the two electrode leads with a Tesla coil or by vibrating the cell. Usually freezing is very rapid, causing profuse, dendritic growth with the impurity dispersed throughout the crystalline mass. After crystallization the cell is cooled to at least 20 degrees below the melting point of the sample.

The sample is then slowly warmed by controlling the temperatures of the two shields. This slow warming allows the crystals to anneal prior to the onset of melting. The impedance of the system and the cell temperature are continuously recorded during the entire experiment. Before the onset of melting the temperature of the inner shield is maintained at no more than 0.2 °C above the cell temperature. During the melting process the temperature difference between the outer container and the cell is maintained at 0.1 °C or less. The average time required for the melting process (excluding the premelting time) is from 6 to 12 hours. The experiment is considered to be complete after the sample has been warmed 5 °C above its melting point.

Since the impedance comparator gives a linear output only when the difference between the reference and sample capacitors is no greater than 5 percent, a technique modification is needed for samples which on melting have a dielectric constant change of more than 10 percent. Nitrobenzene, for example, has a tenfold increase in dielectric constant on melting. For this substance, therefore, the temperature was recorded on an X-time recorder and the nulled value of the impedance comparator was manually recorded on the X-time strip-chart record. This required replotting to obtain the curve of $1/F$ versus T. With this compound the phase angle was balanced with the resistance network prior to the null-balance of the precision capacitor.

There is some experimental difficulty in the determination of the point at which the first melting takes place. Although the impedance (or capacitance) difference is the recorded variable, the impedance comparator also has a meter which shows the phase angle difference. When the sample has an appreciable polarizability or a significant dipole moment, there is a change in the phase angle prior to any noticeable change in the impedance slope. The capacitance value which corresponds to this noticeable change in phase angle is selected as the $F=0$ value. When this is done, there is less than two percent difference between the value of $(\phi_S - \phi_L)$ as determined by this method and that determined by the analysis using the hyperbolic relationship, eq (3). Such a difference causes less than one percent change in N_2^*.

5. Results of Purity Analyses

The method described has been tried for 2-methylnaphthalene, benzene, and naphthalene as examples of compounds with little polarizability and small dipole moment. In addition measurements have been obtained for *p*-dichlorobenzene, which is easily polarized but has no dipole moment. Finally nitrobenzene has been investigated as a typical substance with a large dipole moment. All compounds were distilled, dried with silica gel, and finally purified under vacuum conditions by the fractional melting technique [12]. The two samples analyzed for each compound (except 2-methylnaphthalene) represent the pure fraction and the reject fraction obtained by this technique.

Typical experimental curves and $1/F$ versus T plots are shown in Figures 4 through 8. The appropriate heats of fusion were obtained from the literature references cited in the tables. Tables 1 through 6 show the results of the analyses. For comparison, one sample of each material (except 2-methylnaphthalene) was analyzed by the thermometric (time-temperature) technique.

The linear relationship between capacitance and liquid fraction (cf. sec. 1) is experimentally supported by the data here presented, because the $(C_s - C_x)/(C_s - C_L) \cdot 100$ versus ΔT graphs are hyperbolic corresponding to the generalized van't Hoff eq (3). This linearity is further corroborated by the excellent agreement obtained between the dielectric and the time-temperature analysis.

A remaining uncertainty is due to dissolved atmospheric gases which may show differential

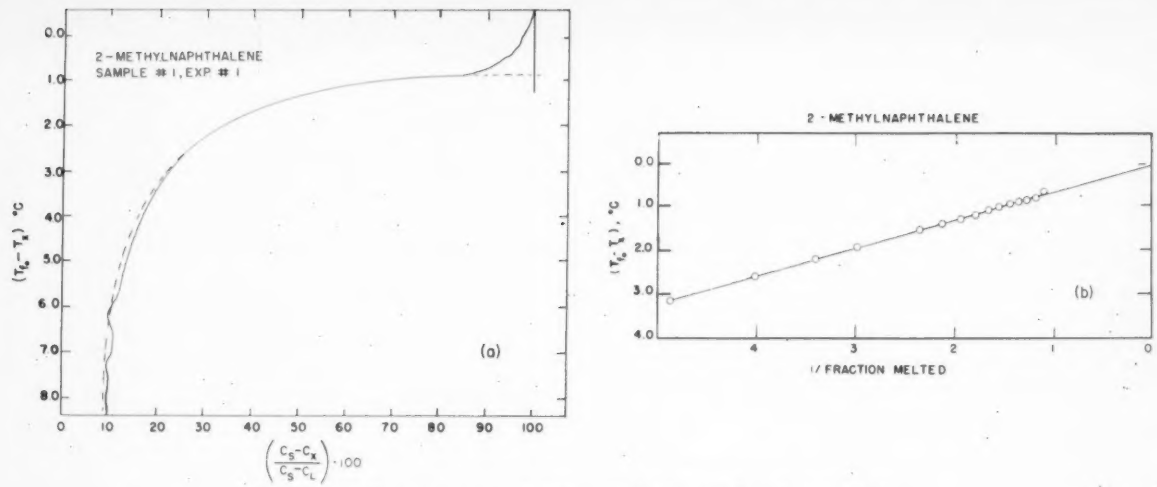

FIGURE 4. *Fusion curve and 1/F presentation for 2-methylnaphthalene.*

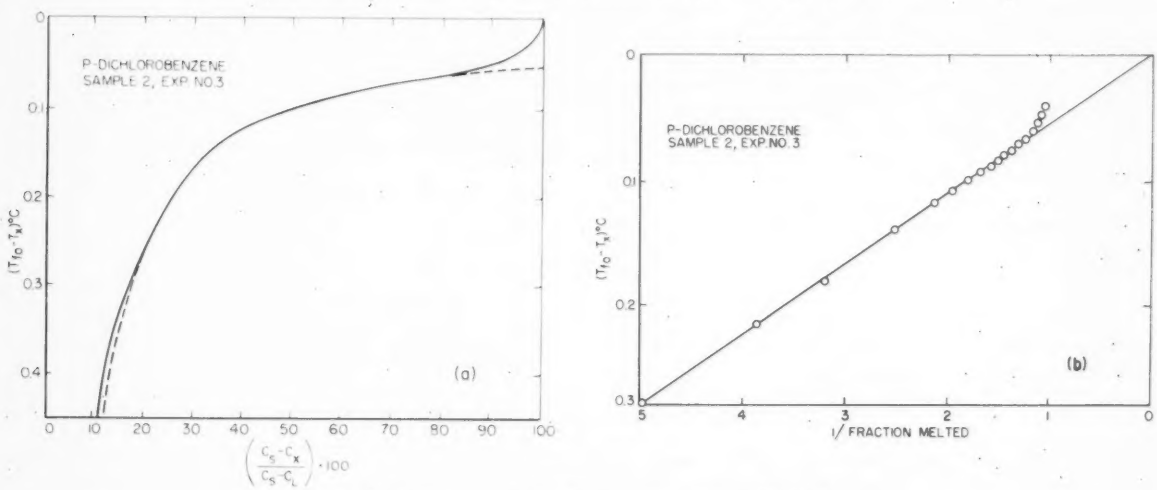

FIGURE 5. *Fusion curve and 1/F presentation for p-dichlorobenzene.*

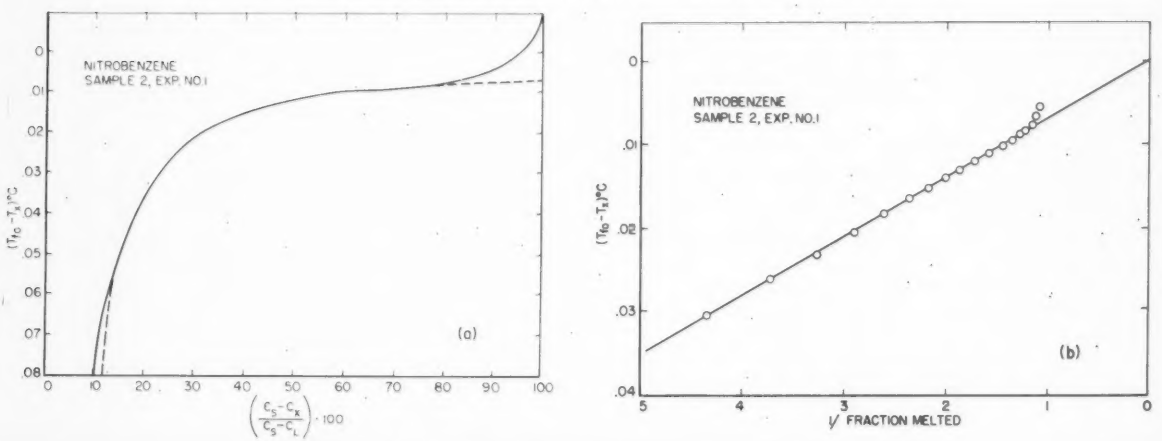

FIGURE 6. *Fusion curve and 1/F presentation for nitrobenzene.*

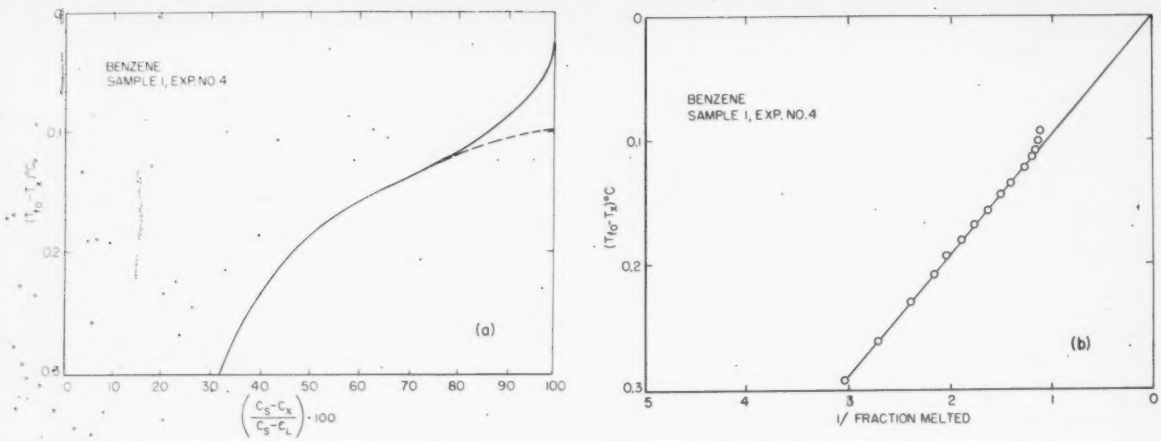

FIGURE 7. *Fusion curve and 1/F presentation for benzene.*

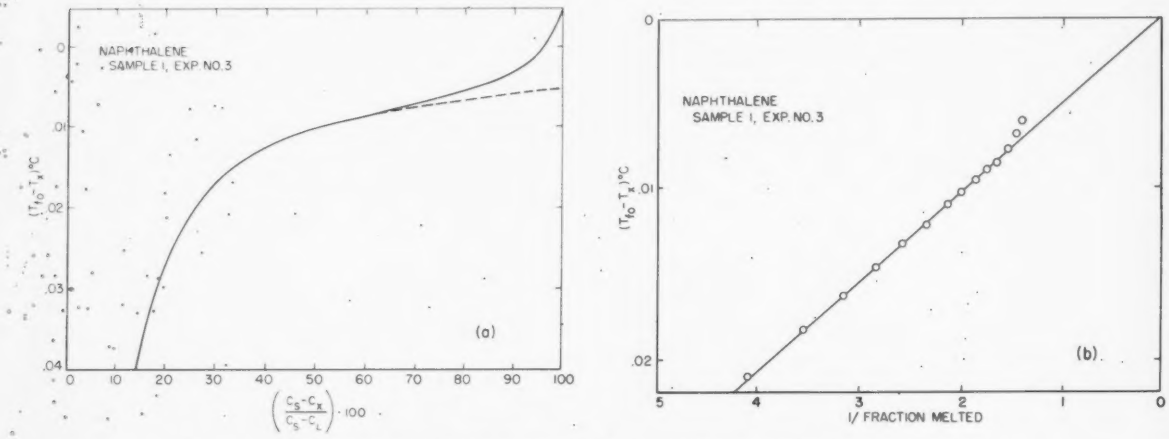

FIGURE 8. *Fusion curve and 1/F presentation for naphthalene.*

solubilities in the liquid and the solid under test. An evacuated sealed cell would constitute an improvement over the apparatus here described. Contamination of the sample from water vapor in the atmosphere would simultaneously be eliminated. In the analyses here given for nitrobenzene and benzene the observed progressive lowering of purity may have arisen from condensed water vapor (see tables 3, 4, and 5).

The experience to date with dielectric cryoscopy is too limited for a numerical estimate of precision to be made with safety. However, it can be claimed without hesitation that this precision exceeds that presently obtainable by thermometric analysis.

TABLE 1. *Purity measurements on 2-methylnaphthalene*

$A=0.01541$*			
Experiment	$(T_{f_0}-T_f)$	Purity	
		Mole %	
1	0.450	99.30	
2	.448	99.31	
3	.456	99.29	

* The cryoscopic constant ($\Delta H_f/RT_{f_0}^2$) was obtained from data given in reference [8].

TABLE 2. *Purity measurements on p-dichlorobenzene*

$A=0.01955$*			
Sample	Experiment	$(T_{f_0}-T_f)$	Purity
			Mole %
1	1	0.0798	99.84
	2	.0782	99.84
	3	.0791	99.84
	4	.0742	99.85
	5	.0763	99.85
	6	.0792	99.84
2	1	.0492	99.90
	2	.0485	99.90
	3	.0497	99.90
	4	.0473	99.90
Thermometric measurement			
1	1		99.8
	2		99.7

*The cryoscopic constant ($\Delta H_f/RT_{f_0}^2$) was obtained from date given in reference [9].

TABLE 3. *Purity measurements on nitrobenzene*

$A=0.01876$*

Sample	Experiment	$(T_{f_0}-T_f)$	Purity
			Mole %
1	1	0.492	99.07_7
	2	.496	99.07_0
	3	.520	99.02_1
	4	.525	99.01_3

*The cryoscopic constant ($\Delta H_f/RT_{f_0}^2$) was obtained from data given in reference [10].

TABLE 4. *Purity measurements on nitrobenzene*[a]

$A=0.01876$*

Sample	Experiment	$(T_{f_0}-T_f)$	Purity
			Mole %
2	1	0.0126	99.976_4
	2	.0128	99.976_0
	3	.0134	99.974_9
	4	.0129[3]	99.975[7]
	5	.0150	99.971_7
Thermometric measurement			
2	1		99.95_7
	2		99.98_9

*The cryoscopic constant ($\Delta H_f/RT_{f_0}^2$) was obtained from data given in reference [10].

[a] This group of experiments was run with a glass-bead matrix between the electrodes.

TABLE 5. *Purity measurements on benzene*

$A=0.01525$*

Sample	Experiment	$(T_{f_0}-T_f)$	Purity
			Mole %
1	1	0.0886	99.86_3
	2	.0903	99.86_7
	3	.0950	99.85_7
	4	.0956	99.85_4
2	1	.0501	99.92_3
	2	.0537	99.91_4
	3	.0510	99.92_2
Thermometric measurement			
1	1		99.87
	2		99.81

*The cryoscopic constant ($\Delta H_f/RT_{f_0}^2$) was obtained from data given in reference [3].

TABLE 6. *Purity measurements on naphthalen*

$A=0.01828$*

Sample	Experiment	$(T_{f_0}-T_f)$	Purity
			Mole %
1	1	0.0051	99.990_{61}
	2	.0052	99.990_{18}
	3	.0051[7]	99.990_{57}
	4	.0051[3]	99.990_{59}
2	1	.0245[1]	99.95_{32}
	2	.0243[7]	99.95_{55}
	3	.0243[8]	99.95_{50}
Thermometric measurement			
1	1		99.990
	2		99.981

*The cryoscopic constant ($\Delta H_f/RT_{f_0}^2$) was obtained from data given in reference [8].

6. Appendix. A Transfer Temperature Standard

The total change in dielectric constant of any given material as it undergoes the solid to liquid phase transition is not directly related to the impurity, providing that the impurity is similar to the major component and that the measurements are conducted in the static frequency range. However, the total change in temperature accompanying such a phase change is directly proportional to the amount of impurity. If one has a thermally stable material whose total impurity content is less than ten parts per million, 90 percent of the total melting or freezing process occurs within a temperature range of approximately one or two thousandths of a degree, assuming an average cryoscopic constant. The total capacitance change of the more pure sample of *p*-dichlorobenzene as plotted on an X-time recorder is shown in figure 9. A plot of the zero stability of the impedance comparator for a similar time interval is included. The series of straight diagonal lines in the figure are a result of changing the value of the balancing precision capacitor to bring the recording on scale. From point A to point B represents a temperature change of 0.01 °C, approximately three fifths of the total melting experiment. Now, when the melting-freezing behavior of the sample is monitored by using the dielectric constant as a means of controlling the heating and cooling of the sample, a stable temperature can be obtained within the cell. When this was done manually, it was easy to maintain the dielectric constant to within 0.2 of one span of the recorded change in dielectric constant with the particular sample. When the temperature was monitored and recorded for several hours, its deviation was no greater than our ability to measure it, namely ± 0.0001 °C. Because of the heavy metal construction of the present cell, overshooting of the heating-cooling cycle was unavoidable. If the monitoring of the heating and

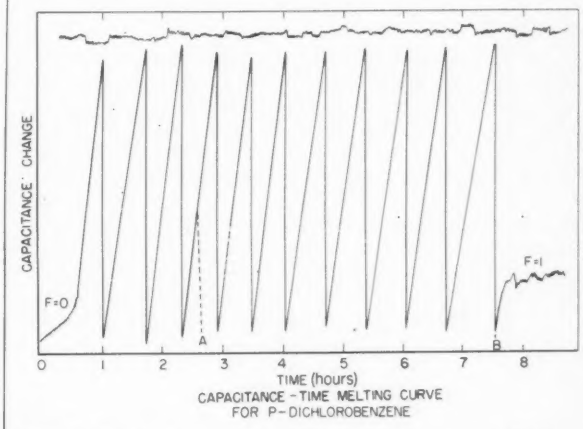

FIGURE 9. *Capacitance-time melting curve for p-dichlorobenzene.*

cooling cycle were automated and controlled within the same temperature limits as was done with the sample of *p*-dichlorobenzene, then direct extrapolation suggests that a cell can be designed whose temperature is stable to within 1 microdegree. In practical applications this is probably impossible, but the production of a stable, relatively sturdy cell, wherein the temperature variation could be controlled to less than 0.0001 °C, seems to be quite possible. Future plans include an attempt to redesign the cell and the shields so that a material of suitable purity can be put in an enclosed cell under its own vapor pressure to obtain transfer temperature standards which have a stability of the previously mentioned order of magnitude.

7. References

[1] W. Swietoslawski, Bull. Acad. Pol. Sci. et Lettres, Classe A **1949,** 113.

[2] T. Plebanski, Bull. Acad. Pol. Sci., Ser. sci. chim. **8,** 125 (1960).

[3] A. R. Glasgow, Jr., G. S. Ross, A. T. Horton, D. Enagonio, H. D. Dixon, C. P. Saylor, G. T. Furukawa, M. L. Reilly, and J. M. Henning, Anal. Chim. Acta **17,** 54 (1957); reprinted in W. M. Smit, Purity Control by Thermal Analysis (Elsevier Publishing Co., Amsterdam, 1957).

[4] J. P. McCullough and G. Waddington, Anal. Chim. Acta **17,** 80 (1957); reprinted in W. M. Smit, Purity Control by Thermal Analysis (Elsevier Publishing Co., Amsterdam, 1957).

[5] A. R. Glasgow, Jr., A. J. Streiff, and F. D. Rossini, J. Res. NBS **35,** 355 (1947) RP1676.

[6] G. S. Ross and H. D. Dixon, J. Res. NBS **67A** (Phys. and Chem.) No. 3, 247 (1963).

[7] Symposium on Cryometric Analysis, presented before the Calorimetry Conference at Ottawa, Canada in 1961. Unpublished data. This comparative study was organized by the International Union of Pure and Applied Chemistry.

[8] J. P. McCullough, H. L. Finke, J. Messerly, S. S. Todd, T. C. Kincheloe, and G. Waddington, J. Phys. Chem. **61,** 1105 (1957).

[9] T. N. Sumarokova and D. Perminova, Izvest. Akad. Nauk Kazakh., SSR, Ser. Khim. No. 1, 12 (1957).

[10] S. S. Parks, S. S. Todd, and W. A. Moore, J. Am. Chem. Soc. **58,** 398 (1936).

[11] C. P. Saylor, Anal. Chim. Acta **17,** 35 (1957); reprinted in W. M. Smit, Purity Control by Thermal Analysis (Elsevier Publishing Co., Amsterdam, 1957).

[12] A. R. Glasgow, Jr., and G. S. Ross, J. Res. NBS **57,** 137 (1956) RP2703.

(Paper 676A–247)

JOURNAL OF RESEARCH of the National Bureau of Standards—A. Physics and Chemistry
Vol. 67A, No. 6, November–December 1963

Adsorption, Desorption, Resorption

William V. Loebenstein

(July 31, 1963)

The complete characterization of batch adsorption from solution, desorption, and related phenomena have been interpreted in the light of a general equation. The forward and reverse adsorption-rate constants and the adsorptive capacity comprise the only parameters. Where adsorption alone is of importance and the desorption-rate constant can be neglected, a simplified form of the theory results in a special equation which may suffice for most adsorption purposes. In either case, the characteristic parameters are determinable from the data and serve as criteria for comparing similar systems. The theory has been confirmed by the data of various investigators taken from the literature. The parameters derived from column adsorption are in agreement with the corresponding batch-derived parameters. The limitations as well as the capabilities of the theory are presented; but even where deviations from the assumed model exist, the results are useful.

1. Introduction

In earlier publications [1, 2][1] the basis was established for characterizing adsorption from solution in terms of just two parameters, namely; the adsorptive capacity per gram of adsorbent, q_0, and the specific adsorption-rate constant, k_1. The values of corresponding parameters derived from batch and from column adsorption were shown to be in substantial agreement with one another, respectively. The two-parameter equations are based on the assumptions that the adsorption step is monomolecular, irreversible, and rate controlling. Furthermore, the assumption of a uniform surface is implicit in the theoretical treatment, since the differential equations used in the derivations are essentially of the Langmuir type. Although these requirements may not be completely applicable in any given instance, the equations are still useful insofar as they provide an approximation of the characteristic parameters which may not be obtainable by other means. The present paper deals, to a considerable extent, with the treatment of data which fall in this category.

In the more general case where reversibility must be reckoned with, but otherwise subject to the same limitations mentioned, a three-parameter batch adsorption equation has been derived [2] which includes the desorption rate constant k_2. For the first time a means is afforded for predicting desorption into solvent as well as adsorption from solution with equal facility. Perhaps even more interesting is the phenomenon of resumed sorption or "resorption" following the interruption of an initial adsorption or desorption step. Should an initial adsorption process, for example, be interrupted and the resumption preceded by a deliberate and sufficient lowering of the concentration, the theory predicts a change to desorption in agreement with experience.

[1] Figures in brackets indicate the literature references at the end of this paper.

2. Two-Parameter Batch Equation

The two-parameter batch adsorption equation previously derived by integrating the irreversible rate equation was shown to be:

$$\frac{q}{q_0}=\frac{1-e^{-\left(\frac{Wq_0}{Vc_0}-1\right)c_0k_1t}}{\frac{Wq_0}{Vc_0}-e^{-\left(\frac{Wq_0}{Vc_0}-1\right)c_0k_1t}} \tag{1}$$

where:

q = the amount of solute adsorbed per gram of the adsorbent at any time, t;
q_0 = the maximum value q would have if all of the adsorption sites were filled;
c = the instantaneous solute concentration whose initial value is c_0;
W = the weight of the adsorbent;
V = the volume of the solution; and
k_1 = the specific adsorption-rate constant.

Methods are available for obtaining values of the parameters q_0 and k_1 which give an optimum fit of eq (1) to the experimental data in the general case where W, V, c_0, and t may all vary from point to point. At best, however, they are cumbersome, and shortcut methods will certainly be preferred wherever they can be used.

One such method was worked out [2] for the special case where both W/V and c_0 are held constant. Under these conditions q values, q_1 and q_2, are determined corresponding to times t_1 and t_2, respectively, such that $t_2=2t_1$. It was then shown that:

$$q_0=\frac{q_1^2\left[q_2\left(\frac{W}{Vc_0}\right)-1\right]}{q_1^2\left(\frac{W}{Vc_0}\right)-2q_1+q_2} \tag{2}$$

and

$$k_1=\frac{\ln\left[\dfrac{q_0-q_1\left(\dfrac{Wq_0}{Vc_0}\right)}{q_0-q_1}\right]}{c_0t_1\left(1-\dfrac{Wq_0}{Vc_0}\right)} \tag{3}$$

Use was made of eqs (2) and (3) in an example taken from published data of Dryden and Kay [3] for the adsorption of aqueous acetic acid on a steam-activated coconut carbon. Good agreement was obtained from three independent determinations of q_0 and k_1. This agreement would not have resulted if the neglected desorption rate constant had been appreciable.

Another special case whose derivation and solution are very similar to the aforementioned method occurs when t is constant providing that a second condition is satisfied. This is the requirement that two values of q can be found, say, $q_1[(W/V)_1, (c_0)_1]$ and $q_2[(W/V)_2, (c_0)_2]$ such that $(W/V)_2=2(W/V)_1$ and $(c_0)_2=2(c_0)_1$. Under these conditions the recurring quantity $\dfrac{Wq_0}{Vc_0}$ which appears so prominently in eq (1) remains unchanged and it follows that

$$q_0=\frac{q_1^2\left[q_2\left(\dfrac{W}{Vc_0}\right)_1-1\right]}{q_1^2\left(\dfrac{W}{Vc_0}\right)_1-2q_1+q_2} \tag{4}$$

and

$$k_1=\frac{\ln\left[\dfrac{q_0-q_1\left(\dfrac{Wq_0}{Vc_0}\right)_1}{q_0-q_1}\right]}{(c_0)_1t\left(1-\dfrac{Wq_0}{Vc_0}\right)_1}. \tag{5}$$

3. Three-Parameter Equation for Batch Adsorption

It has also been shown [2] that where it is desired to retain the desorption rate constant, k_2, in batch adsorption, the integrated equation takes the form:

$$\frac{(M-N)-q}{(M+N)-q}=\frac{M-N}{M+N}e^{-2\left(\frac{W}{V}\right)Nk_1t} \tag{6}$$

where M and N are defined as:

$$M=\frac{V}{2W}\left[\frac{k_2}{k_1}+c_0\left(1+\frac{Wq_0}{Vc_0}\right)\right] \tag{7}$$

$$M^2-N^2=q_0\left(\frac{Vc_0}{W}\right). \tag{8}$$

Here again the parameters q_0, k_1, and k_2 can be readily estimated from a single batch adsorption experiment in the special case where q is determined as a function of t. The solution concentration is measured when t takes on the values[2]: i, $2i$, j, and $2j$. By using the same type of reasoning which led to eqs (2) and (3) from eq (1), it is possible to show from eq (6) that

$$2q_i^2M-(2q_i-q_{2i})(M^2-N^2)=q_i^2q_{2i}. \tag{9}$$

Equation (10) can be written by inspection,

$$2q_j^2M-(2q_j-q_{2j})(M^2-N^2)=q_j^2q_{2j} \tag{10}$$

since it differs from eq (9) only in the subscripts. Equations (9) and (10) constitute a set of simultaneous equations in two unknowns, M and (M^2-N^2), for which the solution is easily obtained. Once these quantities have been found, $(M+N)$ and $(M-N)$ can readily be solved for use in eq (6). Back substitution of one experimental point is sufficient for the determination of k_1. Equation (6) can then be used to predict q for all values of t.

In the event that only the value of q_0 is desired in a given instance, it is only necessary to determine (M^2-N^2) from eqs (9) and (10) for use in eq (8). The quantity (M^2-N^2) is given (according to Cramer's rule) by the ratio:

$$\frac{\begin{vmatrix}2q_i^2 & q_i^2q_{2i}\\ 2q_j^2 & q_j^2q_{2j}\end{vmatrix}}{\begin{vmatrix}2q_i^2 & -(2q_i-q_{2i})\\ 2q_j^2 & -(2q_j-q_{2j})\end{vmatrix}}.$$

Consider the example (Dryden and Kay's Run #201) already cited for the two-parameter equation for purposes of illustration and comparison. The amounts of acetic acid adsorbed per gram of charcoal are repeated in table 1 corresponding to the measured solution concentrations. If, arbitrarily, i and j are taken as 10 min and 15 min, respectively, it follows that

$$q_i=0.3533 \qquad q_j=0.4033$$

$$q_{2i}=0.4667 \qquad q_{2j}=0.5033.$$

Substitution of these values in eqs (9) and (10) results in $M^2-N^2=0.63965$ so from eq (8),

$$q_0=0.627 \text{ meq}\cdot\text{g}^{-1}.$$

To continue with the illustration, $M=0.848$. Thus, $M-N=0.566$ and $M+N=1.130$. By substituting q_0 and M back into eq (7), it can be verified that $k_2/k_1=0.00147$. This confirms that the desorption rate constant is, indeed, very small compared with k_1. One of the adsorption points, say, $q=0.3533$ for $t=10$ may now be substituted back in eq (6) to solve for k_1. The two rate constants are

$$k_1=3.57 \text{ ml}\cdot\text{meq}^{-1}\cdot\text{min}^{-1} \qquad k_2=0.00524 \text{ min}^{-1}$$

[2] Since the three independent parameters must be evaluated from the experimental points, no less than three points are required. The use of four points affords a degree of flexibility in the choice of data. The only restriction is that $i\neq j$, although it is permissible for $2i=j$. In the latter instance, the minimum of three points would, of course, result.

and eq (6), in this particular instance, reduces to:

$$\frac{0.566-q}{1.130-q}=0.501\,e^{-0.0604t}.$$

TABLE 1. *Data of batch adsorption Run #201*
(Dryden and Kay)

Acetic acid: $V=100$ ml, $c_0=0.0306$ meq·ml^{-1}
Coconut charcoal: $W=3.0$ g, Sieve size: (8 on 10)
Temperature: 30 °C, Stirring rate: 400 rpm

t	c	q
min	*meq·ml*$^{-1}$	*meq·g*$^{-1}$
10.0	0.0200	0.3533
15.0	.0185	.4033
20.0	.0166	.4667
30.0	.0155	.5033
45.0	.0147	.5300
60.0	.0140	.5533

It should be pointed out that the value of 0.627 obtained here for q_0 is about 10 percent higher than the corresponding value previously cited [2] for the simpler case where irreversibility was assumed. This (present) value is, moreover, consistent with independent q_0 determinations of 0.666 and 0.641 for combinations of $i=15$ with $j=2i=30$ and for $i=10$ with $j=30$, respectively. The value of 3.57 for k_1 compares well with the corresponding value from the two-parameter equation.

4. Application of Batch Adsorption Theory for Different Values of c_0

A 1944 publication by W. G. Burgers [4] afforded the opportunity to test the applicability of eq (1) and/or eq (6) to the case where the initial concentration differed from batch to batch.

Acetic acid was adsorbed on pulverized "Norit" charcoal at 25 °C with continuous agitation for periods of 2 hr. The volume of solution was held constant at 50 cm^3 while the weight of the carbon and the initial concentration of acid were varied in accordance with table 2 which also lists the corresponding values for the amounts of acetic acid adsorbed per gram. The experimental data of table 2 are reproduced directly from the first two columns of Burgers' *Tableau I, Tableau II, et Tableau III.*

In the estimation of q_0 and k_1 through the application of eqs (4) and (5), the value of 2.024 mM·g^{-1} was selected for q_2 corresponding to $(W/V)_2=0.04$ g·cm^{-3} (i.e., $W_2=2.0$ g) and the corresponding value of $(c_0)_2$ was, consequently, 0.3779 mM·cm^{-3}. No measurement was available for q_1 corresponding to 0.1890 mM·cm^{-3} for $(c_0)_1$ and $(W/V)_1=0.02$ g·cm^{-3}. However, a conventional plot of the data by Burgers showed very little scatter of the points, hence an interpolation was made between the close neighboring values resulting in $q_1\approx 1.683$ mM·g^{-1}.

TABLE 2. *Batch adsorption data for acetic acid on "Norit"*
(W. G. Burgers)
Each determination was carried out at 25 °C with $V=50$ cm^3 and $t=2.0$ hr, but with initial concentrations and adsorbent weights as indicated.

c_0	$q_{(obs)}$		
	$W=1.0$ g	$W=2.0$ g	$W=3.0$ g
mM·cm^{-3}	*mM·g*$^{-1}$	*mM·g*$^{-1}$	*mM·g*$^{-1}$
0.0106	0.354	0.224	-----
.0323	.725	.551	-----
.0489	.908	.737	-----
.0546	-----	-----	0.655
.0643	1.030	.876	-----
.0881	1.199	-----	-----
.0917	1.240	1.124	-----
.1091	-----	-----	1.056
.1796	1.654	1.514	1.396
.2188	1.777	1.646	-----
.2588	1.869	1.750	1.671
.3146	1.957	1.896	-----
.3779	2.082	2.024	1.950

Equation (4) yielded $q_0\approx 2.1$ and this was retained for use with the three-parameter equation. While a somewhat lower value than 6.0 was obtained from eq (5) for k_1, this value was tested along with an estimate for k_2 such that $k_2/k_1\approx 0.02$.

Although lengthy optimizing techniques are available for obtaining a "best" fit of the parameters in eqs (6–8), no improvement was sought in this application. The purpose was to show that the agreement is reasonably close between calculated and experimental values of q despite the use of these rounded off first estimates of q_0, k_1, and k_2. This comparison is shown in the last two columns of table 3. The first two columns identify the points, while the intermediate columns list the values computed for the component parts of eqs (6–8) for each determination.

TABLE 3. *Adsorption calculations from the data of table 2*
Estimated values of 2.1, 6.0, and 0.02 for the parameters q_0, k_1, and k_2/k_1, respectively, were used in the fitting of eq (6).

c_0	W/V	M^2-N^2	M	$M-N$	$M+N$	$2\left(\frac{W}{V}\right)Nk_1t$	$q_{(calc)}$	$q_{(obs)}$
mM·cm^{-3}	*g·cm*$^{-3}$						*mM·g*$^{-1}$	*mM·g*$^{-1}$
0.2588	0.060	9.0573	3.3869	1.8333	4.9405	2.237	1.60	1.671
.1796	.060	6.285	2.713	1.677	3.749	1.492	1.45	1.396
.3779	.060	13.2258	4.3643	1.951	6.777	3.475	1.91	1.950
.0643	.040	3.3758	2.103	1.079	3.127	0.983	0.78	0.876
.3146	.040	16.517	5.232	1.937	8.527	3.163	1.87	1.896
.2188	.040	11.487	4.035	1.845	6.225	2.102	1.68	1.646
.0489	.020	5.1345	2.773	1.175	4.371	0.767	0.72	0.908
.2188	.020	22.974	7.020	1.891	12.149	2.462	1.75	1.777
.0881	.020	9.251	3.752	1.554	5.950	1.055	1.11	1.199

5. Analysis and Comparison of Parameters from Column and Batch Adsorption

An example has already been given in an earlier paper [2] of the application of the present adsorption theory to a batch adsorption run described by Dryden and Kay [3]. That run was part of a wealth of experimental data contained in the Ph.D. Thesis of C. E. Dryden [5]. An interpretation of the results of that data in the light of the present theory can now be readily made. Dryden's experiments consisted of some 20-odd column adsorptions (static bed experiments), a somewhat shorter series of column desorptions, nearly 20 batch adsorptions, and 7 batch desorptions. All runs were carried out at 30 °C using acetic acid together with a steam-activated coconut carbon.

In the column adsorption experiments, a 4-fold variation in column height was used from run to run. Extreme values of volume-flow rate varied over a 20-fold range. Four U.S. Standard sieve sizes of charcoal were used ranging from (8 on 10) to (40 on 60). Two levels of initial acetic acid concentration were employed; namely, 0.10 N and 0.31 N.

In the batch adsorption experiments, the rate of agitation was varied from 0 to 400 rpm of magnetic stirring. The sieve fractions range from (8 on 10) to (80 on 100) in five steps. Water-wetted charcoal was compared with the customary initially dry material. The two levels of initial acetic acid concentration used were 0.03 N and 0.10 N.

5.1 Parameters Derived from Column Adsorption Runs

For each of the column adsorption experiments a semilogarithmic plot of $(c_0/c)-1$ against throughput, y, was made in order to determine the characteristic parameters, q_0 and k_1. This is in accordance with the equation

$$\ln\left(\frac{c_0}{c}-1\right)=\frac{k_1 q_0 x}{\dot{V}}-\frac{k_1 c_0 y}{\dot{V}} \qquad (11)$$

which had been derived and tested in earlier work [1]. In eq (11), $\dot{V}$ is the volume-velocity; x is the mass of adsorbent upstream from the point at which effluent is collected; and y is the throughput or cumulative volume of solution which has passed that point since the start.

The initial (low throughput) points of the curves were not used in fitting to the linear requirement of eq (11). The substitution of solution for the water used to settle the columns is not, strictly speaking, a piston-displacement-like process. Consequently, the early values of c should be abnormally low resulting in initially high values for $(c_0/c)-1$. This phenomenon has been observed in other work [2], as well. The values of the parameters q_0 and k_1 consequently determined from the final points of each plot are shown in table 4 along with the conditions applicable to each run.

TABLE 4. *Characteristic parameters determined from column adsorption experiments*

Results are based on the static-bed data (C. E. Dryden) for acetic acid on coconut charcoal at 30 °C fitted to eq (11).

Run No.	Sieve size	c_0	$\dot{V}$	x	q_0	k_1
		$meq \cdot ml^{-1}$	$ml \cdot min^{-1}$	g	$meq \cdot g^{-1}$	$ml \cdot meq^{-1} \cdot min^{-1}$
18	(8–10)	0.10	21.8	59.8	0.850	0.769
19	(8–10)	.10	35.0	59.2	.676	.575
20	(8–10)	.10	6.99	18.8	.928	.677
21	(8–10)	.10	3.32	18.9	1.176	.379
36	(8–10)	.10	4.88	59.4	1.333	.398
53	(12–16)	.10	9.18	18.1	1.259	1.124
55	(12–16)	.10	3.49	18.5	1.330	0.867
56	(12–16)	.10	22.9	18.4	1.023	1.845
57	(12–16)	.10	23.2	59.1	1.363	1.259
58	(12–16)	.10	64.2	59.1	1.057	2.259
60	(12–16)	.31	3.81	17.9	2.100	0.664
61	(12–16)	.31	45.4	60.6	1.279	.690
75	(24–30)	.10	37.7	55.6	1.542	2.798
76	(24–30)	.10	57.8	17.0	1.336	5.682
77	(24–30)	.10	25.2	17.3	1.625	3.059
78	(24–30)	.10	9.53	16.9	1.583	2.628
79	(24–30)	.10	64.6	55.5	1.358	3.115
83	(40–60)	.10	13.9	15.4	1.470	11.569
84	(40–60)	.10	66.6	15.5	1.406	22.33
90	(40–60)	.10	25.3	15.6	1.443	9.673
91	(40–60)	.31	13.1	15.6	2.210	3.642
92	(40–60)	.31	63.6	15.5	1.935	5.697

a. Agreement With Theory

The most significant result which is immediately evident from table 4 is the degree of agreement among the computed values of q_0. The spread in sieve sizes corresponds to a range in mean particle diameter from about 360 to nearly 2200 microns. The initial concentration varies over three-fold. The velocity of flow ranges from 3.32 $ml \cdot min^{-1}$ to 64.6 $ml \cdot min^{-1}$. The weight of adsorbent varies between about 15.5 g and 60 g. Yet, notwithstanding the interplay of these factors, for the results of the 18 runs at which $c_0=0.10$, there yielded a mean q_0 value of 1.264 $meq \cdot g^{-1}$ with a standard deviation of 0.263.

b. Anomalous Effects

A closer scrutiny of table 4 discloses several interesting facts. The excellent data make it possible to discern "second order" effects which cannot be interpreted in the light of the present simplified theory.

A comparison of Run #55 with #60, of #83 with #91, and of #84 with #92 suggest that the effect of a three-fold increase in the initial concentration, c_0, other things being equal, resulted in an increase in q_0 of about one-and-one-half-fold. This can readily be explained as a departure from idealized Langmuir behavior. The Langmuir model implies a uniform surface. If this is only approximated, then the number of adsorbing sites (a measure of q_0) which could be capable of participating in the case of a much greater initial concentration of solute would include some portions of the surface requiring higher activation energies. If, moreover, adsorption proceeded more slowly at these latter sites, it would result in a lower overall k_1 value.

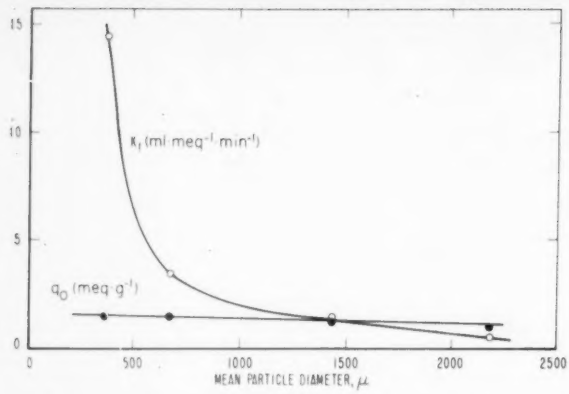

FIGURE 1. *Dependence of parameters on particle size.*

The parameters were computed from column adsorption. Each point on both curves represents the average of three to five individual determinations. Runs with essentially the same initial concentrations were used, namely, 0.10 meq·ml^{-1}

Another "second order" effect appears to be present in considering flow rates. Other things being equal, an increase in velocity results in a lower value for q_0 and a higher value for k_1 as can be seen from table 4. This behavior would be expected based on diffusion considerations which have been entirely neglected in the development of the present simplified theory. The greater the flow rate becomes, the more difficult it is to insure equal access of solute to all of the absorbing sites. Thus, the computed value of q_0 based upon experiments at the higher flow rates would be underestimated. This reasoning is consistent with overestimated values for k_1.

The variation in sieve size (particle diameter) has almost a negligible effect upon q_0 although its influence on k_1 is quite pronounced. These comparisons are portrayed quite strikingly in figure 1. Phenomena such as the very small dependence of q_0 on particle size are of particular interest in confirming the physical significance of the derived parameters. Capacity for adsorption, like surface area, is a quantity measurable only at the molecular level. The process of subdividing a highly porous particle creates very little additional surface not already accessible to a molecule.

5.2 Parameters Derived From Batch Adsorption Runs

The quantities q_0 and k_1 were calculated from the data of each of the batch adsorption runs reported. In general, eqs (2) and (3) were employed for this purpose, the fact having been established that the desorption rate constant k_2 was negligibly small compared with k_1.

As an example to illustrate the procedure, the data and calculations for Batch #221 are typical. These data are given in table 5. The 30 and 60-min points corresponding to 0.245 and 0. 258 meq·g^{-1} for q_1 and q_2, respectively, were selected for use with eqs (2) and (3) to determine q_0 and k_1:

$$q_0=\frac{0.060[0.258(3.268)-1]}{0.060(3.268)-0.490+0.258}=0.262\ \text{meq}\cdot\text{g}^{-1}$$

$$k_1=\frac{\ln\left[\dfrac{0.262-0.245(0.8562)}{0.262-0.245}\right]}{(0.0306)(30)(1-0.8562)}=8.50\text{ml}\cdot\text{meq}^{-1}\cdot\text{min}^{-1}.$$

If one had chosen the 15 and 30-min points instead, the computation for q_0 would have been:

$$q_0=\frac{0.0493[0.245(3.268)-1]}{0.0493(3.268)-0.444+0.245}=0.259\ \text{meq}\cdot\text{g}^{-1}$$

In general, the greater time intervals were consistently chosen and were considered most reliable.

TABLE 5.—*Data of batch adsorption Run #221*
(C. E. Dryden).

Acetic acid:
V=100 ml
c_0=0.0306 meq·ml^{-1}

Coconut charcoal:
W=10.0 g
Sieve size: (8 on 10)

Temperature: 30 °C
Stirring rate: 400 rpm

t	c	q
min	*meq·ml*$^{-1}$	*meq·g*$^{-1}$
0	0.0306	0
10.0	.0100	0.206
15.0	.0084	.222
20.0	.0075	.231
30.0	.0061	.245
45.0	.0053	.253
60.0	.0048	.258
75.0	.0044	.262
∞	.0040	.266

While it is possible to utilize eqs (9) and (10) for determining the parameters in accordance with the general adsorption equation as previously illustrated, this practice is only required when the desorption rate constant, k_2, is appreciable relative to k_1. The simpler method shown here will be preferred wherever it can be used.

In like manner, values for q_0 and k_1 were determined for all of the batch experiments. These results are grouped so as to bring out most effectively the possible influence of each of the factors studied such as rate of stirring, sieve size, etc.

a. Initially Dry Versus Prewetted Adsorbent

A few batch runs were described in Dryden's Thesis [5] in which the adsorbent had been presoaked in water prior to contact with the acetic acid solution. It was hoped to ascertain whether presoaking had any effect upon the adsorption. It now appears clear, in light of the present theory, that the prewetted adsorbent gave rise to q_0 and k_1 values which fell in line with those from the initially dry adsorbent. These results are shown in table 6.

The volume of the solutions were 100 ml and the initial concentration of acetic acid was 0.03 meq·ml^{-1}. There was a slight dilution effect caused by the water contained in the presoaked samples as reflected by the increase in V and decrease in c_0. However, this was limited to 10 percent in all cases and is seen

to have a minor effect at most compared with the influence of changes in W.

The values of q_0 and of k_1, of course, should be constant if the ideal conditions assumed in the derivation of the theory were closely approximated. The observed trend, attributable to the increase in the W/V ratio, is undoubtedly caused by a departure from these conditions.

TABLE 6. *Batch comparisons: the consequences of prewetting and the effect of varying the amount of adsorbent*

Sieve size: (8 on 10) Stirring rate: 400 rpm
Temperature: 30 °C

Run No.	Initial state	W	V	c_0	q_0	k_1
		g	ml	$meq \cdot ml^{-1}$	$meq \cdot g^{-1}$	$ml \cdot meq^{-1} \cdot min^{-1}$
222	dry	1.0	100	0.03	0.726	2.19
236	wet	2.48	108	.027	.594	3.05
201	dry	3.0	100	.03	.565	3.74
238	wet	4.01	107	.026	.474	4.45
220	dry	5.0	100	.03	.421	5.26
221	dry	10.0	100	.03	.262	8.50

b. Effect of W/V

The effect of W/V is equivalent to the effect of W in this work since V was held constant at 100 ml. (Runs #236 and #238, alone, had slightly higher values because of presoaking.) Tables 6 and 7 show the results of increasing adsorbent weight. The essential distinction between the two tables is the sieve sizes although these differences are not pronounced because the sizes are close together. A more searching comparison of the effect of sieve sizes is taken up later. The important point here is that the value determined for the parameter q_0 decreases with increasing W. Both tables confirm that a 10-fold change in W results in about a 3-fold change in q_0. The parameter k_1 is also affected by a change in W. As q_0 decreases, k_1 increases. It is about twice as sensitive as q_0, moreover, to changes in W.

TABLE 7. *Batch comparison: effect of W/V*

V=100 ml Stirring rate: 400 rpm
c_0=0.03 meq-ml^{-1} Sieve size: (12 on 16)
Temperature: 30 °C

Run No.	W	q_0	k_1
	g	$meq \cdot g^{-1}$	$ml \cdot meq^{-1} \cdot min^{-1}$
217-8-9	1.0	0.672	2.64
206	3.0	.562	4.77
210	5.0	.462	5.19
216	10.0	.271	15.9

c. Effect of Stirring Rates

The rate of stirring was varied in three steps from 0 to 400 rpm within each of two sets of experiments. The sets differed from one another in regard to sieve size. The results are shown in tables 8–a and 8–b. Within each set there is no apparent correlation of parameters with stirring rate. The observed spread in values of q_0 are entirely within experimental error. The same is true for k_1, except perhaps for the unusually high value obtained in Run #209. No reason can be found for this singular anomaly.

TABLE 8. *Batch comparison: effect of stirring rate*

V=100 ml W=3.0 g
c_0=0.03 meq-ml^{-1} Temperature: 30 °C

Run No.	Stirring rate	q_0	k_1
		8–a	
		Sieve size: (12 on 16)	
	rpm	$meq \cdot g^{-1}$	$ml \cdot meq^{-1} \cdot min^{-1}$
208	0	0.522	2.97
207	120	.541	6.16
206	400	.562	4.77
		8–b	
		Sieve size: (8 on 10)	
203	0	0.500	1.26
209	150	.498	14.6
201	400	.565	3.74

d. Effect of Initial Concentration

The influence of c_0 on the results of batch adsorption are strikingly similar to those for column. Although only two batch runs were made at c_0=0.10, these are sufficient for comparison purposes. Tables 9–a and 9–b compare these batches (Runs #202 and #215) with other batch runs which differed only with respect to initial concentration. The q_0 values of 1.425 and 1.201 meq·g^{-1} obtained in Runs #202 and #215, respectively, compare well with 1.264 meq·g^{-1}, the average of the 18 column runs previously computed for the same initial concentration. While k_1 seems to be more sensitive to variations in conditions than does q_0, its magnitude is also consistent with the corresponding column results.

It is interesting that a three-fold increase in initial concentration from 0.03 to 0.10 meq·ml^{-1} (as seen in tables 9–a and 9–b) resulted in nearly a three-fold increase in q_0. However, at higher initial concentrations the effect was much less pronounced. This can be seen from table 4 by comparing Run #55 with Run #60; Run #83 with Run #91; and Run #84 with Run #92. In each of these comparisons where factors other than c_0 were essentially constant, the initial concentration increased from 0.10 to 0.31 meq·ml^{-1}; yet the increase in q_0 was limited to about 50 percent.

TABLE 9. *Batch comparison: effect of c_0*

V=100 ml Stirring rate: 400 rpm
Temperature: 30 °C

Run No.	c_0	q_0	k_1
		9–a	
W=3.0 g		Sieve size: (8 on 10)	
	$meq \cdot ml^{-1}$	$meq \cdot g^{-1}$	$ml \cdot meq^{-1} \cdot min^{-1}$
201	0.03	0.57	3.74
202	.10	1.425	0.819
		9–b	
W=5.0 g		Sieve size: (12 on 16)	
210	0.03	0.462	5.19
215	.10	1.201	0.905

e. Effect of Sieve Size

The influence of particle size on the parameters derived from the batch adsorption experiments confirms the findings of the column runs. Very little, if any, change in q_0 is evident from table 10–b, although the sieve size ranges in five steps from (8 on 10) through (80 on 100), other factors being constant. At the same time, however, the accompanying value of k_1 increased markedly with decreasing particle size. Tables 10–a, 10–c, and 10–d show the same lack of dependency of q_0 although only two runs were available for comparison in each case.

In a preceding paper [2], the adsorbent involved was a service bone char which had been subjected to numerous cycles of adsorption, partial desorption, drying, and kilning. Its prior history may have been reflected in its dependence of q_0 on sieve size in contrast with the present study. This very point was discussed in some detail at that time.

TABLE 10.—*Batch comparison: effect of particle size*

c_0=0.03 meq· ml^{-1} Stirring rate: 400 rpm

Temperature: 30°C

Run No.	Sieve size	q^0	k_1
	10–a	W=1.0 g	
		meq· g^{-1}	ml· *meq*$^{-1}$· *min*$^{-1}$
222	(8 on 10)	0.726	2.19
217–8–9	(12 on 16)	.672	2.64
	10–b	W=3.0 g	
201	(8 on 10)	0.565	3.74
206	(12 on 16)	.562	4.77
212	(24 on 30)	.608	15.22
213	(40 on 60)	.567	71.5
214	(80 on 100)	.653	110.5
	10–c	W=5.0 g	
220	(8 on 10)	0.421	5.26
210	(12 on 16)	.462	5.19
	10–d	W=10.0 g	
221	(8 on 10)	0.262	8.50
216	(12 on 16)	.271	15.9

6. Adsorption—Desorption—Resorption

Much has been written in the preceding sections of this paper regarding the limitations of the present theory. Examples have been given and comparisons made showing the extent of departure from ideal conformity with the model assumed, although plausible explanations were offered for most of the observed discrepancies. Despite these shortcomings, the theory has much to recommend it including applications which have not heretofore been discussed. One such application is in desorption. It is clear, of course, that the simplified two-parameter equation cannot be used in this application, since it neglects entirely the desorption rate constant, k_2. Furthermore, it would be extremely desirable to be able to use only one equation for both adsorption and desorption.

The difference between the two processes should be reflected only in the boundary conditions. In the derivation of the adsorption equation the initial conditions required all of the adsorbable species to be in the solution phase. Conversely, for desorption the adsorbable species initially would be entirely in the adsorbed phase. To proceed one step further, it might be stipulated that both adsorption and desorption should be considered, from this point of view, as special cases of an initial condition where some of the adsorbable species may exist in solution while the remainder is adsorbed. The process which would subsequently take place might either be adsorption or desorption, depending upon the levels of the interrelated variables. These various concepts may be reconciled by use of the term "resorption" to define this resumed sorption process.

In the original derivation of eq (6), the quantity c_0 was defined as the concentration of the adsorbable solute before any adsorption had taken place. For the general case (applicable as well in the original case), c_0 should be redefined as follows:

c_0=the concentration that would exist at any time if all of the adsorbable species were assumed to be in the solution phase.

Two new symbols can now be defined as c_I and q_I to correspond to the concentration and the amount adsorbed per gram, respectively, which exist at the onset of a sorption process.

Since the conservation equation holds under all conditions, it follows here that

$$c_0=\frac{W}{V}q_I+c_I \tag{12}$$

and the general form of the integrated equation becomes

$$\frac{(M-N)-q}{(M+N)-q}=\frac{(M-N)-q_I}{(M+N)-q_I}e^{-2\left(\frac{W}{V}\right)Nk_1t} \tag{13}$$

while M and M^2-N^2 retain their definitions as given by eqs (7) and (8), respectively.

It is seen that the only difference between eq (13) and eq (6) is the appearance of q_I in numerator and denominator of the coefficient of ϵ. Reference to eq (12) confirms that for an adsorption process q_I=0 and $c_0=c_I$. Under these conditions eq (13) reduces to eq (6) as a special case. For a desorption process where the adsorbent containing adsorbate is added to pure solvent, c_I vanishes and eq (12) shows that $Vc_0/W=q_I$. Obviously, in any case, it is always true that $q^0 \geq q_I$. Since q_I is different from zero in this instance (desorption), eq (13) would apply.

6.1. Desorption

The consequence of subtracting q_1 from the numerator and denominator of the coefficient of e in eq (13) can impart a negative value to this factor which immediately identifies the process as one of desorption. It is instructive to consider the batch desorption data of table 11 as an example of the use of eq (13) in this capacity. The table contains the data collected by Dryden in Run #224.

Amount of acetic acid preadsorbed on the charcoal	7.26	meq
Weight of wet charcoal	8.036	g
Weight of dry charcoal (W)	5.221	g
Difference (assumed to be excess water)	2.82	ml
Water added	100.00	ml
Total water present, (V)	102.82	ml

$$q_1=\frac{7.26}{5.221}=1.391 \text{ meq}\cdot\text{g}^{-1};\ c_0=\frac{7.26}{102.82}$$
$$=0.07061 \text{ meq}\cdot\text{ml}^{-1}.$$

While it is possible, analytically, to solve the desorption equation using a method based on the same principles as in the case of adsorption, it is considerably more involved. It is extremely sensitive both to the accuracy of each of the three or four measured points used, as well as to the slightest departure from the assumed model. For these reasons the usefulness of this method for determining the parameters is purely academic.

TABLE 11. *Data of batch desorption Run #224*

(C. E. Dryden)

Acetic acid: Coconut charcoal:
Stirring rate: 400 rpm Sieve size: (8 on 10)

Temperature: 20 °C

t	c	q
min	*meq·ml⁻¹*	*meq·g⁻¹*
1.0	0.0102	1.190
2.0	.014	1.115
3.0	.0169	1.058
4.0	.0188	1.020
5.0	.0204	0.989
7.5	.0221	.955
10.0	.0243	.912
15.0	.0266	.867
20.0	.0275	.849
30.0	.0282	.835
45.0	.0293	.814
60.0	.0299	.802

For the example used in this illustration, a reasonably fair agreement with the desorption data can be obtained using the approximate values:

$$q_0=2.0 \text{ meq}\cdot\text{g}^{-1}$$
$$k_1=1.0 \text{ ml}\cdot\text{meq}^{-1}\cdot\text{min}^{-1}$$
$$k_2=0.045 \text{ min}^{-1}.$$

It is noteworthy that the magnitude of each of these parameters is consistent with corresponding values derived from adsorption. Equation (13) can now be evaluated. It is first determined by eq (7) that $M=2.138$ under the conditions of the experiment. Next, it is ascertained by use of eq (8) that $N=1.338$. The coefficient of t in the exponent of eq (13) can now be determined as well as the factor:

$$\frac{(M-N)-q_1}{(M+N)-q_1}.$$

Accordingly, the desorption equation reduces to:

$$\frac{0.800-q}{3.476-q}=-0.283\ e^{-0.136t}.$$

It can be seen that as t becomes large, the right side of the equation approaches zero. Therefore, the limiting value of q must be 0.800 in agreement with table 11. At the other extreme the value of q predicted for 1 min is 1.33 compared with 1.190 as seen from the table. The remaining desorption experiments reported by Dryden [5] yield results in substantial agreement with the example given here.

6.2. Resorption

The remarkable versatility of eq (13) cannot be fully appreciated until some examples of resorption are considered. Fortunately, it is not necessary to redesign additional experiments to illustrate these applications.

For the first example, consider desorption Run #224 just discussed. The desorption equation predicts $q=0.81$ meq·g^{-1} for $t=30$ min. Suppose that after desorption had progressed for 10 min, the process were halted by physically separating the adsorbent from solution for an indefinite period of time. Ultimately, adsorbent and solution could be recombined, thus permitting the desorption process to be resumed. Reference to table 11 discloses that when $t=10$ min, 0.912 meq·g^{-1} is the observed value of q which, consequently, would become the new value for q_1 in the resorption process. Neither M nor N would change, since the weight, volume, concentration, etc., were not altered. The new coefficient of the exponential in eq (13) would be:

$$\frac{0.800-0.912}{3.476-0.912}=-0.0437$$

while the only change in the exponent, itself, would be the substitution of $(t-10)$ for t. Almost by inspection, therefore, the new resorption equation could be written:

$$\frac{0.800-q}{3.476-q}=-0.0437\ e^{-0.136(t-10)}.$$

The 30 min point is again calculated to be 0.81 meq·g^{-1}, in agreement with the original desorption equation.

The same treatment can be applied to interrupted adsorption. Consider the illustration given earlier in connection with table 1. If the adsorption had been interrupted after having been allowed to

proceed for, say, 20 min, and the amount adsorbed per gram at that time were considered the new initial conditions; what would the resultant resorption equation become? Again, M and N would be unchanged, but now q_I (instead of being zero as at the beginning of the original experiment) would take on the new value of 0.4667. Immediately, the resorption equation in that instance could be written:

$$\frac{0.566-q}{1.130-q}=+0.150\ e^{-0.0604(t-20)}$$

where the coefficient +0.150 is determined from

$$\frac{0.566-q_I}{1.130-q_I}$$

according to eq (13). The fact that the coefficient 0.150 remains greater than zero shows that the resorption in this case is an adsorption process.

If after 20 min in this same illustration, the solution had been diluted by adding water until its volume, V, became, say, 500 ml the situation would have changed considerably. While q_I would still be 0.4667, the initial concentration c_I would now become (0.0166)/5 or 0.00333 meq·ml^{-1}. The new value of c_0 according to eq (12) would be 0.00613. It would now be possible to recompute M from eq (7) and then to redetermine N from eq (8). The new values would be $M=0.947$; $N=0.506$. The resorption equation would then reduce to

$$\frac{0.441-q}{1.453-q}=-0.0264e^{-0.0217(t-20)}$$

and since the coefficient is now negative, the resumed process would have changed from adsorption to desorption. Clearly, if the degree of dilution had been but slight, the resorption would have continued as an adsorption process but to a diminished extent.

It is instructive to select the final illustration from an experiment cited by Bürgers [4] in referring to a paper by Freundlich [6] published nearly 60 years ago. Freundlich compared two batch adsorption runs using 1g of blood charcoal as the adsorbent in each run and acetic acid as the adsorbate. The second run used twice the initial concentration, but only half of the volume. However, after a reasonably long period of time, the second batch was diluted with an equal volume of water and stirring was continued for an additional hour—presumably long enough to re-establish equilibrum. Both runs ended under comparable conditions, yet the final solution concentration was slightly lower in the second experiment than in the first. Freundlich ignored the difference and used the illustration to prove the reversible nature of adsorption. It should be possible in light of the present theory to re-examine the data quantitatively in an attempt to account for the observed discrepancy.

Freundlich's measurements are shown in table 12. For his first batch, the initial value of c was also c_0, since all of the acetic acid was in solution. The final condition corresponded to a q value of 0.802 meq·g^{-1} as indicated in the last column of table 12. In his second batch before dilution, c_0 was 0.1376 meq.ml^{-1} while after dilution, it reverted back to 0.06880 meq·ml^{-1}. The final concentration of the second batch after dilution corresponded to $q=0.816$ meq·g^{-1}.

If the present theory applies to Freundlich's experiment, it ought to be possible to assign reasonable values to the three parameters, q_0, k_1, and k_2, consistent with results already discussed for similar systems under substantially the same conditions. If it is estimated that

$q_0=1.07$ meq·g^{-1}.
$k_1=30.0$ ml·meq^{-1}·hr^{-1} (0.5 ml·meq^{-1}·min^{-1})
$\frac{k_2}{k_1}=0.02$ meq·ml^{-1},

the sorption equations applicable to both batches are determined as follows:

TABLE 12. *Freundlich's experiment*

	W	V	t	c	q
	g	*ml*	*hr*	*meq.ml*$^{-1}$	*meq.g*$^{-1}$
First batch					
Initial state	1.0	100.0	0	0.06880	0
Final state	1.0	100.0	20.5	.06078	0.802
Second batch					
Before dilution:					
Initial state	1.0	50.0	0	.1376	0
Final state	1.0	50.0	21.0		( )
After dilution:					
Initial state	1.0	100.0	21.0		( )
Final state	1.0	100.0	22.0	.0064	0.816

For the first batch:

$$M=\frac{100}{2}\left[0.02+0.06880\left(1.000+\frac{1.00\times1.07}{100\times0.06880}\right)\right]=4.975$$

and

$$M^2-N^2=(1.07)(6.880)=7.362 \qquad \text{so, } N=4.170$$

hence,

$$\frac{M-N}{M+N}=+0.0880.$$

Finally, the adsorption equation takes the form:

$$\frac{0.805-q}{9.145-q}=0.0880e^{-2.502t}$$

which may be solved for q when $t=20.5$ hr to give $q=0.805$ meq.g^{-1} compared with 0.802 in table 12.

For the second batch—before dilution:

$$M=\frac{50}{2}\left[0.02+0.1376\left(1.000+\frac{1.00\times1.07}{50\times0.1376}\right)\right]=4.475$$

$M^2-N^2=(1.07)(6.880)=7.362$, as before; but now $N=3.559$

so in this instance $\frac{M-N}{M+N}=0.1140$. Therefore, the adsorption equation applicable to this case becomes:

$$\frac{0.916-q}{8.034-q}=0.1140e^{-4.271t}.$$

This would require that at the time of dilution; namely, when $t=21.0$ hr, the value of q would have been 0.916 meq.g^{-1} (although it was not actually measured).

For the second batch—after dilution: The addition of 50 ml of water would have the effect on M and N of causing them to revert back to the values 4.975 and 4.170, respectively, which applied to the first batch. This is evident from the definitions of M and of M^2-N^2 in eqs (7) and (8). The only difference is that q_1 would now be 0.916 meq.g^{-1} where originally it was zero. Therefore, the coefficient of the exponential becomes:

$$\frac{0.805-0.916}{9.145-0.916}=-0.0135$$

which, being negative, means desorption. The final resorption equation can therefore be written by inspection:

$$\frac{0.805-q}{9.145-q}=-0.0135e^{-2.502t}.$$

The final condition after dilution and resorption was reached 1 hr later. By substitution of $t=1.0$ in this equation, it is found that $q=0.814$ meq.g^{-1} which is in good agreement with 0.816 in table 12.

7. Summary

Batch adsorption from solution can be characterized and interpreted in terms of the parameters q_0, k_1, and k_2 whose values best fit the general adsorption equation, eq (6).

In the special case where the desorption rate constant can be neglected, a simplified two-parameter equation is adequate for adsorption. Short-cut methods have been found for evaluating the parameters from the data:

(a) when the adsorption is a function of time

or

(b) when the adsorption is a function of both W/V and c_0.

Values of the parameters can also be determined for the general case where the adsorption data are time dependent.

The characteristic parameters determined from batch adsorption are in agreement with corresponding values determined from column adsorption.

Some deviations in the results have been observed in certain instances and can be explained in terms of a slight departure from the theoretical model.

Even the general adsorption equation, eq (6), can be considered as a special case of eq (13) which, differing only in initial conditions but utilizing the same set of parameters, will, in fact, predict with equal facility desorption, interrupted sorption, and sequential combinations of adsorption and desorption as the case may be.

8. References

[1] W. V. Loebenstein, Proc. of Fifth Tech. Sess. on Bone Char, 253 (1957).
[2] W. V. Loebenstein, J. Res. NBS **66A** (Phys. and Chem.) No. 6, 503 (1962).
[3] C. E. Dryden and W. B. Kay, Ind. Eng. Chem. **46,** 2294 (1954).
[4] W. G. Burgers, Rec. Trav. Chim. **63,** 46 (1944).
[5] C. E. Dryden, Ph.D. thesis: The kinetics of sorption of acetic acid in water-carbon systems (The Ohio State University, 1951).
[6] H. Freundlich, Z. Physik. Chem. **57,** 385 (1907).

(Paper 67A6–248)

JOURNAL OF RESEARCH of the National Bureau of Standards—A. Physics and Chemistry
Vol. 67A, No. 6, November–December 1963

Color Phenomena in Polymer Fracture*

Sanford B. Newman and Irvin Wolock**

(July 18, 1963)

Thin layers derived from the matrix are produced in the fracture plane of some polymers prior to ultimate failure. A certain amount of the evidence would indicate that these layers consist of an oriented array of molecules. Fracture isolates these molecular segments in a thin film with physical properties differing from that of the matrix in which they originated. These films produce interference phenomena which in some cases are useful in elucidating structure and origin.

1. Introduction

It is difficult to ascertain when the strong colors on the fracture surfaces of polymers were first observed. In 1956 Busse, Orowan, and Neimark [1][1] exhibited some surfaces produced by fracturing large notched plates of polymethyl methacrylate. About a year before, somewhat more diffuse colors had been observed on tensile specimens broken under static conditions [2] at the National Bureau of Standards [3]. Although Wolock et al. [4] and Berry [5] both reported observing colors associated with specific fracture markings, the first detailed discussion of the phenomenon was published by Higuchi [6]. Many of the same observations were made independently and reported by Wolock et al. [7] and Berry [8].

It is entirely possible, of course, that colored fracture surfaces were observed earlier than the period mentioned. Higuchi, for example, indicates that the experiments of Benbow and Roesler [9] must have produced such surfaces. Thus far almost all colored surfaces that have been studied have been produced on polymethyl methacrylate.

2. Fracture Color Patterns

The colors arising from interference in subsurface cracks are not considered in this discussion. Although they produce an optical effect which often appears quite close to the surface its origin is obvious and easily ascertained.

There is considerable variety in the color patterns obtained by various fracturing techniques. Those found on statically tested tensile specimens are weak, usually located about the periphery of the mirror area and are found on relatively few specimens. They are not usually associated with an individual structure, such as parabolas, but cover an area which encompasses a number of figures or structures without any specificity of color or tint for each element. Fractures exhibited by Busse and his coworkers were more brilliant and formed bands transverse to the direction of fracture. Higuchi used notched sheets 3–5 mm thick and 40 mm wide. The exact conditions of test are not described. His figures show a variety of patterns. Most of the conic sections are differentiated in color from their surround and occasional transverse bands cause a reversal of colors in the banded area. He finds that the colors on the two fracture surfaces are generally complementary and that the red areas are raised and the green are depressed relative to the specimen matrix.

Wolock [7] produced similar colors on fracture surfaces of polymethyl methacrylate specimens which had been broken by rapid overstress. Films of diffuse color were formed on surfaces of cast polystyrene broken in the same fashion. Specific colors, however, were not related to the individual structures on the polystyrene fracture faces. Somewhat later, Wolock noted the intense differential color produced on the relatively smooth fracture surfaces of specimens of polymethyl methacrylate tested for resistance to crack propagation. Many of the observations to be discussed were made on fractures produced in these specimens (fig. 1), which were broken by loading through a cross head moving at 0.008 mm/sec (0.02 in./min). These contain four types of color patterns or characteristics (fig. 9). The first is observed in the slow-growth area and actually consists of two types of patterns, namely, multicolored areas (fig. 9b) and single-colored areas (fig. 9a). The next pattern (fig. 9c) is composed of irregularly shaped elongated figures. These figures develop, in the third pattern of this series (fig. 9d) into oriented forms that lead, in many cases, into parabolas. The last area (fig. 9e) is darker (less reflective) with little or no color and containing many crowded parabolas in which only the foci are very distinct. The significance of the geometric markings on the fracture surfaces have been dealt with extensively in the literature [10–12] and will not be discussed in this paper.

A characteristic blue color is also found on fracture surfaces of hot-stretched polymethyl methacrylate. These surfaces are produced by cleaving the stretched sheets through the thickness dimension. The colors are not associated with specific markings.

*Presented at the Symposium on Adhesion and Cohesion, General Motors Corporation Research Center, Detroit, Mich. Color plates were made available through the courtesy of the General Motors Corporation.

**Naval Research Laboratory.

[1] Figures in brackets indicate the literature references at the end of this paper.

3. Optics of Color Formation

It can be demonstrated that the strongly colored areas of the fracture surfaces produced in crack propagation specimens are covered with a soft thin film. The presence of this film is a prerequisite for the development of color. In figure 10 a soft swab has been wiped across a fracture surface with removal of essentially all of the tint. Under room conditions the color will disappear from crack propagation specimen surfaces over a period of months. The time for color disappearance varies greatly, however. Colors on ordinary tensile specimens and on cleaved, stretched material faded in the course of a few weeks, whereas those of Busse et al. [1] were still intense after almost a year. Storage at temperatures of 50 to 60 °C causes rapid loss of color in crack propagation specimens in well under an hour. Loss of color under these circumstances is not necessarily associated with complete loss of the film. Even when the colors have completely disappeared an oily film still occupies the surface. The disappearance of color by aging or heating takes place by fading of the original tint without any pronounced color shift [6, 7].

Concentrated vapors of a number of organic solvents such as toluene and methyl chloride will often eliminate colors in a matter of minutes. In this case a change in tint is involved as can be seen in figure 11. The first color changes seem concentrated along level difference lines and a few other structures on the fracture face.

Another method of affecting color intensity of parts of the film is by exposure to low pressure. This can be demonstrated by placing one of the matching surfaces of a crack propagation specimen in a container maintained at approximately $1 \cdot 10^{-5}$ mm Hg pressure. After removal it will be found that almost all of the color is removed from the slow growth area. The color intensity over the remainder of the fracture is apparently the same as that of the matching surface which had been stored outside of the vacuum chamber. Microscopic examination and micromanipulation of the film on the slow-growth area of the fracture surface indicates that this portion is thicker than the rest of the film.

The fact that much of the surface is little affected by high vacuum makes it possible to apply the methods of multiple-beam interference microscopy to the study of the color phenomenon. Figure 2 is a multiple-beam interferogram of a portion of a fracture produced in a crack propagation specimen. The field shows a portion of the first parabola-containing area. A layer of silver has been deposited over the surface film and the fringe displacement over the composite surface is shown. It would appear that the adjacent areas covered by the contribution of different secondary fractures are consistently displaced by about 1500 Å. When the color is removed by aging or heating before the specimen is prepared for interference microscopy this displacement remains about the same.

Assuming first-order interference Higuchi [6] has estimated a film thickness range of 400 to 700 mμ from the observed colors. Using a soft swab to remove the film produces a swath with a depth of less than 200 mμ in the surface as measured by multiple-beam techniques (fig. 3). This experiment was repeated by focusing the radiation from a zirconium arc lamp on a small area of the fracture surface until all the color had disappeared and continuing the treatment until the film was scarcely detectable in the irradiated portion by microscopical examination. The depth of the circular depression was again found to be somewhat less than 200 mμ. Although the film in the slow growth area may exceed this figure, its sensitivity to vacuum prevents direct measurement. Figure 3 also shows the increased reflectivity of the treated area. Apparently swabbing or heating tends to produce a surface that is smoother than the original face of the film.

The presence of the film led Higuchi [6], Wolock et al. [7], and Berry [5, 8] to postulate its formation by the pulling out of chain ends and the scission of chains. These segments would have been extended in the fracture process and thus could have a somewhat different density than the matrix. The chain segments in only a relatively small thickness of material would be extended during the fracture process. Oriented layer and matrix would differ sufficiently in refractive index to lend themselves to the development of thin film interference as shown figure 4. In any given region, an average height would predominate which would result in the color observed. As the chain segments composing the film relax, the distribution of heights remains the same but the number of segments remaining in the film decreases so that the same color is present but is diminished in intensity. This would account for the fading observed with no change in color. Solvent vapors produce different changes in the structure reflected by the change in color withdrawal. The derivation of the film from the matrix would lead to a structure whose properties would differ from the matrix to the greater degree at the exposed face and tend to blend into the matrix at the other limit. Although the blending section close to the matrix could contribute to the optical effect, it would be difficult to establish its boundary by the methods described. Hence failure to realize the theoretical film thickness is probably to be expected.

Tolansky's thin film technique [13] permits corroboration of this explanation of the origin of the color phenomenon with a simple model. A fracture surface with the colors removed by aging or some other method is covered with a totally reflected film of silver *in vacuo*. A drop of a dilute solution of Canada balsam in xylene is placed on the silvered surface and allowed to drain by tilting the specimen. The surface of the film of Canada balsam in contact with the fracture surface replicates the topography of the surface. The upper surface of the film, however, does not contour the fracture surface but stretches itself into a single plane for considerable distances. On illuminating such a surface two-beam interference fringes will be formed. Figure 12 illustrates a portion of a fracture colored by thin

film interference. The wrinkling probably caused by solvent attack on the silver and plastic substrate is noticeable but otherwise there is considerable similarity to the fracture-produced colors. Even the slight coloring observed in the rough, low-reflecting zone is almost identical (fig. 13) with that observed on the original fracture surface.

Considerable fringe broadening is apparent in the interferogram in figure 2. This is at a minimum in the initial, smooth, slow growth area and increases toward the crowded parabola portion. An electron micrograph of these two areas, figures 5 and 6, shows the change in surface granularity responsible for the fringe broadening. Although the surface is sufficiently smooth up to the first parabolas to permit the use of multiple-beam interference, the final surface is so rough that the method fails. Figure 6 reveals this surface to be sculptured with thin leaf-like projections. It is doubtful that a fragile film in the millimicron thickness range could be formed there. Only isolated fragments of color are found in this area.

Replicas for electron microscopy were produced by allowing a dilute solution of methyl cellulose to dry on the fracture surface. Despite its limited resolution, which is well illustrated in figure 6, this method was chosen because it would impose the least abuse on the polymer matrix. On stripping the film from a surface originally bearing color, the surface was found to be colorless. A carbon replica was made from the negative and shadowed by vacuum deposition. The loss of color would be caused either by the stripping of all or part of the interference film with the cellulosic replica or by disorienting it with the replicating solution.

Before replicating the surfaces in figures 5 and 6, an attempt was made to remove thoroughly the surface film by heating for 96 h at 50°C. For purposes of comparison replicas were also prepared from a surface bearing bright interference colors. In most cases the replicas from the unheated colored surfaces bore numerous droplets over a considerable portion of the fields examined, as in figure 7. It would seem that a portion of the film is removed and subsequently disrupted by the replicating process. These observations, moreover, pinpoint one of the difficulties encountered in preparing high resolution replicas of a polymer fracture.

This discussion has been limited almost entirely to polymethyl methacrylate. Attempts to produce color on a number of other polymers by varying loading rates and thermal conditions have been largely unsuccessful. However, polystyrene has occasionally yielded colored surfaces, as shown in figure 14.

4. Color Patterns in Crazing

Niegisch [14] has recently convincingly demonstrated the presence of oriented material in craze cracks produced in long-time tests of polycarbonates. Although this polymer did not exhibit brittle fracture under the test conditions, the ultimate elongation being about 100 percent, some evidence of similar "craze matter" in polystyrene and polymethyl methacrylate was also presented. From these data, Spurr and Niegisch [15] have offered an attractive theory for the development and structure of craze cracks in thermoplastics. Probably the most important contribution of their observations is the support they provide for the conclusion that the appearance of crazing does not mean the end of structural integrity or continuity in the stressed specimen.

The matter in polycarbonate cracks is visible by difference in refractive index probably coupled with some scattering from micropores. However, during some routine tests of standard tensile specimens [2] of acrylonitrile-styrene copolymer, a striking color phenomenon was also noted in the craze cracks of this material, as seen in figure 15. These specimens were injection molded and the stressed skin was apparently responsible for the formation of internal cracks which sometimes encompassed one-half or more of the specimen cross section. These tensile specimens, when loaded at a head speed of 0.008 mm/sec have the load-elongation characteristics shown in figure 8. The large internal cracks suddenly appear apparently full grown at the top of the straight line portion of the curve but without any discontinuities in loading. Ultimate failure occurs through one of these large cracks.

It was originally assumed that the optical effect was due to an interference system involving a void. On examining the fracture surface, however, it was found that a pattern similar to that noted in the intact craze cracks was found on one surface or parts of one surface, as shown in figure 16. The matching surface was devoid of color. Colors observed in the intact cracks are more intense than those found on fracture surfaces. Critical microscopical examination established the presence of a film on the color-bearing surface. Unlike the film found on polymethyl methacrylate fracture surfaces, the film is integral and shears cleanly from one of the crack faces. Edges of the film are sometimes curled free of the matrix on which they lie but mechanical removal of any significant amount of film appears impractical.

If the film-bearing surface of the fracture is examined at higher magnification, some additional details can be resolved. As in the intact cracks the peripheral area of the fractured craze is covered with fringes of equal thickness. The film in figure 17 bears first to fourth order colors which indicates a thickness of approximately 2 μ. Thicknesses of this magnitude are not uncommon although many cracks with much thinner films are found. In general, however, the film is much thicker than those found on the fracture surfaces discussed in the earlier section.

The center of the film-bearing area is likely to show more disorder. Colors are bright and the fringe pattern has contours that seem unrelated to film thickness. Such an area occupies about half the field in figure 18. The film is wrinkled and stretched, especially in the regions surrounding the

small holes. Evidently it has been slightly dislodged from the substrate during fracturing.

In a few small areas the conic sections characteristic of brittle failure sculpture the face of the fractured craze crack as shown in figure 19. If the crack surfaces are connected by a thin layer of oriented molecules as originally suggested by Bessonov and Kuvshinskii [16] and developed by Spurr and Niegisch [15], the connection may not be as tenuous as might be suggested by a consideration of the properties of the film on polymethyl methacrylate surfaces. Besides its association with the brittle mode of failure, the crack material is much more resistant to heat, aging, and solvents. Exposure in an oven at 70 °C for 48 h produced little change in the appearance of the film on the acrylonitrile-styrene copolymer fracture surface. Prolonged heating at this temperature caused some fading of the colors and a great increase in the pitting, which is visible in the periphery of the film in figure 17. Colors in the intact cracks were unaffected by weeks of heating at 70 °C or exposure to solvent vapors that did not cause gross matrix deterioration.

Spurr and Niegisch [15] detected "craze matter" in cracks of polystyrene and polymethyl methacrylate. Its presence was much more difficult to demonstrate than in polycarbonate and it was possible to record photographically. Recently,however, the description of the work of Bessonov and Kuvshinskii [17] became available. They had observed phenomena closely related to those described in our acrylonitrile-styrene copolymer in specimens of "annealed polystyrene." Their specimens with a section of 2×2 mm and a free length of 15 mm were maintained at a temperature of 110 °C for 30 min and then cooled rapidly by plunging them into liquid nitrogen. These specimens were then loaded to failure at a rate of deformation equal to 0.04 mm/sec. The pretreatment resulted in the formation of a stressed skin and a 20 percent increase in tensile strength. Failure was preceded by the formation of large internal cracks as in the acrylonitrile-styrene copolymer. They report that the material filling these cracks remains on the fracture surface. Part of this forms interference fringes and clings to the matrix but part can be stripped. They suggested that the film consists of the bundles of linear polymers discussed by Hsiao and Sauer [18] and Kargin et al. [19].

Since certain details necessary for comparison with previous results were not given in this report, the work was repeated using standard tensile specimens [2]. The preliminary heating was extended to 2 hr in view of the larger cross section. These specimens were loaded to failure at a head speed of 0.008 mm/sec Large internal cracks formed shortly before failure and failure occurred through cracks encompassing one-third to one-half of the cross section. No color phenomenon was visible in any of the cracks on gross examination.

On microscopically examining the fracture surface a few faint interference bands could be observed. The film responsible for these adhered strongly to one of the surfaces. The remainder of the crack was partly covered on both faces by a transparent film. The film was partly detached and partly loosely attached to the surface. It was easily stripped and pieces 5 or 6 mm^2 were removed with forceps. The film was lower in refractive index than the matrix. It appears to have good physical properties and the relatively large areas available should permit the use of transmission electron microscopy, infrared spectroscopy, and other instrumental techniques in elucidating their structure and mode of formation.

Attempts to produce large cracks in specimens of polymethyl methacrylate by this technique have thus far been unsuccessful.

5. Summary

Thin layers derived from the matrix are produced in the fracture plane of some polymers prior to ultimate failure. A certain amount of the evidence would indicate that these layers consist of an oriented array of molecules. Fracture isolates these molecular segments in a thin film with physical properties differing from that of the matrix in which they originated. These films produce interference phenomena which in some cases are useful in elucidating structure and origin.

The suggestion has been made that these oriented layers provide structural continuity in polymers after optical inhomogeneities are produced by stress. This is supported, at least superficially, by observations on polycarbonate and acrylonitrile-styrene copolymer. In these materials intact craze cracks appear to be filled with homogeneous or oriented material. The film observed in intact cracks of "annealed" polystryene, however, shows some disorder. Folds and wrinkles are almost always present and it is difficult to attribute any load-bearing function to this structure.

It is possible that the two types of film formation may not be as closely related as has been assumed during much of this discussion. Further experimentation may provide the necessary data for supporting the assumption. If the mechanism proposed for the formation of these films is correct, we would expect to detect them on a wide range of polymers when failure is produced under suitable conditions. The search for, and study of, these films is continuing.

The authors acknowledge valuable discussions with Dr. Samuel G. Weissberg.

6. References

[1] W. F. Busse, E. Orowan, and J. E. Neimark, Morphology of Fractures in Polymethyl Methacrylate, Am. Phys. Soc., Philadelphia, Pa., March 1957; also Symposium on Ultimate Strength of Polymers, Brooklyn, Nov. 1956, Polytechnic Institute of Brooklyn.

[2] Method of Test for Tensile Properties of Plastics, Am. Soc. for Testing Materials, D-638.

[3] S. B. Newman and I. Wolock, unpublished data.

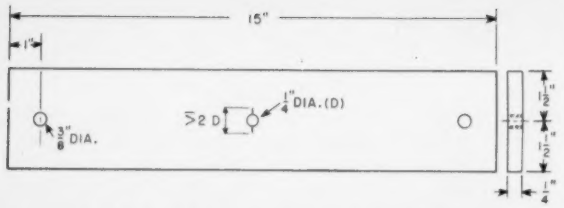

FIGURE 1. *Schematic diagram of crack propagation specimen.*
Small variations in overall dimensions and position of loading pin holes do not significantly affect fracture characteristics.

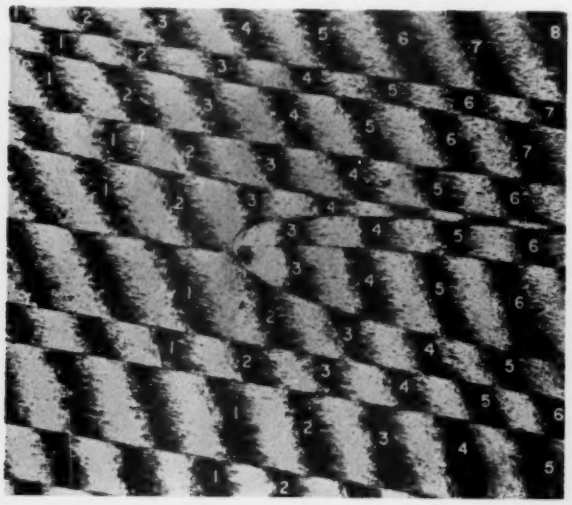

FIGURE 2. *Multiple-beam interferogram of parabola-bearing portion of a polymethyl methacrylate crack propagation specimen fracture surface.*
Numbers identify components of the same fringe. Source was the 5461 Å mercury line.

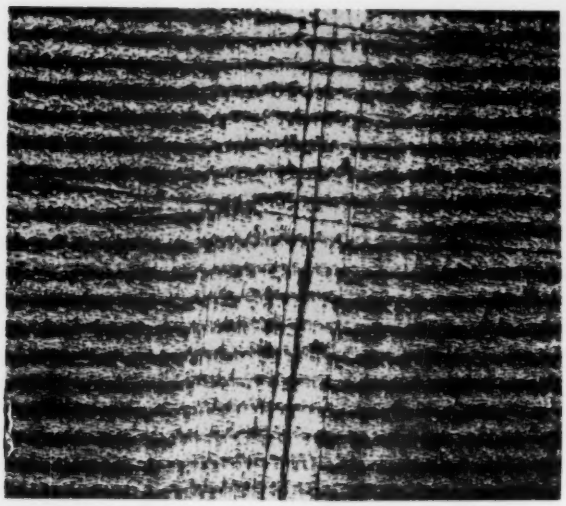

FIGURE 3. *Multiple-beam interferogram of the swabbed area of the fracture surface of a crack propagation specimen of polymethyl methacrylate.*
Source was the 5461 Å mercury line.

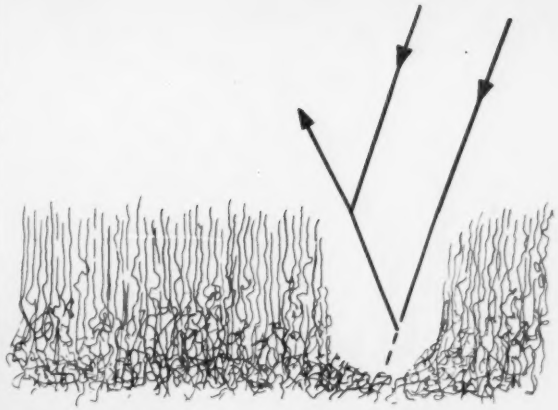

FIGURE 4. *Diagrammatic representation of interference in the oriented film of the fracture of polymethyl methacraylate.*
(Modified from Higuchi [6])

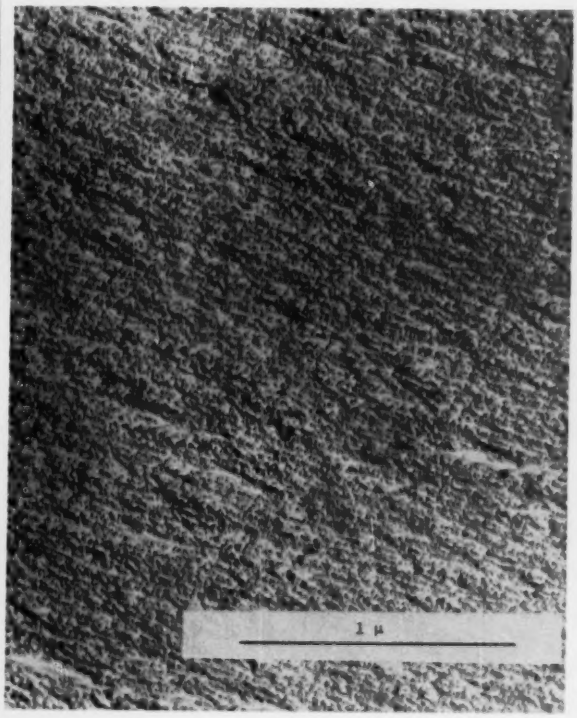

FIGURE 5. *Electron micrograph of a replica of the fracture surface of a crack propagation specimen of polymethly methacrylate.*
The area shown is from the slow-growth region.

[4] I. Wolock, J. A. Kies and S. B. Newman, Fracture Phenomena in Plastics, in B. L. Averback, D. K. Felbeck, G. T. Hahn and D. A. Thomas (editors), Fracture, p. 250 (Technology Press and Wiley, New York, 1956).

[5] J. P. Berry (discussion) in B. L. Averbach, D. K. Felbeck, G. T. Hahn and D. A. Thomas (editors), Fracture, p. 263. (Technology Press and Wiley, New York, 1959).

699-332—63——9

FIGURE 6. *Electron micrograph of a replica of the fracture surface of a crack propagation specimen of polymethyl methacrylate.*
The area shown is from the crowded parabola region.

FIGURE 7. *Electron micrograph of a replica of a fracture surface of polymethyl methacrylate broken by rapid overstress.*
The surface is covered by droplets derived from the surface film.

[6] M. Higuchi, On the Color of the Fracture Surface of Polymethyl Methacrylate Plate, Colorless and Transparent in Itself, Repts. Research Inst. Appl. Mech., Kyushu University VI, No. 24, (1958).
[7] I. Wolock, S. B. Newman, and S. G. Weissberg, Color Phenomena in Polymethyl Methacrylate Fractures, Meeting Div. of High Polymer Physics of Am. Phys. Soc., Detroit, Mich., (March 1960).
[8] J. P. Berry, Nature, **171,** 91 (1960).
[9] J. J. Benbow and F. C. Roesler, Proc. Phys. Soc. (London), B **70,** 201 (1957).
[10] J. A. Kies, A. M. Sullivan and G. R. Irwin, J. Appl. Phys. **21,** 716 (1950).
[11] F. Zandman, Étude de la Déformation et de la Rupture des Matières Plastiques, Publ. sci. et tech. ministère de l'Air (France), No. 291, (1954).
[12] V. F. Schwarzl and A. J. Staverman, Bruchspannung und Festigkeit von Hochpolymeren, in H. A. Stuart (editor), Die Physik der Hochpolymere, **IV,** 165 Springer Verlag, Berlin (1965).
[13] S. Tolansky and M. Omar, Nature **170,** 81 (1952).
[14] W. D. Niegisch, The Morphology of Crazing in Some Amorphous Thermopolastic Polymers, Polymer and Fiber Microscopy Soc. Meeting, Norwalk, Conn., (May 1961).
[15] O. K. Spurr and W. D. Niegisch, Stress Crazing of Some Amorphous Thermoplastics, J. Appl. Polymer Sci., **6,** 585 (1962).
[16] M. I. Bessonov and E. V. Kuvshinskii, Fiz. Tverd. Tela, Akad. Nauk S.S.S.R., Sbornik Statei, **1,** 1321 (1960).
[17] M. I. Bessonov and E. V. Kuvshinskii, Vyskomolekulyarnye Soediniya, 1 (1959) 1561.
[18] C. C. Hsiao and J. A. Sauer, J. Appl. Phys., 21, 1071 (1950).
[19] V. A. Kargin, A. I. Kitaigorodskii and G. L. Slonimskii, Kolloid. Zhur., **19,** 131 (1957).

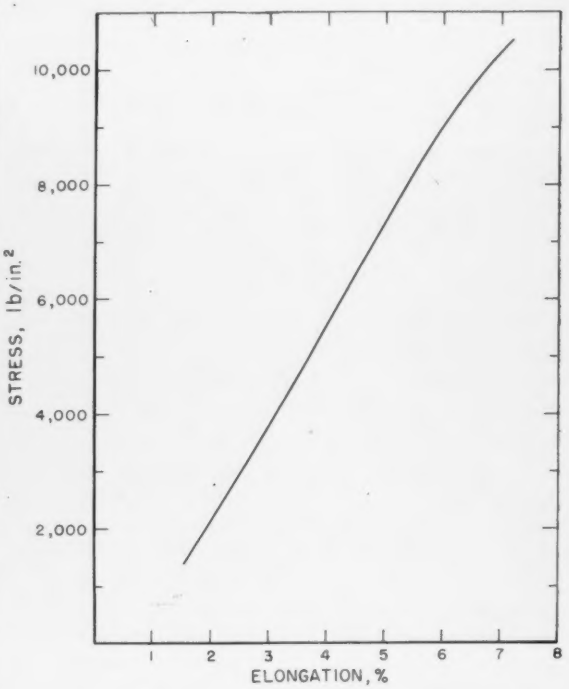

FIGURE 8. *Stress-elongation characteristics of acrylonitrile-styrene copolymer.*

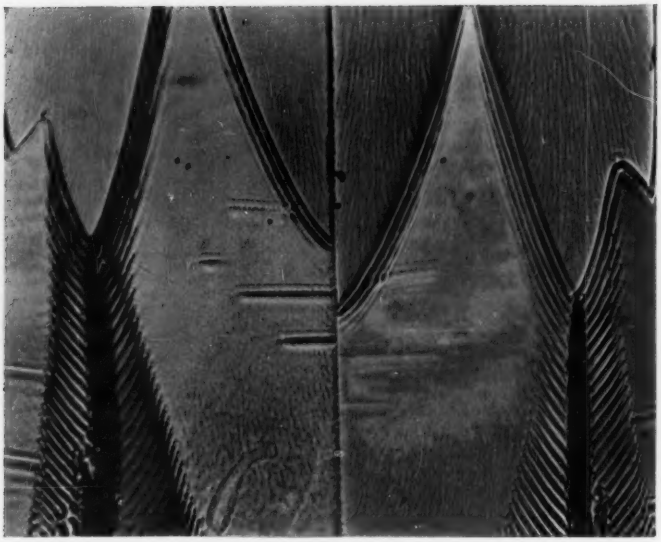

FIGURE 9a. *Single colored area in the slow-growth region of a fracture produced in a crack propagation specimen of polymethyl methacrylate.*

The matching faces are shown side by side.

FIGURE 9b. *Multicolored area in the slow-growth region of a fracture produced in a crack propagation specimen of polymethyl methacrylate.*

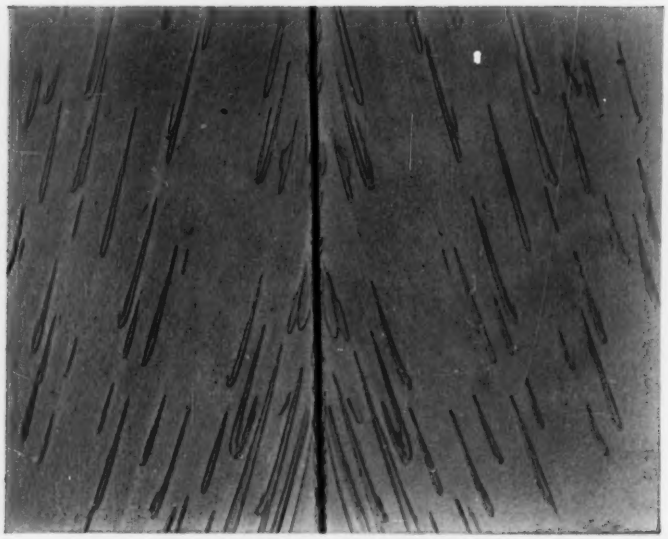

FIGURE 9c. *Area of irregularly shaped elongated figures on a fracture surface produced in a crack propagation specimen of polymethyl methacrylate.*

The matching faces are shown side by side.

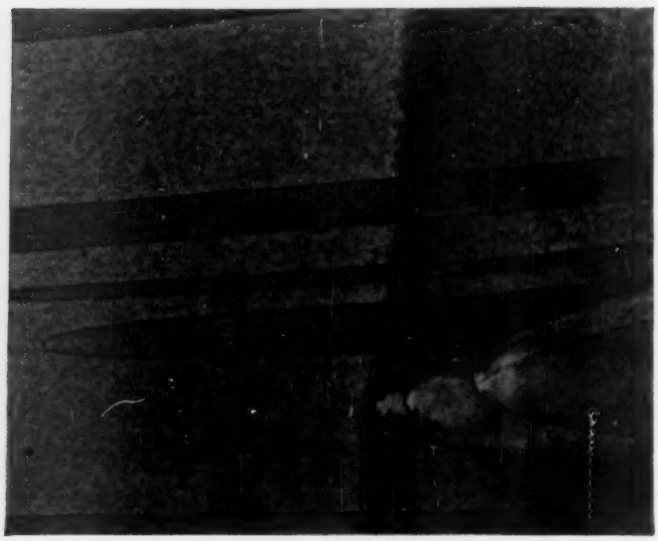

FIGURE 9d. *Detail from an area on the fracture face of a crack propagation specimen of polymethyl methacrylate in which the elongated figures merge into the parabola-containing region.*

Note the same structures bearing complementary colors on opposite sides of the transverse color interface.

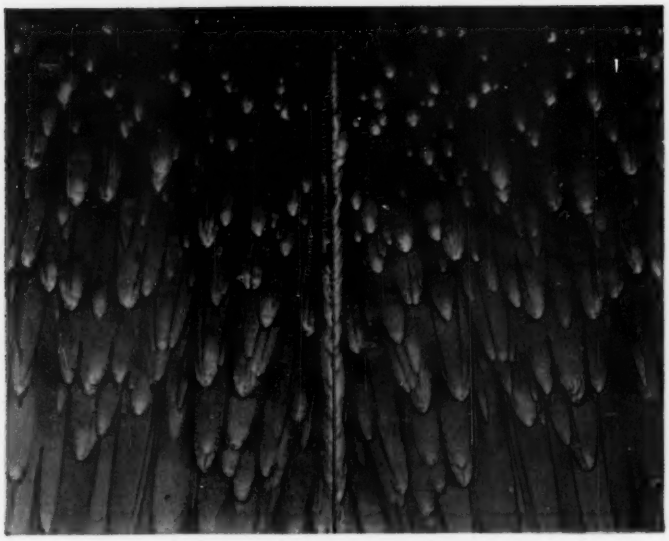

FIGURE 9c. *Area of crowded parabolas on a fracture surface produced in a crack propagation specimen of polymethyl methacrylate.*

The matching faces are side by side.

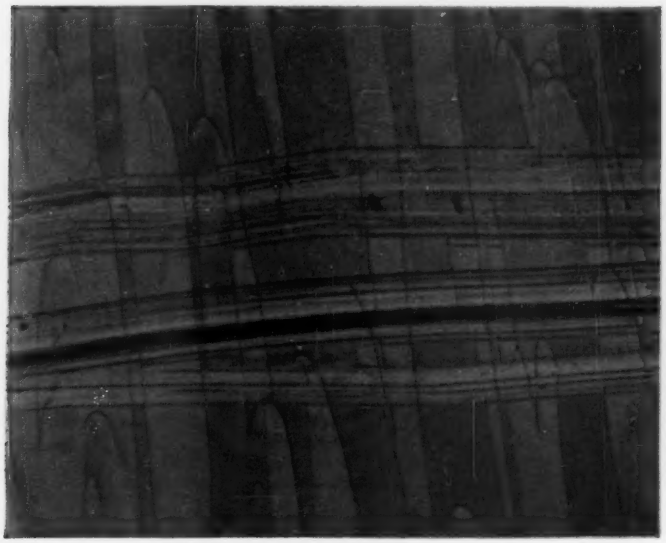

FIGURE 10. *Area of the parabola-bearing region on the surface of a fracture produced in a crack propagation specimen of polymethyl methacrylate.*

A soft swab has produced swaths through the surface film. Note the loss of color in the swaths which have not disturbed the geometric structures.

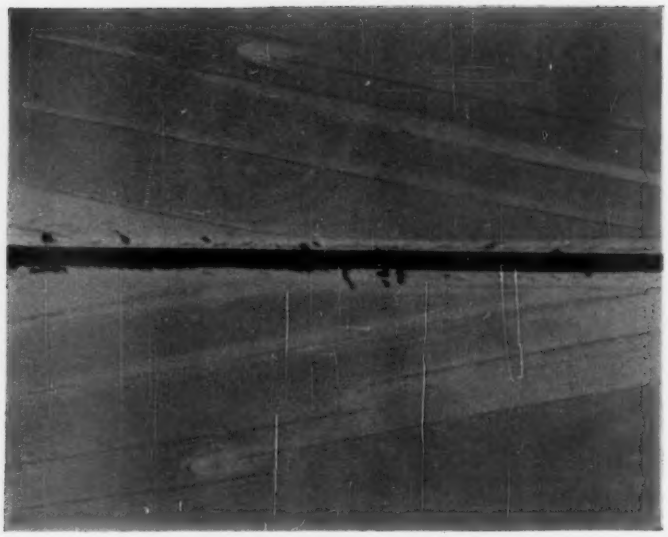

FIGURE 11. *Part of the surface of a fracture produced in a crack propagation specimen of polymethyl methacrylate.*

The surface shows the effect of exposure to vapors of methyl chloride (upper half). The lower section is the untreated matching surface.

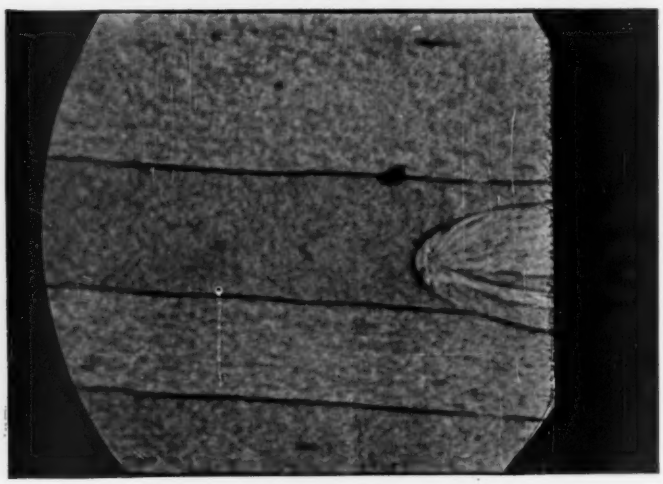

FIGURE 12. *Fracture surface colors produced by thin-film interference.*

A reflecting layer of silver was deposited on the fracture surface *in vacuo* and subsequently a thin solution of Canada balsam was deposited over the silver.

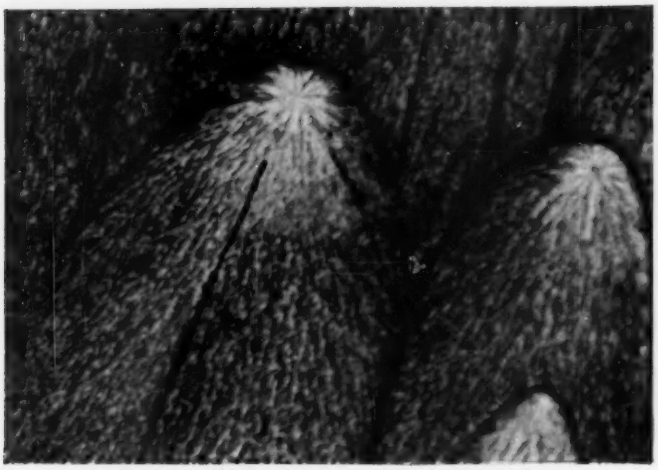

FIGURE 13. *Thin-film interference on the crowded parabola portion of the surface of a fracture produced in a crack propagation specimen of polymethyl methacrylate.*

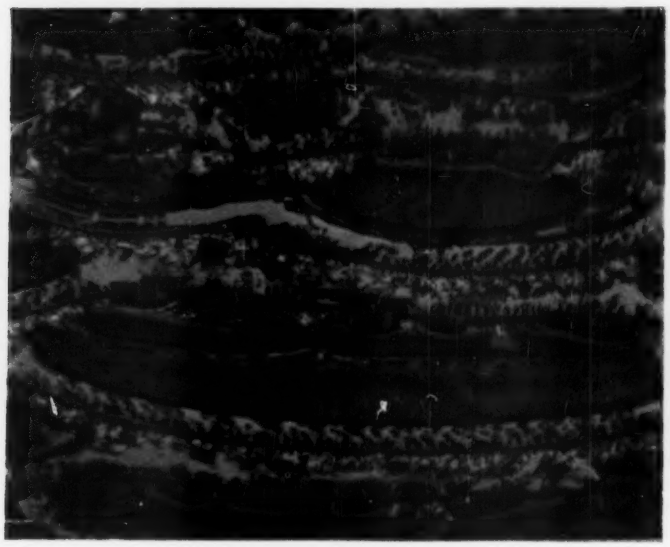

FIGURE 14. *Fracture surface of a tensile specimen of molded polystyrene.*

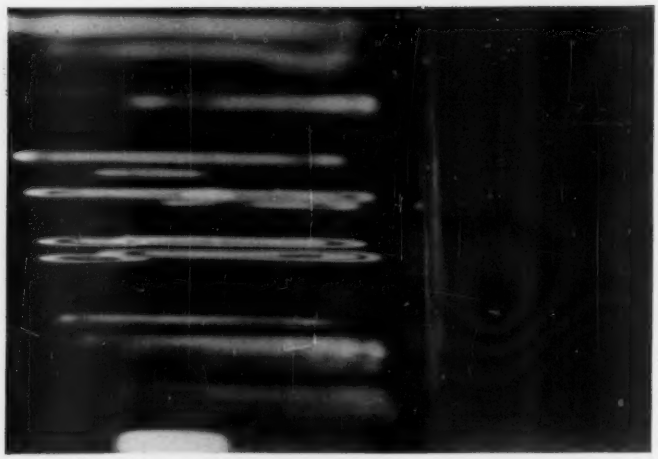

FIGURE 15. *Large internal craze cracks in a tensile specimen of molded acrylonitrile-styrene copolymer.*

The specimen was loaded to failure through a crosshead moving at 0.02 in./min.

FIGURE 16. *Matching fracture faces of a tensile specimen of acrylonitrile-styrene copolymer.*

The specimen was loaded to failure through a crosshead moving at 0.02 in./min.

FIGURE 17. *Detail from a fractured craze crack of acrylonitrile-styrene copolymer.*
The periphery of the crack is in the upper left-hand corner. The film displays fringes of at least four orders.

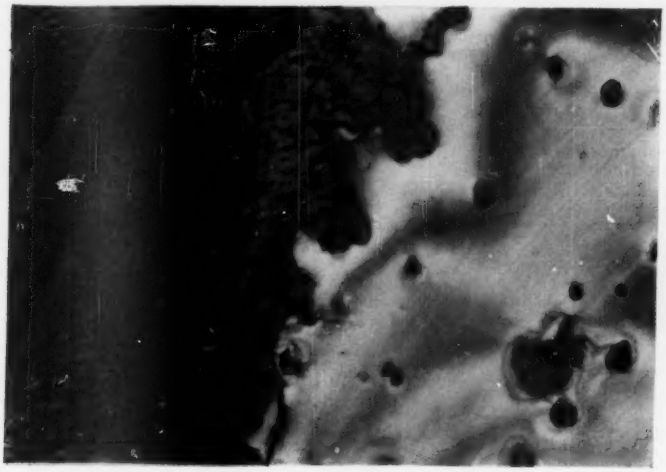

FIGURE 18. *Detail from a fractured craze on acrylonitrile-styrene copolymer.*
The area bearing fringes of equal thickness is at the left. The bright fringes cover a portion of the film which is slightly wrinkled and also stretched in the vicinity of the holes.

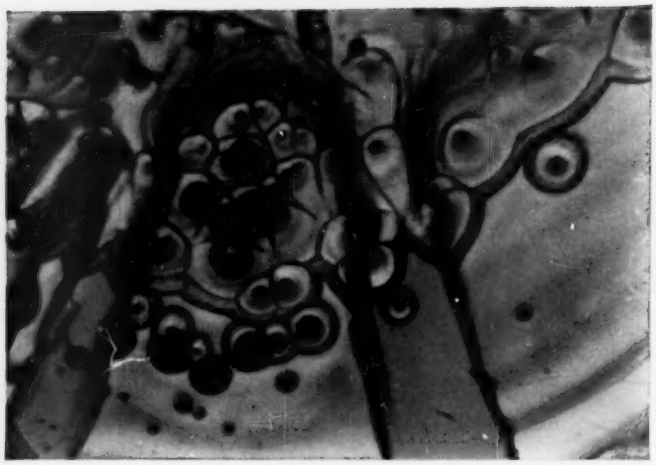

FIGURE 19. *Detail from the center of a fractured craze crack of acrylonitrile-styrene copolymer.*

Conic sections characteristic of brittle failure are associated with the surface film.

JOURNAL OF RESEARCH of the National Bureau of Standards—A. Physics and Chemistry
Vol. 67A, No. 6, November–December 1963

Publications of the National Bureau of Standards*

Selected Abstracts

On the index of refraction of air, the absorption and dispersion of centimeter waves by gases, G. Boudouris. *Translated from French by G. Wm. Curtis, J. Res. NBS 67D (Radio Prop.), No. 6, (Nov.–Dec. 1963).*

The index of refraction, the absorption and dispersion are studied for several gases and vapors (pressure from 0 to 1 atm, temperature from 0 to 50° C, frequency from 7,000 to 12,000 Mc/s). The first part is devoted to a description of the microwave spectrometer used, while the second part is a survey of the several theories implied in the interpretation of the results.

In the third part, we present first the results concerning the index of refraction of atmospheric gases, of dry air, and of damp air. Then we study the absorption and dispersion by several vapors, and of ammonia and chloroform, principally. Finally, we indicate a new method making use of gaseous mixtures.

Our original results are discussed and presented within the frame of reference of works of other authors by means of comparison and intensive bibliographies.

Tensile and impact properties of selected materials from 20 to 300°K, K. A. Warren and R. P. Reed, *NBS Mono. 63 (June 28, 1963), 35 cents.*

The tensile and impact properties of structural materials were experimentally determined at temperatures from 20 to 300 °K. Tensile properties of a few materials were also determined at 4 °K. The materials included forty-two commercial alloys of iron, aluminum, titanium, copper, nickel, and cobalt, and two metal-bonded carbides. The properties experimentally determined were the yield strength, tensile strength, elongation, and reduction of area, the stress versus strain curve, and the impact energy. The test equipment and procedures are described. The individual data are presented in tables, and the average results are displayed in graphs.

Refractive indices and densities of aqueous solutions of invert sugar, C. F. Snyder and A. T. Hattenburg, *NBS Mono. 64 (June 7, 1963), 15 cents.*

The refractive indices and densities of aqueous solutions of invert sugar have been determined, at temperatures of 15, 20, 25, and 30 °C, for concentrations up to about 82 percent of invert sugar (by weight). From the results, equations have been derived which relate the refractive index and percent of invert sugar (weight in air) at each temperature. Other equations relate the absolute density and percent of invert sugar (weight in vacuum) at each temperature. Five-decimal tables giving the refractive indices and densities of invert sugar solutions containing 1 to 85 percent of sugar are given for each percentage of invert sugar at the four temperatures.

Reduction of data for piston gage pressure measurement, J. L. Cross, *NBS Mono. 65 (June 17, 1963), 15 cents.*

Pressure measurements made with piston gages are affected by gravity, temperature, pressure, and several other variables. For accurate determinations of pressure the calculations must take these variables into account. A general equation is developed and simplified procedures for calculating pressure are illustrated.

Tabulation of data on receiving tubes, C. P. Marsden and J. K. Moffitt, *NBS Handb. 83 (May 23, 1963), $1.25. (Supersedes Handb. 68.)*

A tabulation of Receiving-Type Electron Tubes with some characteristics of each type has been prepared in the form of two major listings, a Numerical Listing in which the tubes are arranged by type number, and a Characteristic Listing in which the tubes are arranged by tube type and further ordered on the basis of one or two important parameters. The tabulation is accompanied by a listing of similar tube types and basing connections for the listed tubes.

Impedance of commercial Leclanché dry cells and batteries, R. J. Brodd and H. J. Dewane, *NBS Tech, Note 190 (July 5, 1963), 40 cents.*

An extensive study of the impedance characteristics of the most commonly used sizes of commercial Leclanché type dry cells and batteries has been made through the frequency range of 50 to 50,000 cycles. Changes in impedance due to aging and use were determined. Open-circuit voltages and flash currents were measured, and capacities determined on standard tests in an effort to find a possible correlation between any of those three parameters and residual capacity. Data obtained are displayed in tabular form and on Argand diagrams.

Tables describing small-sample properties of the mean, median, standard deviation, and other statistics in sampling from various distributions, C. Eisenhart, L. S. Deming, and C. S. Martin, *NBS Tech. Note 191 (June 14, 1963), 20 cents.*

This note includes a collection of tables useful for study of the sampling distributions of some frequently-used statistics, with brief discussions of their construction and use. (1) The probability level $P(\epsilon,n)$ of any continuous parent distribution corresponding to level ϵ of the distribution of the median. (2) Probability points of certain sample statistics for samples from six distributions: normal and double-exponential (mean, median), rectangular (mean, median, midrange), Cauchy, Sech, Sech ^{2} (median). In all the above tables, the sample size $n=3(2)15(10)95$ and the probability levels are $\epsilon=.001$, .005, .01, .025, .05, .10, .20, .25. Together with the tables listed under (2) are given the values of certain ratios useful for comparing the various statistics. (3) Probability that the standard deviation of a normal distribution will be underestimated by the sample standard deviation s and by unbiased estimators of σ based on s, on the mean deviation, and on the sample range. Divisors are given for obtaining the corresponding "median unbiased" estimators.

Calculations of the potential and effective diffusion constant in a polyelectrolyte solution, S. R. Coriell and J. L. Jackson, *NBS Tech. Note 192 (June 28, 1963), 25 cents.*

The results of numerical computations of the electrostatic potential and the effective diffusion constant of counterions in a polyelectrolyte solution are given. The potentials for various polyion charge densities and polyion sizes are presented graphically. The calculated diffusion constants are compared with experimental data on the diffusion of labeled sodium ions in polyacrylis acid-sodium hydroxide solutions.

National standard reference data program, background information, *NBS Tech. Note 194 (June 1963), 25 cents.*

Plans are proposed for a National Standard Reference Data System that will provide critically evaluated data in the physical sciences on a national basis. It will be conducted as a decentralized operation across the country, with central coordination and administration by NBS. Data will be centrally stored at NBS and disseminated through a series of services tailored to user needs in science and industry.

Microwave spectrum of tertiary butyl chloride, A. Comparison of tertiary butyl structures, D. R. Lide, Jr., and M. Jen, *J. Chem. Phys.* **38,** *No. 7, 1504–1507 (Apr. 1, 1963).*

The rotational constants of $(C^{12}H_3)_3C^{12}Cl^{35}$, $(C^{12}H_3)_3C^{12}Cl^{37}$,

$C^{12}H_3)_3C^{13}Cl^{35}$, $(C^{12}H_3)_3C^{13}Cl^{37}$, and $(C^{13}H_3)(C^{12}H_3)_2(C^{12}Cl^{35})$ have been measured. The r_s structure of the *t*-butyl chloride skeleton calculated from these constants is: $r(CCl)=1.803\pm0.002$ A, $r(CC)=1.530\pm0.2002$ A, $\angle CCC=110.9°\pm0.1°$. The quadrupole coupling constant for Cl^{35} is -66.9 ± 1.5 Mc. The structures of a number of *t*-butyl compounds are compared. The *t*-butyl group is practically unaffected by substitution, while the CX bond in $(CH_3)_3CX$ is systematically longer than in CH_3X molecules. Conventional concepts of valence theory do not provide a satisfying explanation for this behavior.

Calorimetric calibration of the electrical energy measurement in an exploding wire experiment, D. H. Tsai and J. H. Park, *Exploding Wires* **2,** *27–107 (Plenum Press, Inc., New York, N.Y., 1962).*
A discussion is presented on the requirements and methods for measuring the current and voltage during the transient discharge of a capacitor bank being employed in an exploding wire experiment. A method is described for accurately calibrating the measured current, voltage, and electrical energy by comparing the calorimetric heating of a resistance element of essentially constant resistance with the electrical energy dissipated in the element. Results show that the accuracy of the energy measurement is about 1–2%.

Quasi-equilibrium theory of mass spectra, H. M. Rosenstock and M. Krauss, *Book, Mass Spectrometry of Organic Ions, pp. 1–64 (Academic Press, Inc., New York, N.Y., 1963).*
The essential features of the ionization and dissociation of diatomic molecules by electron impact are well understood. The process of ionization produces a vertical or Franck-Condon transition to one or another of the potential curves of the ion. Fragmentation occurs in that fraction of the ions initially formed above the dissociation limits of the potential curve.

Electrode potentials in fused systems. VI. Membrane potentials, K. H. Stern, *Phys. Chem.* **67,** *893–895 (1963).*
Membrane potentials have been measured for the cells $Ag\,AgCl(X_1)$, $NaCl(1-X_1)$ vycor glass $AgCl(X_2)$, $NaCl(1-X_2)Ag$. In contrast to the simple liquid junction whose potential is zero in this system (the transport number equals the mole fraction), most of the current is carried through the glass by the sodium ion and $t_{Na^+}=0.95$, independent of melt composition. Cells in which $X_1\cong1$, i.e. reagent grade AgCl, also operate as concentration cells with a Na^+ impurity ($X_{Na^+}\cong 2\times10^{-4}$). The use of these cells for reference electrodes is discussed.

Electron spin resonance spectra of aged, γ-irradiated polystyrenes, R. E. Florin, L. A. Wall, and D. W. Brown, *J. Polymer Sci. Pt. A.* **1,** *1521–1529 (1963).*
The electron spin resonance spectrum of polystyrene which has been γ-irradiated at −196°C changes gradually from a broad three-peaked structure with outer derivative peaks at ±46 gauss to a much narrower structure with poorly separated outer derivative peake at ±21 to 24 gauss. The deuterated polystyrenes behave likewise in general. The aged radicals of α,β,β-trideuterostyrene and β,β dideuterostyrene exhibit only a single peak with derivative maxima at ± 7 or 8 gauss from center. The aged spectra are all consistent with the hypothesis of major hyperfine interaction with β hydrogens. During the aging about 80% of the original radicals are lost, but the remainder are very long-lived. Poorly evacuated samples or those with added benzene decay much more rapidly.

Numerical computation of time-dependent properties of isotopically disordered one-dimensional harmonic crystal lattices, R. J. Rubin, *J. Phys. Soc. Japan* **18,** *Suppl. II, 63–69 (1963).*
The principal purpose of this work is to investigate numerically the statistical dynamical properties of isotopically disordered harmonic crystal lattices. Two properties are studied in detail: 1) The decay of initial periodic disturbances $\dot{Q}_k(\tau)$ which are normal modes of the same lattice structure when all particles have the same mass; and 2) the dipole moment correlation function $\langle\dot{M}(o)\,M(\tau)\rangle$. The numerical calculation of the time evolution of either $\dot{Q}_k(t)$ or $\langle\dot{M}(o)M(\tau)\rangle$ involves the solution of a single initial value problem for a given random distribution of the isotope masses on the lattice sites. The time evolution is investigated for values of the isotope mass ratio m_1/m_2 and of K for which the perturbation results of Maradudin, Weiss, and Jepsen are not applicable. A new formulation of the formal solution of the normal mode decay problem is proposed. This formulation should make it possible to calculate the initial stages of decay in an infinite lattice for the extreme values of m_1/m_2 and K studied in this paper.

Symmetry conditions for internal friction caused by jumping of point defects in crystals, J. B. Wachtman, Jr., and H. S. Peiser, *J. Appl. Phys. Letter* **1,** *No. 1, 20–22 (Sept. 1962).*
Symmetry conditions for the existence of internal friction are given which require only a knowledge of the behavior of a defect-free crystal under strain and a knowledge of which sites the defect occupies. These conditions predict that in rutile under strain ϵ_{xx} oxygen vacancies should not and titanium interstitials should produce internal friction. An observed internal friction peak suggests the existence of titanium interstitials in lightly reduced rutile.

Measurement of the lattice constants of neon isotopes in the temperature range 4°–24°K, L. H. Bolz and F. A. Mauer, *Proc. 11th Annual Conf. Applications of X-ray Analysis, Denver Res. Inst. (Plenum Press, Inc., New York, N.Y., 1962).*
Using an X-ray diffractometer cryostat, the lattice constants of the isotopes ^{20}Ne and ^{22}Ne as well as the naturally occurring mixture have been measured throughout most of the temperature range in which they exist as solids (0° to approximately 24 °K). The heavier isotope has the smaller lattice constant, the values obtained at 4.2 °K being: ^{20}Ne—4.462_4 A, $^{22}Ne-4.454_9$ A, and natural neon—4.462_2 A. The absolute error in these values is believed to be no greater than 0.001 A. The volume expansion coefficient, which does not appear to differ significantly in the three cases, increases to a value of 6.3×10^{-3}/°K at 24 °K.

Design of an interferometric oil manometer for vacuum measurement, A. M. Thomas, D. P. Johnson, and J. W. Little, *1962 Trans. Ninth Natl. Vacuum Symp., Am. Vacuum Soc., pp. 468–473 (1962).*
The oil manometer under discussion is one which uses an interferometer to measure the changes in height of the oil surfaces as a change in pressure is applied. Interference fringes are developed between the lower surface of an optical flat and the oil surfaces of the manometer. Di-octyl sebacate is distilled into the manometer after outgassing the system and oil. A fringe shift of fifty-five fringes is produced by a pressure of 10^{-3} torr. A sensitivity of 2×10^{-6} torr can be attained by detecting a shift of one-tenth of a fringe.

Analysis of the third spectrum of praseodymium, J. Sugar, *J. Opt. Soc. Am.* **53,** *No. 7, 831–838 (July 1963).*
The spectrum of doubly-ionized praseodymium was recorded and analyzed, with the result that 118 energy levels of odd parity and 130 levels of even parity were derived. These include nearly all the levels of the $4f^3$, $4f^25d$, $4f^26s$, $4f^26p$ configurations as well as some low levels of the $4f5d^2$ and $4f^26d$ configurations. Electrostatic and spin-orbit parameters were determined for the $4f^26s$ configuration. From the *hfs* of the $4f^26s$ levels, a magnetic dipole interaction constant of 0.46 cm^{-1} was obtained. An ionization potential of 23.2 volts was calculated from levels of the $4f^25d$ and $4f^26d$ series.

Photodisintegration of light nuclei, E. Hayward, *Rev. Mod. Phys.* **35,** *No. 2, 324–331 (Apr. 1963).*
The data from some recent experiments on the photoeffect in light nuclei (Z= 6–20) are summarized. It is shown that the so-called giant resonance for these nuclei really consists of the superposition of many resonances, more than is consistent with a simple shell-model. The absorption cross section integrated over the giant resonance varies from 50 to 90 percent of the classical dipole sum, a large fraction of the nuclear oscillator strength being associated with the high energy quasideuteron effect.

Very low temperature data. Properties of paramagnetic salts, R. P. Hudson, *AIP Handb. 2d Ed. Sec. 5g, pp. 222–223 (1963).*
A revision of Section 4b of the American Institute of Physics Handbook, on the properties of paramagnetic salts at very low temperatures, has been made. The original discussion has been completely rewritten and brought up to date, and extended to other substances which have recently acquired importance.

Collective correlation of plasma, C. M. Tchen, *Czechoslovak J. Phys., Proc. 2d Conf. Electronics* **XXI,** *No. 5–6, 516–521 (Apr. 1962).*
The one-particle distribution function is described by the BBGKY equation, while the correlation function is determined by an equation of the Vlasov type (with self-consistent field, but without collision). Oscillations of small amplitudes are considered. The dispersion relation is obtained, and the Landau damping is calculated.

Pressure broadening as a prototype of relaxation, U. Fano, *Phys. Rev.* **131,** *No. 1, 259–268 (July 1, 1963).*
The theoretical results of Baranger, Kolb and Griem on pressure broadening are rederived by a more compact and flexible procedure directly applicable to other relaxation processes. Pressure broadening is worked out to first order in the pressure, including previously disregarded corrections. The procedure adapts the concepts and techniques of scattering theory to the Louville representation of density matrices. Its key quantity is a frequency dependent relaxation operator $<M_c(\omega)>$ introduced by Zwanzig.

The atomic spectra of the rare earths: their presence in the sun, C. E. Moore, *Appl. Opt.* **2,** *No. 7, 665–674 (July 1963).*
A summary of the present state of analysis of the first and second spectra of the rare-earth elements is presented with an extensive bibliography. The astrophysical importance of these spectra is stressed. Counts are given of the number of lines of each rare-earth spectrum identified at present in the accessible solar spectrum. Most of them appear only in the singly-ionized state; exceptions are Eu I, Tm I?, and Yb I. The possible presence of the strongest laboratory line of Co III in the solar spectrum is suggested. If correct, this is the first evidence of a third spectrum line in the accessible range of the solar spectrum ($\lambda > 3000$ Å).

The conductive-disk method of measuring the thermal conductivity of insulations, H. E. Robinson, *Suppl., Bull. Intern. Inst. Refrigeration, Annexe 1962–1, 43–50 (Aug. 1962).*
A comparative method of a new type for determining the thermal conductivity of isotropic insulations is described. It employs a circular disk of a material of suitable conductivity and thickness, which is sandwiched between two flat specimens of the material to be measured, the outer faces of which are put in contact with uniform-temperature cooling plates. The rim of the disk is heated uniformly, and as a result of heat flow from the disk through the specimens to the cooling plates, the steady-state temperature of the disk decreases toward its center. Measurements are made of the surface temperature of the disk at its center, and at a suitable radius, and also of that of the cooling plates. The conductivity of the specimen is determined from these data, together with the dimensions of the system and the conductivity of the disk material. If the conductivity of the disk material is not known, a calibration curve for the disk can easily be developed by means of a few tests made on specimens of known conductivity.

Electron affinity of atomic iodine, B. Steiner, M. L. Seman, and L. M. Branscomb, *J. Chem. Phys.* **37,** *No. 6, 1200–1202 (June 1962).*
Photodetachment of I^- ions has been observed in a crossed beam experiment. The apparatus used was essentially similar to that in previous photodetachment experiments. Use of four Sharp Cut filters provided good "effective" resolution close to threshold but did not permit an independent determination of the behavior of the cross section as a function of wavelength. A step function cross section, shown by Berry and co-workers to approximate closely the true cross section behavior, was used to provide an upper energy limit to the electron affinity shown to be close to the actual value. The value of the electron affinity thus determined, $3.076 \pm .005$ ev, is in excellent agreement with the shock wave determination of Berry, $3.074 \pm .003$. The absolute magnitude of the cross section in the region 0.3 ev above threshold was determined to be $1.5 \pm 0.8 \times 10^{-17}$ cm^2.

Field-emission study of carbon monoxide on tantalum, R. Klein and L. B. Leder, *J. Chem. Phys.* **38,** *No. 8, 1866–1872 (Apr. 15, 1963).*
Adsorbed carbon monoxide shows three states of binding on tantalum. The weakest of these is desorbed at temperatures above 125°K with no observable surface migration. The bonding with the surface is of the Van der Waal's type. This is in contrast with the second state, which is chemisorbed above 650°K. The third state is dissociated before desorption to give the oxygen on tantalum pattern. Surface migration involving the second adsorbed state occurs with an activation energy of 38 k cal. The work function of a carbon monoxide covered tantalum surface, obtained by spreading a CO shadowed tip at 40°K, is 0.8 ev greater than that of the corresponding clean tantalum. Fowler-Nordheim plots of clean and shadowed tips show that at least under these conditions the infinite field extrapolation of $\ln i/V^2$ is proportional to the emitting areas.

Field emission observations of carbon on tantalum, R. Klein and L. Leder, *J. Chem. Phys.* **38,** *No. 8, 1863–1866 (Apr. 1963).*
The carbon-tantalum system, observed with field emission, shows the temperature effects on the solubility and precipitation of the carbide phase. Carbon, once deposited on tantalum, cannot be removed by high temperature treatment, as in the case of tungsten. With low carbon contamination the 334 planes appear as dark areas, just as for carbon on tungsten. At temperatures in the region of 950°K, platelets, presumably Ta_2C, form and migrate to the [111] zones of the emitter single crystal tip. The energy of activation of this surface migration process is 54 k cal.

Electron energy levels and their relationship to lattice defects in reduced rutile, J. H. Becker and W. R. Hosler (*Proc. Intern. Conf. Crystal Lattice Defects*), *J. Phys. Soc. Japan* **18,** *Suppl. II, 152–160 (1963).*
Electrical conduction mechanisms and defect structure are studied by measurements of the Hall coefficient and electrical resistivity from 300°K to about 2°K, for samples of reduced rutile with $\rho \| c$ (300°K) ~1 to 5 ohm-cm. Virtually identical results are obtained for samples reduced in vacuum at 1000°C or hydrogen at 600°C. The anisotropic nature of the Hall coefficient and resistivity tensora (with two independent elements in each for this tetragonal system) is taken into account. The data are suggestive of conduction in impurity levels at very low temperatures ($<\sim$ 4°K), a narrow Ti^{3+} conduction band (No. 1) at low temperatures ($\sim$7−30°K) and additional contributions at intermediate temperatures ($\sim$ 30°−300°K) from another Ti^{3+} conduction band (No. 2). Recent evidence concerning the defects in reduced rutile is discussed; it appears that most of the data are more consistent with a model of Ti^{3+} ions at interstitial positions which act as donors than with a model of oxygen vacancies, as concluded previously by several authors.

New autoionizing atomic energy levels in He, Ne, and A, R. P. Madden and K. Codling, *Phys. Rev. Letters* **10,** *No. 12. 516–518 (June 15, 1963).*
The NBS 180 MeV electron synchrotron has been used as a continuum light source for absorption spectroscopy in the λ180–470Å region. Two-electron transitions to states which autoionize have been observed in He; transitions to autoionizing states have also been observed in Ne and A.

A modification of the Born-Mayer potential function as applied to the crystalline alkali halides, T. B. Douglas, *J. Chem. Phys.* **38,** *No. 10, 2461–2466 (May 15, 1963).*

In an attempt to improve the applicability of the Born-Mayer equation to more extreme conditions than those in the pure alkali halides, the repulsion constant ρ is assigned values different for like and unlike ion pairs in such a way that large

699-332—63——10

deviations from the observed compressibilities of the lithium halides attributable to marked anion-anion repulsion are removed. It is then found that the "basic radii" can be assigned values which give lattice parameters in excellent agreement with the experimental ones, and that the calculated electron affinities still agree approximately with the most precise directly observed values. A general condition imposed by the Born-Mayer equation is pointed out which is not satisfied by the data for several of the alkali halides.

Microbalance techniques for high temperature applications—further developments, N. J. Carrera and R. F. Walker, *Book, Vacuum Microbalance Techniques, 3, 153–177 (Plenum Press, Inc., New York, N.Y., 1963).*

A description is given of recent improvements to and plans for a microbalance technique for studying the rates of vaporization of refractory substances, generally in the temperature range of 1600–2500° C. An ion pumping system is described which permits the attainment of 1×10^{-9} torr without bakeout. The apparatus, apart from the pump, can be completely enclosed in a bakeout oven to attain still lower residual pressures. The design of a variable-capacitance recording system for the Gulbransen-type microbalance has commenced, and preliminary features of this system are presented. It has been found possible to include a black body hole in the small samples suspended from the microbalance, thus improving the precision of temperature measurements. Some preliminary work on the application of reimaging techniques for the heating of samples is also described.

High resolution spectra in the region from 2 to 6μ, E. K. Plyler and E. D. Tidwell (*Proc. Intern. Molecular Conf.), Book, Advances in Molecular Spectroscopy, pp. 1336–1342 (Pergamon Press Inc., New York, N.Y., 1962).*

A grating spectrometer has been built which has high resolution in the region from 2 to 6μ. Three gratings are used to cover the region and they have 7500. 10,000, and 15,000 lines/in. and their ruled area is about 5×8 in. The instrument can be used single pass or double pass. Under the most favorable conditions partial resolution is obtained of lines separated by 0.025 cm^{-1}.
The absorption spectra of several polyatomic molecules have been measured and molecular constants calculated. This report discusses the spectra of the $2\nu_4$ bands of fluoroform and chloroform. Molecular constants of fluoroform have been calculated from the spectra and have the following values, $\nu_0=2710.25_5$ cm^{-1}, $B''=.34521_5$, $B'=.34452_6$, $D=3.97_5\times10^{-7}$

Theory of the electronic polarizabilities of ions in crystals: Application to the alkali halide crystals, A. R. Ruffa, *Phys. Rev.* **130,** *No. 4, 1412–1423 (May 15, 1963).*
A theoretical estimate of the polarizabilities of ions in the alkali halides is made by means of a procedure based upon the product approximation which distinguishes the ionic constituents in the crystal but allows for their overlap and mutual interaction. Analysis by means of the Thomas-Kuhn sum rule is used allowing the sum representing the ionic polarizability to be represented by one effective parameter, which is calculated for the free ions from the Pauling theoretical values. The change in this parameter when the ion is transported into the crystalline environment is estimated by an energy level analysis used previously by Seitz.
It is shown that this procedure accounts for most of the quantitative features of the polarizabilities of the alkali halides. Moreover, the implications of these results are strongly at variance with the usual view concerning the polarizabilities of ionic crystals, since the additivity rule appears as an accidental result of the qualitative similarily of the interactions in many crystals, and the possibility of large fluctuations in the polarizability of a given ion in different crystalline environments is made evident.

Atomic flame reactions involving N-atoms, H-atoms and ozone, D. Garvin and H. P. Broida, *9th Intern. Combustion Symp., pp. 678–688 (1963).*
The low pressure reaction between H, N and O_3 has been studied by emission and absorption spectroscopy. When all three of these reactants are present together two types of flames are formed. One of these, a pink brush-like reaction zone represents a low temperature regime, while the other, a well formed white flame is probably a high temperature phenomenon. Electronic spectra in emission of OH, NH, NO and N_2 (1st positive) are found in the former. The latter has the same bands plus emission from NH_2 and the OH vibration-rotation bands.
The reaction mechanism is discussed. It is shown that H-atoms serve as a catalyst and suggested that vibrationally excited OH is responsible for the formation of NH and excited nitrogen molecules ($B^3\pi$)

Infrared spectrum of acetylene-d_1, W. J. Lafferty, E. K. Plyler, and E. D. Tidwell, *J. Chem. Phys.* **37,** *No. 9, 1981–1988 (Nov. 1962).*
The high resolution absorption spectrum of C_2HD has been studied in the 1900 to 3400 cm^{-1} region. Several bands at lower frequencies have been examined with medium resolution. Nineteen bands were analyzed for their rotational constants. Combination differences of four transitions from the ground state were averaged and the rotational constants $B_0=0.99156\pm.00004$ cm^{-1} and $D_o=1.17\pm.07\times10^{-6}$ cm^{-1} obtained. This B_o value together with those recently obtained for C_2H_2 and C_2D_2 have been used to calculate the ground state and equilibrium state bond distances of the acetylene molecule. The *l*-doubling constants for the degenerate modes were determined to be $q_4=4.4_2\times10^{-3}cm^{-1}$ and $q_5=3.4\times10^{-3}$ cm^{-1}. The frequencies of the bending modes have been calculated by use of difference bands to be $\nu^l_4=518.38$ cm^{-1} and $\nu^l_5=677.77$ cm^{-1}.

Audiofrequency dispersion effects in lanthanide salts at low temperatures, R. P. Hudson and B. W. Mangum, *Book, Magnetic and Electric Resonance and Relaxation, Ed. J. Smidt, pp. 135–146 (North-Holland Publ. Co., Amsterdam, The Netherlands, 1963).*
Measurements have been made of the quadrature components of the audiofrequency susceptibility of three rare-earth paramagnetic salts in the liquid helium region and in the presence of an external magnetic field. The susceptibilities and derived values of the spin-lattice relaxation time are compared with theory and suggestions put forward to explain major anomalies in the case of dysprosium ethylsulfate.

An LCAO-MO-SCF study of the structure of HO_2, M. E. Boyd, *Program Comm. Intern. Symp. on Molecular Structure and Spectroscopy, pp. B404-1–B404-4 (Science Council of Japan, Tokyo, 1962).*
A priori computations by the self-consistent field molecular orbital method have been performed on the radical HO_2 in an effort to determine its geometry. For a linear configuration the energy was computed as a function of internuclear distances. Fixing these at the value giving the lowest energy, calculations were performed of energy as a function of the HOO angle, and gave an energy minimum for an isosceles triangle geometry having $D(O_2-H)$ 4 e.v. and an ionization potential of 10.95 e.v. in reasonable agreement with mass spectrometer data.

Dependence of the electrical conductivity and thermoelectric power of pure and aluminum-doped rutile on equilibrium oxygen pressure and temperature, J. Yahia, *Phys. Rev.* **130,** *No. 5, 1711–1719 (June 1, 1963).*
Several defect models for the production of charged carriers in pure and Al-doped rutile are discussed in this paper. For the case of pure rutile, it is shown that the anion-vacancy model does not lead to the observed pressure dependence of the conductivity whereas the titanium interstitials model does lead to the proper result. For the case of Al-doped rutile, the anion vacancy model combined with a certain choice of reaction constants gives a pressure dependence of the density of electrons (and holes) that is close to that observed. The titanium interstitials model is not solved explicitly for this case (as for the anion vacancy calculation) but it is shown that it may give rise to the right pressure dependence of the electron and hole concentration. The two-band formalism of Becker and Frederikse is applied to an analysis of our data and shown to be in reasonable conformity with the observations. There are some indications that the hole mobilities $\sim$ 180 cm^2/volt-sec at 1000°K. As a consequence of this, an effective mass for the hole $\sim 10^{-2}$

m_o is deduced, assuming high temperature polar scattering to take place. These hole mobilities are considerably larger than those expected for electrons at those temperatures.

Other NBS Publications

J. Research NBS 67C (Eng. and Instr.), No. 4 (Oct.–Dec. 1963), 75 cents.

Limitations on electron beam density of unipotential electron guns at low voltages. J. A. Simpson and C. E. Kuyatt.

New radiofrequency mass spectrometer having high duty cycle. R. H. Mills.

A power-series buildup factor formulation. Application to rectangular and off-axis disk source problems. J. B. Hubbell.

An alinement interferometer. J. B. Saunders.

Determination of optical path difference for a photographic objective. F. E. Washer and W. R. Darling.

Development of filters for a thermoelectric colorimeter. S. H. Emara and R. P. Teele.

Application of air bearings to an electrodynamic vibration standard. T. Dimoff and B. F. Payne.

Leak-resistant rotation seal for vacuum applications. F. L. Howard.

Studies on the tungsten-rhenium thermocouple to 2000 °C. D. B. Thomas.

J. Research NBS 67D (Radio Prop.), Np. 6 (Nov.–Dec. 1963), 70 cents.

A radiometeorological study, part I. Existing radiometeorological parameters. J. A. Lane and B. R. Bean.

A radiometeorological study, part II. An analysis of VHF field strength variations and refractive index profiles. B. R. Bean, V. R. Frank, and J. A. Lane.

A radiometeorological study, part III. A new turbulence parameter. B. R. Bean, E. J. Dutton, J. A. Lane, and W. B. Sweezy.

Reflection of radio waves from undulating tropospheric layers. A. T. Waterman, Jr., and J. W. Strohbehn.

Oblique propagation of groundwaves across a coastline—Part I. J. R. Wait.

Oblique propagation of groundwaves across a coastline—Part II. J. R. Wait and C. M. Jackson.

On the index of refraction of air, the absorption and dispersion of centimeter waves by gases. Georges Boudouris. Translated from French by G. Wm. Curtis. (See above abstracts.)

A numerical approach to the solution of radio diffraction problems. J. K. Hargreaves and S. Hargreaves.

Inversion of radio wave absorption data to establish ionospheric properties. I. Nondeviative absorption. A. D. Wheelon.

Radiation in a lossless magneto-ionic medium at frequencies high relative to the electron gyrofrequency. J. W. Marini.

Radiation through cylindrical plasma sheaths. J. H. Harris.

Chart for determining the effects of ionospheric tilts using an idealized model. T. A. Croft and R. B. Fenwick.

Reflection of VLF radio waves from an inhomogeneous ionosphere. Part III. Exponential model with hyperbolic transition. J. R. Wait and L. C. Walters.

Families of distributions for hourly median power and instantaneous power of received radio signals. M. M. Siddiqui and G. H. Weiss.

Statistical methods in radar astronomy. Determination of surface roughness. H. S. Hayre.

Electrical conductivity of the Great Lakes. L. H. Doherty.

Quarterly radio noise data, September, October, November 1962, W. Q. Crichlow, R. T. Disney, and M. A. Jenkins, NBS Tech. Note 18–16 (June 10, 1963), 60 cents.

Phototypesetting of computer output, an example using tabular data, W. R. Bozman, NBS Tech. Note 170 (June 25, 1963), 10 cents.

A bibliography of foreign developments in machine translation and information processing, J. L. Walkowicz, NBS Tech. Note 193 (July 10, 1963), $1.00.

Table of attenuation error as a function of vane-angle error for rotary vane attenuators, W. Larson, NBS Tech. Note 177 (May 20, 1963), 75 cents.

Tabulation of published data on Soviet electron devices, C. P. Marsden, NBS Tech. Note 186 (June 3, 1963), 45 cents.

Instability of the equatorial F layer after sunset, W. Calvert, J. Geophys. Res. **68,** 2591–2593 (May 1, 1963).

A simple environmental chamber for rotating beam fatigue testing machines, J. A. Bennett, Mater. Res. Std. **3,** No. 6, 480–482 (June 1963).

Standard potential of the silver-silver chloride electrode and activity coefficients of hydrochloric acid in aqueous methanol (33.4 Wt. %) with and without added sodium chloride at 25°, R. G. Bates and D. Rosenthal, J. Phys. Chem. **67,** 1088–1090 (1963).

International standardization. A new responsibility of the engineer, A. T. McPherson, Natl. Acad. Sci.-Natl. Res. Council Div. of Eng. and Ind. Res. Newsletter, No. 26, 2–4 (June 1, 1963).

Path antenna gain and comments on "Properties of 400 Mc/s long-distance tropospheric circuits," W. J. Hartman. Proc. IEEE **51,** 847–848 (May 1963).

Absorption and scattering of photons by deformed nuclei, E. G. Fuller, Proc. 2d All-Union Conf. Nuclear Reactions at Low and Intermediate Energies, p. 419, 1960 (Russian Academy of Science, U.S.S.R., 1962).

Search for a slow component in alpha ionization, Z. Bay and R. M. Pearlstein, Phys. Rev. **130,** No. 1, 223–227 (Apr. 1963).

Evidence regarding the mechanism of fatigue from studies of environmental effects, J. A. Bennett, Acta Met. **11,** No. 7, 799–800 (July 1963).

Dielectric friction on a rotating dipole, R. Zwanzig, J. Chem. Phys. **38,** No. 7, 1605–1606 (Apr. 1, 1963).

Field-aligned E-region irregularities identified with acoustic plasma waves, K. L. Bowles, B. B. Balsley, and R. Cohen, J. Geophys. Res. **68,** 2485–2501 (May 1, 1963).

The association of plane-wave electron-density irregularities with the equatorial electrojet, R. Cohen and K. L. Bowles, J. Geophys. Res. **68,** 2603–2611 (May 1. 1963).

Determination of differential X-ray photon flux and total beam energy, J. S. Pruitt and H. W. Koch, Book, Nuclear Physics 5, Ch. 2.8.2, Pt. B, 508–553, Ed. L. C. L. Yuan and C. Wu (Academic Press, Inc., New York, N.Y., 1963).

Index to the communications of the ACM, 1958–1962, W. W. Youden, Comm. ACM **6,** No. 3, 1–32 (Mar. 1963).

Magnetic properties of acetinide element alloys and compounds, J. C. Eisenstein, Book, Landolt-Bornstein, 6 Ed. 2, Pt. 9, p. 3.236 (Springer-Velag, Berlin, Germany 1962).

Planar twin boundary in aluminum, T. H. Orem, Trans Met. Soc. AIME **227,** 786–788 (June 1963).

Radio noise anomalies in August 1958, C. A. Samson, J. Geophys. Res. **68,** 2719–2726 (May 1, 1963).

Optical studies of the formation and breakdown of passive films formed on iron single crystal surfaces in inorganic inhibitor solutions, J. Kruger, J. Electrochem. Soc. **110,** No. 6, 654–663 (June 1963).

The importance of enviroment in fatigue failure of metals, J. A. Bennett, W. L. Holshouser, and H. P. Utech, Book, Fatigue of Aircraft Structures, pp. 1–18 (Pergamon Press, Inc., London, England, 1963).

Production of Lyman alpha radiation in ion-atom collisions, G. H. Dunn, R. Geballe, and D. Pretzer, Phys. Rev. **128,** No. 5, 2200–2206 (Dec. 1, 1962).

Microwave spectrum of aluminum monofluoride, D. R. Lide, Jr., J. Chem. Phys. **38,** No. 8, 2027 (Apr. 15, 1963).

Some limits on the effect of coronal self-emission upon the excitation state of coronal ions, R. N. Thomas and C. Pecker, Astrophys. J. **137,** No. 3, 967–980 (1962).

Oil baths for saturated standard cells, P. H. Lowrie, Jr., ISA J. **9,** No. 12, 47–50 (Dec. 1962).

Performance of the barium fluoride film hygrometer element on radiosonde flights, F. E. Jones, J. Geophys. Res. **68,** No. 9, 2735–2751 (May 1, 1963).

Radiation induced polymerization of propylene at high pressure, D. W. Brown and L. A. Wall, J. Phys. Chem. **67,** 1016–1019 (1963).

Dielectric friction on a moving ion, R. Zwanzig, J. Chem. Phys. **38,** No. 7, 1603–1605 (Apr. 1, 1963).

Survey of Rb^{85}/Rb^{87} ratios in minerals, W. R. Shields, E. L. Garner, C. E. Hedge, and S. S. Goldich, J. Geophys. Res. **68,** No. 8, 2331–2334 (Apr. 15, 1963).

Dissociation constant of pyrrolidinium ion and related thermodynamic quantities from 0 to 50°, H. B. Hetzer, R. G. Bates, and R. A. Robinson, J. Phys. Chem. **67,** 1124–1127 (1963).

Introduction to the International Symposium on Equatorial Aeronomy, R. Cohen and K. L. Bowles, J. Geophys. Res. **68,** 2359–2361 (May 1, 1963).

Interference fringes with long path difference using He-Ne laser, T. Morokuma, K. F. Nefflen, T. R. Lawrence, and T. M. Klucher, J. Opt. Soc. Am. **53,** No. 3, 394–395 (Mar. 1963).

Hydrogen retention system for pressure calibration of microphones in small couplers, W. Koidan, J. Acoust. Soc. Am. **35,** No. 4, 614 (Apr. 1963).

The National Bureau of Standards; Where measurement is the central theme, C. S. McCamy, Ind. Phot. **11,** No. 8, 28 (Aug. 1962).

Statistical computation of configuration and free volume of a polymer molecule with solvent interaction, J. Mazur and L. Joseph, J. Chem. Phys. **38,** No. 6, 1292–1300 (Mar. 15, 1963).

A comparison of two independent atomic time scales, J. Newman, L. Fay, and W. R. Atkinson, Proc. IEEE **51,** No. 3, 498–499 (March 1963).

Change in occlusion of complete dentures caused by a pipe habit: a case report, J. B. Woefel and G. C. Paffenbarger, J. Am. Dental Assoc. **66,** No. 4, 478–485 (Apr. 1963).

Measurement of a maximum in the isothermal crystallization rate-temperature curve for polypentene-1, F. A. Quinn, Jr., and J. Powers, Polymer Letters (J. Polymer Sci., Pt. B) **1,** No. 7, 341–344 (July 1963).

Pressure induced shifts of infrared lines due to polar molecules, E. K. Plyler, M. A. Hirshfield, and J. H. Jaffe, J. Chem. Phys. **38,** No. 1, 257–258 (Jan. 1963).

The maximum number of zeros in the powers of an undecomposable matrix, M. Marcus and F. May, Duke Math. J. **29,** No. 4, 581–588 (Dec. 1962).

Radio spectrum of SH, H. E. Radford and M. Linzer, Phys. Rev. Letters **10,** No. 10, 443–444 (May. 15, 1963).

Electrophoretic deposits of barium titanate, V. A. Lamb and H. I. Salmon, J. Am. Ceram. Bull. **41,** No. 11, 781 (1962).

Thermodynamic properties of gases, J. Hilsenrath, Am. Inst. Phys. Handb. 2d Ed., Sec. 4h, 101–157 (1963).

The decoration of dislocations in aluminum oxide, H. E. Bond and K. B. Harvey, J. Appl. Phys. **34,** No. 2, 440–441 (Feb. 1963).

The effect of geomagnetic crochet on cosmic ray intensity, C. S. Warwick, J. Geophys. Res. **68,** No. 10, 3303–3304 (May 15, 1963).

Absorption bands of carbon dioxide from 5.3 to 4.6 microns, A. Maki, E. K. Plyler, and R. J. Thibault, J. Chem. Phys. **37,** No. 8, 1899–1900 (Oct. 1962).

Packing inequalities for circles, P. J. Davis, Michigan Math. J. **10,** 25–31 (1963).

Lower bounds to eigenvalues using operator decompositions of the form B*B, N. W. Bazley and D. W. Fox, Arch. Rat. Mech. Anal. **10,** p. 352 (1962).

Transference numbers in pure molten sodium nitrate, R. J. Labrie and V. A. Lamb, J. Electrochem. Soc. **110,** No. 7, 810–814 (July 1963).

Unstable detonation near a hypervelocity missile, F. W. Ruegg and W. W. Dorsey, Ninth Symp. Intern. Combustion, pp. 476–477 (1963).

Vacuum-tight cylinder joints and ball-and-socket joints, L. A. Guildner and H. F. Stimson, Rev. Sci. Instr. **34,** No. 6, 658–659 (June 1963).

Statistical interpretations, W. J. Youden, Book, Standard Methods of Chemical Analysis, IIA, Ch. 16, pp. 319–325 (D. Van Nostrand Co., Princeton, N.J., 1963).

Exchange processes in the reaction of boron trichloride with triethylamine-boron trifluoride, T. D. Coyle, Proc. Chem. Soc. (London), p. 172 (June 1963).

Study of Knudsen's method of pressure division as a means of calibrating vacuum gauges, S. Schuhmann, Trans. Ninth Natl. Vacuum Symp. Am. Vacuum Soc., pp. 463–467 (1962).

Design of low voltage electron guns, J. A. Simpson and C. E. Duyatt, Rev. Sci. Instr. **34,** No. 3, 265–268 (Mar. 1963).

Classification of two-electron excitation levels of helium, J. W. Cooper, U. Fano, and F. Prats, Phys. Rev. Letters **10,** No. 12, 518–521 (June 1963).

Solid state physics, H. P. R. Frederikse (editor and part author), Book, Am. Inst. Phys. Handbook Sec. 9, 2d Ed. (McGraw Hill Book Co., New York, N.Y., 1963).

VLF propagation—theory and experiment, J. R. Wait, Monograph, Electromagnetic Waves in Stratified Media, Ch. IX, pp. 264–288 (Pergamon Press, Inc., Oxford, England, 1962).

Plastics, G. M. Kline, Americana Annual, p. 535 (Americana Corp., Chicago, Ill., 1963).

Precision of simultaneous measurement procedures, W. A. Thompson, Jr., J. Am. Stat. Assoc. **58,** No. 302, 474–479 (June 1963).

Sum rules relating coherent X-ray scattering data to the diamagnetic nuclear shielding constant and to the self-energy of the charge distribution of the scatterer, J. N. Silverman and Y. Obata, J. Chem. Phys. **38,** No. 5, 1254–1255 (1963).

Determining fastest routes using fixed schedules, B. M. Levin and S. Hedetniemi, Proc. Conf. American Federation for Information Processing Soc. **23,** pp. 1–9 (1963).

Dielectric relaxation in a high temperature dipole lattice, R. Zwanzig, J. Chem. Phys. **38,** No. 11, 2766 (1963).

Present status of our knowledge of atomic transition probabilities, W. L. Wiese, Proc. Xth Colloq. Spectroscopicum Intern., pp. 37–56 (Ed. E. R. Lippincott and M. Margoshes, Spartan Books, Washington, D.C., 1963).

Double-photon photodetachment of negative ions, S. Geltman, Phys. Rev. Letters **4,** No. 3, 168–169 (Apr. 1, 1963).

Mathematical analysis of thermal environment in underground shelters, P. R. Achenbach, T. Kusuda and F. J. J. Drapeau, ASHRAE Symp. Survical Shelters, pp. 9–33 (June 1962).

Effect of insulation on the weathering of smooth-surfaced, built-up roofs exposed to solar heating, W. C. Cullen and W. H. Appleton, Am. Roofer and Building Improvement Building Contractor Mag. Pt. I, **53,** No. 3, 19–22 (Mar. 1963); Pt. II, **53,** No. 4, 14 (Apr. 1963)

The precise evaluation of lens distortion, F. E. Washer, Photogrammetric Eng. XXXI, No. 3, pp. 327–332 (Mar. 1963).

Electrodeposition of alloys. Principles and practice. Vol. I, General Survey, principles, and alloys of copper and of silver, and Vol. II, Practical and specific information, A. Brenner, Book, Academic Press, Inc., New York, N.Y., 1963.

Factorial designs and the direct product, B. Kurkjian and M. Zelen, Bull. Intern. Stat. Inst. **XXXIX,** Pt. 2, 509–519 (1962).

The contact properties of thin films on semiconductors, T. Higier and G. G. Harman, November 1961 Contact Symp. Proc. Univ. Maine (Mar. 20, 1963).

Temperature scales, thermocouples and resistance thermometers, H. F. Stimson, J. F. Swindells, and R. E. Wilson, Am. Inst. Phys. Handb. 2d Ed., Sec. 4a, pp. 2–21 (1963).

Electron impact ionization of atomic hydrogen, S. Geltman, M. R. Rudge, and M. J. Seaton, Proc. Phys. Soc. **81,** Pt. 2, No. 520, 375–377 (Feb. 1, 1963). Some free products of cyclic groups, M. Newman, Michigan Math. J. **9,** 369–373 (1962).

Addendum: Vibration-rotation spectra of BrCN, A. Maki, J. Chem. Phys. **38,** No. 5, 1261–1262 (May 1963).

The present status of radiometric calibrations in the ultraviolet spectrum, R. Stair, Symp. on Military Applications of Ultraviolet Radiation, Rept. No. LAS–TR–199–37 (Nov. 1962).

Acoustic properties of liquids, M. Greenspan, Am. Inst. Phys. Handb. 2d Ed. Sec. 3e, pp. 71–82 (1963).

Reflection mechanisms for sporadic *E*, K. Tao and J. R. Wait, Book, Ionospheric Sporadic *E*, Ed. E. K. Smith and S. Matsushita, Ch. 4, Pt. II, pp. 13–27 (Pergamon Press, Inc., Oxford, England, 1962).

Gas measurement and other services of the National Bureau of Standards, C. T. Collett, Am. Gas Assoc. Preprint DMC–63, pp. 1–3 (1963).

Review of reviews of atomic spectra, W. Meggers, Appl. Opt. **2,** No. 7, 657–663 (July 1963).

Molecular parameters of ethane, W. J. Lafferty and E. K. Plyler, J. Chem. Phys. **37,** No. 11, 2688–2692 (Nov. 1962).

Multipliers of difference sets, M. Newman, Can. J. Math. **13,** 121–124 (Nov. 1961).

The segemental variation of Blaschke products, G. T. Cargo,

Duke Math. J. **30,** No. 1, 143–150 (Mar. 1963).

The structure of some subgroups of the modular group, M. Newman, Illinois J. Math. **6,** No. 3, 480–487 (Sept. 1962).

Discussion of errors of a recommended standard resistor-noise test system, N. Newman and G. T. Conrad, Jr., IRE Trans. Component Parts **CP–9,** No. 4, 180–192 (Dec. 1962).

Conditions for second-order waves in hypo-elasticity, B. Bernstein, Trans. Soc. Rheology **VI,** No. 1, 263–273 (1962).

Research in American Society for Testing Materials, B. L. Wilson, Mater. Res. Std. **2,** No. 8, 694–695 (Aug. 1962).

Heat capacities, G. T. Furukawa and T. B. Douglas, A.m. Inst. Phys. Handb. 2d Ed., Sec. 4e, pp. 47–63 (1963)

Impressions of Japan, R. S. Marvin, Japanese J. Kobunshi (High Polymers), Soc High Polymers **12,** No. 130, 53 (1963).

Annual report for IAU Commission 14, C. E. Moore, Trans. Astronomical Union XIA97–XIB, 208 (1962).

The effect of moisture on heat transfer through insulated flat-roof constructions, F. J. Powell, Suppl. Bull. Intern. Inst. Refrigeration, Annexe 1962–1, 61–70 (Aug. 1962).

Nickel and alloys, M. R. Meyerson, Encyclopedia of Engineering Materials and Processes, pp. 439–442 (Reinhold Publ. Corp., New York, N.Y., 1963).

Some problems in temperature measurements from line spectra, J. T. Jefferies, Book, Temperature, Its Measurement and Control in Science and Industry 3, No. 1, 703–711 (1962).

The invariance of symmetric functions of singular values, Pacific J. Math. **12,** No. 1, 327–332 (1962).

Bounds for cofactors and arithmetic minima of quadratic forms, M. Newman. J. London Math. Soc. **38,** 215–217 (Apr. 1963).

Non-linear effects in spectra of the iron group, R. E. Trees, Phys. Rev. **129,** No. 3, 1220–1224 (Feb. 1, 1963).

Nonreciprocity of propagation of VLF radio waves along the magnetic equator, D. D. Crombie, Proc. IEEE **51,** No. 4, 617–618 (Apr. 1963).

Infrared spectrum of carbon tetrafluoride, A. Maki, E. K. Plyler and R. Thibault, J. Chem. Phys. **37,** No. 8, 1899–1900 (Aug. 1962).

Convergence to normality of powers of a normal random variable, N. Severo and L. J. Montzingo, Jr., Bull, Intern. Stat. Inst. **XXXIX,** Pt. 2, 491–500 (1962).

Matrix effects in the gaseous H atom–condensed olefin system; surface reaction–olefin diffusion model, R. Klein and M. D. Scheer, J. Phys. Chem. **66,** No. 12, 2677–2681 (Dec. 1962).

Normal functions, the Montel property, and interpolation in H^{∞}, G. T. Cargo, Michigan Math. J. **10,** 141–146 (1963).

A Note on domain conversions of $BaTiO_3$, P. H. Fang and W. S. Brower, J. Appl. Phys. **34,** No. 5, 1516 (May 1963).

Stability relations of dravite, a tourmaline, C. R. Robbins and H. S. Yoder, Jr., Geophysical Laboratory Yearbook 1961–62 (Note) (Carnegie Institute of Washington, Feb 1963).

An alignment interferometer, J. B. Saunders, Appl. Opt. **2,** No. 5, 541 (May 1963).

An application of the peek-a-boo principle to information retrieval, J. Stern, Proc. Symp. Materials Information Retrieval, pp. 93–115 (Nov. 28–29, 1962).

Critical review of sugar color and turbidity measurements F. G. Carpenter and V. R. Dietz, Sugar Ind. Tech. **21,** Paper 65, 32–52 (1962).

Molecular vib-rotors. The theory and interpretation of high resolution infrared spectra, H. C. Allen, Jr., and P. C. Cross, Book, John Wiley & Sons, Inc., New York, N.Y., 1963.

Copositive and completely positive quadratic forms, M. Hall, Jr., and M. Newman, Proc. Camb. Phil. Soc. **59,** 329–339 (1963).

On the vacuum ultraviolet reflectance of evaporated aluminum before and during oxidation, R. P. Madden, L. R. Canfield, and G. Haas, J. Opt. Soc. Am. **53,** No. 5, 620–625 (May 1963).

Covers and packings in a family of sets, J. Edmonds, Bull. Am. Math. Soc. **LXVIII,** No. 5, 494–499 (Sept. 1962).

On the pedestrian queueing problem, G. Weiss, Bull. Intern. Stat. Inst. **XXXIX,** No. 4, 163–168 (1962).

Burning behavior of building finish materials: Two-test methods, A. R. Robertson, Spec. Publ. Fed. Fire Council, pp. 21–35 (Apr. 1962).

The kinetics of description II: Ca^+ and Ba^+ from rhenium, M. D. Scheer and J. Fine, J. Chem. Phys. **38,** No. 2, 307 (Jan. 1963).

A computer for the Abel inversion, C. R. Yokley and J. B. Shumaker, Rev. Sci. Instr. **34,** No. 5, 551–557 (May 1963).

Rotation-vibration constants of acetylene, E. K. Plyler, E. D. Tidwell, and T. A. Wiggins, J. Opt. Soc. Am. **53,** No. 5, 589–593 (May 1963).

Calculation of crystallite size distributions from X-ray line broadening, A. Bienenstock, J. Appl. Phys. **34,** No. 5, 1391 (May 1963).

Osmotic and activity coefficients of tetraethylammonium iodide in aqueous solution at 25°, V. E. Bower and R. A. Robinson, Trans. Faraday Soc. **59,** No. 488, 1717–1719 (Aug. 1963).

A connection between Tauberian theorems and normal functions, G. T. Cargo, Bull. Am. Math. Soc. **68,** No. 4, 400–401 (July 1962).

A portable impedance tube, R. D. Berendt and H. A. Schmidt, Jr., J. Acoust. Soc. Am. **35,** No. 7, 1049–1052 (July 1963).

Inertial seismograph design—limitations in principle and practice, B. S. Melton and D. P. Johnson, Proc. IRE **50,** No. 11, 2328–2339 (Nov. 1962).

Nuclear moment of Ni^{61} from nuclear resonance studies in steady external magnetic fields, R. L. Streever, Phys. Rev. **128,** No. 4, 1632–1633 (Nov. 15, 1962).

Electromagnetic waves in stratified media, J. R. Wait, Book, Pergamon Press, Inc., New York, N.Y., 1962).

Linear velocity-gradient term in time-dependent pair distribution function, R. E. Nettleton, J. Chem. Phys. **38,** No. 8, 1791–1802 (Apr. 1963).

Absolute magnetic susceptibilities by the Gouy and the Thorpe-Senftle methods, G. A. Candela and R. E. Mundy, IRE Trans. Instr. **I–11,** No. 3–4, 106–109 (Dec. 1962).

** Publications for which a price is indicated are available by purchase from the Superintendent of Documents, U.S. Government Printing Office, Washington, D.C., 20402 (foreign postage, one-fourth additional). Reprints from outside journals and the NBS Journal of Research may often be obtained directly from the authors.*

JOURNAL OF RESEARCH of the National Bureau of Standards—A. Physics and Chemistry
Vol. 67A, No. 6, November–December 1963

INDEX TO VOLUME 67A

January to December 1963

A

Page

A note on the galvanomagnetic and thermoelectric coefficients of tetragonal crystalline materials ... 293
Absolute calibration of the National Bureau of Standards thermal neutron flux ... 215
Absolute configuration and chemical topology ... 591
Absorption bands of carbon dioxide from 5.3 to 4.6 microns ... 219
Absorption spectrum of muscovite sheet mica on the basis of color, and optic angle ... 309
Adiabatic calorimeters, heat exchange ... 331
Adsorption, batch (and column) ... 615
Adsorption from solution ... 615
Adsorption kinetic ... 615
Adsorption, polyester, on glass, reversibility ... 601
Afterglows and atomic flames, color phenomena associated with energy transfer ... 379
Aldoses-1-t, isotope effects in oxidation ... 569
Allen, H. C., Jr., Wm. B. Olson, On the fourth order Hamiltonian of an asymmetric rotor molecule of orthorhombic symmetry ... 359
—, —, *E. K. Plyler*, Analysis of two infrared bands CH_2D_2 ... 27
Ambrose, J. R., W. H. Johnson, Heat of oxidation of aqueous sulfur dioxide with gaseous chlorine ... 427
Analysis of families of curves ... 259
Analysis of the spectrum of neutral atomic bromine (Br I) ... 505
Analysis of two infrared bands CH_2D_2 ... 27
Analyzers and oscillatory systems, resolution limits ... 461
Antonucci, J. M., L. A. Wall, W. J. Pummer, J. E. Fearn, Reactions of polyfluorobenzenes with nucleophilic reagents ... 481
Arc, gas-stabilized, a study of, as an emission source for the measurement of oscillator strengths. Determination of some relative *gf*-values for Fe I ... 561
Atmosphere chamber, controlled ... 269
Atomic bromine (Br I), spectrum of neutral atomic, analysis ... 505
Atomic flames, color phenomena ... 379
Arton, E. J., An absolute calibration of the National Bureau of Standards thermal neutron flux ... 215

B

Barium borosilicate, vitreous, radial distribution study ... 37
Barnes, M. W., S. Ruthberg, R. H. Noyce, Correlation of muscovite sheet mica on the basis of color, apparent optic angle, and absorption spectrum ... 309
Bass, A. M., H. P. Broida, Color phenomena associated with energy transfer in afterglows and atomic flames ... 379
Bates, R. G., M. Paabo, R. A. Robinson, Buffer solutions of potassium dihydrogen phosphate and sodium succinate at 25 °C ... 573
Belcher, H. V., J. E. McKinney, Dynamic compressibility of poly(vinyl acetate) and its relation to free volume ... 43
Belknap, M. A., H. J. Keegan, J. C. Schleter, Recalibration of the NBS glass standards of spectral transmittance ... 577
Berman, H. A., E. S. Newman, Heat of formation of calcium aluminate monosulfate at 25 °C ... 1
Beryllium oxide and magnesium oxide, thermodynamic properties from 298 to 1,200 °K ... 325
Block, S., G. J. Piermarini, Radial distribution study of vitreous barium borosilicate ... 37
Brauer, G. M., R. W. Morris, W. B. Howe, Synthesis of isomers of eugenol ... 253
Broadening of the rotational lines of carbon monoxide by HCl and by argon ... 113
Broadhurst, M. G., Thermodynamic properties of polyethylene predicted from paraffin data ... 233
Broida, H. P., A. M. Bass, Color phenomena associated with energy transfer in afterglows and atomic energy ... 379
Bromine (Br I), spectrum of neutral atomic, analysis ... 505
Buffer solutions of potassium dihydrogen phosphate and sodium succinate at 25 °C ... 573
Burley, G., Photolytic behavior of silver iodide ... 301
Burns, C. L., D. F. Taylor, An investigation of the constitution of the mercury-tin system ... 55

C

Calcium aluminate monosulfate at 25 °C, heat of formation ... 1
Calorimeters, adiabatic, heat exchange ... 331
Carbon dioxide, absorption bands, from 5.3 to 4.6 microns ... 219
Carbon monoxide, broadening of the rotational lines of, by HCl and by argon ... 113
Carbon monoxide, self-broadening, in the 2ν and 3ν bands ... 229
CH_2D_2, two infrared bands, analysis ... 27
Chemical purity by dielectric cryometry ... 607
Chemical topology, absolute configuration ... 591
Chlorine, gaseous, heat of oxidation of aqueous sulfur dioxide ... 427
Color phenomena associated with energy transfer in afterglows and atomic flames ... 379
Color phenomena in polymer fracture ... 625
Colored glass standards ... 577
Compere, E. L., Jr., T. W. Mears, C. L. Stanley, F. L. Howard, Synthesis, purification, and physical properties of seven twelve-carbon hydrocarbons ... 475
Compressibility—of parahydrogen, 15 to 100 °K, to 350 atm ... 173
Controlled atmosphere chamber ... 269

Page

Corliss, E. L. R., Resolution limits of analyzers and oscillatory systems ... 461
Correlation of muscovite sheet mica on the basis of color, apparent optic angle, and absorption spectrum ... 309
Coulometric titrations of halides ... 31
Coulometric titrations, precise, of potassium dichromate ... 453
Cryometry, dielectric, chemical purity by ... 607
Cryometry, time-temperature, purity analysis of highly purified materials ... 247
Crystal point defects, trapped, relaxation modes ... 217
Crystals, anhydrous single, rare-earth halides, preparation ... 343
Crystals, oxide, symmetry splitting of equivalent sites in, and related mechanical effects ... 281
Curves, analysis of families ... 259
Cyclic polyhydroxy ketones. I. Oxidation products of hexahydroxybenzene (benzenehexol) ... 153

D

Davis, M. M., M. Paabo, Spectrophotometric determination of the thermodynamic pK value of picric acid in water at 25 °C ... 241
Decolorization by adsorption ... 615
de Vore, R. V., K. N. Roa, E. K. Plyler, Wavelength calibrations in the far infrared (30 to 1000 microns) ... 351
Dickson, R. W., H. S. Peiser, J. B. Wachtman, Jr., Reduction of space groups to subgroups by homogeneous strain ... 395
Dielectric cryometry, chemical purity by ... 607
Diffraction, X-ray ... 149
Digital computer, quantitative metallography with, application to a Nb-Sn superconducting wire ... 127
Diller, D. E., R. D. Goodwin, H. M. Roder, L. A. Weber, Pressure-density-temperature relations of fluid parahydrogen from 15 to 100 °K pressures to 350 atmospheres ... 173
2,3-Dimethylpentane and 2-methylhexane as a test mixture for evaluating highly efficient fractionating columns ... 15
Dixon, H. D., G. S. Ross, Purity analysis of highly purified materials by time-temperature cryometry ... 247
Douglas, T. B., High-temperature thermodynamic functions for zirconium and unsaturated zirconium hydrides ... 403
—, *A. C. Victor*, Thermodynamic properties of magnesium oxide and beryllium oxide from 298 to 1,200 °K ... 325
Dynamic compressibility of poly(vinyl acetate) and its relation to free volume ... 43

E

Effect of methyl bromide additions on the flame speed of methane ... 71
Effect of pressure and temperature on the refractive indices of benzene, carbon tetrachloride, and water ... 163
Elastic constants of a cubic crystal from velocity measurements in a single arbitrary direction; application to $SrTiO_3$, a method for determining ... 193
Electron configurations $np^2\ n'\ p$ and $np^4\ n'\ p$, matrices of spin-orbit interaction ... 555
Electron microscopy, polymers ... 625
Ellipsometry, thickness of absorbed polystyrene layers ... 431
Ellipsometry, measurement of the thickness and refractive index of very thin films and the optical properties of surfaces ... 363
Equivalent sites in oxide crystals, symmetry splitting of, and related mechanical effects ... 281
Eugenol, synthesis of isomers ... 253

F

Families of curves, analysis ... 259
Fatiadi, A. J., H. S. Isbell, Cyclic polyhydroxy ketones. I. Oxidation products of hexahydroxybenzene (benzenehexol) ... 153
Fearn, J. E., L. A. Wall, W. J. Pummer, J. M. Antonucci, Reactions of polyfluorobenzenes with nucleophilic reagents ... 481
Films, very thin, measurement of the thickness and refractive index of, and the optical properties of surfaces by ellipsometry ... 363
Flames speed of methane, effect of methyl bromide additions ... 71
Fracture, polymer, color phenomena in ... 625
Franklin, A. D., Relaxation modes for trapped crystal point defects ... 291
Frolen, L. J., G. S. Ross, Chemical purity by dielectric cryometry ... 607

G

Galvanomagnetic and thermoelectric coefficients of tetragonal crystalline materials, a note on ... 293
Gas-stabilized arc as an emission source for the measurement of oscillator strengths, a study. Determination of some relative *gf*-value for Fe I ... 561
Glass, reversibility of polyester adsorption on ... 601
Glass standards of spectral transmittance, NBS, recalibration ... 577
Goodwin, R. D., D. E. Diller, H. M. Roder, L. A. Weber, Pressure-density-temperature relations of fluid para hydrogen from 15 to 100 °K pressures to 350 atmospheres ... 173
Gordon, C. L., R. B. Johannesen, A controlled atmosphere chamber ... 269
Grant, W. H., R. R. Stromberg, Reversibility of polyester adsorption on glass ... 601

H

Page

Halides, rare-earth, preparation of anhydrous single crystals ... 343
Halides, titrations of, precise coulometric ... 31
Halpern, C., Effect of methyl bromide additions on the flame speed of methane ... 71
Heat exchange in adiabatic calorimeters ... 331
Heat of formation of calcium aluminate monosulfate at 25 °C ... 1
Heat of oxidation of aqueous sulfur dioxide with gaseous chlorine ... 427
Hernandez, W. C., Jr., A. H. Kahn, A note on the galvanomagnetic and thermoelectric coefficients of tetragonal crystalline materials ... 293
Hexahydroxybenzene (benzenehexol), cyclic polyhydroxy ketones, oxidation products ... 153
High-temperature thermodynamic functions for zirconium and unsaturated zirconium hydrides ... 403
Howard, F. L., T. W. Mears, C. L. Stanley, E. L. Compere, Jr., Synthesis, purification, and physical properties of seven twelve-carbon hydrocarbons ... 475
Howe, W. B., G. M. Brauer, R. W. Morris, Synthesis of isomers of eugenol ... 253
Hydrocarbons, twelve-carbon, synthesis, purification, and physical properties of seven ... 475
Hydrogen (para)—compressibility data, 15 to 100 °K, to 350 atomspheres ... 173

I

Infrared, absorption of carbon dioxide from 5.3 to 4.6 microns ... 219
Infrared, far, (30 to 1000 microns) wavelength calibrations ... 351
Infrared spectrum of the ν_2-ν_3 band of $C^{13}C^{12}H_6$ ... 225
Interference, X-ray ... 149
Investigation of the constitution of the mercury-tin system ... 55
Isbell, H. S., A. J. Fatiadi, Cyclic polyhydroxy ketones. I. Oxidation products of hexahydroxybenzene (benzenehexol) ... 153
—, *L. T. Sniegoski*, Tritium-labeled compounds. IX. Determination of isotope effects in reactions yielding water-*t* from nonvolatile reactants. Oxidation of aldoses-*l*-*t* with iodine ... 569
Isomers of eugenol, synthesis ... 253
Isotope effects, determinations of ... 569

J

Jaffe, J. H., R. J. Thibault, E. K. Plyler, Broadening of the rotational lines of carbon monoxide by HCl and by argon ... 113
Johannensen, R. B., C. L. Gordon, A controlled atmosphere chamber ... 269
Johnson, W. H., J. R. Ambrose, Heat of oxidation of aqueous chlorine ... 427

K

Kahn, A. H., W. C. Hernandez, Jr., A note on the galvanomagnetic and thermoelectric coefficients of tetragonal crystalline materials ... 293
Keegan, H. J., J. C. Schleter, M. A. Belknap, Recalibration of the NBS glass standards of spectral transmittance ... 577
Ketones, cyclic polyhydroxy, oxidation products of hexahydroxybenzene (benzenehexol) ... 153
Kiess, N. H., Preparation of anhydrous single crystals of rare-earth halides ... 343
Kinetics of adsorption ... 615
Kuehner, E. C., 2,3-Dimethylpentane and 2-methylhexane as a test mixture for evaluating highly efficient fractionating columns ... 15

L

Lafferty, W. J., E. K. Plyler, Infrared spectrum of the ν_2-ν_3 band of $C^{13}C^{12}H_6$ ... 225
Lamellar thickness, change of, and melting temperature with time for bulk polyethylene ... 441
Langmuir adsorption kinetics ... 615
Levine, E. P., J. B. Watchman, Jr., H. S. Peiser, Symmetry splitting of equivalent sites in oxide crystals and related mechanical effects ... 281
Loebenstein, W. V., Adsorption, desorption, resorption ... 615

M

Magnesium oxide and beryllium oxide, thermodynamic properties from 298 to 1,200 °K ... 325
Maki, A. G., E. K. Plyler, R. J. Thibault, Absorption bands of carbon dioxide from 5.3 to 4.6 microns ... 219
Mandel, J., F. L. McCrackin, Analysis of families of curves ... 259
Margoshes, M., B. F. Scribner, A study of the gas-stabilized arc as an emission source for the measurement of oscillator strengths. Determination of some relative *gf*-values for Fe I ... 561
Marinenko, G. J. K. Taylor, Precise coulometric titrations of halides ... 31
—, —, Precise coulometric titrations of potassium dichromate ... 453
Marzullo, S., J. B. Wachtman, Jr., M. I. Wheat, A method for determining the elastic constants of a cubic crystal from velocity measurements in a single arbitrary direction; application to $SrTiO_3$ ... 193
Matrices of spin-orbit interaction in the electron configuration $np^2\,n'p$ and $np^4\,n'p$ ... 555
McCrackin, F. L., J. Mandel, Analysis of families of curves ... 259
—, *F. Passaglia, R. R. Stromberg, H. L. Steinberg*, Measurement of the thickness and refractive index of very thin films and the optical properties of surfaces by ellipsometry ... 363
McKinney, J. E., H. V. Belcher, Dynamic compressibility of poly(vinyl acetate) and its relation to free volume ... 43
Mears, T. W., C. L. Stanley, E. L. Compere, Jr., F. L. Howard, Synthesis, purification, and physical properties of seven twelve-carbon hydrocarbons ... 475
Measurement of the thickness and refractive index of very thin films and the optical properties of surfaces by ellipsometry ... 363
Mechanical effects, related, of symmetry splitting of equivalent sites in oxide crystals ... 281
Melting temperature and change of lamellar thickness with time for bulk polyethylene ... 441
Mercury-tin system, an investigation of the constitution ... 55
Metallic surfaces, theory of frustrated total reflection ... 115
Method for determining the elastic constants of a cubic crystal from velocity measurements in a single arbitrary direction; application to $SrTiO_3$ ... 193
Methyl bromide additions on the flame speed of methane, effect ... 71
Mica, muscovite sheet, thermal behavior ... 585
Microscopy, polymers ... 625
Moire fringes produced by a point projection X-ray microscope ... 149
Moore, G. A., L. L. Wyman, Quantitative metallography with digital computer; application to a Nb-Sn superconducting wire ... 127
Morris, R. W., G. M. Brauer, W. B. Howe, Synthesis of isomers of eugenol ... 253
Muscovite sheet mica on a basis of color, apparent optic angle, and absorption spectrum, correlation ... 309
Muscovite sheet mica, thermal behavior ... 585

N

Neutron flux, thermal, an absolute calibration of the National Bureau of Standards ... 215
Newman, E. S., H. A. Berman, Heat of formation of calcium aluminate monosulfate at 25 °C ... 1
Newman, S. B., Moire fringes produced by a point projection X-ray microscope ... 149
—, *I. Wolock*, color phenomena in polymer fracture ... 625
Niobium-tin superconducting wire, quantitative metallography of, with a digital computer ... 127
Noyce, R. H., S. Ruthberg, M. W. Barnes, Correlation of muscovite sheet mica on the basis of color, apparent optic angle, and absorption spectrum ... 309
Nucleophilic reagents, reactions of polyfluorobenzenes ... 481

O

Olsen, Wm. B., H. C. Allen, Jr., On the fourth Hamiltonian of an asymmetric rotor molecule of orthorhombic symmetry ... 359
—, —, *E. K. Plyler*, Analysis of two infrared bands CH_2D_2 ... 27
On the fourth order Hamiltonian of an asymmetric rotor molecule of orthorhombic symmetry ... 359
Optic angle, apparent, and absorption spectrum of muscovite sheet mica on the basis of color and absorption spectrum ... 309
Optical properties of surfaces by ellipsometry, measurement of the thickness and refractive index of very thin films ... 363
Oscillator strengths, gas-stabilized arc as an emission source for measurement ... 561
Oscillatory systems and analyzers, resolution limits ... 461
Oxalic acid/acetic acid/water: its significance in oxalic acid crystal growth; phase study of the system ... 347
Oxidation, heat of, of gaseous sulfur dioxide with gaseous chlorine ... 427
Oxidation of aldoses with iodine ... 569
Oxidation products of hexahydroxybenzene (benzenehexol), cyclic polyhydroxy ketones ... 153
Oxide crystals, symmetry splitting of equivalent sites in, and related mechanical effects ... 281

P

Paabo, M., R. G. Bates, R. A. Robinson, Buffer solutions of potassium dihydrogen phosphate and sodium succinate at 25 °C ... 573
—, *M. M. Davis*, Spectrophotometric determination of the thermodynamic *pK* value of picric acid in water at 25 °C ... 241
Palladium (Pd III), third spectrum ... 87
Paraffin data, thermodynamic properties of polyethylene predicted ... 233
Passaglia, E., F. L. McCrackin, R. R. Stromberg, H. L. Steinberg, Measurement of the thickness and refractive index of very thin films and the optical properties of surfaces by ellipsometry ... 363
—, *R. R. Stromberg, D. J. Tutas*, Thickness of adsorbed polystyrene layers by ellipsometry ... 431
Peiser, H. S., J. B. Wachtman, Jr., R. W. Dickson, Reductions of space groups to subgroups by homogeneous strain ... 395
—, —, *E. P. Levine*, Symmetry splitting of equivalent sites in oxide crystals and related mechanical effects ... 281
Phase equilibrium relations in the Sc_2O_3–Ga_2O_3 system ... 19
Phase study of the system; oxalic acid/acetic acid/water; its significance in oxalic acid crystal growth ... 347
Photolytic behavior of silver iodide ... 301
Physical properties, synthesis, and purification of seven twelve-carbon hydrocarbons ... 475
Picric acid in water at 25 °C, spectrophotometric determination of the thermodynamic *pK* value ... 241
Piermarini, G. J., S. Block, Radial distribution study of vitreous barium borosilicate ... 37
Plyler, E. K., W. J. Lafferty, Infrared spectrum of the ν_2-ν_3 band of $C^{13}C^{12}H_6$ ... 225
—, *A. G. Maki, R. J. Thibault*, Absorption bands of carbon dioxide from 5.3 to 4.6 microns ... 219
—, *W. B. Olsen, H. C. Allen, Jr.*, Analysis of two infrared bands CH_2D_2 ... 27
—, *K. N. Roa, R. V. de Vore*, Wavelength calibrations in the far infrared (30 to 1000 microns) ... 351
—, *R. J. Thibault*, Self-broadening of carbon monoxide in the 2ν and 3ν bands ... 229
—, —, *J. H. Jaffe*, Broadening of the rotational lines of carbon monoxide by HCl and by argon ... 113
Point projection X-ray microscope moiré fringes produced ... 149
Polyester adsorption on glass, reversibility ... 601
Polyethylene, bulk, melting temperature and change of lammellar thickness with time ... 441
Polyethylene, thermodynamic properties of, predicted from paraffin data ... 233
Polyfluorobenzenes with nucleophilic reagents, reactions ... 481
Polymer adsorption ... 601
Polymer fracture, color phenomena ... 625
Polymethyl methacryiate, fracture ... 625
Polystyrene, crazing ... 625
Polystyrene layers, thickness of adsorbed, by ellipsometry ... 431
Poly(vinyl acetate) and its relation to free volume, dynamic compressibility ... 43
Potassium dichromate, precise coulometric titrations ... 453
Potassium dihydrogen phosphate and sodium succinate at 25 °C, buffer solutions ... 573
Precise coulometric titrations of halides ... 31
Precise coulometric titrations of potassium dichromate ... 453
Preparation of anhydrous single crystals of rare-earth halides ... 343

Page

Pressure-density-temperature relations of fluid para hydrogen from 15 to 100 °K at pressures to 350 atmospheres ... 173
Pummer, W. J., L. A. Wall, J. E. Fearn, J. M. Antonucci, Reactions of polyfluorobenzenes with nucleophilic reagents ... 481
Purification, synthesis, and physical properties of seven twelve-carbon hydrocarbons ... 475
Purity analysis of highly purified materials by time-temperature cryometry ... 247

Q

Quantitative metallography with a digital computer; application to a Nb-Sn superconducting wire ... 127

R

Radial distribution study of vitreous barium borosilicate ... 37
Rao, K. N., R. V. de Vore, E. K. Plyler, Wavelength calibrations in the far infrared (30 to 1000 microns) ... 351
Rare-earth halides, preparation of ahhydrous single crystals ... 343
Reactions of polyfluorobenzenes with nucleophilic reagents ... 481
Recalibration of the NBS glass standards of spectral transmittance ... 577
Reduction of space groups to subgroups by homogeneous strain ... 395
Refractive indices of benzene, carbon tetrachloride, and water, effect of pressure and temperature ... 163
Refractive index of very thin films, measurement of the thickness, and the optical properties of surfaces by ellipsometry ... 363
Relaxation modes for trapped crystal point defects ... 291
Resolution limits of analyzers and oscillatory systems ... 461
Reversibility of polyester adsorption on glass ... 601
Robinson, R. A., M. Paabo, R. G. Bates, Buffer solutions of potassium dihydrogen phosphate and sodium succinate at 25 °C ... 573
Roder, H. M., R. D. Goodwin, D. E. Diller, L. A. Weber, Pressure-density-temperature relations of fluid para hydrogen from 15 to 100 °K at pressures to 350 atmospheres ... 173
Ross, G. S., H. D. Dizon, Purity analysis of highly purified materials by time-temperature cryometry ... 247
—, *L. J. Fralen,* Chemical purity by dielectric cryometry ... 607
Rothrock, B. D., T. R. Young, Theory of frustrated total reflection involving metallic surfaces ... 115
Ruthberg, S., Thermal behavior of muscovite sheet mica ... 585
—, *M. W. Barnes, R. H. Noyce,* Correlation of muscovite sheet mica on the basis of color, apparent optic angle, and absorption spectrum ... 309

S

Sc_2O_3-Ga_2O_3 system, phase equilibrium relations ... 19
Schleter, J. C., H. J. Keegan, M. A. Belknap, Recalibration of the NBS glass standards of spectral transmittance ... 577
Schneider, S. J., J. L. Waring, Phase equilibrium relations in the Sc_2O_3-Ga_2O_3 system ... 19
Scribner, B. F., M. Margoshes, A study of the gas-stabilized arc as an emission source for the measurement of oscillator strengths. Determination of some relative *gf*-values for Fe I ... 561
Self-broadening of carbon monoxide in the 2σ and 3σ bands ... 229
Shenstone, A. G., Third spectrum of palladium (Pd III) ... 87
Silver iodide, photolytic behavior ... 301
Sniegoski, L. T., H. S. Isbell, Tritium-labeled compounds. IX. Determination of isotope effects in reactions yielding water-*t* from nonvolatile reactants. Oxidation of aldoses-*1-t* with iodine ... 569
Sodium succinate at 25 °C and potassium dihydrogen phosphate, buffer solutions ... 573
Space groups, reduction of, to subgroups by homogeneous strain ... 395
Spectrophotometric determination of the thermodynamic *p*K value of the picric acid in water at 25 °C ... 241
Spectrophotometry standards ... 577
Spectrum of neutral atomic bromine (Br I) ... 505
Standards, NBS glass, of spectral transmittance, recalibration ... 577
Stanley, C. L., T. W. Mears, E. L. Compere, Jr., F. Howard, Synthesis, purification, and physical properties of seven twelve-carbon hydrocarbons. ... 475
Steinberg, H. L., F. L. McCrackin, E. Passaglia, R. R. Stromberg, Measurement of the thickness and refractive index of very thin films and the optical properties of surfaces by ellipsometry ... 363
Strain, homogeneous, reduction of space groups ... 395
Strassburger, J., J. L. Torgesen, Phase study of the system: oxalic acid/acetic acid/water; its significance in oxalic acid crystal growth ... 347
Stromberg, R. R., W. H. Grant, Reversibility of polyester adsorption on glass ... 601
—, *F. L. McCrackin, E. Passaglia, H. L. Steinberg,* Measurement of the thickness and refractive index of very thin films and the optical properties of surfaces by ellipsometry ... 363
—, *E. Passaglia, D. J. Tutas,* Thickness of adsorbed polystyrene layers by ellipsometry ... 431
Strontium titanate ($SrTiO_3$), elastic constants of a cubic crystal from velocity measurement in a single arbitrary direction, a method for determining ... 193
Study of the gas-stabilized arc as an emission source for the measurement of oscillator strengths. Determination of some relative *g*-values for Fe I ... 561
Sulfur dioxide, aqueous, with gaseous chlorine, heat of oxidation ... 427
Symmetry splitting of equivalent sites in oxide crystals and related mechanical effects ... 281
Synthesis of isomers of eugenol ... 253
Synthesis, purification, and physical properties of seven twelve-carbon hydrocarbons ... 475

T

Page

Tauber, S. J., Absolute configuration and chemical topology ... 59
Taylor, D. F., C. L. Burns, An investigation of the constitution of the mercury-tin system ... 55
Taylor, J. K., G. Marinenko, Precise coulometric titrations of halides ... 31
—, —, Precise coulometric titrations of potassium dichromate ... 453
Tech, J. L., Analysis of the spectrum of neutral atomic bromine (Br I) ... 505
—, Matrices of spin-orbit interaction in the electron configurations np^3 $n'p$ and np^4 $n'p$ ... 555
Temperature, melting, and change of lamellar thickness with time for bulk polyethylene ... 441
Test mixture for evaluating highly efficient fractionating columns, 2,3-dimethylpentane and 2-methylhexane ... 15
Tetragonal crystalline materials, a note on the galvanomagnetic and thermoelectric coefficients of tetragonal crystalline materials ... 293
Theory of frustrated total reflection involving metallic surfaces ... 115
Thermal behavior of muscovite sheet mica ... 585
Thermodynamic functions for zirconium and unsaturated zirconium hydrides, high-temperature ... 403
Thermodynamic *p*K value of the picric acid in water at 25 °C, spectrophotometric determination ... 241
Thermodynamic properties of magnesium oxide and beryllium oxide from 298 to 1,200 °K ... 325
Thermodynamic properties of polyethylene from paraffin data ... 233
Thibault, R. J., J. H. Jaffe, E. K. Plyler, Broadening of the rotational lines of carbon monoxide by HCl and by argon ... 113
—, *A. G. Maki, E. K. Plyler,* Absorption bands of carbon dioxide from 5.3 to 4.6 microns ... 219
—, *E. K. Plyler,* Self-broadening of carbon monoxide in the 2σ and 2σ bands ... 229
Thickness of adsorbed polystrene layers by ellipsometry ... 431
Third spectrum of palladium (Pd III) ... 87
Titrations of halides, precise coulometric ... 31
Titrations of potassium dichromate, precise coulometric ... 453
Topology, chemical, absolute configuration ... 591
Torgesen, J. L., J. Strassburger, Phase study of the system: oxalic acid/acetic acid/water; its significance in oxalic acid crystal growth ... 347
Transition probabilities ... 561
Tritium-labeled compounds. IX. Determination of isotope effects in reactions yielding water-*t* from nonvolatile reactants. Oxidation of aldoses-*1-t* with iodine ... 569
Tutas, D. J., R. R. Stromberg, E. Passaglia, Thickness of adsorbed polystyrene layers by ellipsometry ... 431

V

Victor, A. C., T. B. Douglas, Thermodynamic properties of magnesium oxide and beryllium oxide from 298 to 1,200 °K ... 325
Vitreous barium borosilicate, radial distribution study of ... 37

W

Wachtman, J. B., Jr., H. S. Peiser, R. W. Dickson, Reduction of space groups to subgroups by homogeneous strain ... 395
—, —, *E. P. Levine,* Symmetry splitting of equivalent sites in oxide crystals and related mechanical effects ... 281
—, *M. L. Wheat, S. Marzullo,* A method for determining the elastic constants of a cubic crystal from velocity measurements in a single arbitrary direction; application to $SrTiO_3$ ... 193
Wall, L. A., W. J. Pummer, J. E. Fearn, J. M. Antonucci, Reactions of polyfluorobenzenes with nucleophilic reagents ... 481
Waring, J. L., S. J. Schneider, Phase equilibrium relations in the Sc_2O_3-Ga_2O_3 system ... 19
Water-*t* determination of isotope effect in formation of ... 569
Wavelength calibrations in the far infrared (30 to 1000 microns) ... 351
Wazler, R. M., C. E. Weir, Effect of pressure and temperature on the refractive indices of benzene, carbon tetrachloride, and water ... 163
Weber, L. A., R. D. Goodwin, D. E. Diller, H. M. Roder, Pressure-density-temperature relations of fluid para hydrogen from 15 to 100 °K at pressures to 350 atmospheres ... 173
Weeks, J. L., Melting temperature and change of lamellar thickness with time for bulk polyethylene ... 441
Weir, C. E., R. M. Wazler, Effect of pressure and temperature on the refractive indices of benzene, carbon tetrachloride, and water ... 163
West, E. D., Heat exchange in adiabatic calorimeters ... 331
Wheat, M. L., J. B. Wachtman, Jr., S. Marzullo, A method for determining the elastic constants of a cubic crystal from velocity measurements in a single arbitrary direction; application to $SrTiO_3$ ... 193
Wolock, I., S. B. Newman, Color phenomena in polymer fracture ... 625
Wyman, L., G. A. Moore, Quantitative metallography with a digital computer; application to a Nb-Sn superconducting wire ... 127

X

X-ray microscope, point projection, moire fringes produced ... 149

Y

Young, T. R., B. D. Rothrock, Theory of frustrated total reflection involving metallic surfaces ... 115

Z

Zirconium, high-temperature thermodynamic functions ... 403
Zirconium hydrides, correlation of thermodynamic properties ... 403
Zirconium hydrides, unsaturated, high-temperature thermodynamic functions for ... 403

U.S. GOVERNMENT PRINTING OFFICE: 1963

UNITED STATES
GOVERNMENT PRINTING OFFICE
DIVISION OF PUBLIC DOCUMENTS
WASHINGTON, D.C. 20402
OFFICIAL BUSINESS

PENALTY FOR PRIVATE USE TO AVOID PAYMENT OF POSTAGE, $300 (GPO)

JOURNAL OF RESEARCH of the National Bureau of Standards Vol. 67A, No. 6 November–December 1963
A. Physics and Chemistry

Contents

	Page
Analysis of the spectrum of neutral atomic bromine (Br I). Jack L. Tech.	505
Matrices of spin-orbit interaction in the electron configurations $np^3\ n'\ p$ and $np^4\ n'\ p$. Jack L. Tech.	555
A study of the gas-stabilized arc as an emission source for the measurement of oscillator strengths. Determination of some relative gf-values for Fe I. Marvin Margoshes and Bourdon F. Scribner.	561
Tritium-labeled compounds. IX. Determination of isotope effects in reactions yielding water-t from nonvolatile reactants. Oxidation of aldoses-1-t with iodine. Horace S. Isbell and Lorna T. Sniegoski.	569
Buffer solutions of potassium dihydrogen phosphate and sodium succinate at 25 °C. Maya Paabo, Roger G. Bates, and Robert A. Robinson.	573
Recalibration of the NBS glass standards of spectral transmittance. Harry J. Keegan, John C. Schleter, and Marion A. Belknap.	577
Thermal behavior of muscovite sheet mica. Stanley Ruthberg.	585
Absolute configuration and chemical topology. Stephen J. Tauber.	591
Reversibility of polyester adsorption on glass. Robert R. Stromberg and Warren H. Grant.	601
Chemical purity by dielectric cryometry. Gaylon S. Ross and Lois J. Frolen.	607
Adsorption, desorption, resorption. William V. Loebenstein.	615
Color phenomena in polymer fracture. Sanford B. Newman and Irvin Wolock.	625
Publications of the National Bureau of Standards.	639
Index to volume 67A. Physics and Chemistry, January to December 1963.	647

Library of Congress Catalog Card Number: 62–37059

For sale by the Superintendent of Documents, U.S Government Printing Office, Washington, D.C., 20402. Price 70 cents (single copy Subscription $4.00 a year; 75 cents additional for foreign mailing.
UNITED STATES GOVERNMENT PRINTING OFFICE, WASHINGTON : 1963

6